Generation of a novel mouse model for the study of autoimmune liver disease overlap syndrome

Dissertation
zur Erlangung des Doktorgrades
der Naturwissenschaften

Vorgelegt beim Fachbereich 14 Biochemie, Chemie und Pharmazie
der Johann Wolfgang Goethe-Universität
in Frankfurt am Main

von
Sina Fuchs
aus Gießen

Frankfurt am Main, 2019

vom Fachbereich 14 Biochemie, Chemie und Pharmazie der Johann Wolfgang Goethe-Universität als Dissertation angenommen.

Dekan: Prof. Dr. C. Glaubitz
Gutachter: Prof. Dr. R. Fürst
Prof. Dr. U. Christen

Datum der Disputation:

To my family

Table of contents

I List of figures

II List of tables

III List of abbreviations

Aa	Amino acid
AD	Autoimmune disease
Ad-2D6	Adenovirus expressing CYP2D6
Ag	Antigen
AIH	Autoimmune hepatitis
AIRE	Autoimmune regulator
ALT	Alanine aminotransferase
AMA	Anti-mitochondrial antibodies
ANA	Anti-nuclear antibodies
AP	Alkaline phosphatase
APC	Antigen presenting cell

APECED	Autoimmune polyendocrinopathy candidiasis ectodermal dystrophy
AST	Aspartate aminotransferase
Auto-Ag	Auto-antigen
B cells	B lymphocytes
BEC	Biliary epithelial cell
BMDC	Bone marrow derived dendritic cell
CD	Cluster of differentiation
CK19	Cytokeratin 19
CTL	Cytotoxic T lymphocyte
CTLA	T lymphocyte-associated antigen
CYP2D6	Cytochrome P450 2D6
D	Days
DC	Dendritic cell
Dex	Dexamethasone
EAE	Experimental autoimmune encephalitis
ECDI	1-ethyl-3-(3-dimethy-laminopropyl) carbodiimide
E. coli	*Escherichia coli*
EMA	European Medicines Agency
ERCP	Endoscopic retrograde cholangiopancreatography
FACS	Fluorescence-activated cell sorting
FCS	Fetal calf serum
FDA	Food and Drug Administration
$Foxp3^{+}$	Forkhead box protein 3
FVB	Friend leukemia virus B
GATA-3	GATA-binding protein 3
GGT	Gamma glutamyltransferase
GM-CSF	Granulocyte-macrophage colony-stimulation factor
HEPES	2-(4-(2-Hydroxyethyl)- 1-piperazinyl)-ethansulfonsäure
HLA	Human leukocyte antigen

HSC	Hepatic stellate cell
IAIHG	International AIH Group
IBD	Inflammatory bowel disease
ICCS	Intra cellular cytokine stain
IFN γ	Interferon γ
Ig	Immunoglobulin
IL-	Interleukin-
i.n.	Intranasal
i.p.	Intraperitoneal
i.v.	Intravenous
KC	Kupffer cell
LC-1	Liver cytosol-1 antibody
LKM-1	Liver/kidney microsomal type 1
LSEC	Liver sinusoidal endothelial cell
MALT	Mucosal-associated lymphoid tissue
MBP	Myelin basic protein
M cell	Microfold cell
mCyp	Mouse cytochrome P450 family molecules
Mdr2	*Multidrug resistance gene 2*
MHC	Major histocompatibility complex
MRCP	Magnetic resonance cholangiopancreatography
MS	Multiple sclerosis
NALT	Nasal-associated lymphoid tissue
NK	Natural killer
NOD	Non-obese diabetic mouse
NP	Nanoparticles
OGDC-E2	2-oxo-glutarate dehydrogenase
OS	Overlap syndrome
PAMPs	Pathogen-associates molecular patterns

pANCA	Anti-neutrophil cytoplasmic antibodies
PBC	Primary biliary cholangitis
PBMC	Peripheral blood mononuclear cell
PDC-E2	Subunit E2 of the pyruvate dehydrogenase complex
PD-L1	Programmed death ligand 1
Pen/Strep	Penicillin/Streptomycin
Pfu	Plaque forming unit
PLG	Poly-lactide-co-glycolide
PLP	Proteolipid protein
Poly IC	Polyinosinic-polycytidylic acid
PRRs	Pathogen-recognition receptors
PSC	Primary sclerosing cholangitis
RA	Rheumatoid arthritis
RORγt	Retinoic acid-related orphan receptor-γt
RT	Room temperature
SDS-PAGE	Sodium dodecyl sulphate - Polyacrylamide gel electrophorese
SLE	Systemic lupus erythematosus
SMA	Smooth muscle antibody
STAT4	Signal Transducer and Activator of Transcription 4
T1D	Type 1 diabetes
T-bet	T-box-expressed-in-T cell
T cells	T lymphocytes
TCM	Tissue culture medium
TCR	T cell receptor
tDC	Tolerogenic dendritic cell
T_{eff}	Effector T cell
TGF-β	Transforming growth factor β
T_H cell	T helper cell
TNFα	Tumor necrosis factor α

T_{reg}	Regulatory T cell
UDCA	Ursodeoxycholic acid
US	Ulcerative colitis
VitD3	Vitamin D

1. **Summary**

The three major autoimmune diseases (ADs) of the liver are primary biliary cholangitis (PBC), primary sclerosing cholangitis (PSC), and autoimmune hepatitis (AIH). All of those diseases show an aggressive immune reaction resulting in the destruction of liver tissue and finally to the development of hepatic fibrosis.

PSC is an autoimmune mediated disease of unknown etiology. It is characterized by inflammation of intra- and extrahepatic bile ducts. The progressive destruction of the bile ducts can lead to liver cirrhosis and finally to liver failure. Clinical signs for PSC are increased alkaline phosphatase (AP) and gamma glutamyltransferase (GGT) levels, presence of perinuclear anti-neutrophil cytoplasmic antibodies (pANCA) and bile ducts with characteristic strictures and dilations of the biliary tree as well as onion skin fibrosis surrounding the damaged bile ducts. Currently, there is no established treatment for PSC patients. The administration of ursodeoxycholic acid (UDCA) is being use as a therapy. However, it merely serves a symptomatic treatment to reduce serum AP and GGT as well as the formation of gallstones. In the advanced stage of PSC, liver transplantation is the last therapeutic option. *Mdr2*$^{-/-}$ mice are an excepted mouse model for human PSC. Such mice show lymphocytes infiltration into the liver, bile duct lesions, as well as the presence of the typical onion skin-like pericholangitis and periductal fibrosis.

AIH is a rare chronic autoimmune disease of the liver that results from the loss of self-tolerance to hepatocytes and leads to destruction of the hepatic parenchyma with the onset of cirrhosis. Clinical signs for AIH are elevated alanine aminotransferase (ALT) and aspartate transaminase (AST) levels, hypergammaglobulinemia and different types of autoantibodies. In addition, interphase hepatitis with lymphocytic and plasmacellular infiltrates in the periportal field are characteristic for AIH. Two different subtypes of AIH exist and depending on their autoantibody profile they can be distinguished into AIH type 1 which is characterized by the presence of anti-nuclear (ANA) and/or anti-smooth muscular (SMA) autoantibodies, and AIH type 2 showing liver/kidney microsomal autoantibodies (LKM-1). LKM-1 recognizes the major autoantigen, the 2D6 isoform of the cytochrome P450 enzyme family (CYP2D6). One mouse model for AIH is the CYP2D6 model in which the injection of Ad-2D6 leads to a breakdown of the immune tolerance by the destruction of hepatocytes.

There are some patients with autoimmune diseases of the liver who have both cholestatic and hepatic liver enzymes and histological features suggestive of two different liver diseases. These patients are diagnosed with an overlap syndrome (OS).

In my thesis I generated an animal model with characteristics of both diseases, which would mimic features of human PSC-AIH OS. *Mdr2*$^{-/-}$ mice which spontaneously develop PSC were infected with Ad-2D6 to trigger the autoimmune-driven hepatic injury. Pathogenesis of PSC-AIH OS mice was compared to mice with solitary PSC or AIH. Naïve FVB wild type mice have been used as healthy controls. The characterization of the PSC-AIH OS model was done by analyzing serological parameters like ALT, AP, different antibodies like pANCA, LKM-1 like CYP2D6 and total IgG. Additionally, fibrosis and cholangitis were analyzed by immunohistochemistry and Western blotting. Moreover, cellular infiltrations of $CD4^+$ and $CD8^+$ T cells, dendritic cells (DCs), monocytes/macrophages and neutrophils were determined with immunohistochemistry. Finally, the overall immune balance in the liver and the frequency of CYP specific T cells were analyzed via flow cytometry. Our new mouse model indeed represents the characteristics of both PSC and AIH and mimics features of the human PSC-AIH OS. It allows studying the development of a PSC-AIH OS and how the two overlapping diseases are influencing one another. In a second approach I wanted to induce CYP2D6-specific tolerance in AIH mice. Therefore, I tried four different approaches, namely intranasal peptide administration, injection of tolerogenic DCs, antigen-coupled splenocytes, and Ag-coupled nanoparticles (NP) and evaluated their potential to induce CYP2D6 specific T_{reg} with the capacity to prevent AIH in mice. Unfortunately, the intranasal peptide administration and also the injection of tolerogenic DCs did not increase the amount of CYP2D6 specific T_{reg} which would lead to a reduction of the frequency of inflammatory T cells. Surprisingly, the injection of antigen-coupled splenocytes showed the opposite effect characterized by a very strong cytokine secretion in the tolerized mice. The use of NPs led to an increase in CYP2D6 specific T_{reg} as well as in decrease in the frequency of inflammatory T cells and finally has the potential for a therapeutic approach.

In summary, the generated PSC-AIH OS model represents many clinical signs which can also be observed in PSC-AIH OS patients. This model can be used to study the etiology of this overlap syndrome and further to test potential therapeutic approaches. The

different immune tolerance induction pathways which I tried in the AIH model show that NPs have to potential to induce immune tolerance but this approach has to be refined and the outcome has to be characterized in more detail.

2. **Zusammenfassung**

Die drei häufigsten Autoimmunerkrankungen der Leber sind primäre biliäre Cholangitis (PBC), primäre sklerosierende Cholangitis (PSC) und Autoimmunhepatitis (AIH). All diese Erkrankungen weisen eine aggressive Immunreaktion auf, die zur Zerstörung des Lebergewebes und schließlich zur Leberfibrose führt.

PSC ist eine autoimmun basierte Lebererkrankung unklarer Ätiologie. Sie ist gekennzeichnet durch eine Entzündung des außerhalb und innerhalb der Leber gelegenen Gallengangsystems. Die fortschreitende Zerstörung der Gallengänge kann über eine Leberzirrhose bis zu einem Leberversagen führen. Die klinischen Auffälligkeiten, die für eine PSC sprechen, sind erhöhte Werte der alkalischen Phosphate (AP) sowie der Gamma Glutamlytransferase (GGT). Die Präsenz von perinuklearen Anti-Neutrophile cytoplasmatische Antikörper (pANCA) und Gallengänge mit Verengungen sowie Fibrose in Form von Zwiebelschalen ähnlichen Strukturen um die Gallengänge herum, deuten ebenfalls auf eine PSC hin. PSC tritt häufig in Zusammenhang mit Colitits ulcerosa auf. Männer sind zweimal häufiger betroffen als Frauen. Aktuell gibt es keine etablierte medikamentöse Therapie für Patienten mit PSC. Die Gabe von Ursodeoxycholsäure (UDCA) ist eine mögliche Therapiemaßnahme, um die AP und GGT im Serum zu senken und um die Bildung von Gallensteinen zu vermindern. Im fortgeschrittenen Stadium der PSC ist eine Lebertransplantation die letzte Therapiemaßnahme. 40% aller Patienten mit PSC benötigen einen Lebertransplantation 10-15 Jahren nach Auftreten der ersten Symptome. Die *Mdr2*$^{-/-}$ Maus ist ein etabliertes Mausmodel für humane PSC. Solche Mäuse zeigen lymphozytäre Infiltrationen in der Leber, Gallengangsschädigungen sowie Cholangitis und Fibrose in Form von typischen zwiebelschalenartigen Strukturen um die Gallengänge herum. Die *Mdr2*$^{-/-}$ Maus hat einen Gendefekt im Multidrug Resistenz Gen 2, welches zu einer fehlerhaften Sekretion von Phospholipiden in die Galle führt. Die dadurch austretende toxische Gallensäure führt zur Schädigung des umliegenden Gewebes. Interessanterweise führt eine Mutation in einem stark verwandten menschlichen Gen ABCB4 (MDR3) ebenfalls zur autoimmun-basierten Cholangitis mit starken Ähnlichkeiten zur *Mdr2*$^{-/-}$ Maus.

AIH ist eine seltene chronische Autoimmunerkrankung der Leber, die aus dem Verlust der Selbsttoleranz gegenüber den Hepatozyten resultiert und zur Zerstörung des

hepatischen Parenchyms mit dem Übergang zu einer Zirrhose führt. Klinische Auffälligkeiten, die für eine AIH sprechen, sind erhöhte Serumwerte von Alanin Aminotransferase (ALT) und Aspartat Transaminase (AST), Hypergammaglobulinämie und die Präsenz verschiedener Autoantikörper. Darüber hinaus ist histologisch eine „Interphase"-Hepatitis mit lymphozytären und plasmazellulären Infiltraten im Periportalfeld charakteristisch für AIH. Es gibt zwei verschiedene Typen der Autoimmunhepatitis, diese sind abhängig von der Art der Autoantikörper. Man unterscheidet AIH Typ 1, welcher über die Präsenz von Antikörpern gegen Zellkerne (ANA) und Antikörpern gegen glatte Muskulatur (SMA) charakterisiert ist und dem AIH Typ 2, der mit Leber-Niere-Mikrosomen Antikörpern (LKM-1) auftritt. Der Krankheitsverlauf von AIH Typ 2 ist im Vergleich zum AIH Typ 1, ein akuterer, denn er geht meist schneller in eine Zirrhose über. Patienten mit AIH werden erhalten nach der Diagnose einer sofortigen immunsuppressiven Therapie unterzogen. Diese setzt sich aus der alleinigen Gabe von Glukokortikoiden wie beispielsweise Prednison oder Budesonid zusammen, oder sie werden mit dem Zytostatikum Azathioprin kombiniert. Bei guter Verträglichkeit erfolgt diese Therapie erfolgt lebenslang. Leider ist die Therapie aber nicht immer erfolgreich, sodass viele Lebertransplantationen aufgrund von AIH durchgeführt werden müssen. Die Krankheitsursachen, die zu einer AIH führen, sind noch nicht geklärt. Man geht davon aus, dass ein Zusammenspiel von genetischen und umweltbedingten Faktoren die Krankheit verursacht und/oder fördert. Ein Tiermodell, welches viele Aspekte der humanen AIH widerspiegelt, stellt das CYP2D6 Mausmodell dar. In diesem Modell werden Mäuse mit einem Adenovirus, das das menschliche CYP2D6 exprimiert (Ad-2D6), infiziert. Das Ad-2D6 infiziert Leberzellen und sorgt für eine Expression des CYP2D6 in den infizierten Zellen. Aufgrund einer molekularen Mimikry zwischen CYP2D6 und den strukturell ähnlichen Maus Zytochromen (Cyp) wird die Toleranz gegenüber Cyp durchbrochen und eine chronische autoimmune Lebererkrankung induziert. Die resultierenden Autoantikörper zeigen die gleiche Spezifität wie die menschlichen LKM-1 Antikörper. Darüber hinaus weisen Ad-2D6 infizierte Tiere erhöhte Werte der Leberenzyme ALT und AST auf und zeigen eine hepatische Fibrose mit fusionierten Leberlappen, lymphozytären und plasmazellulären Infiltrate sowie Nekrose.

Es gibt Patienten mit Autoimmunerkrankungen der Leber, die sowohl cholestatische Veränderungen, als auch erhöhte hepatische Leberenzyme und histologische Merkmale aufweisen, welche für zwei verschiedene Lebererkrankungen sprechen. Diese Patienten werden mit einem Überlappungssyndrom (OS) diagnostiziert. Die Prävalenz von Patienten mit AIH und PBC liegt bei 7-13%, ergänzend dazu tritt AIH mit PSC in 6-11% der Fälle auf. Patienten mit einem PSC-AIH OS können histologisch eine „Interphase"-Hepatitis mit Plasmazellinfiltrationen, Fibrose und Cholangitis aufzeigen. Darüber hinaus können folgende Leberenzyme erhört sein: ALT, AST, AP und GGT. Die Antikörper, welche in PSC-AIH OS Patienten detektiert werden können, sind unterschiedlich. Jedoch sprechen erhöhte Werte von γ-Globulin und IgG sowie der Nachweis von pANCA, ANA und SMA, für einen PSC-AIH OS. Bis heute gibt es keine einheitliche Therapiemaßnahme für die Behandlung von PSC-AIH OS. Der Hauptgrund dafür liegt an dem fehlenden Wissen über die Krankheitsursachen und der Immunpathogenese des mit den bereits charakterisierten Einzelerkrankungen der Leber vergleichsweise seltenen OS. Zudem fehlt ein repräsentatives Tiermodell, welches die Charakteristiken des PSC-AIH OS im Menschen aufzeigt.

Das Ziel dieser vorliegenden Arbeit war zunächst die Etablierung eines Tiermodells zur Charakterisierung des Überlappungssyndroms der PSC und AIH, welches das Krankheitsbild im Menschen widerspiegelt. Darüber hinaus wurden im Rahmen dieser Arbeit verschiedene potentielle Therapieansätze, basierend auf der Induktion der immunen Toleranz im Tiermodell der AIH, getestet.

2.1. Etablierung eines Tiermodells zur Charakterisierung des Überlappungssyndroms von PSC-AIH im Menschen

Die Etablierung eines Tiermodells zur Charakterisierung des Überlappungssyndroms der PSC und AIH erfolgte unter der Verwendung von *Mdr2*$^{-/-}$ Mäusen, welche bereits als etabliertes Tiermodell der humanen PSC darstellen. Diese Mäuse wurden mit dem Adenovirus Ad-2D6, welches das humane Cytochrom P4502D6 exprimiert, infiziert, um den autoimmunen Leberschaden zu erzeugen. Die Pathogenese der PSC-AIH OS Mäusen

wurde sowohl mit naiven *Mdr2*$^{-/-}$ Tiere verglichen als auch mit Ad-2D6 infizierte FVB Wildtyp Mäusen, welche die Auswirkung von AIH als Einzelerkrankung aufzeigen. Ergänzend zu diesen verschiedenen Mausmodellen wurden darüber hinaus noch naive FVB Wildtyp Mäuse als zusätzliche Kontrolle verwendet. Die Charakterisierung des PSC-AIH OS Tiermodells wurde zunächst anhand von serologischen Analysen vorgenommen, welche die Detektion der Leberenzyme ALT und AP und der Autoantikörper LKM-1 und pANCA, sowie die Gesamtmenge von IgG beinhaltete. In den Tieren des PSC-AIH OS wurden die höchsten ALT und AP Werte gemessen. Diese Tiere zeigten ebenfalls die stärkste pANCA Aktivität sowie ähnlich hohe IgG und LKM-1 Antikörper Titer wie AIH Mäuse auf. Ergänzend zu den serologischen Analysen erfolgten histologische Analysen zur Charakterisierung des PSC-AIH OS Tiermodells. Dabei wurden Gewebeschnitte der Leber hinsichtlich Fibrose für Collagen III Ablagerungen gefärbt, als auch Cholangitis durch die Verwendung von Anti-Cytokeratin 19 Antikörpern visualisiert. Die Quantifizierung dieser Färbungen zeigte, dass die Tiere des PSC-AIH OS im Vergleich zu den Tieren der anderen Modelle am stärksten von Fibrose und Cholangitis betroffen waren. Histologische Analysen wurden ebenfalls hinsichtlich zellulärer Infiltrate von $CD4^+$ und $CD8^+$ T Zellen, Monozyten und Makrophagen sowie von Dendritischen Zellen und Neutrophilen durchgeführt. Die meisten infiltrierenden Zellen waren in den PSC-AIH OS Tieren zu finden. Interessanterweise zeigten die PSC-AIH OS Tiere sowohl das Muster der einzelnen, verstreut vorkommenden Zellinfiltraten, welche charakteristisch für AIH sind, als auch das Muster der Clusterung von dichten Zellinfiltraten auf, welches wiederrum typisch für PSC ist. Aufgrund der bereits identifizierten Peptide des AIH Modells, war es möglich, die Frequenz von Autoantigen-spezifischen inflammatorischen T Zellen in den verschiedenen Tieren zu messen. Hinsichtlich der inflammatorischen $CD4^+$ T Zellen war kein Unterschied zwischen den AIH und PSC-AIH OS Tieren zu sehen, jedoch zeigten die PSC-AIH OS Tiere eine zweifach höhere CYP2D6 spezifische $CD8^+$ T Zellantwort. Die Charakterisierung der Immunantwort der T Zellen in den verschiedenen Tiermodellen hat ergeben, dass AIH Tiere aufgrund der Virusinfektion eine stärkere Typ 1 T Zellantwort aufweisen. Im Vergleich dazu zeigten PSC Tiere eine Zunahme der Typ 17 T Zellantwort auf. In den PSC-AIH OS Tieren wurde sowohl eine dominante Typ 1 T Zellantwort als auch eine starke Typ 17 T Zellantwort gemessen, welches zu einer Reduktion der Typ 2 T Zellantwort führte.

Im Rahmen dieser Arbeit konnte das Ziel erreicht werden, ein Tiermodell zu etablieren, welches die Aspekte eines Überlappungssyndroms von PSC-AIH in vielen Hinsichten widerspiegelt. Dieses Tiermodell erlaubt die Immunpathogenese des PSC-AIH OS im Detail zu studieren und darüber hinaus potentielle therapeutische Interventionen für den Menschen zu untersuchen.

2.2. **Therapieansätze für AIH basierend auf Toleranzinduktion**

Die Wiederherstellung der verlorengegangenen Toleranz gegenüber den spezifischen Autoantigenen, die in einer Autoimmunerkrankung attackiert werden, ist ein vielversprechendes Ziel einer maßgeschneiderten Therapiemaßnahme für Autoimmunerkrankungen. Um dies zu erreichen, muss das Gleichgewicht zwischen Effektor- und regulatorischen T Zellen (T_{reg}) wiederhergestellt werden. Dabei kann entweder die Zahl der autoreaktiven T Zellen reduziert oder alternativ die Zahl der T_{reg} erhöht werden. Tiermodelle der experimentellen Autoimmun-Encephalomyelitis (EAE) und Typ 1 Diabetes in denen die nasale Verabreichung von löslichen Autoantigenen erfolgte, zeigten eine Zunahme von T_{reg} und eine Verhinderung der Erkrankung. Die Applikation von tolerogenen Dendritischen Zellen, die zur Induktion T_{reg} führen, ist ebenfalls eine vielversprechende Therapiemaßnahme. Die intravenöse Verabreichung von Splenozyten, bei welchen Autoantigene über einen Crosslinker verbunden sind, stellt ebenfalls einen möglichen Therapieansatz zur Toleranzinduktion dar. Anstelle der verwendeten Splenozyten gibt es auch chemisch hergestellte Nanopartikel, die ebenfalls als Träger von Antigenen eingesetzt werden können.

In dieser Arbeit wurde in dem Tiermodell für AIH sowohl die nasale Verabreichung von CYP2D6 Peptiden mit verschiedenen Adjuvantien getestet, als auch die Injektion von CYP2D6 beladen tolerogenen Dendritischen Zellen. In diesen beiden Therapieansätzen konnte im Vergleich mit nicht tolerisierten Tieren kein signifikanter Unterschied in der Menge an inflammatorischen T Zellen detektiert werden. Der dritte Ansatz beinhaltete die Verabreichung von Splenozyten, die über einen Crosslinker mit den CYP2D6 Peptiden verbunden wurden. Dieser Ansatz erbrachte den gegenteiligen Effekt und zeigte eine sehr starke Zytokinausschüttung in den tolerisierten Tieren. Als weiteren

therapeutischen Ansatz erfolgte der Einsatz von Nanopartikeln, die tatsächlich zu einer Zunahme von T_{reg} sowie einer temporären Abnahme von Effektor T Zellen in tolerisierten Tieren führten. Dieser Ansatz muss aber noch weiter verfeinert werden, um einen permanenten therapeutischen Erfolg zu erzielen.

Die Analysen der AIH infizierten Tiere mit den verschiedenen Therapiemaßnahmen der Toleranzinduktion hat ergeben, dass in einigen Fällen zwar die Zahl der T_{reg} in den tolerisierten Tieren erhöht werden konnte, jedoch konnte aufgrund des nicht wieder vollständig hergestellten Immungleichgewichts eine AIH in diesen Tieren nicht verhindert werden.

3. Introduction

3.1. The immune system

The immune system is a complex defense system which protects the host from pathogenic microorganisms such as viruses, bacteria, fungi, parasites, and tumors. The main function of the immune system is accomplished by the capability to recognize “non-self” and “altered-self” structures on infected or transformed cells. A failure in these complex defense mechanisms often leads to allergies, the development of autoimmune diseases or tumors.

The immune system can be divided into two components based on the recognition and elimination of pathogen structures. The non-antigen specific defense is ensured by the innate immune system, whereas the adaptive immune system is responsible for the antigen specific recognition and elimination. Besides, the adaptive immune system is characterized by an immunological memory that allows a very fast and effective immune response against a pathogen which is already known [2–4].

3.2. Innate immune system

The innate immune system is the first line of defense against invading pathogens and prevents the entrance and establishment of infection agents. It does not require sensitization to antigens and has a very fast response. The first barriers of the innate immunity are anatomical barriers like the skin and the mucous membranes to block the entry of microbes into the body. Moreover, physiological barriers include body temperature, low pH, and chemical barriers like the complement system, interferons or lysozymes belong to the innate immune system. The innate immune system contains a variety of cells, like monocytes/macrophages, natural killer (NK) cells, dendritic cells (DCs), neutrophils as well as several plasma proteins like the complement system which create the phagocytic or endocytic barrier. Innate immune cells recognize and bind to microbial structures, called pathogen-associates molecular patterns (PAMP). PAMPs are recognized via pathogen-recognition receptors (PRRs) which are either attached on the membrane of immune cells or are soluble receptors in the cytosol. The binding initiates

effector functions of the cells, like phagocytosis, opsonization, and lysis via the complement system and finally elimination of the pathogen. The innate immune system is also able to initial release of chemokines and cytokines which are needed to activate the adaptive immune system [2–4].

3.3. **Adaptive immune system**

In contrast to the innate immune system, the adaptive immune system is highly specific and is able to recognize and eliminate pathogens effectively. The cell types which belong to the adaptive immune system are T and B lymphocytes (T and B cells) and their products, such as antibodies. These cells are able to recognize a high diversity of individual molecules of pathogens, called antigens via their antigen receptors on their surface. Depending on the type of response, the adaptive immune response can be subdivided into cell-mediated (T cells) and humoral (B cells) responses. Moreover, the adaptive immune system has the ability to distinguish self from non-self. A response only to non-self-molecules is critical because a failure in such a self-tolerance of the immune system might lead to autoimmune diseases (ADs). In contrast to the innate immune system, the adaptive immune system is able to memorize specific antigens. This immunological memory enables the immune system to respond faster and more effectively to a secondary infection with the same pathogen and finally to avoid or weaken the development of the disease [2–4].

3.4. **T lymphocytes**

T cells together with B cells belong to the adaptive immune system and are responsible for the cell-mediated immune response. In contrast to the B cells, which are generated in the bone marrow and mature there, the bone marrow-derived hematopoietic progenitors T cell mature under stricter controls in the thymus. First, positive selection ensures that only T cells bearing a functional antigen receptor (T cell receptor, TCR) can interact with molecules presented by the major histocompatibility complex (MHC). T cells which do not bind to MHC undergo apoptosis. In contrast, negative selection ensures that T cells that recognize the host own peptide antigens are eliminated to

maintain self-tolerance. After successful differentiation the naïve T cells are allowed to leave the thymus and recirculate in the bloodstream, lymphatics, and secondary lymphatic organs where they wait for activation signals [5, 6].

Detection of invading pathogens requires presentation of their antigens on the cell surface of antigen presenting cells (APC), such as macrophages, B cells, DCs, and monocytes. Naïve cluster of differentiation (CD) 8^+ T cells only interact with peptides presenting by MHC class I molecule that is expressed on all nucleated host cells [7]. In addition to the recognition of antigens through the TCR, co-stimulatory molecules like CD28 are needed, which interacts with CD80 or CD86 expressed on APCs. Moreover, cytokine secretion is necessary for a successful T cell activation. After activation $CD8^+$ T cells differentiate into cytotoxic T lymphocytes (CTL) which are able to eliminate tumor cells and protect against viruses. For this ability CTL release the cytotoxins perforin, granzymes, and granulysin which allow eliminating infected endogenous cells. Moreover, $CD8^+$ T cells can produce interferon γ (IFN γ) which directly activates macrophages [8].

$CD4^+$ T cells play an important role in the adaptive immune response and are responsible for generating the appropriate immune response against different pathogens. Naïve $CD4^+$ T cells interact with peptides presented via MHC class II molecules which are expressed on B cells, macrophages, and especially DCs [9]. After activation, naïve $CD4^+$ T cells differentiate into one of several subpopulations like T-helper cells type (T_H1), T_H2, T_H17 or regulatory T (T_{reg}) depending on the surrounding cytokine milieu (Figure 1) [10–12]. These different subpopulations of T_H cells distinguish from each other in their cytokine production as well as their functions [13]. However, it is known that after differentiation, the cells still have the opportunity to develop into another effector cell type. This indicates the presence of plasticity within the subpopulations [12, 14].

The differentiation to T_H1 cells takes place in the presence of IFNγ or interleukin 12 (IL-12) [15]. Moreover, the transcription factors Signal Transducer and Activator of Transcription 4 (STAT4) and T-box-expressed-in-T cells (T-bet) play a crucial role in T cell maturation into T_H1 cell [16]. Additionally, T_H1 cells interact mainly with macrophages as well as $CD8^+$ T cells or B cells [13]. The main products which are released by T_H1 cells are IFNγ, IL-2 and tumor necrosis factor α (TNFα). T_H1 cells mediate protection against intracellular pathogens and viruses, which is promoted by IFNγ-induced macrophage

activation [17]. T_H2 cells mature in response to IL-4. GATA-binding protein 3 (GATA-3) as a transcription factor is known to induce the differentiation of T_H2 cells which are characterized by the secretion of IL-4, IL-5, IL-10, as well as IL-13. Moreover, T_H2 cells stimulate B cells to produce all immunoglobulin classes, recruit eosinophilic granulocytes and thus contribute to the elimination of extracellular pathogens [13, 17, 18]. In addition, T_H2 cells are involved in the development of allergies such as allergic asthma [19]. T_H17 cells, which differentiate in the presence of IL-6, IL-21, and Transforming Growth Factor β (TGF-β) are characterized by IL-17, IL-21, and IL-22 secretion and play an important role in the defense against microbial pathogens [20, 21]. The transcription factor retinoic acid-related orphan receptor-γt (RORγt) is known to be characteristic for T_H17 cells which are involved in the development of ADs such as multiple sclerosis (MS) and rheumatoid arthritis (RA) [22, 23]. To protect against ADs, the body has another effector population, the T_{reg}. Their task is to suppress immune reactions against self-molecules and to inhibit the activity of autoreactive T cells [24] The secreted cytokines such as IL-10 and TGF-β provide this anti-inflammatory environment [25]. The presence of IL-2 and TGF-β lead to the differentiation of naïve T cells to T_{reg} , which express the transcription factor forkhead box protein 3 ($Foxp3^+$) by the induction of TGF-β [26–28]. T_{reg} can be divided into two distinct subpopulations: induced T_{reg} and natural T_{reg}.

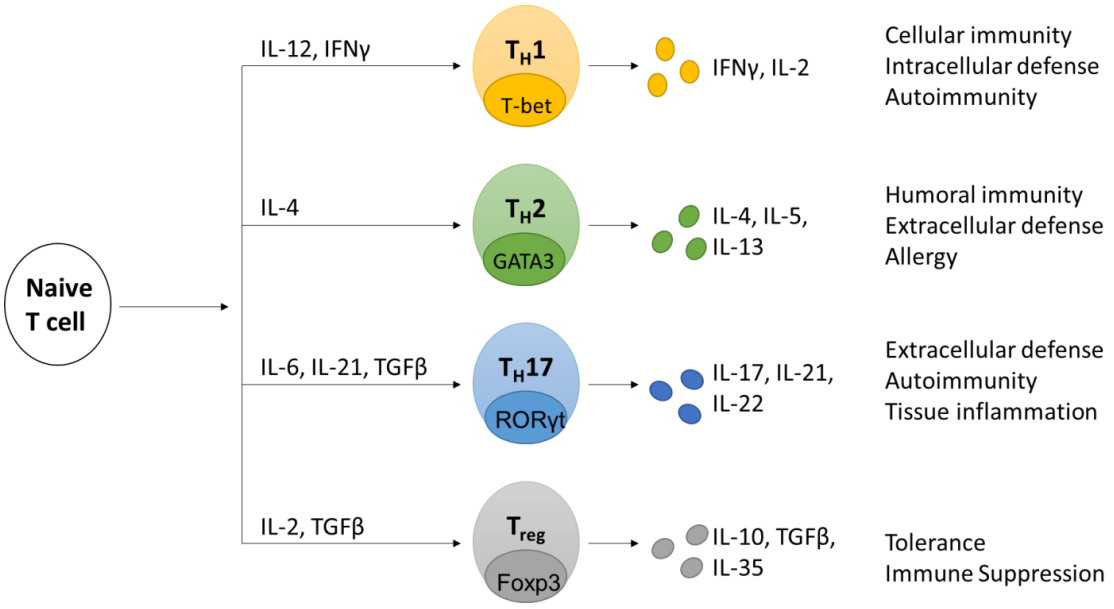

Figure 1: Differentiation of naïve T cell into different CD4⁺ T cell subsets characterized by their cytokine production, transcription factor and effector functions
Scheme modified after Pietropapolo et al., 2008 [1].

3.5. **Tolerance**

Tolerance is a state of unresponsiveness in which the immune response prevents against a particular antigen. The immune system is generally tolerant of self-antigens. However, when tolerance is lost, disorders like ADs or allergy may occur. There are different types of tolerance, the central as well as the periphery tolerance.

3.5.1. Central and peripheral tolerance

T cells have to go through several levels to prevent from uncontrolled self-reactivity. Central tolerance is the first mechanism to tolerize the immune system towards self (Figure 2). It takes place in the thymus where pre-T cells undergo a stringent process and in which 95% of the pre-T cells are eliminated [29]. The first selection process is called positive selection and involves the presentation of self-peptides to T cells [4]. At this time, $CD4^+$ $CD8^+$ double-positive T cells interact with either MHC I or MHC II molecules are positive selected and get the chance to mature to $CD4^+$ or $CD8^+$ single-positive T cells

[4]. T cells which react to self-antigens presented by MHC molecules too strong, die through apoptosis at an early state in their development. This process allows eliminating self-reactive T cells and is called negative selection. After a successful first tolerance, which known as central tolerance, lymphocytes will leave the thymus and circulate in the periphery.

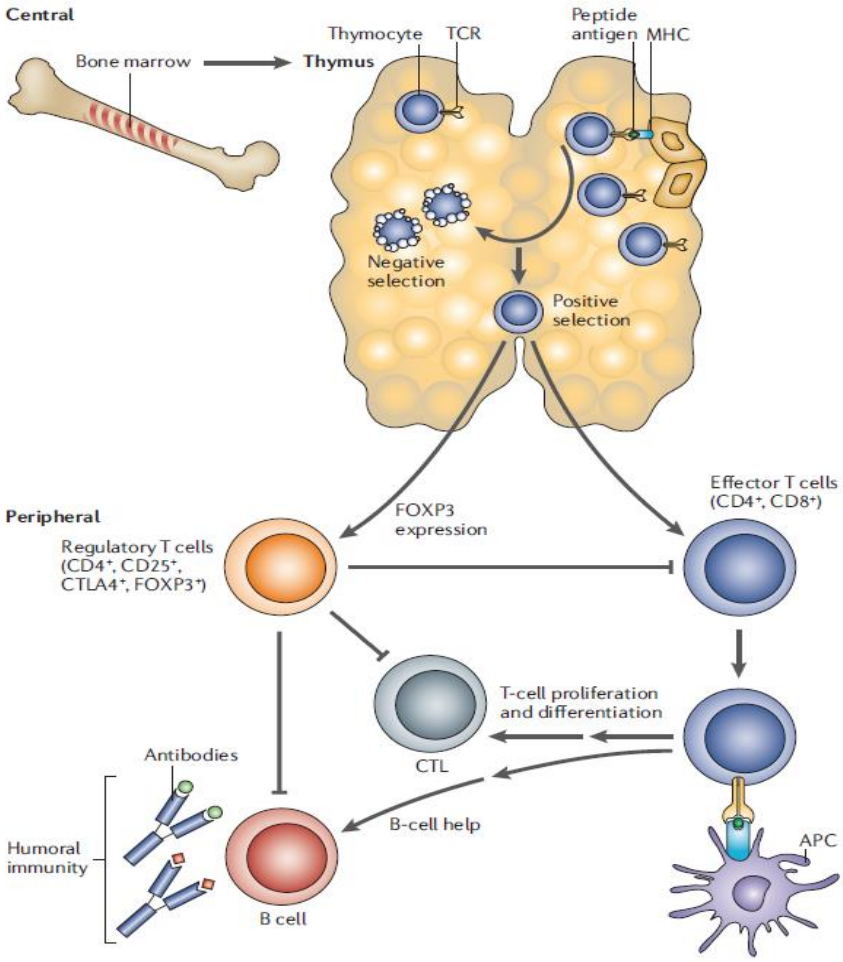

Figure 2: Central and peripheral tolerance mechanisms
Bone marrow lymphoid cells migrate into the thymus where they are undergoing negative and positive selection. After successful maturation T cells will leave the thymus and will develop into either $CD4^+$ or $CD8^+$ T cells or T_{reg} expressing Foxp3. Once in the periphery, T_{reg} are important for peripherl tolerance. Figure from Gregersen et al., 2006 [31].

Not all self-proteins can be presented during the time of maturation in the thymus. Therefore, another type of tolerance is needed that controls maturated lymphocytes, which is called peripheral tolerance. Mature lymphocytes have to distinguish between

self and non-self even if they have not seen the antigen before during their maturation. This very critical process has to be controlled carefully. When self-reactive lymphocytes escape into the periphery tolerance can be induced by three different mechanisms. Firstly, an induction of anergy, a state of inactivation in which lymphocytes remain alive but are unable to respond to antigen. Secondly, a deletion of autoreactive T cells via apoptosis. Thirdly, an indication of T_{reg} which are able to suppress the activation and proliferation of other lymphocytes in multiple ways [30].

3.6. **Autoimmunity**

The immune system has to distinguish self from non-self to maintain the balance of immunity of the host (Figure 3) [32]. Interference with this important process can result in overactivity to self-antigens, leading to autoimmunity. During the last decades there is a significant increase in the incidence of ADs worldwide [33]. ADs have high prevalence (~8%) in the population [34]. Depending on which parts of the body are affected by the ADs, they can be categorized into organ-specific or systemic ADs. Type 1 diabetes (T1D), in which insulin producing β cells of the pancreas get destroyed, MS, which involved a destruction of myelin sheathing axons in the central nervous system, Graves' disease, which is caused by damage to the thyroid-stimulating hormone receptor, and autoimmune hepatitis (AIH), which is described by the destruction of hepatocytes, all belong to organ-specific ADs. In addition to the organ-specific ADs, systemic ADs like lupus erythematosus (SLE) or RA cause inflammation in multiple tissues in the whole body. All these different ADs can be mediated by CTL or autoantibodies, but in all cases, T_H cells are involved. Moreover, it is known that a close interplay between environmental factors like vitamin D (VitD3), toxins, infections, life-style, diet, and genetic factors is responsible for the loss of immune tolerance and autoimmunity (Figure 3)[35, 36].

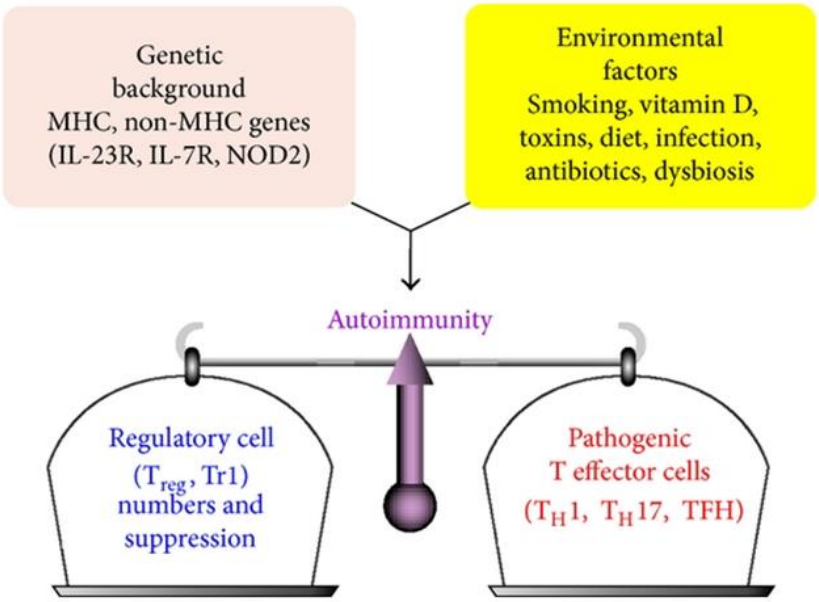

Figure 3: The balance of immunity
A combination of genetic predisposition and environmental factors can lead to autoimmunity. A balance between T_{reg} and pathogenic T effecor cells is needed for immunity. Figure from Vojdani et al., 2014 [37].

3.6.1 Genetic predisposition

ADs effects 5-9% of the general population but the etiology for most ADs is still unclear [37]. Some individuals have a higher risk to develop an AD; a circumstance which is deeply rooted in their genetic predisposition. It is known that genetic susceptibility factors like the MHC haplotype and polymorphisms in other genes that are involved in establishing self-tolerance and immune regulation are linked to the development of ADs. The most common risk factors for autoimmune disorders are genetic variations in the MHC genes [3, 4, 38]. The MHC haplotype can influence the susceptibility to get an AD in two ways. On the one hand, an enhanced presentation of peptide epitopes in the periphery, leads to an increase of T cell activation. On the other hand, an ineffective presentation of self-antigens in the thymus, results in a fewer numbers of T_{reg} and more aggressive T cells in the periphery. It is already shown that HLA-DRB1 and –DQB1 are linked to type 1 AIH [39] whereas HLA-DRB1 is also connected to RA [40]. Moreover, HLA-

DRB3 is associated with Graveś disease [41] and HLA-DR3 is a genetic predisposition for SLE [42].

Polymorphic gene expression in the cell-surface protein cytotoxic T-lymphocyte-associated protein-4 (CTLA-4) which is a key negative regulator of T cell activation has been associated with Graves´ diseases, T1D, MS and AIH [4, 6]. In addition to CTLA-4, the protein tyrosine phosphatase non-receptor type 22 has also an influence on the development of autoimmunity because it is involved in the negative control of T cell activation and development [6]. Moreover, autoimmune regulator (AIRE) is another risk factor for ADs [43]. It is known that a defective expression of AIRE is responsible for the human multi-organ AD, called autoimmune polyendocrinopathy candidiasis ectodermal dystrophy (APECED) [44]. APECED is characterized by variable ADs attacking the endocrine tissue resulting in T1D or Addison´s diseases [45]. 20% of patients with a AIRE deficiency develop an AIH [46]. Research on AIRE-deficient mice shows that AIRE regulates autoimmunity by promoting the peripheral tissue-restrict antigens in the thymus. Absence of AIRE shows the inability to present these antigens in the thymus which finally leads to an immune disorder [45]. Genetic predisposition plays a role in the development of ADs but studies on monozygotic twins show that the concordance rate is not higher that 30% meaning that there are other factors needed for the development of ADs [47, 48].

3.6.2. Environmental factors

The observed overall north-south geographical gradient of ADs in the northern hemisphere put the thought forward that environmental factors play an essential role in autoimmunity. There are many studies investigating the association between VitD3 deficiency and ADs [49–52]. Low levels of VitD3 have been linked with ADs, such as SLE, MS, T1D and RA [53]. It is published few months ago that severe VitD3 deficiency is a prognostic biomarker in AIH. [54]It is known that VitD3 has a potential role in the regulation of immune response towards the stimulation of secretion of T_H2 cells and T_{reg} as well as its protective function in the inhibition of the generation of proinflammatory cytokines like IL-1,-2,-12,-17 or TNFα [55].

A significant increase in the incidence of ADs like T1D and MS could be observed in industrialized counties over recent decades which led to the postulation that diet is a potential environmental risk factor for ADs. The human microbiome which depending on the diet might be a major player in autoimmunity because changes in microbial composition can lead to the loss of immune tolerance [56, 57]. Microbiota studies of the fecal samples of children with T1D show a lower diversity of bacteria than healthy controls [58]. Additionally, studies of human patients with PSC compared to healthy control show distinct differences in the global bacterial community [59, 60]. These studies show that there is an association between the bacteria *Veillonella* and other chronic inflammatory and fibrotic conditions and *Veillonella* was enriched in PSC patients. Moreover, the present of *Veillonella* in PSC patients could be a possible biomarker to differentiating PSC and healthy controls [61]. Alterations of microbiome, called 'dysbiosis' can induce autoimmune disorders in people who have a genetic predisposition as well as other environmental factors which favored the development of ADs.

A closer look at the diet shows that there is a link between gluten sensitive and gluten ingestion enteropathies [62]. Recently, it is published that a high level of dietary sodium affects the immune system in that way that it can influence T_H cell differentiation towards T_H1 and T_H17. The suppressive effects of T_{reg} are reverse and finally high level of dietary sodium promotes the development of ADs [63]. Cigarette smoking as an environmental factor may be one of the important risk factors for ADs, especially for RA. The effect of cigarette smoking may be related to an increase in the level of proinflammatory cytokines, DNA methylation or an increased oxidative stress [64, 65].

In addition to the diet and the lifestyle in the western countries there is another fact linked to these countries which has an impact in the development of ADs and is described as 'hygiene hypothesis'. It has been observed that there is a relationship between the size of a family and the development of immune disorders. The hypothesis postulates that a reduction in the frequency of infections in western countries contributes directly to the increase in ADs and allergies. Parasite exposures like helminths infections in the early childhood are considered to have an influence of the immune system. These infections are supposed to promote the T_H2 response and to

stimulate the secretion of IL-10 and TGFβ and therefore to protect from the development of autoimmune disorders [66].

3.6.3. Pathogen-induced autoimmunity

Pathogen infections either by bacteria or virus lead to the initiation of an innate and adaptive immune response and therefore they are known to implicate in the development of many ADs. Infections with viruses result in an inflammatory milieu with a strong type 1 response which is much higher as required for the elimination of intracellular pathogens and finally modulate the immune system in the direction of autoimmunity [67, 68]. It is difficult to demonstrate an association between the pathogen infections and the ADs because the infection might have occurred years to decades before the diagnosis of the disease so the pathogen is no detectable in the host [69]. This process is described as ʾhit-and-runʾ event. In addition to this process there are others which described possible mechanism how pathogens might initiate autoimmune disorders. Bystander activation which is characterized by a strong pathogen infection leading to a highly inflammatory milieu in which autoreactive T cells can activated. In other possible pathway, described as molecular mimicry shows that pathogen infection can break self-tolerance by sharing similar epitopes to the host which results to a cross-reactive immune response [70]. Molecular mimicry might play a role in the development of PBC, since the anti-mitochondrial antibodies (AMA) of PBS patients attack the lipoic acid moiety of the 2-oxoacid dehydrogenase enzyme family also show a cross-reactivity to the components of the bacterium *Novosphingobium aromaticivorans* [71, 72]. Bacteria and viruses are able to produce superantigens as a defense mechanism against the host immune system. These superantigens can cause a T_H1 cytokine storm in which T_H1 cells get activated and might react to self-components [73]. Interestingly, there are certain pathogen infections, like infections by helminths, which are known to protect from autoimmune disorders rather to initiate or enhance an immune reaction [74]. In summary, it is a complex and dynamic interaction of genetic and environmental factors and there are many factors needed to break the self-tolerance and lead to an AD.

3.7. **The liver**

3.7.1. Anatomy and function of the liver

The liver is the largest internal organ in the body. It is very important for the detoxification of metabolites and removal of waste products. Moreover, it is also involved in the glucose, lipid and protein metabolisms as well as in the production and secretion of bile. Bile is a complex aqueous secretion that is produced by the hepatocytes and is modified via a complex network in the bile duct epithelium. Finally, it converges into the common bile duct which is entering into the gallbladder before it will secrete to the intestinal lumen. Biliary epithelial cells (BEC) which have the major function to modify the bile before its secretion are also constitute the main target cells in cholestatic diseases [75].

The human liver consists of two lobes, a smaller lobe on the left side and a lager one on the right side [4]. A closer look inside shows that the liver is divided into small units, called liver lobule (Figure 4, A). Each liver lobule is composed of a central vein in the middle, from which hepatocytes radiate to the portal tracts in the periphery. Each portal triad also called Glisson Triad consists of one hepatic portal vein, one hepatic artery together with one bile duct [76, 77].

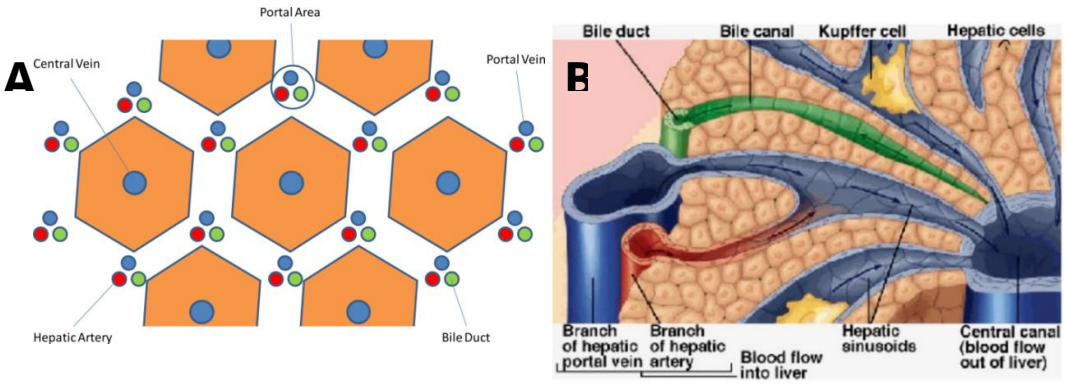

Figure 4: Anatomic structure of a liver lobule and the hepatic microenvironment
The hepatic lobule is the structural unit of the liver. Each liver lobule contains a central vein from which the hepatocytes radiate towards the periphery, where the portal triads are located. Each portal triad contains one hepatic artery, one portal vein, and one bile duct. Figure is modified after Bogdanos et al., 2013 & PathologyOutlines.com [76].

The liver has a dual blood supply, one from the hepatic arteries and one form the portal veins (Figure 4, B). The hepatic artery provides oxygen-rich blood from the system circulation, while the portal vein received nutrient and antigen-rich blood from the digestive system. Blood enters the liver mainly through the portal vein, flows through a highly branched vascular system, called sinusoids and leaves the liver via the central veins. The sinusoids are lined by an endothelium, known as liver sinusoidal endothelial cells (LSEC) and contain a lot of additional cell types like liver resident macrophages, known as Kupffer cells (KCs), hepatocytes, hepatic stellate cells (HSCs), immature DCs, and hepatic lymphocytes. All these cells are important for the first line of defense against infectious or toxic pathogen arriving from the gut [78].

3.7.2. Liver immunology

The liver plays an essential role in immune tolerance. On one hand the liver has to be tolerant against harmless food derived antigens arriving from the gut, but on the other hand the liver has to efficiently eliminate pathogenic microorganisms to avoid liver damage. Therefore, the liver has to switch from a tolerant to a responsive state every time [79]. Experimental transplantation in the past shows that liver allografts in many species were more tolerant compared to other transplanted organs [80]. This leads to conclude that the immune status of the liver is predominantly tending tolerance rather than a reactive state which would result in organ rejections. Liver-resident cells responsible for the liver immunology are KCs which are strategically positions in the sinusoids and play an important role in the first line of defense against invading microorganisms. KCs are able to produce cytokines after bacterial stimulation which further lead to an immune response [81]. It has been observed that KCs are able to activate and induce the differentiation of NK cells by the release of IL-12 and IL-18 [82]. Upon activation of NK cells are also able to release cytokines like IFNγ, which result in the expression of chemokines by LSECs and the recruitment of T cells [83]. LSECs as well as KCs are able to endocytose, process and present antigens to T cells which leads to T cell activation. On one hand KCs are known to act as effective APC, resulting in T cell proliferation and cytokine secretion but on the other hand KCs are able to induce

immune tolerance by synthesis of nitric oxide which leads to the suppression of T cell activation [84].

Another cell type which has also the ability to act as APCs but is limited in this function is the HSC [85–87]. HSCs are located between hepatocytes and LSECs in the space of Disse where they control the blood flow through the sinusoidal system. After activation HSCs are able to differentiate into myofibroblasts and generate fibrous matrix leading to liver fibrosis.

3.7.3. Liver tolerance

The first liver immune tolerance was observed in porcine liver allo-transplantation in the 1960s. Later it was found to be indispensable for the maintenance of oral tolerance toward harmless food and bacteria antigens from the gut [88]. The liver-mediated immune tolerance needs a complex interaction of hepatocytes, liver non-parenchymal cells and immune cells. To induce immune tolerance in the liver several types of conventional and nonconventional APC as well as T_{reg} are needed. The role of LSECs in hepatic tolerance and generation of immune tolerance in the liver is often observed. LSECs are known to be an efficient APC with multiple functions [89, 90]. They have efficient scavenger functions, that keep the blood vessels clean form bacterial and antigens compounds [91]. Moreover, LSECs have the capacity to present antigens to $CD4^+$ and $CD8^+$ T cells [90]. However, under non-inflammatory conditions, these interactions fail to activate an immune response [92]. In this case, immune tolerance is induced in which T cells start to secrete suppressive cytokines like IL-4 and IL-10 [93]. Other resistant liver cells, such as KCs, are known to have the tolerogenic capacity to allergic and drug-induced reactions [94, 95]. Under normal conditions, KCs do not get triggered by soluble antigens, since they do not express MHC class II or co-stimulatory molecules [94, 96]. KCs can interact with LSECs or T_{reg}, which leads to IL-10 secretion and thus to an immunosuppressive environment [97, 98]. During inflammation in the liver, immune tolerance can be broken and KCs can get activated to induce T cell proliferation [99]. Loss of liver tolerance leads to auto-aggressive phenomena which further can lead to autoimmune liver diseases if it could not control by T_{reg}. Many publications focus on the

capacity of the liver to induce tolerance by expression of autoantigens to generate autoantigen-specific T_{reg} which suppressed ADs like EAE in mice [100]. Moreover, the expression of autoantigens like myelin basic protein (MBP) on the surface of nanoparticles (NP) which stuck in the liver, led to T_{reg}-induced control of autoimmunity by liver sinusoidal endothelia cells and prevented EAE in mice [101].

3.8. **Autoimmune liver diseases**

The three major ADs of the liver are primary biliary cholangitis (PBC), primary sclerosing cholangitis (PSC), and autoimmune hepatitis (AIH). All of those diseases are considered be of autoimmune origin and show an aggressive immune reaction leading in destruction of liver tissue and finally to the development of hepatic fibrosis. Autoimmune liver diseases can be divided into two categories: those with a predominance of cholestatic features like PBC with a lymphatic cholangitis and PSC including fibrosis sclerotic cholangiopathy and those with a hepatic predominance like AIH with interface hepatitis [102, 103]. If both clinical features, cholestatic and hepatic, appear in a patient, then the disease is called an overlap syndrome (OS).

3.8.1. Primary biliary cholangitis

PBC is a chronic inflammatory autoimmune liver disease which is characterized by destruction of the medium-size and small intrahepatic bile ducts and eventually leads to fibrosis, cirrhosis and liver failure [104]. PBC is ten-fold more common in women than men and the median age of diagnosis is about 50 years [104, 105]. Moreover, a strong association with recurrent urinary tract infections could be observed [106–109]. *Escherichia coli* (*E. coli*) are the most frequent cause of these infections. This leads to the assumption that *E. coli* infections trigger autoimmune responses by molecular mimicry [106, 107, 109, 110]. Genetic and familial factors play a major role in PBC [111]. The HLA-DR7 as well as –DR8 are risk factors for PBC, whereas HLA-DR11 and –DR13 are protective factors [112]. Liver biopsy of PBC patients show nonsuppurative destructive

cholangitis and interlobular bile duct destruction [113]. Circulating AMA are present in nearly 95 % of the PBC patients and are one of the major diagnostic criteria for PBC [114–116]. The target antigens for AMA are localized to the inner membrane of the mitochondria. The E2-subunit of the pyruvate dehydrogenase complex (PDC-E2) has been identified as the major autoantigen of PBC and it has a strong reactivity of AMA [117, 118]. Moreover, the other members of the 2-oxo-acid dehydrogenase family, 2-oxo-glutarate dehydrogenase (OGDC-E2) as well as branched chain 2-oxo acid dehydrogenase (BCOADC-E2) are also attacked by an aggressive autoimmune response because of the loss of self-tolerance [116]. Currently, ursodeoxycholic acid (UDCA) is the primary therapy for PBC. It can reduce the concentration and injury from relatively toxic bile acids but up to 40 % of the patients response sub optimally to UDCA treatment [119]. In this case a combination therapy of UDCA with obeticholic acid is used as the new drug in almost 20 years to treat patients with PBC [120]. Liver transplantation remains as an option when therapy with medications is no longer effective. Results of liver transplantation are about 70% of 10-year survival after transplantation [113].

3.8.2. Primary sclerosing cholangitis

PSC is a chronic, progressive cholestatic liver disease characterized by inflammation, fibrosis and destruction of intra- and extrahepatic bile ducts and possible cirrhosis and malignance [121]. The majority of PSC patients develops cirrhosis within 10-20 years and finally requires liver transplantation for survival [122, 123]. PSC has an annual, incidence of approximately 1 in 100.000 [124]. Two thirds of the patients are male in a median age of 30–40 years [125]. It also attacks children and young adults [126] PSC is strongly associated with ulcerative colitis (US) and inflammatory bowel disease (IBD) (70-80%) [127, 128]. Genetic susceptibility is associated in genes of the HLA complex. An increase in HLA-DR6 has been found in PSC patients [129]. Other risk-associated genes which are known to play a role in the development of PSC are *IL2; MDR3,* v-rel reticuloendotheliosis viral oncogene homolog and *caspase recruitment domain-containing protein 9* [130]. PSC is specifically diagnosed by the detection of increased liver enzymes like gamma glutamyltransferase (GGT), alkaline phosphatase (AP), a slight increase in alanine

aminotransferase (ALT) / aspartate aminotransferase (AST) levels and a rise in serum bilirubin in advanced stages [125, 131, 132]. To date, there are no PSC-specific autoantibodies, but a screening can be useful in differential diagnosis [133, 134]. For example, the detection of perinuclear anti-neutrophil cytoplasmic antibodies (pANCA) can be observed in about 90 % of patients. AMA is a typical hallmark for PBC, but can also be found in very few patients with PSC; it is most useful when searching for a cholestatic disease [135]. An important tool for the diagnosis of PSC is the use of magnetic resonance cholangiopancreatography (MRCP) or endoscopic retrograde cholangiopancreatography (ERCP) that enables to analyze the structure of bile ducts and to diagnose PSC (**Figure 5**). Most PSC patients display damage to the large bile ducts (90-95%) with characteristic strictures and dilatations of the biliary tree as well as onion skin fibrosis surrounding the damaged ducts. There are no effective specific medical treatments for PSC till now. Most patients are treated with immunosuppressive drugs and the administration of UDCA [125, 131, 132].

Figure 5: Cholangiogram of a PSC patient showing beading and dilation of the intra- and extrahepatic bile ducts
Figure from Chapman et al., 2008 [128].

3.8.3. *Mdr2*$^{-/-}$ mice as a model for human PSC

The multidrug resistance gene 2 (*Mdr2*) encodes for the main biliary phospholipid flippase *Mdr2* which is responsible for the package of bile acids into phospholipid vesicles [136, 137]. It is highly expressed in the bile canalicular membrane of hepatocytes

[138]. A lack in this gene leads to an incorrect secretion of phospholipids into the bile resulting in toxic bile acid-induced bile duct damage and finally leads to sclerosing cholangitis [136, 139, 140]. Already one day after birth, livers of *Mdr2*$^{-/-}$ mice display alterations, like proliferation fibroblast, neutrophil-granulocytic infiltrate and a ductular reaction in lager portal tracts, compared to age matched control mice [141]. Histological hematoxylin and eosin staining of liver from *Mdr2*$^{-/-}$ compared to FVB wild type mice confirm the typical PSC features in this animal model (Figure 6). This model is very common for studying the pathogenesis of PSC. Interestingly, a mutation in the human orthologous gene ABCB4 (MDR3) also leads to autoimmune-mediated cholangitis characterized by lymphocytes infiltration, bile duct lesions, and presence of the typical onion skin-like pericholangitis and periductal fibrosis [139, 142–144].

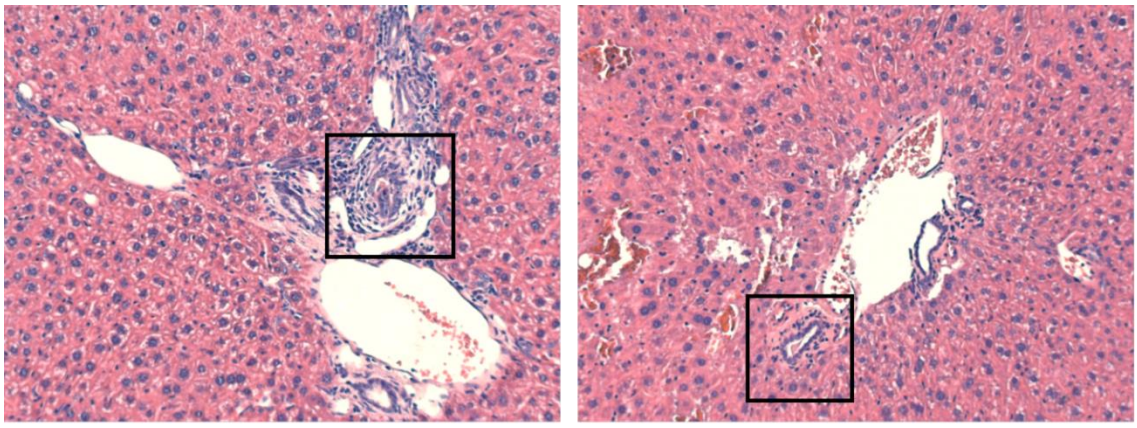

Figure 6: Histological analysis of the liver pathology in *Mdr2*$^{-/-}$ mouse compared to FVB wild type mouse
Representative pictures of hematoxylin and eosin stained livers of 8-week old *Mdr2*$^{-/-}$ mouse (left side) compared to FVB wild type mouse (right side). Note the onion skin concentric fibrosis around the bile ducts in *Mdr2*$^{-/-}$ mouse which are not present in FVB wild type (boxed area). 40x magnification.

3.8.4. Autoimmune hepatitis

AIH is an autoimmune disease which is characterized by a chronic inflammation and the destruction of parenchyma resulting in liver chronic fibrosis [145]. AIH affects individuals of all ages and different ethnologies and the causes are still unknown [146, 147]. It has a female predominance of 3.6:1 [148]. People who are diagnosed with AIH suffering from fatigue, lethargy, malaise, nausea, jaundice, mild pain [149]. Histological staining of liver

biopsies from AIH patients show interface hepatitis with plasma and T cell infiltration, piecemeal necrosis affecting patches of hepatocytes and fibrosis [150–153]. In addition to the histological features, elevated serum levels of the liver enzyme AST and ALT as well as hypergammaglobulinemia of immunoglobulin (IgG) are also characteristic for AIH. Depending on the different autoantigens that are recognized by autoantibodies, AIH can be divided into type 1 and type 2 AIH. Type 1 AIH is defined by the presence of anti-nuclear (ANA) and/or anti-smooth muscle (SMA) autoantibodies, whereas type 2 AIH is characterized by liver/kidney microsomal type 1 (LKM-1) and/or anti-liver cytosol type 1 (LC-1) autoantibodies [154, 155]. It is known that LKM-1 autoantibodies mainly target cytochrome P450 2D6 (CYP2D6). Thus, CYP2D6 is described as the major autoantigen and LKM-1 as major autoantibody of type 2 AIH [156–158]. Individuals exhibiting MHC class I HLA-B8 and/or MHC class II HLA-DR3 show a genetic predisposition and an increased risk of both types of AIH [159–162]. In addition, the presence of MHC class II molecule HLA-DR4 genetically predisposes for AIH-1, whereas the MHC class II molecule HLA-DR7 is allied with the development for AIH-2. The diagnosis of AIH is somewhat difficult because not all of the patients show the same symptoms but the International AIH Group (IAIHG) generated a simplified scoring system which helps to diagnose AIH [163–167]. The current standard therapy is a treatment with glucocorticoids like prednisone and budesonide alone or in combination with another immunosuppressive drugs like azathioprine [147, 150, 168, 169]. 80%-90% of treated patients achieve remission, but may experience a relapse [170]. Alternative treatments like budesonide and cyclosporine A as a calcineurin inhibitor as well as tacrolimus could be used for AIH patients who relapses after corticosteroid withdrawal [171, 172]. If there is no response, the immunosuppressant mycophenolate mofetil, a cytostatic drug can be used for patients who are intolerant to azathioprine [170, 173–178]. However, during standard therapy, adults rarely achieve resolution of their laboratory and liver tissue abnormalities in less than 12 months and withdrawal of therapy after two years leads to relapse in 85% of cases [150]. AIH patients who are untreated have a poor prognosis [170], therefore it is needed to find new therapeutic approach for AIH.

3.8.5. The CYP2D6 mouse model for AIH

There are many mouse models for AIH available; one of them is the CYP2D6 mouse model. The CYP2D6 mouse model is induced by injection of an adenovirus which is encoding the human autoantigen CYP2D6 (Ad-2D6), which is the main target of LKM-1 in the human disease (Figure 7). The human CYP2D6 has a strong similarity to the mouse Cyp isoenzymes and therefore the CYP2D6 model is based on the concept of molecular mimicry. Wild type mice of the FVB strain are tolerant to their own mouse cytochrome P450 family molecules (*mCyp*). Ad-2D6 infection leads to local inflammation and destruction of some infected hepatocytes. In parallel, Ad-2D6 infection causes KCs and HSCs to release chemokines and cytokines resulting in an activation of lymphocytes. CYP2D6-specific lymphocytes expand and rapidly try to eliminate the virus. After virus elimination, CYP specific lymphocytes attack the homologues isoenzymes of the mCyp family that carry a sufficient degree to similarity to the humans CYP2D6.There are four different mouse Cyps, namely Cyp2D9, Cyp2D11, Cyp2D22, and Cyp2D26 which have a peptide sequence similarity up to 75% to the human CYP2D6. Ad-2D6 induced AIH-like disease is characterized by cellular infiltration, hepatic fibrosis and fused liver lobules. Moreover, the mice generate CYP2D6-specific T cells, show elevated ALT and AST levels and produce LKM-1 like auto antibodies [179, 180]. This CYP2D6 mouse model represents the main features of human AIH and its pathogenesis can divided into two phases of liver damage. The first and acute phase results from the direct adenovirus-infection and is characterized by transiently elevated serum aminotransferase levels. This phase is followed by a second, autoimmune phase, which is persistent and results in chronic hepatic damage, characterized by massively changes in liver morphology, extensive subcapsular and per-vascular infiltration of different cell types. Moreover, high titers of anti-CYP2D6 antibodies, high frequencies of CYP2D6-specific T cells and massive liver fibrosis can be observed in the chronic autoimmune phase.

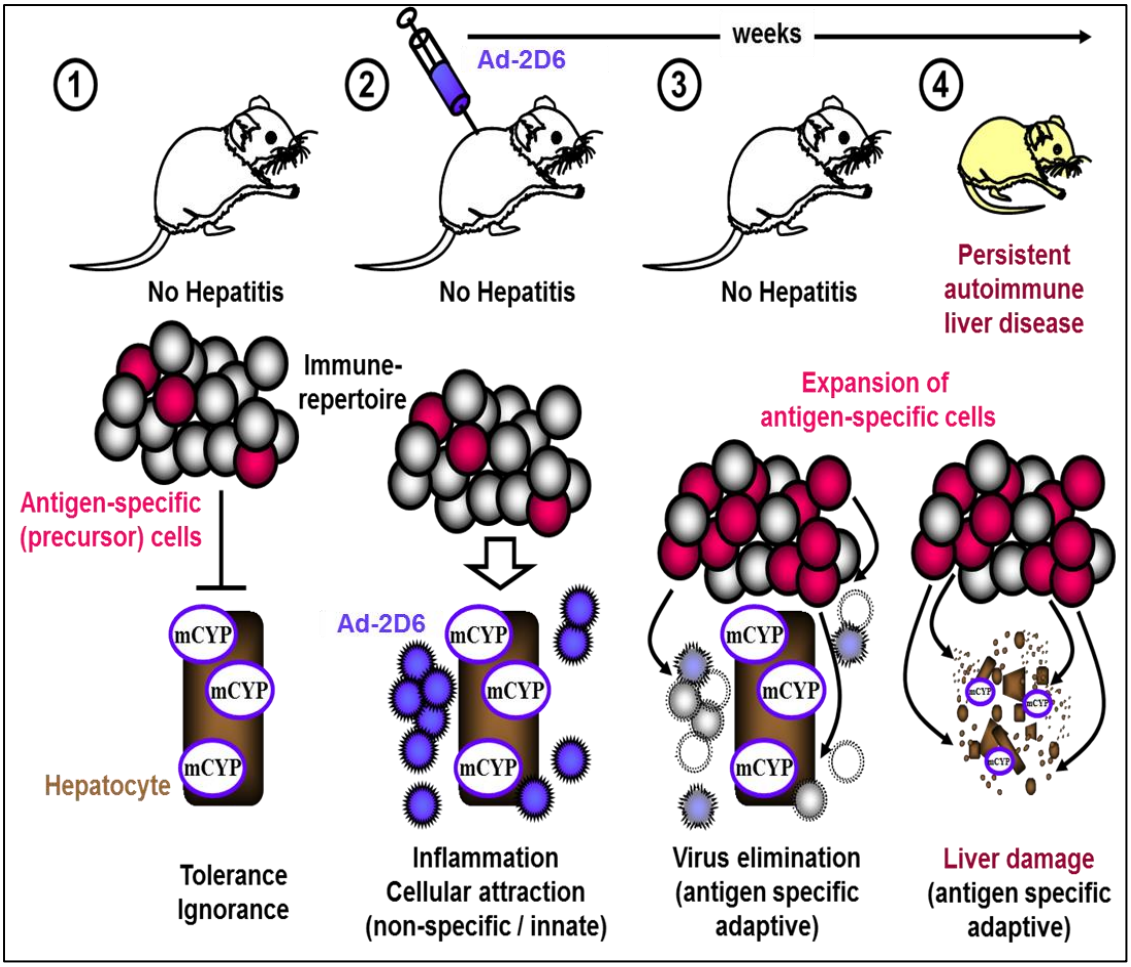

Figure 7: The CYP2D6 mouse model for autoimmune hepatitis
(1) FVB wild type mice express mice cytochrome P450 family molecules (mCYP). (2) Infection with the adenovirus which is expressing the human cytochrome P450 2D6 (Ad-2D6) leads to a strong inflammation in the liver. Therefore, leukocytes attract to the side of the liver inflammation. (3) CYP2D6-specific lymphocytes expand and rapidly eliminate the virus. (4) Activated CYP2D6-specific lymphocytes attack the mouse isoenzymes of the CYP superfamily, which are very similar but not identical to the human CYP2D6. This leads to the destruction of hepatocytes, liver fibrosis and cirrhosis. Figure modified after Christen & Herrath, 2004 [180].

3.8.6. Overlap syndromes

There are some patients within the spectrum of autoimmune liver diseases who present with both cholestatic and hepatic serum liver enzymes and have histological features of both AIH and PBC or PSC [181]. These are commonly classified as having an OS [182]. The prevalence of AIH in patients with PBC is about 7-13 % and 6-11% for PSC [183]. While AIH-PBC OS is predominantly found among adults, PSC-AIH OS have mainly

observed in children, teenager and young adults [184–186]. The “Paris criteria” are the most commonly used tool for the diagnosis of the AIH-PBC OS. A larger study including 134 PBC, AIH, or AIH-PBC OS patients confirmed that these criteria has a high sensitivity (92%) and specificity (97%) for AIH-PBC OS diagnosis [187]. When using the Paris criteria for establishing AIH-PBC OS diagnosis, at least two of the three criteria per disease have to be fulfilled. For the PBC part one criterion is elevated serum levels exceeding two times higher than the upper limit of normal values for AP or five times higher than the upper limit of normal for GGT. Second criterion is the presence of AMA and the third criterion includes liver biopsy with a florid bile duct lesion. For the AIH part the first criterion is an ALT level five times higher than the upper limit of normal. Next criterion is serum level of IgG which is two times higher than the upper limit of normal or a positive anti-SMA detection. The last criterion for AIH is a liver biopsy with periseptal or periportal lymphocytic necrosis [188]. The treatment for PBC-AIH OS patients includes a combination therapy of UDCA which is well-established for patients with PBC and an immunosuppression regimen normally used for the AIH part[189–191].

PSC-AIH OS is another of the cholestatic phenotypes of AIH which is characterized by having negative AMAs and cholangiographic alternations [192]. In histology, patients with a PSC-AIH OS may show interface hepatitis with or without the presence of plasma cells, fibrosis or portal edema. Furthermore, ductal distortion, ductular proliferation, ductopenia, or fibro-obliterating cholangitis may be observed [192]. Cholangiography of the biliary tree of AIH patients may also show dilations and focal strictures of them which are typical for PSC patients. Liver enzymes which are typically elevated in PSC-AIH OS patients are ALT, AST, AP and GGT. The antibody profile is variable but increased γ-globulin as well as IgG levels are present [183]. A study of 16 patients with an PSC-AIH OS shows that 81% of the patients were found to be positive for pANCA, 62.5% for ANA, and 50% for SMA [193]. To date, there is no uniform treatment recommendation for the PSC-AIH OS requiring a carefully individual evaluation of the patient [192]. Treatment with UDCA in combination with an immunosuppressive regimen like prednisolone and azathioprine results in a good biochemical response and may represent an adequate medical treatment for most patients [194]. Dependent on its clinical manifestations it is advisable to treat either the more dominant disease of the OS or to go for a combination therapy targeting both diseases. The main reason for the fact that there is no current

therapy available, is the lack of knowledge on the etiology and the immunopathogenesis of the very rare OS compared to the solitary autoimmune liver diseases. However, such knowledge is hard to come by, since there is no animal model available that represents the clinical features of human OS.

3.9. **Immune tolerance induction as a therapy for autoimmune diseases**

Immune tolerance induction as a treatment for immune-mediated diseases is a very promising strategy. There are many different pathways with the aim to reestablish immune tolerance in patients with ADs. In the past it could be shown that the presentation of disease specific auto-antigens either via crosslink to nanoparticles or splenocytes or via intranasal delivery of soluble auto-antigen can lead to immune tolerance by increasing the amount of T_{reg}. T_{reg} are essential for the immune balance which was shown in a spontaneous development of AD in normal rodents when T_{reg} were depleted [195]. This experiment displays that lack or dysfunction of natural T_{reg} alone is enough to break self-tolerance and generate autoimmunity. It is known that T_{reg} are the main mediators of peripheral tolerance [196]. T_{reg} can influence the immune system on different ways. First, T_{reg} are able to produce inhibitory cytokines like IL-10 and TGFβ to suppress effector T cells (T_{eff}). Second, T_{reg} are able to induce the expression of Foxp3 gene in naïve T cells and convert them into T_{reg}-like cells [197–199]. Third, suppression by cytolysis in which T_{reg} may kill T_{eff} as well as B cells by a granzyme-B-dependent mechanism [200, 201]. Fourth, T_{reg} can interact in T_{eff} function by taken up local IL-2 and induce cytokine-deprivation-mediated apoptosis in these cell types. Another ability of T_{reg} is the suppression of maturation and function of DCs in which T_{reg} are able to downregulate the two co-stimulatory molecules, CD80 and CD86 on DCs which are needed for the activation of T cells. This leads to a reduced activation of T_{eff} [202]. All these different abilities of T_{reg} show how different they can interact in the immune system and how important they are for the immune balance. Thus, ADs can result from an immune disbalance with a stronger T_{eff} response that exceeds the T_{reg} capacity for

immune regulation. Therefore, one strategy to reestablish immune tolerance is to increase the number of T_{reg}.

3.9.1. Therapeutic application of tolerogenic dendritic cells

DCs are professional APCs which are creating the bridge between innate and adaptive immune responses. A major role of DCs is to take up and process antigens and finally to present them to T cells. The activation of T cells trough DCs also needs co-stimulatory molecules such as CD80 and CD86. These molecules together with MHC class II and CD11c are characteristic for DCs. Moreover, DCs are able to induce an immune response as well as immune tolerance [203]. DCs which have tolerogenic function, called tolerogenic DCs (tDCs) can induce T cell anergy and generate T_{reg}.. These special type of DCs is characterized by phenotypic markers like low expression of MHC class II and co-stimulatory molecules expression but increase in programmed death ligand 1 (PD-L1). In addition to these surface molecules, typical cytokines like IL-10 and TGF-β which are released by tDCs can promote tolerance.

Modification of DCs in the laboratory can increase and stabilize their tolerogenic function. Induction of stable tDCs could be a successful antigen-specific treatment of ADs. tDCs can be generated by the isolation of bone marrow-derived DCs cultivating in media containing IL-2 and granulocyte-macrophage colony-stimulation factor (GM-CSF) for 6 to 10 days [204, 205]. Furthermore, the media has to be complemented with agents such as VitD3 and Dexamethasone (Dex) to turn DCs into tDCs. VitD3as an organic molecule is well-known as a tolerogenic reagent. The active form of VitD3, $1,25(OH)_2D_3$ is able to induce tolerogenic surface molecules as well as to support the production of anti-inflammatory cytokines. The cultivation of DCs together with Dex leads to a down-regulation of co-stimulatory and MHC class II molecules, which results in an impaired T cell response [206–210].

tDCs are a promising tool to suppress the immune response in ADs and transplantations. *Ex vivo* manipulation of DCs can retained an immature phenotype and induces tolerance *in vivo.* For this, tDCs have to be tailored for the respective AD which can be achieved by loading the tDCs with diseases specific Ag. These antigen-loaded tDCs are able to induce

immune tolerance, by promoting antigen-specific T_{reg} differentiation (Figure 8) [211, 212]. Administration of antigen-loaded tDCs has shown efficacy in mouse models of T1D and RA as well as phase I studies in humans [213]. Finally, tDCs can be used as a new therapeutic strategy to reestablish immune tolerance or to prevent ADs [209, 214].

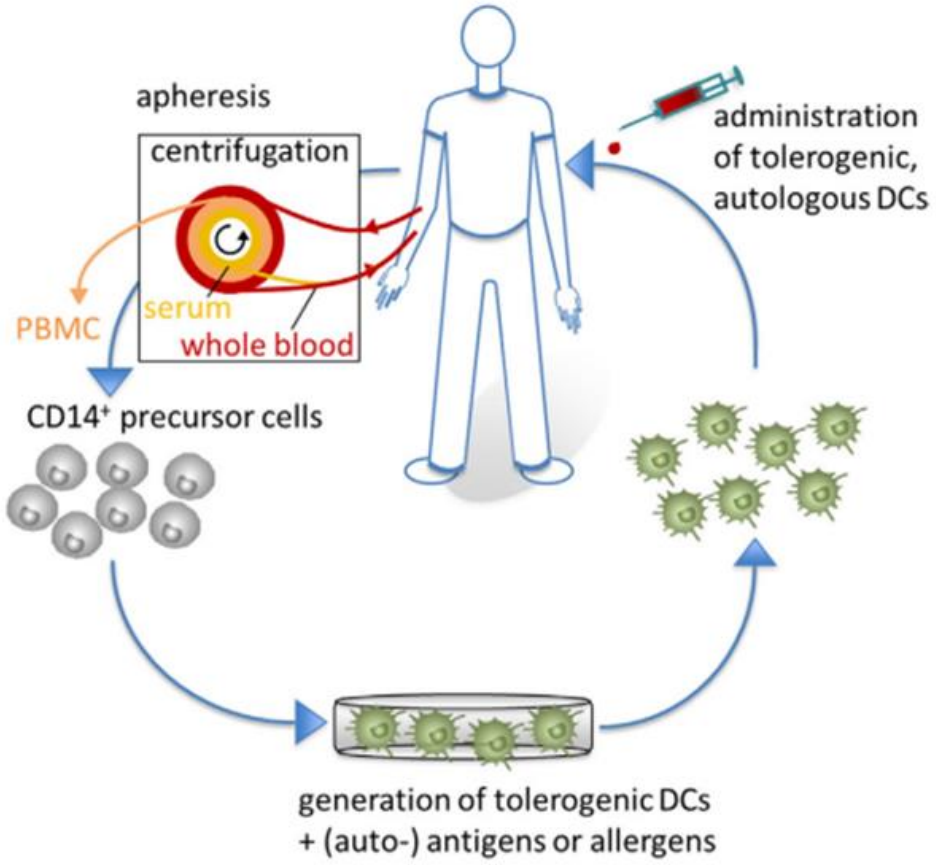

Figure 8: Clinical application of tolerogenic DCs
$CD14^+$ monocytes are isolated from apheresis to generate tDCs which are loaded with auto-Ag to become specific for a particular AD. Antigen-loaded tolerogenic DCs are reinjected into the patient to reestablish the immune balance. Figure is from Domagalla et al., 2017 [211].

3.9.2. Intranasally induced immune tolerance

Nasal-associated lymphoid tissue (NALT) belongs to the mucosal-associated lymphoid tissue (MALT) and has the same function as other mucosal lymph nodes, called Payer´s patches, in the gut. One big difference lays in the development of NALT which in contrast to other MALT develops only after birth. Lymphotoxin is known to be essential for the development of NALT [215, 216]. Studies on germ-free mice compared to wild type mice

show that NALT needs the interaction with indigenous bacteria to develop after birth [217]. NALT is important for the induction and regulation of mucosal immunity in the upper respiratory tract. It is located on the nasal cavity side of the upper palate [218]. The strategic location of this lymphoid tissue suggests that it is directly involved in handling inhalant antigens and pathogens as well as immune activation after intranasal (i.n.) immunization. Immune cells which are responsible for this function and located in the NALT are T cells, B cells, DCs, macrophages, and microfold cells (M cells) [218–220]. M cells are located in the epithelium overlying the NALT and have the function to transported inhalant antigens to the NALT, where the antigens are taken up by DCs which further processed and presented these antigen to T cells (Figure 9) [216]. This leads to T cell activation which results in secretion of cytokines and interaction with B cells. B cells develop into IgA committed B cells which move to the effector site to produce antigen-specific IgA and finally protect the host for pathogen invasion [221].

A lot of experiments have been done with mice which were treated i.n. with auto-Ag of a particular disease to induce immune tolerance. I.n. treatment with different auto-Ag like ovalbumin in an animal model for allergic asthma have been demonstrated to induce immune tolerance by an increase in the amount of antigen-specific T_{reg} that can transfer their regulatory capacity to naïve $CD4^+$ T cells [222]. I.n. treatment of T1D mice with insulin did not delay loss of β-cell function but it can be used to prevent diabetes in an individual at risk [223]. Moreover, i.n. administration of a set of minor histocompatibility antigens leads to a transplantation tolerance [224]. Additionally, i.n. application of the recombinant adenoviral vaccine shows protection against the aerosol challenge with *Mycobacterium tuberculosis* [225]. Taken together many studies have been done in rodents which clearly implicate the involvement of NALT in the i.n. immune tolerance induction. However, the challenge remains to transfer these findings into human patients where NALT is quite unorganized and it is hard to reach [226].

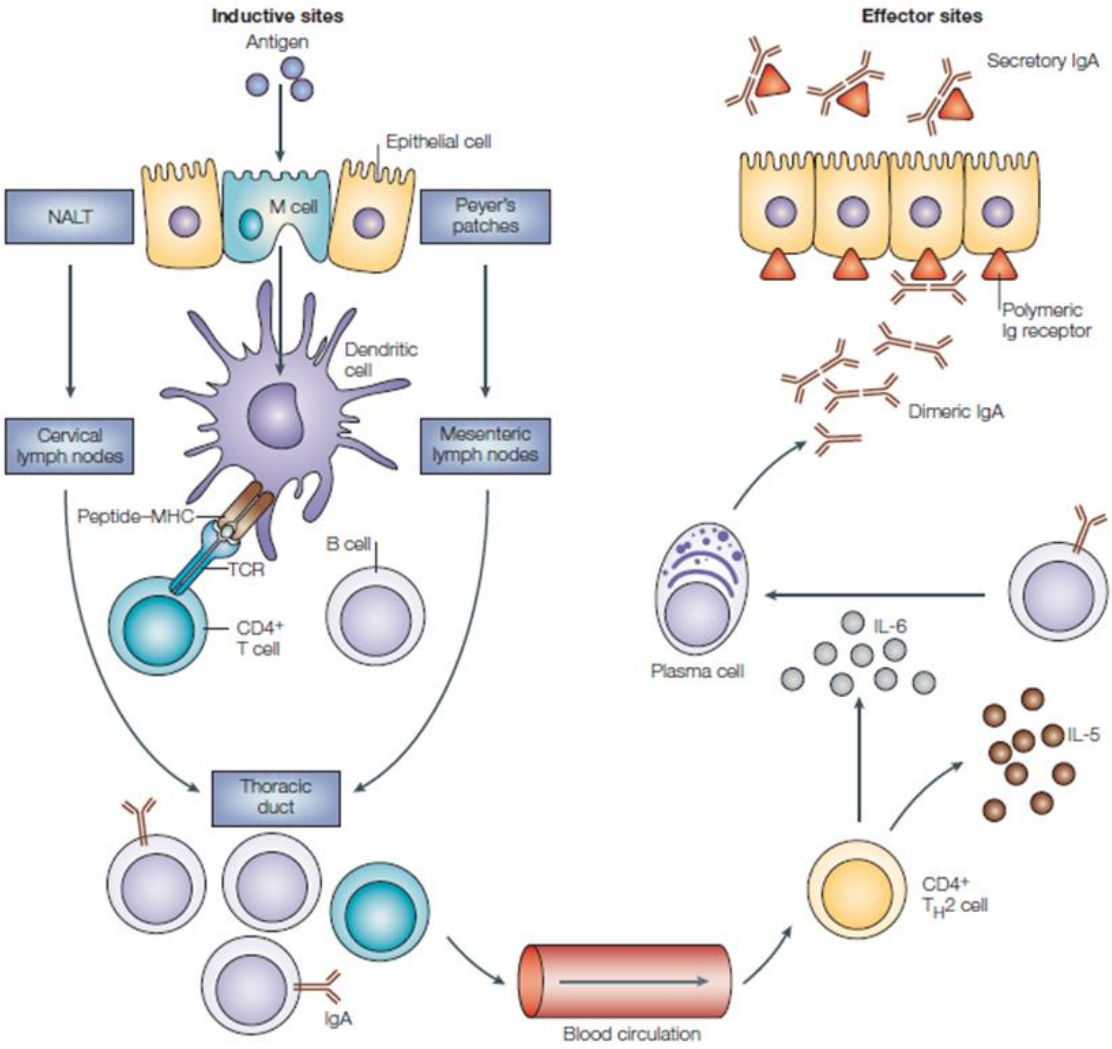

Figure 9: The mucosal immune system including NALT
Inhalant antigens are transported to the NALT via M cells which are located in the epithelium overlying NALT. Further, antigens are taken up by DCs where they are processed and presented to T cells. Such a T cell activation further leads to the generation of antigen-specific T_H2-cell-dependent IgA response, and T_H1-cell- and CTL-dependent immune response as a first defense at mucosal surfaces. Figure from Kiyono et al., 2004 [216].

3.9.3. Induction of cell-mediated immunity and tolerance with antigen-coupled splenocytes

Antigen-specific tolerance is a highly promising therapy for ADs. In 1979, the use of splenocytes which were crosslinked with 1-ethyl-3-(3-dimethy-laminopropyl) carbodiimide (ECDI) to the auto- antigen for the specific disease was described the first time [227]. The fixation of antigens to donor cells via ECDI results in the formation of

peptide bonds between free amino and carboxyl groups and which binds the peptide to the cells [228]. I.v. infusion of protein/peptide antigens linked via ECDI to splenocytes (Ag-SP) prevents and even reverses $T_H1/17$-mediated ADs such as MS or T1D as well as allograft rejection [229–232]. I.v. injection of myelin-Ag-coupled cells leads to a rapid and long-lived antigen-specific tolerance in an experimental autoimmune encephalitis (EAE) model. Other disease models which also show a successful induction of tolerance by Ag-SP treatment are uveitis, neuritis, and T1D [233–235]. Ag-SP therapy seems to have no-toxic side-effects and is well tolerated during the treatment. This is unlike soluble-peptide therapies, in which the injected antigens can induce an anaphylactic response regardless of the antigens use [236, 237]. The fact that there are currently phase I/II clinical trials investigating the safety and efficacy of myelin peptide-coupled peripheral blood lymphocytes in human MS patients shows that this method has promising advantages [238]. In addition to MS studies, clinical trials of insulin-coupled autologous PBMCs controlled by the Immune Tolerance Network for T1D patients are also running.

3.9.4. Nanoparticles as a therapy for autoimmune diseases

Over the last 20 years the interest in the use of nanoparticle (NP) as drug delivery vehicle has increased gradually. Nanoparticles are characterized by a size of 1-1000 nm and can be classified depending on their constituent like poly(amino acids), polysaccharides and poly(alpha-hydroxy acids) as well as gold, silver, carbon, iron and silica [239, 240]. Moreover, NP which are synthesize from biocompatible and biodegradable polymers such as poly-lactide-co-glycolide (PLG) are very common in the field of immune modulatory therapeutics [240]. PLG-NP have been used extensively for the delivery and release of drugs and are already approved by regulatory authorities like the Food and Drug Administration (FDA) and the European Medicines Agency (EMA) [241]. NPs can be generate to deliver proteins (hormones and antibodies), peptides (for vaccine or immune tolerance induction), and/or small-molecule drugs (immune suppressants or chemotherapeutic) [242]. Moreover, NPs are tested to be safe, cost-effective, and highly efficient alternatives to cellular carriers, like SP to present auto-Ag. NP in comparison to splenocytes have the advantages that they are of much lower cost, do not require the

complexity of ex vivo laboratory manipulation, as well as have no limitations regarding autologous donor cell requirements [243]. The combination of NP with specific auto-antigens on the surface which are chemically conjugated to NPs using ECDI can be used to restore peripheral immune tolerance and reserve ADs [244, 245]. There are many crosslinkers available, like carboxymethylcellulose, hyaluronic acid or poly 9,9-dioctylfluorene-alt-benzothiadiazole which can be used for NPs crosslinking but the most common one is ECDI [246, 247]. NPs have to be loaded with the correct antigen which should have the capacity to induce immune tolerance in the specific disease. These auto-antibodies delivering on NP target to APCs capable of reducing T cell function and inducing T_{reg}. For many ADs the main epitopes associated with the disease are known and can be used for immune tolerance induction via NP. This has already been shown in different autoimmune models like in non-obese diabetic (NOD) mice for T1D or EAE for MS in which EAE mice were protected in a T_{reg}-dependent manner by i.v. injection of peptide-coupled poly-coated NP [101, 244, 245, 248–250].

4. **Aims of the study**

AIH is an AD of the liver, resulting in liver damage including fibrosis, increased levels of auto-antibodies and immune cell infiltrations. PSC has an izmmune-mediated origin, leading to the destruction of the intra- and extrahepatic biliary trees with fibrosis sclerotic cholangiopathy and possible cirrhosis and malignance. To date, for both diseases AIH and PSC, there is no diseases-specific treatment available. Current therapy is still restricted to the administration of corticosteroids and cytostatic drugs or liver transplantation. Interestingly, some patients show features of both AIH and PSC, they are described as having an overlap syndrome. Until now, there is no animal model available which represents the clinical features of human OS and can be used to study the etiology and immunopathogenesis of the PSC-AIH OS.

The combination of the CYP2D6 mouse model for AIH which was developed in our lab and the well accepted *Mdr2*$^{-/-}$ mouse model for PSC allows generating a PSC-AIH OS mouse model. In comparison to the *Mdr2*$^{-/-}$ mouse model in which the auto-Ag are unknown, the big advantage lays in the CYP2D6 AIH model in which the auto-Ag are already identified and can be used to induce CYP2D6 specific tolerance.

Such a PSC-AIH mouse model with overlapping characteristics would help to investigate immunoregulatory mechanisms leading to auto-aggressive destruction of hepatocytes and cholangiocytes.

Aim 1: Generation of a PSC-AIH OS model

The first aim was the generation of a novel animal model with characteristics of both diseases, which would mimic features of human PSC-AIH OS. To achieve this aim *Mdr2*$^{-/-}$ mice which spontaneously develop PSC were infected with adenovirus encoding human Cytochrome P4502D6 to trigger the autoimmune-driven hepatic injury in these mice (Figure 10). Pathogenesis of PSC-AIH OS mice was compared to mice with solitary PSC or AIH or FVB wild type mice as controls.

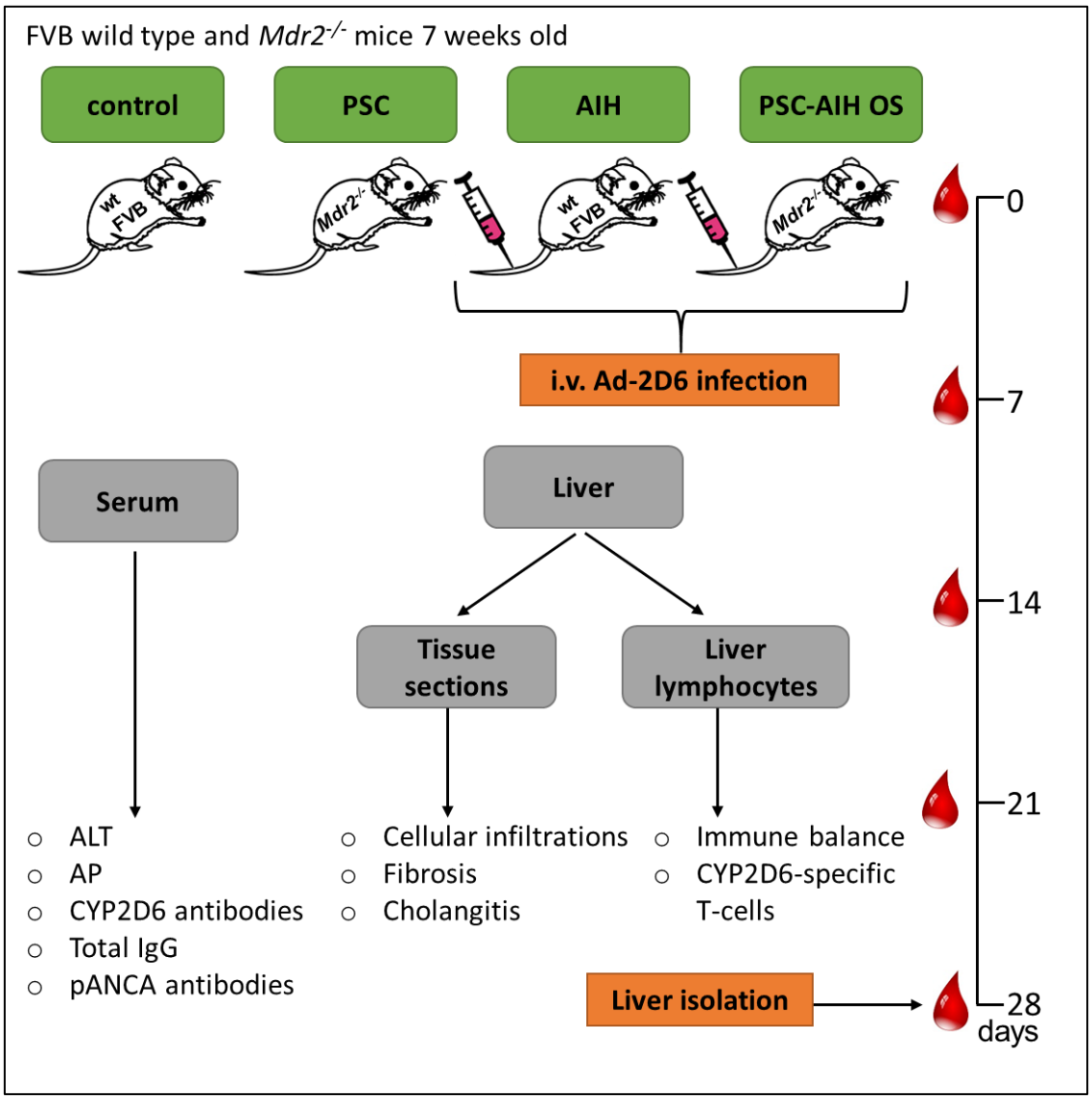

Figure 10: Generation of a PSC-AIH OS model

<u>Aim 2:</u> Therapeutic tolerance induction as a therapy for AIH

The second aim was to find a novel therapy based on immune tolerance induction to treat AIH in mice. Four different pathways, namely intranasal peptide administration, injection of tolerogenic DCs, antigen-coupled splenocytes, and antigen-coupled NP were evaluation for their potential to induce CYP2D6 specific T_{reg} with the capacity to prevent AIH in mice (Figure 11).

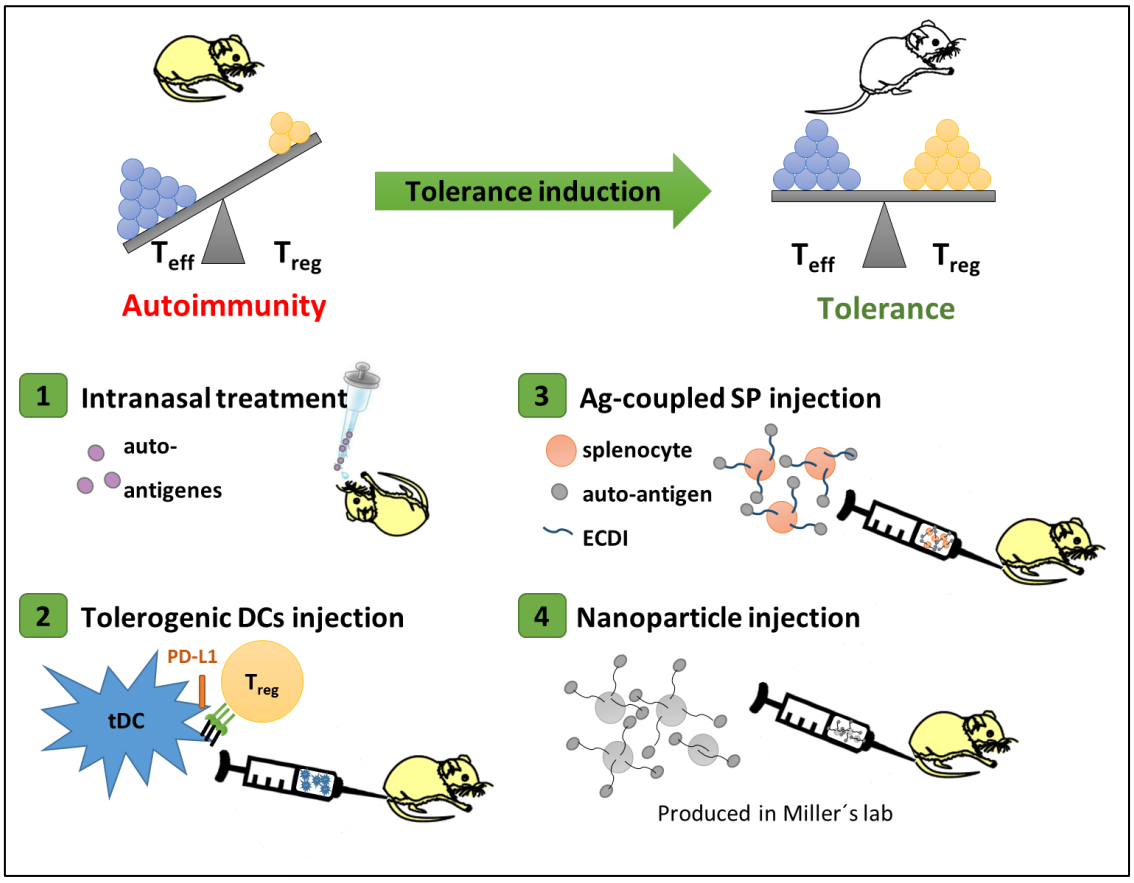

Figure 11: Different ways of immune tolerance induction in AIH mice

5. Results

5.1. Generation of a PSC-AIH OS model

In order to generate a novel PSC-AIH OS mouse model existing PSC and AIH models were combined. Thereby, *Mdr2*$^{-/-}$ mice were infected with 3 x 10^8 pfu Ad-2D6 at an age of seven weeks which formed the PSC-AIH OS group. In order to investigate PSC-AIH OS pathogenesis, such Ad-2D6 infected *Mdr2*$^{-/-}$ mice were compared with naïve *Mdr2*$^{-/-}$ mice representing solitary PSC. As solitary AIH group wild type FVB mice were infected with 3 x 10^8 pfu Ad-2D6. Hence, in contrast to our regular CYP2D6 AIH model, the mice were exclusively infected by the intravenous route to avoid massive sub-capsular fibrosis that was observed after the additional intraperitoneal infection [251]. Naïve FVB wild type mice were used as healthy controls.

5.1.1. Serologic diseases markers like AP and ALT were enhanced in PSC-AIH OS mice

Most patients with ALD show elevated serum levels of liver damage markers such as alkaline phosphatase (AP), an enzyme which gets released during biliary obstruction and is the most common biochemical abnormality in PSC [252] and is often elevated at least 2 – 3 fold in patients with PSC [253]. Alanine aminotransferase (ALT) is typically elevated in AIH and indicates the destruction of hepatocytes [254].

Blood was taken at the beginning of the experiment as well as every week after the Ad-2D6-infection to track the liver damage over time (Figure 12). As a result, a two to threefold increase in AP levels was detected in PSC mice compared to naïve FVB mice (Figure 12, left side). In contrast, AIH mice showed only a minor increase in AP levels at week one and two after Ad-2D6 infection. However, these levels detected in AIH mice were reduced over time. Mice of the PSC-AIH OS group had the highest AP levels, which did not decrease over time. The results of the ALT measurements showed that PSC mice have elevated ALT levels compared to naïve FVB wild type mice (Figure 12, right side).

The serum levels of AIH mice declined from week one to two after the Ad-2D6 infection. This time point was the acute phase and remained above baseline at week four after infection. ALT levels of mice from the PSC-AIH OS group were already higher than in age-matched uninfected AIH mice. After infection of PSC-AIH OS mice the ALT levels got a peak after one week. ALT levels of this group were still elevated from week two to four after the Ad-2D6-infection. Interestingly, as highlighted in Figure 12 in the PSC-AIH OS group the kinetic pattern of ALT seemed to follow the pattern found for solitary AIH with a peak at week one post-infection (green). In contrast, the kinetic pattern found for AP in PSC-AIH OS mice followed the one from the solitary PSC group (purple).

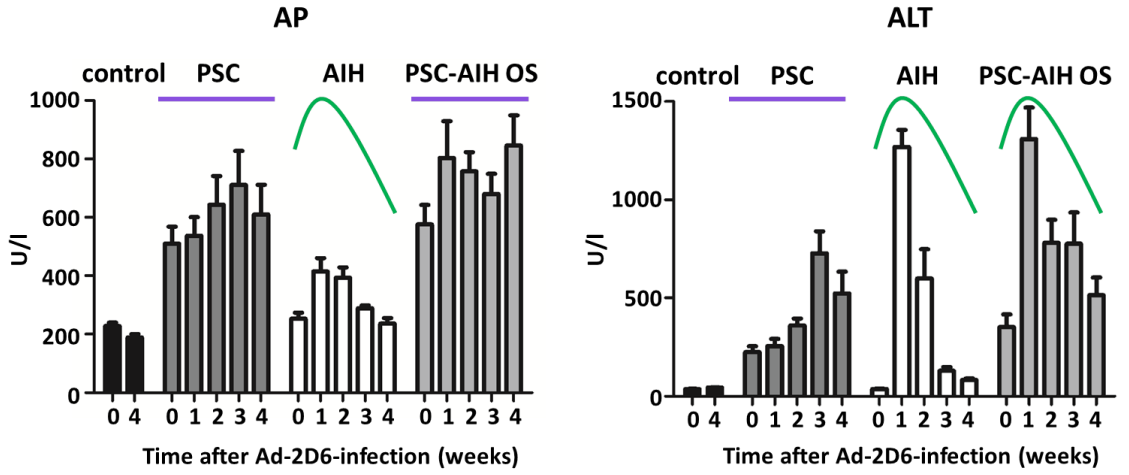

Figure 12: Serum levels of AP and ALT in naïve and Ad-2D6 infected FVB and *Mdr2*$^{-/-}$ mice at different points in time
Alkaline phosphatase (AP) and alanine aminotransferase (ALT) levels in naïve and Ad-2D6-infected FVB and *Mdr2*$^{-/-}$ mice were measured in 10 mice per group at different points in time by a Reflotron analyzer (Roche). Note that *Mdr2*$^{-/-}$ mice had enhanced enzyme levels already before the infection took place (week 0). Ad-2D6 infection resulted in a higher elevation of the serum levels at week one post-infection. Typical kinetic patterns of AIH and PSC are labeled in green and purple, respectively. Data are mean ± SEM, n=10.

5.1.2. Detection of AIH- and PSC-specific autoantibodies

Screening for autoantibodies, produced by humoral immune response against self-antigens, is often part of the diagnostic analysis of autoimmune liver diseases and has clinical relevance for diagnosis, disease activity and prognosis [135]. Hypergammaglobulinemia is frequently observed in patients with ALD. As stated by

Czaja, elevated levels of serum IgG about 1.2 – 3 times higher than normal is a characteristic laboratory marker of AIH, whereas hypergammaglobulinemia is not common for PSC patients [252, 255].

Thus, sera of naïve and Ad-2D6 infected FVB and *Mdr2*$^{-/-}$ mice were analyzed for the presence of AIH- and PSC-specific autoantibodies at week four after infection (Figure 13). As highlighted in Figure 13, a similar titer of total IgG was found in PSC and control mice. The titer of total IgG was approximately 4 – 16 times higher in AIH and PSC-AIH OS mice.

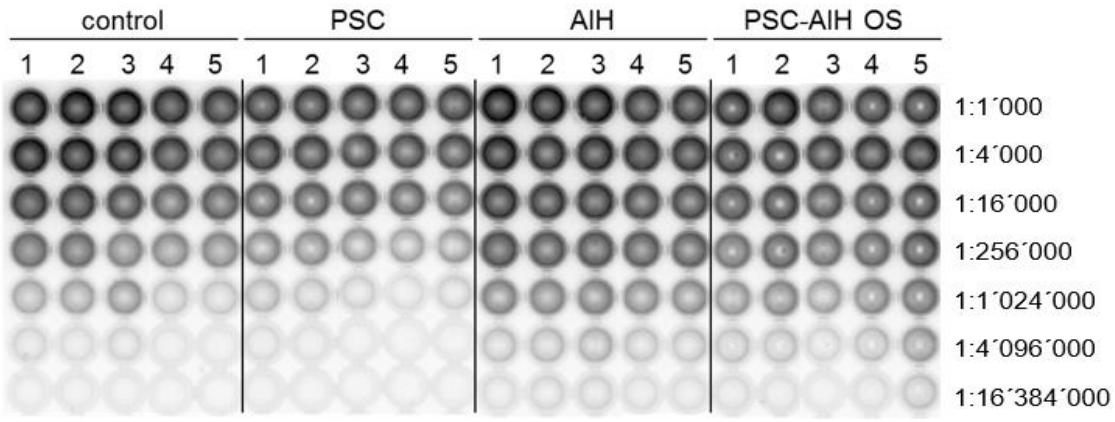

Figure 13: Total IgG titer detection in different mouse models
Serum titer of total IgG in naïve and Ad-2D6 infected FVB wild type was well as in *Mdr2*$^{-/-}$ mice. Assembled microtiter plates from the ELISA using murine IgG as a target for sera obtained at week four after Ad-2D6 infection (n=5). Note that total IgG titers were highest and in a similar amount in AIH and PSC-AIH OS mice.

In order to investigate whether Ad-2D6 infection leads to a production of LKM-1-like anti-hCYP2D6 autoantibodies the serum titers of anti-hCYP2D6 antibodies were determined by ELISA at week four after the infection (Figure 14). The titer of anti-hCYP2D6 antibodies was similar in mice with solitary AIH and PSC-AIH OS. As expected, there were no LKM-1-like anti-hCYP2D6 antibodies detectable in sera of solitary PSC and control mice (Figure 14).

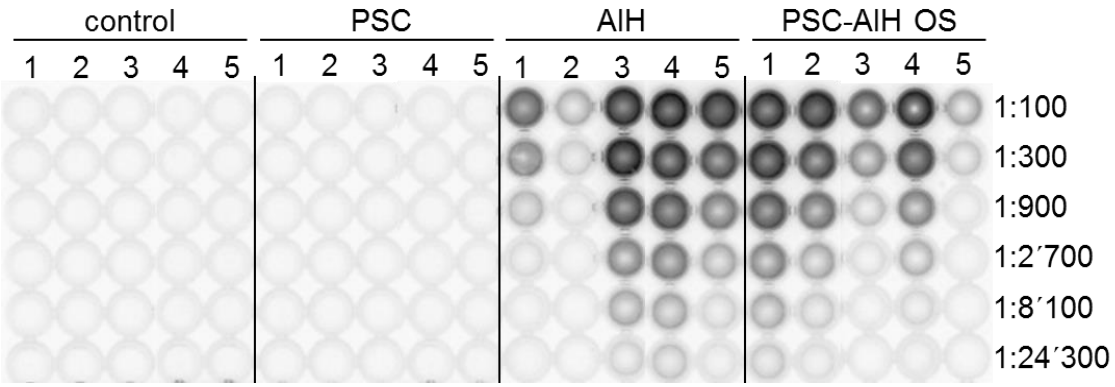

Figure 14: hCYP2D6 specific antibodies were detected in sera of AIH and PSC-AIH OS mice

ELISA using recombinant hCYP2D6 as a target for sera of naïve FVB wild type (control), naïve *Mdr2*$^{-/-}$ (PSC), Ad-2D6 infected FVB (AIH), and Ad-2D6 infected *Mdr2*$^{-/-}$ (PSC-AIH OS) mice was collected at week four after infection. Note that LKM-1 like anti-hCYP2D6 antibodies were detectable in Ad-2D6 infected FVB and *Mdr2*$^{-/-}$ mice at comparable titers.

Generally, PSC patients can carry many circulating autoantibodies. Although not used as *bona fide* diagnostic markers perinuclear anti-neutrophil cytoplasmic antibodies (p-ANCA) are the most common antibodies found in PSC [135]. However, they are also detectable in some patients with AIH.

In the next experiment, human promyelocytic leukemia HL-60 cells were used as a target to detect the reactivity of pANCA- like antibodies [256]. Cells were incubated with the sera of naïve and Ad-2D6-infected FVB and *Mdr2*$^{-/-}$ mice collected at week four after infection (Figure 15, right side). In parallel, sera of diagnosed PSC patients and healthy individuals were used as a control mechanism (Figure 15, left side). The presence of pANCA- like antibodies was visualized with a fluorochrome-labelled anti-mouse or anti-human IgG 2nd antibody (green). A much higher reactivity was found with sera collected from mice with PSC-AIH OS compared to mice with solitary PSC. Sera of mice with AIH showed also a high reactivity of pANCA- like antibodies but less than the sera of PSC-AIH OS mice.

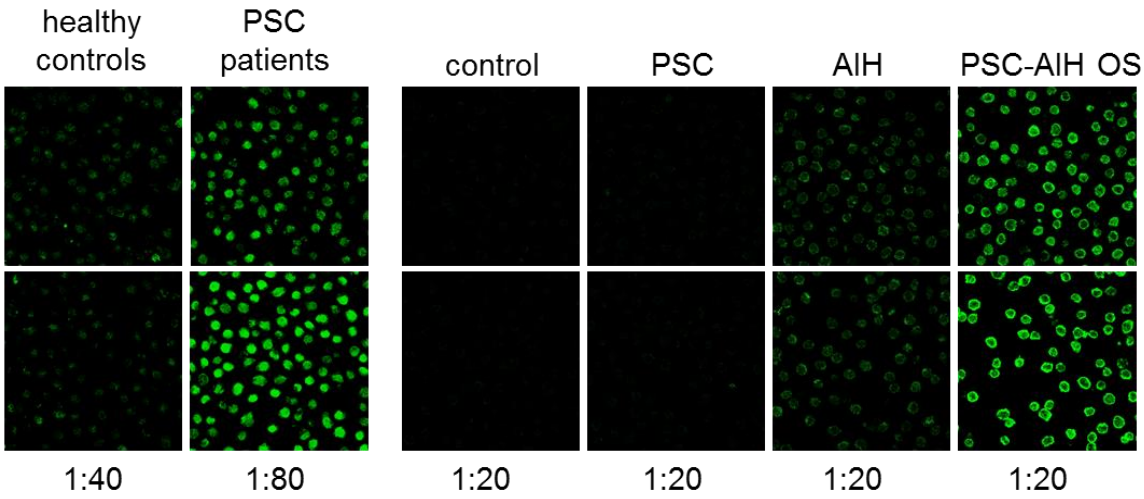

Figure 15: Serum reactivity of pANCA- like antibodies to human promyelocytic leukemic HL-60 cells
Serum of naïve FVB (control), naïve *Mdr2*$^{-/-}$ (PSC), Ad-2D6-infected FVB (AIH), and Ad-2D6-infected *Mdr2*$^{-/-}$ (PSC-AIH OS) mice was collected at week four after infection and was incubated with human promyelocytic leukemia HL-60 cells. Two representative examples out of ten mice per group are shown. Sera of diagnosed PSC patients and healthy individuals were used as controls. Presence of perinuclear anti-neutrophil cytoplasmic (pANCA) - like antibodies was visualized with a fluorochrome-labelled secondary anti-mouse or anti-human 2nd antibody (green). Note that this experiment was done by PD Dr. Edith Hintermann.

5.1.3. Characterization of cholangitis and fibrosis in different mouse models

To characterize cholangiocyte proliferation and hepatic fibrosis livers were harvested at week four after Ad-2D6 infection and quick-frozen for immunohistological stainings. Moreover, an anti-cytokeratin 19 (CK19) antibody was used as a selected marker for cholangiocytes and bile ducts. Histological sections of PSC mice showed a strong cholangiocyte proliferation in comparison to the control group (Figure 16, A upper row). This proliferation was further increased after Ad-2D6 infection in PSC-AIH OS mice. These animals showed the highest cholagiocytes expansion as indicated by CK 19 signals which were strongly clustered and spread over the whole tissue. Cholangitis detection in AIH mice was also increased after Ad-2D6 infection but to a lesser degree than in solitary PSC mice.

Further, hepatic fibrosis was characterized by anti-collagen III antibody staining in the different mouse models. AIH mice showed a stronger collagen III staining compared to control mice (Figure 16, A lower row). In these animals the collagen III staining was localized around blood vessels. The fibrosis staining in PSC mice was higher than in AIH mice. PSC mice showed strong clustered regions around blood vessels and also some bridging fibrosis could be observed. The strongest fibrosis was found in the PSC-AIH OS group, which developed a pattern of typical fibrotic chicken wires covering the entire tissue. Quantification of the cholangitis and fibrosis staining was done with the Keyence BZ-II analysis software and revealed that the observed differences were highly significant (Figure 16, B).

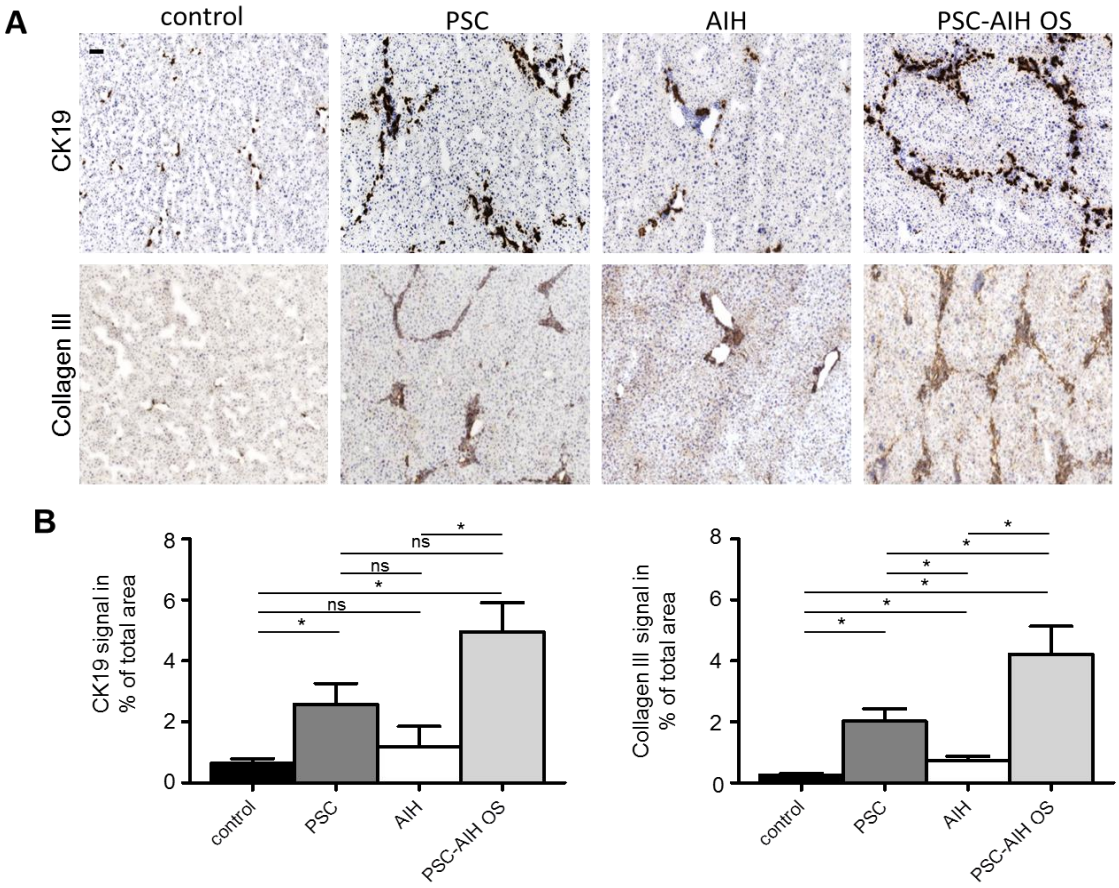

Figure 16: Cholangitis and fibrosis staining in naïve and Ad-2D6 infected FVB and *Mdr2*$^{-/-}$ mice at week four after infection

(A) Immunohistochemistry staining of quick-frozen liver sections from naïve FVB (control), naïve *Mdr2*$^{-/-}$ (PSC), Ad-2D6 infected FVB (AIH), and Ad-2D6 infected *Mdr2*$^{-/-}$ (PSC-AIH OS) mice at week four after infection. Cholangiocytes were visualized by using CK19 antibodies (top row) and collagen III antibody were used to visualize peri-ductal and bridging fibrosis (upper row). Representative pictures of liver sections of 10 mice

per group are depicted. Bar, 50 µm. (B) Quantification of CK19 and collagen III staining was done with the Keyence BZ-II analysis software. Presented values are the mean ± SEM (n = 5) of the whole liver section excluding the capsule. Significant differences ($p < 0.05$, unpaired, two-tailed t-test) are indicated (*).

5.1.4. Myofibroblast activation in PSC-AIH OS mice

Myofibroblasts are the mesenchymal cells responsible for wound healing. A dysregulation of normal wound healing results in liver fibrosis. The activation of myofibroblasts leads to the production of fibrotic ECM and can be analyzed by assessing the expression of SMA. Western blot analysis was used to detect the protein expression of αSMA protein. As Figure 17 shows the αSMA expression in PSC mice was slightly but not significantly upregulated compared to control mice. A comparison of AIH mice to the control group showed no significant difference. The highest αSMA protein expression (twofold higher as the control) was observed in mice with PSC-AIH OS (Figure 17, right side). These data indicate that the mice with PSC-AIH OS had the strongest fibrotic activity and confirm the results obtained from the histological staining for CK19 and collagen III.

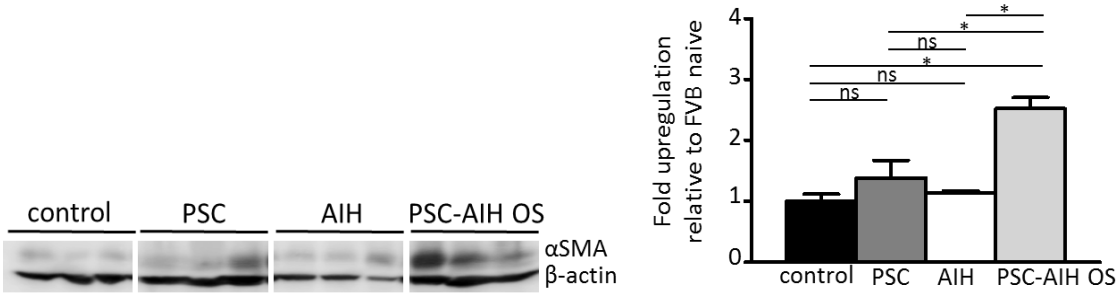

Figure 17: αSMA protein expression was the highest in PSC-AIH OS mice
Western blot detection of αSMA protein from liver homogenates of naïve FVB wild type (control), naïve *Mdr2*$^{-/-}$ (PSC), Ad-2D6 infected FVB (AIH), and Ad-2D6 infected *Mdr2*$^{-/-}$ (PSC-AIH OS) mice at week four after infection. Selected are three representative examples per group are shown. β-actin was used as loading control. Expression levels of naïve FVB mice were set at 1 (mean ± SD, n = 4). Significant differences ($p < 0.05$, unpaired, two-tailed t-test) are indicated (*).

Further, to find out which cell type was responsible for the αSMA activation, a closer look at HSCs and portal fibroblasts (PFs) which can be identified by anti-desmin and anti-elastin staining, respectively was done. The anti-desmin DAB staining revealed that liver

sections of PSC mice had a high number of HSCs which clustered predominantly around the portal field but were also found scattered in the entire liver parenchyma. In AIH mice HSCs were also mainly located around the portal field albeit to lesser degree than in PSC mice. Importantly, PSC-AIH OS mice showed the highest number of HSCs compared to the mice with solitary PSC or AIH (Figure 18, upper row).

In addition, a co-staining with a fluorescent anti-desmin (HSCs) and anti-CK19 (cholangiocytes) antibodies was done (Figure 18, lower row). This staining also showed that FVB mice had much less HSCs compared to *Mdr2*$^{-/-}$ mice and confirmed that the Ad-2D6 infection led only to a small increase in the number of HSCs in control mice compared to AIH mice and PSC mice to the PSC-AIH OS model. Moreover, that staining showed HSCs proliferation and accumulation were mainly in the portal fields in periductal areas in which also strong collagen III staining was detected (Figure 18, lower row).

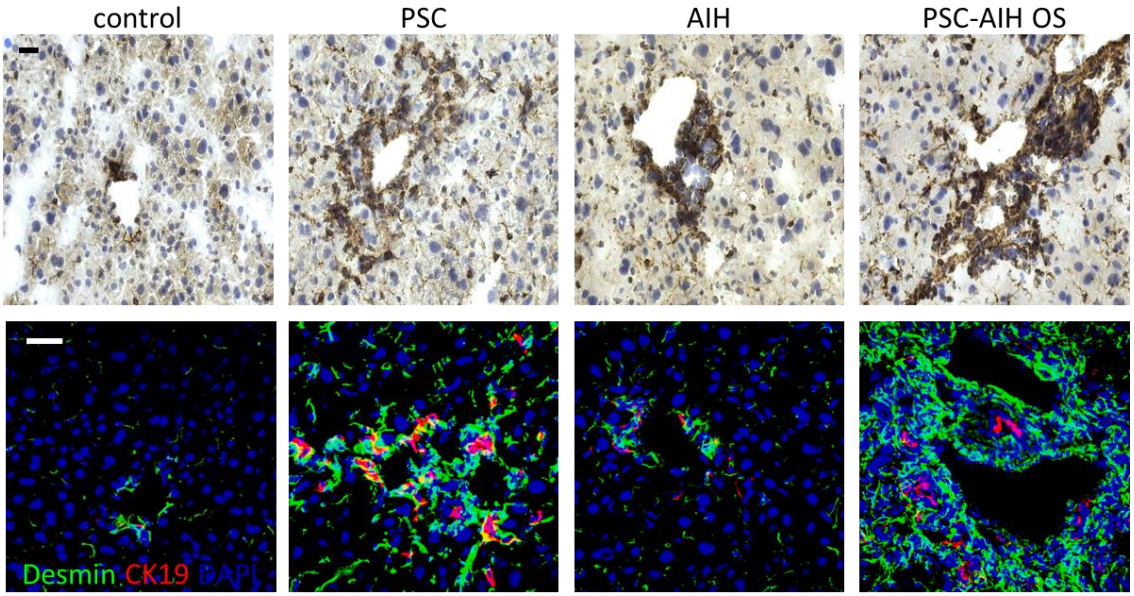

Figure 18: Analysis the presence of desmin in PSC, AIH and PSC-AIH OS mouse models
Immunohistochemistry staining of quick-frozen liver from 11-week old naïve and 4-week Ad-2D6 infected FVB and *Mdr2*$^{-/-}$ mice. Liver sections were stained for desmin a marker for HSCs. Bar, 50 µm (upper row). Co-staining of desmin (green) and CK19 (red) in the portal tract of different mouse models. Nuclei were stained with DAPI (blue). Bar, 20 µm (lower row).

Next, the expression of desmin was determined by western blot analysis in which liver homogenates were used at week four after Ad-2D6 infection. Desmin expression in PSC mice was significantly twofold upregulated compared to the control group (Figure 19). The strongest desmin expression was detected in the PSC-AIH OS mice which was nearly comparable to mice with solitary PSC. Ad-2D6 infection led to a little not significantly increase in the desmin expression from naïve FVB to AIH mice and naïve *Mdr2*$^{-/-}$ to PSC-AIH OS mice (Figure 19).

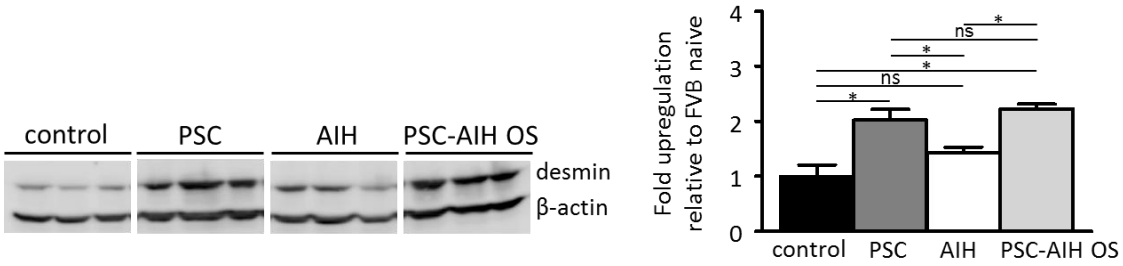

Figure 19: Desmin protein expression was upregulated in solitary PSC and PSC-AIH OS mice
Western blot detection of desmin from liver homogenates of naïve FVB wild type (control), naïve *Mdr2*$^{-/-}$ (PSC), Ad-2D6 infected FVB (AIH), and Ad-2D6 infected *Mdr2*$^{-/-}$ (PSC-AIH OS) mice at week four after infection. Selected are three representative examples per group. β-actin was used as loading control. Expression levels of naïve FVB mice were set at 1 (mean ± SD, n = 4). Significant differences ($p < 0.05$, unpaired, two-tailed t-test) are indicated (*).

In addition to the desmin analysis which is specifically used to show the presence of HSCs, PFs were also analyzed. Therefore, an anti-elastin antibody was used as a selective marker for PFs. Liver sections of PSC mice showed a strong elastin staining around the blood vessels and in the tissue of the portal field (Figure 20, upper row). AIH mice showed elastin positive staining only around the blood vessels similar to the mice of the control group. PSC-AIH mice showed the highest elastin expression compared to the mice with solitary PSC. Lastly, a co-staining was done in which PFs were visualized in green and cholangiocytes in red. That staining confirmed the DAB staining and further demonstrated that elevated expansion of cholangiocytes was attended by the presence of a high number of PFs in the fibrotic periductal region (Figure 20, lower row). The characterization of cholangiocyte proliferation and hepatic fibrosis showed the worst case in PSC-AIH OS mice which had the highest number of activated HSCs and PFs.

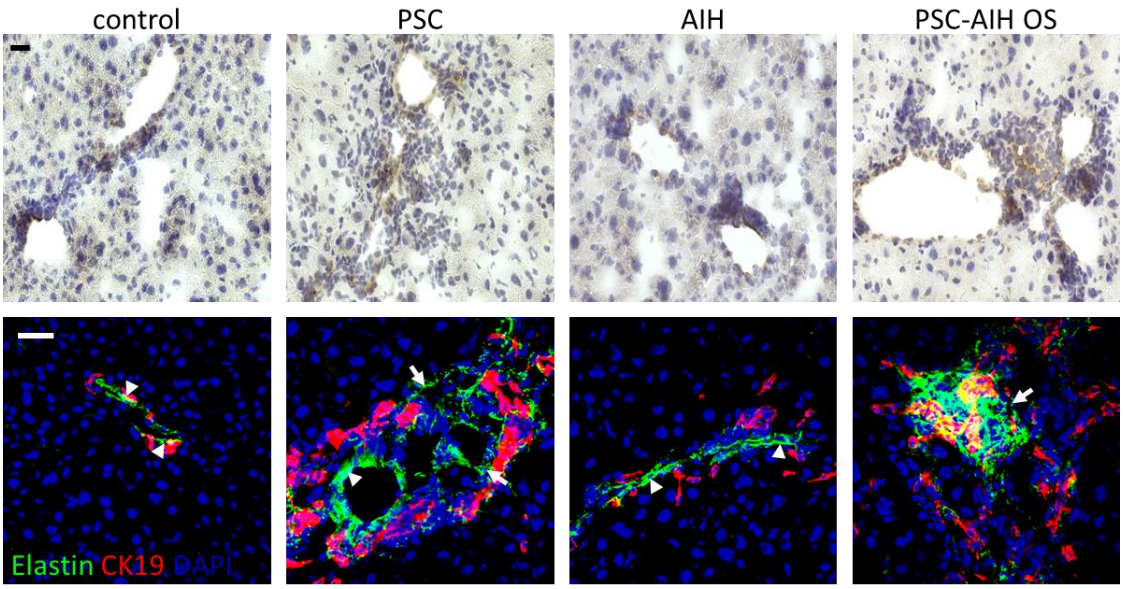

Figure 20: Analysis the presence of elastin in PSC, AIH and PSC-AIH OS mouse models
Immunohistochemistry staining of quick-frozen liver from 11-week old naïve and 4-week Ad-2D6 infected FVB and *Mdr2*$^{-/-}$ mice. Liver sections were stained for elastin a marker for activated PF. Bar, 50 µm (upper row). Co-staining of elastin (green) and CK19 (red) in the portal tract of different mouse models. Note that the elastin staining which surrounded blood vessels in the control and AIH groups, resulted mainly from smooth muscle cells (arrow heads). The elastin staining in PSC and PSC-AIH mice resulted from activated PFs (arrows). Nuclei are stained with DAPI (blue). Bar, 20 µm (lower row).

5.1.5. Cellular infiltrations of different cell types were the highest in PSC-AIH OS mice

To evaluate the cellular infiltration in different mouse models, livers of naïve and Ad-2D6-infected FVB and *Mdr2*$^{-/-}$ mice were harvested at week four after infection. Tissue sections were generated and stained for the presence of infiltrating cells of the innate and adaptive immune system by immunohistochemistry. CD11b and CD11c were used as markers for monocytes / macrophages and DCs, respectively (Figure 21 A, upper and middle panel). Moreover, neutrophils were visualized with a Ly6G antibody (Figure 21 A, upper panel).

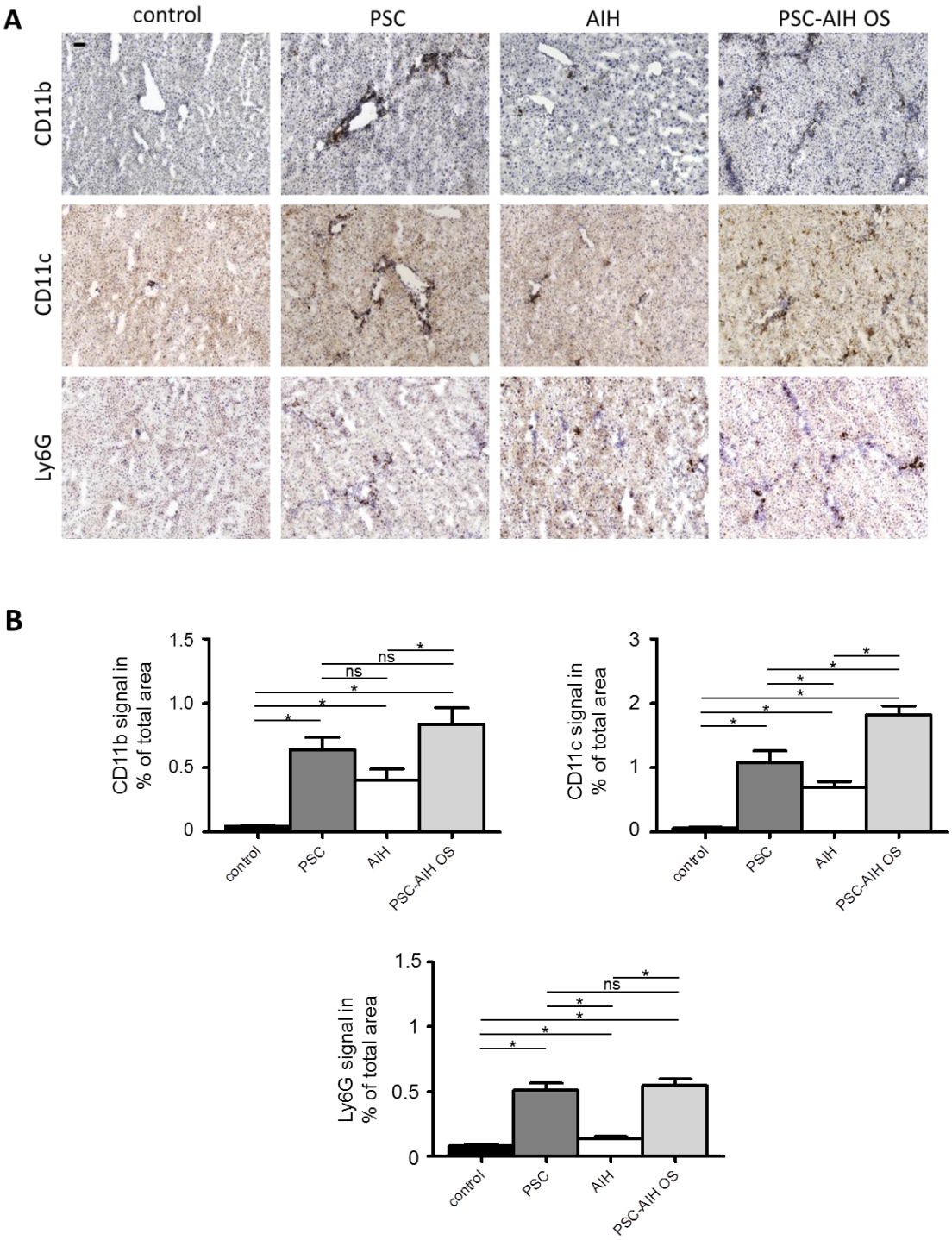

Figure 21: Innate cellular infiltration analysis in naïve and Ad-2D6-infected FVB and *Mdr2*$^{-/-}$ mice at week four after infection

(A) Immunohistochemistry of quick-frozen liver sections from naïve FVB wild type (control), naïve *Mdr2*$^{-/-}$ (PSC), Ad-2D6 infected FVB (AIH), and Ad-2D6 infected *Mdr2*$^{-/-}$ (PSC-AIH OS) mice at week four after infection. Liver sections were staining for macrophages and monocytes (CD11b, upper row), DCs (CD11c, middle row) and neutrophils (Ly6G, lower row). Bar, 50 µm (B) Quantification of CD11b, CD11c and Ly6G signals was done with the Keyence BZ-II Analysis Software. Values are the mean ± SEM (n = 15) of three areas per liver section per mouse with five mice per group. Significant differences ($p < 0.05$, unpaired, two-tailed t-test) are indicated (*).

Monocytes / macrophages, DCs and neutrophils were numerous and localized in big clusters around the blood vessels in the PSC mice. In contrast, liver sections of AIH mice displayed scattered cells covering the entire tissue. Interestingly, the PSC-AIH OS mice showed the highest cellular infiltration and literal overlap of the pattern specific for PSC mice with typical cell clusters and the one of AIH mice with many scattered cells covering the entire tissue. Quantification of the immunohistochemistry data demonstrated that the observed differences were highly significant (Figure 21 B). It was planned to confirm these data by flow cytometry, but the extensive liver fibrosis in *Mdr2*$^{-/-}$ mice impeded the isolation of infiltrating cells. Therefore, the quantity of isolated cells from fibrotic livers does not reflect the actual degree of cellular infiltration.

Secondly, cells of the adaptive immune system like CD4^{+} T cells (Figure 22 A, upper panel) and CD8^{+} T cells were analyzed (Figure 22 A, lower panel). In liver sections of PSC mice many CD8^{+} T cells were found mainly clustered around the blood vessels. Interestingly, livers of PSC mice showed less CD4^{+} than CD8^{+} T cells. In contrast, in livers of AIH mice CD4^{+} and CD8^{+} T cells were predominantly scattered throughout the entire tissue. Just like for the innate immune cells, the PSC-AIH OS mice showed the highest cellular infiltration with a literal overlap of the pattern found for PSC and AIH mice. Quantification of the immunohistochemistry data demonstrated that the observed differences are highly significant (Figure 22 B).

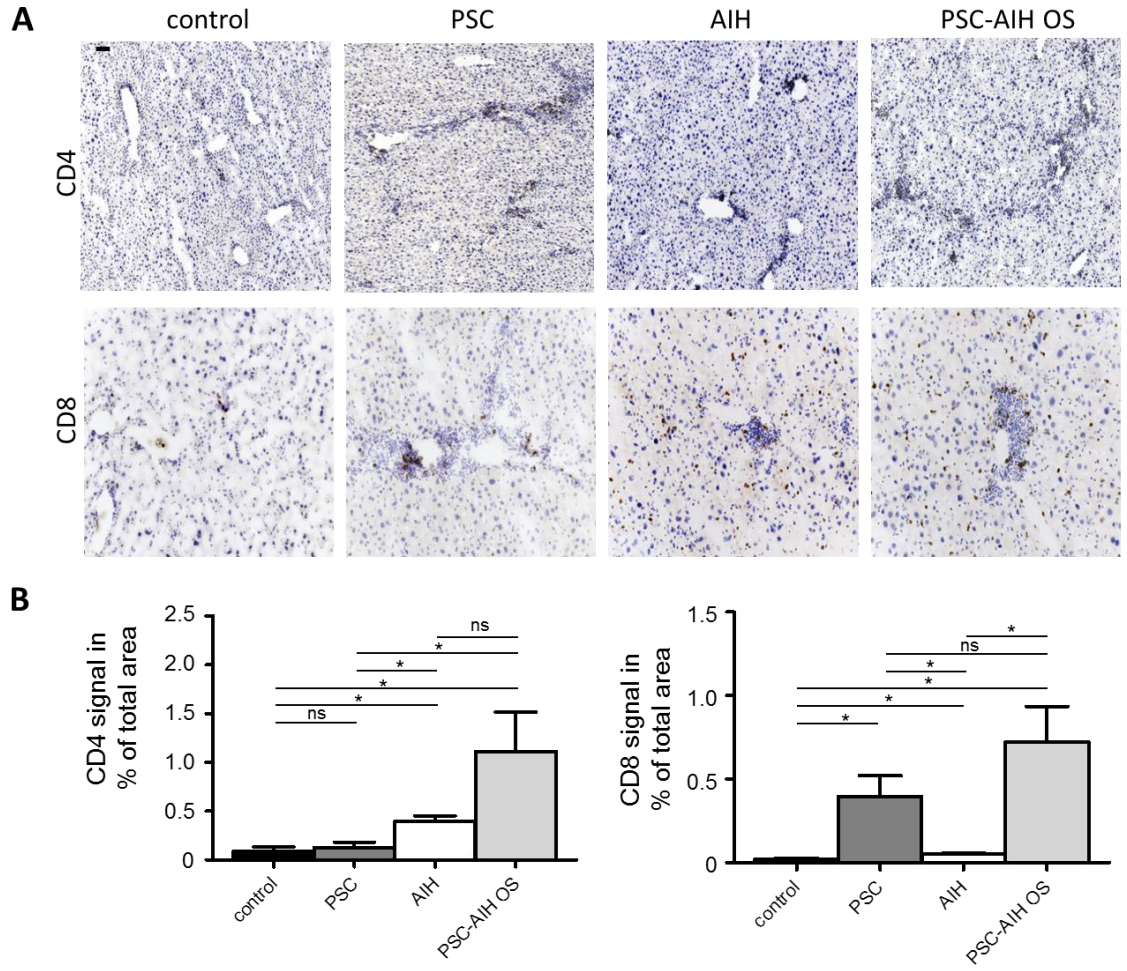

Figure 22: Adaptive cellular infiltration analysis in naïve and Ad-2D6-infected FVB and *Mdr2*$^{-/-}$ mice at week four after infection

(A) Immunohistochemistry of quick-frozen liver sections from naïve FVB wild type (control), naïve *Mdr2*$^{-/-}$ (PSC), Ad-2D6 infected FVB (AIH), and Ad-2D6 infected *Mdr2*$^{-/-}$ (PSC-AIH OS) mice at week four after infection. Adaptive cell types were visualized by using an anti-CD4 antibody for CD4^{+} T cells (upper row) and an anti-CD8 antibody for CD8^{+} T cells (lower row) Bar, 50 µm (B) Quantification of CD4^{+} and CD8^{+} signals was done with the Keyence BZ-II Analysis Software. Values are the mean ± SEM (n = 15) of three areas per liver section per mouse with five mice per group. Significant differences ($p < 0.05$, unpaired, two-tailed t-test) are indicated (*).

5.1.6. Characterization of auto-aggressive immune cells & immune balance

In addition to the histological characterization of the adaptive immune system, the hCYP2D6-specific T cell response at week four post-infection of wild type FVB and *Mdr2*$^{-/-}$ mice was also analyzed. Since the immunodominant hCYP2D6 epitopes for CD8^{+} and

$CD4^+$ T cells are known, liver lymphocytes were isolated and stimulated with those peptides overnight [257]. The intracellular IFNγ production was analyzed by flow cytometry and the frequency of hCYP2D6-specific T cells was quantified. For the analysis of the flow cytometry data, the events were first gated for lymphocytes and then for $CD4^+$ and $CD8^+$ T cells producing IFNγ (Figure 23).

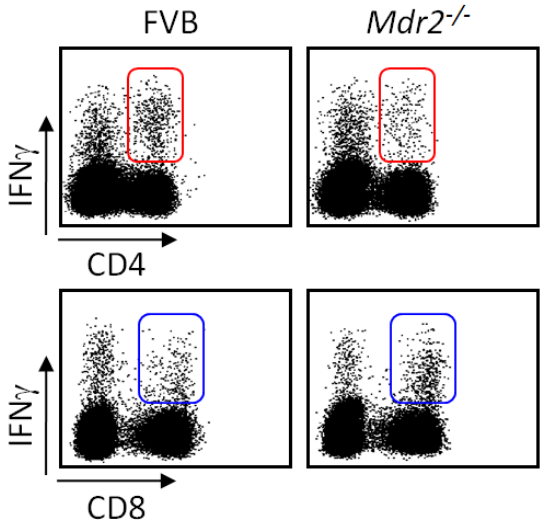

Figure 23: hCYP2D6-specific T cell analysis in Ad-2D6-infected FVB and *Mdr2*$^{-/-}$ mice
Livers were harvested from Ad-2D6 infected FVB or *Mdr2*$^{-/-}$ mice at week four after infection. Lymphocytes were isolated and stimulated with hCYP2D6-specific $CD4^+$ or $CD8^+$ T cell peptides overnight. Intracellular IFNγ staining was analyzed by flow cytometry. Events gated for lymphocytes have been further gated for $CD4^+$ (red) and $CD8^+$ (blue) T cells producing IFNγ.

A significant increase in the frequency of hCYP2D6-specific $CD8^+$ T cells in the PSC-AIH OS mice compared to mice with solitary AIH was detected (Figure 24, left side). The frequency of hCYP2D6-specific $CD4^+$ T cells was similar in mice with PSC-AIH OS and solitary AIH (Figure 24, right side).

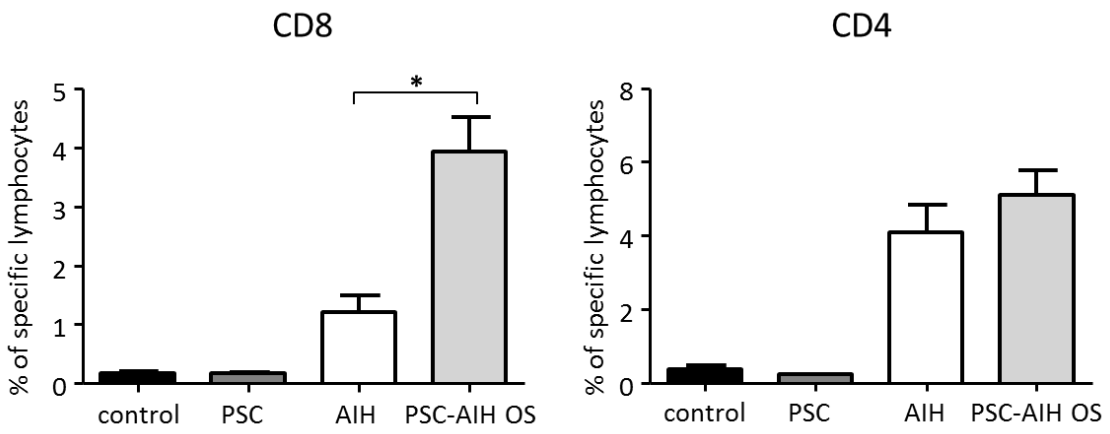

Figure 24: CYP2D6-specific CD8$^+$ T cell response was highest in PSC-AIH OS mice
Livers were harvested from naïve or Ad-2D6-infected FVB or *Mdr2*$^{-/-}$ mice at week four after infection. Lymphocytes were isolated and stimulated with hCYP2D6-specific CD4$^+$ or CD8$^+$ T cell peptides overnight. Intracellular IFNγ staining was analyzed by flow cytometry. Cells were gated for lymphocytes and for CD4$^+$ and CD8$^+$ T cells. Values are mean ± SEM (n = 12) in % of total CD4$^+$ or CD8$^+$ T cells. Significant differences ($p < 0.05$, unpaired, two-tailed t-test) are indicated (*).

Further, the overall T cell balance in the different mouse models was characterized. Therefore lymphocytes were stimulated with anti-CD3 and anti-CD28 antibody as well as IL-2 overnight and the frequency of CD4$^+$ T cells and CD8$^+$ T cells producing IL-10, IFNγ, IL-4 or IL-17 were measured by flow cytometry (Figure 25). The immune response of naïve FVB mice showed a baseline / steady-state CD4$^+$ T cell immune balance between type 1 CD4$^+$ T cell response, which is characterized by IFNγ production, and type 2 CD4$^+$ T cell response which is characterized by IL-4 production (Figure 25, upper row). PSC mice revealed a rather similar type 1 and type 2 CD4$^+$ T cell balance like naïve FVB mice but in addition they also showed an elevated type 17 CD4$^+$ T cell response characterized by IL-17 release. The immune response of AIH mice was characterized by an imbalance toward a strong type 1 CD4$^+$ T cell response which led to a decreased of the type 2 CD4$^+$ T cell response and also a reduction in the type 17 CD4$^+$ T cells. Interestingly, the immune response of PSC-AIH OS mice showed an overlap of the immune balance observed in solitary AIH (strong type 1 CD4$^+$ T cell response) and solitary PSC (higher type 17 CD4$^+$ T cell response) and a reduction of the type 2 CD4$^+$ T cells. All mouse models revealed a similar frequency of CD4$^+$ T_{reg} characterized by an IL-10 production. Analysis of the shift in the immune balance analysis of CD8$^+$ T cells in comparison with naïve mice showed a

very strong IFNγ production which was dominant in all mouse models (Figure 25, lower row). As to be expected the Ad-2D6 infection of FVB mice (AIH model) resulted in an enhanced type 1 $CD8^+$ T cell response and a reduction of type 2 $CD8^+$ T cells. However, also in the PSC group, which did not received any liver-trpic virus, an increase of type 1 $CD8^+$ T cells compared to the naïve FVB mice was observed. Interestingly, the type 17 $CD8^+$ T cell response was more extensive in PSC mice was bigger than in AIH mice, but similar in PSC-AIH OS mice. PSC-AIH OS mice showed again a literal overlap of the immune balance shifts observed in mice with solitary AIH and solitary PSC.

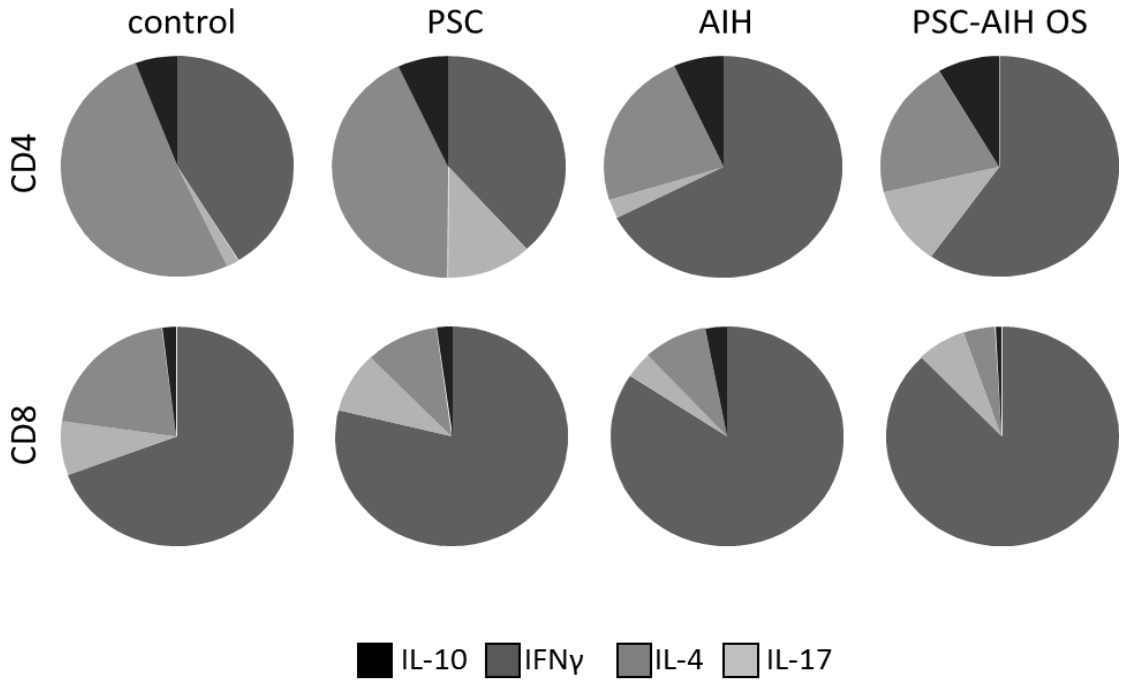

Figure 25: Characterization of the T cell immune response in control, PSC, AIH, and PSC-AIH mice
Liver lymphocytes analysis of naïve or Ad-2D6 infected FVB or *Mdr2*$^{-/-}$ mice at week four after infection. Lymphocytes were isolated and stimulated with anti-CD3 and anti-CD28 antibody in the presence of IL-2 overnight and were then stained for intracellular IL-10, IFNγ, IL-4 or IL-17 production were acquired by flow cytometry. Events were gated for lymphocytes and further gated for $CD4^+$ T cells (upper row) and $CD8^+$ T cells (lower row). Pie charts were created using the mean of data from 6 – 10 mice per group.

5.2. **Novel therapies for the resolution of AIH based on antigen-specific immune tolerance induction**

In previous studies of the research group showed that the immunodominant hCYP2D6 $CD4^+$ and $CD8^+$ T cell epitopes were identified [257]. The highest frequency of hCYP2D6-specific $CD4^+$ T cells was found after overnight stimulation with peptide 6 (aa position 41-60; PGLGNLLHVDFQNTPYCFDQ) (Figure 26, left panel). In contrast, they found several peptides that activated hCYP2D6-specific $CD8^+$ T cells, namely peptide 21 (aa position 161-180; CAAFANHSGRPFRPNGLLDK), peptide 25 (aa position 193-212; RRFEYDDPRFLRLLDLAQEG) and peptide 28 (aa position 217-236; SGFLREVLNAVPVLL89HIPAL) (Figure 26, right panel) [257]. Based on this information, antigen-specific immune tolerance induction was planned on different ways. In a first approach, tolerogenic DCs were to be generated by isolation of bone marrow derived DCs that were stimulated with VitD3 and Dexamethason and pulsed with hCYP2D6 peptides. These tolerogenic DCs were then injected into Ad-2D6 infected mice to assess whether these animals have a lower frequency of inflammatory cells in the liver compared to untreated mice. In a second approach, hCYP2D6-specific T_{reg} were to be generated by the intranasal treatment with hCYP2D6 peptides together with different adjuvants. This approach should have led to an increase in the frequency of FoxP3-positiv T_{reg} in the NALT which then are supposed to travel to the liver shift the skewed immune balance towards a more regulatory phenotype. In a third approach, a tolerization towards hCYP2D6 was attempted by crosslinking hCYP2D6 peptides to splenocytes with ECDI. These splenocytes were then injected into AIH mice to ablate the aggressive hCYP2D6 specific immune response. Finally, in a fourth approach, which was very similar to the hCYP2D6 peptide crosslinked splenocytes, nanoparticles were crosslinked with the hCYP2D6 peptides and then injected into AIH mice to induce immune tolerance.

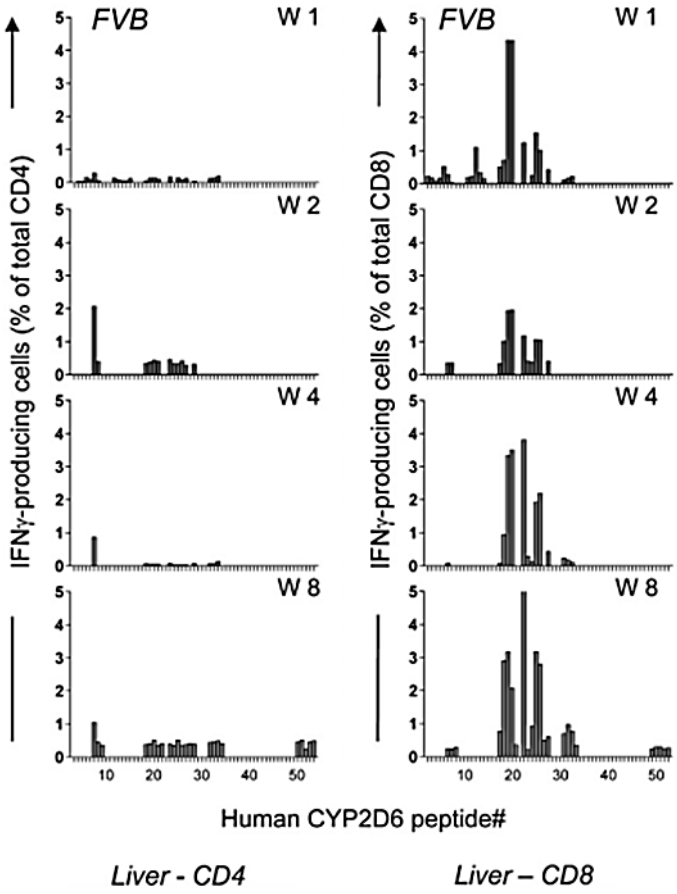

Figure 26: Frequency of hCYP2D6 peptide-specific T cells in the liver
Ehser et al., infected FVB mice with Ad-hCYP2D6 at different time points. After infection liver lymphocytes were isolated and stimulated overnight. For the stimulation peptides covering the entire hCYP2D6 sequence were used. After stimulation, the frequencies of hCYP2D6 peptide-specific $CD4^+$ (left panel) and $CD8^+$ (right panel) T cells producing IFNγ were measured by flow cytometry. Figure is from Ehser et al., 2013 [257].

5.2.1. Transfer of Dexamethasone- and Vitamin D3-modulated DC carrying hCYP2D6-peptides

To generate tolerogenic DCs, bone marrow was harvested from femurs of mice (Figure 27). Cells were isolated and cultured with GM-CSF and IL-4 to induce the initial differentiation of DCs. For the final differentiation of tDCs, cells were treated with either Dex, VitD3 or a mixture of both (VitD3+Dex). These different treatment conditions were compared to the control DCs which were not stimulated with either Dex, VitD3 or VitD3+Dex. After six days of differentiation cells were pulsed with the immunodominant $CD4^+$ T cell epitope peptide p6 and the immunodominant $CD8^+$ T cell epitope peptide

p21 to ensure their antigen-specificity for the use in AIH mice. Before DCs were injected into AIH mice, they were analyzed by flow cytometry to confirm a successful tDCs differentiation.

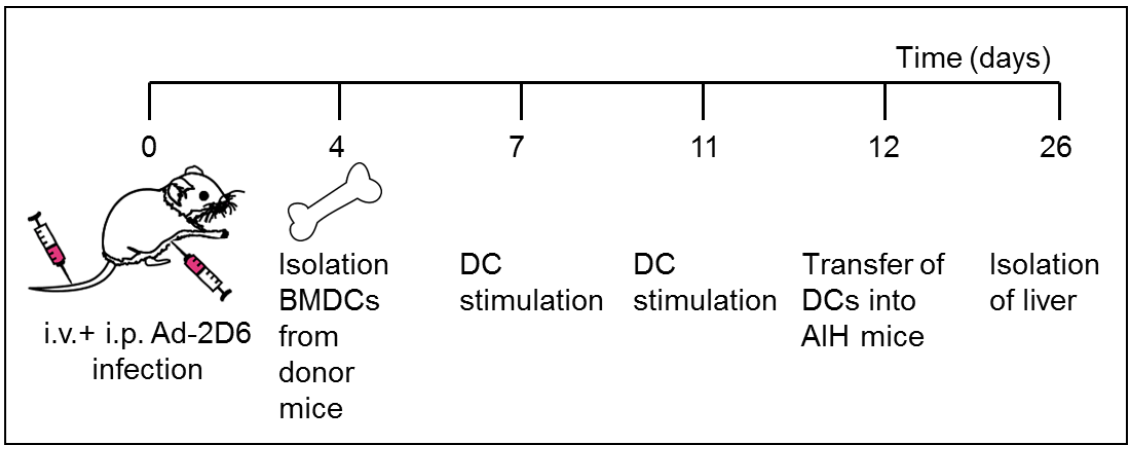

Figure 27: Initial treatment protocol of AIH mice with VitD3+Dex DCs
Mice were infected with Ad-2D6 four days before BMDCs were isolated from donor mice. Cells were cultured for several days. After successful differentiation DCs were transferred into recipient AIH mice, 12 days post infection. Mice were sacrificed two weeks after cell transfer and livers were harvested for flow cytometry analysis.

For the differentiation under normal condition, a mature phenotype with a high expression of MHC class II and CD86 was expected. The DCs differentiation under VitD3+Dex conditions was expected to generate a semi-mature phenotype which is characterized by a low expression of MHC class II and CD86. After VitD3 treatment, an increase of PD-L1 expression was expected as well as a ratio of PD-L1 to CD86 which is associated with impaired dendritic cell function. Several rounds of BMDCs isolation and differentiation were performed and a representative example of the flow cytometry phenotype analysis of a successful differentiation of DCs is shown in Figure 28.

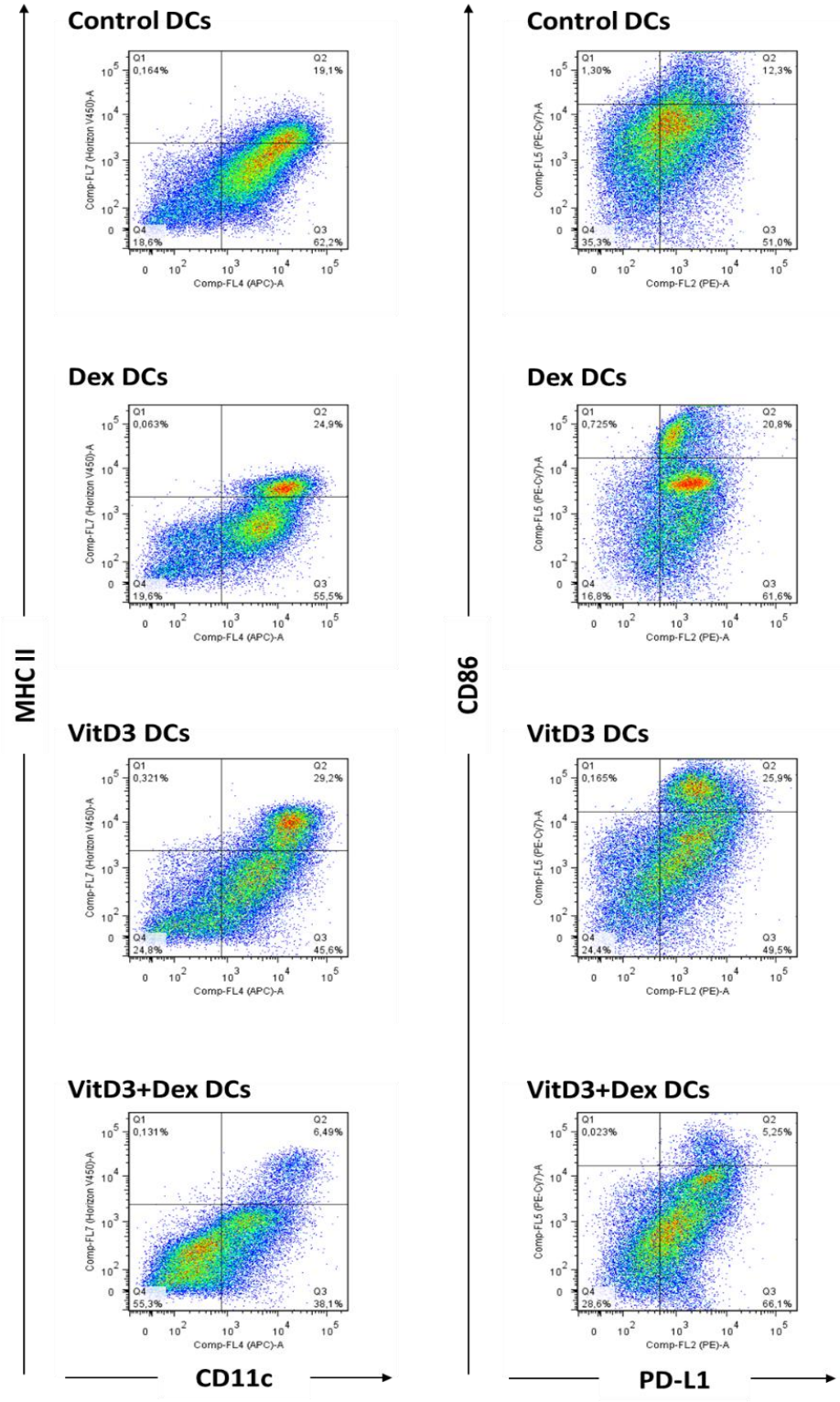

Figure 28: Flow cytometry dot plot analysis of DC differentiation under different treatment conditions

On the left side the frequency of MHC class II and CD11c expressing cells is shown for four different groups depending on their treatment condition (control, Dex, VitD3, VitD3 +Dex). On the right side the frequency of CD86 and PD-L1 positive cells is shown.

After a successful differentiation of DCs, the effectiveness of VitD3+Dex DCs as a tolerance inducing therapy for AIH in the Ad-2D6 infected mice was tested. The cell transfer of either VitD3+Dex DCs or control DCs was done at day 12 after the adenovirus infection which is shortly after the acute phase of infection. Therefore, one group received control DCs, another group received VitD3+Dex DCs and the third group received no treatment (control group). Two weeks after the transfer the livers were harvested and liver lymphocytes were isolated and stimulated with the immunodominant $CD4^+$ and $CD8^+$ T cell epitopes p6 and p21, respectively. The next day, intracellular cytokine staining for IFNγ production was performed and cells were analyzed by flow cytometry. Events gated for lymphocytes have been further gated for $CD4^+$ or $CD8^+$ T cells producing IFNγ.

The frequency of $CD4^+$ T cells producing IFNγ are the same in both groups which received DCs, independent if they were treated with mature (control) or semi- mature (VitD3+Dex) DCs. The untreated AIH mice showed a little lower but not significantly decreased frequency of $CD4^+$ T cells producing IFNγ (Figure 29, A). In terms of $CD8^+$ T cells producing IFNγ no difference can be observed (Figure 29, B).

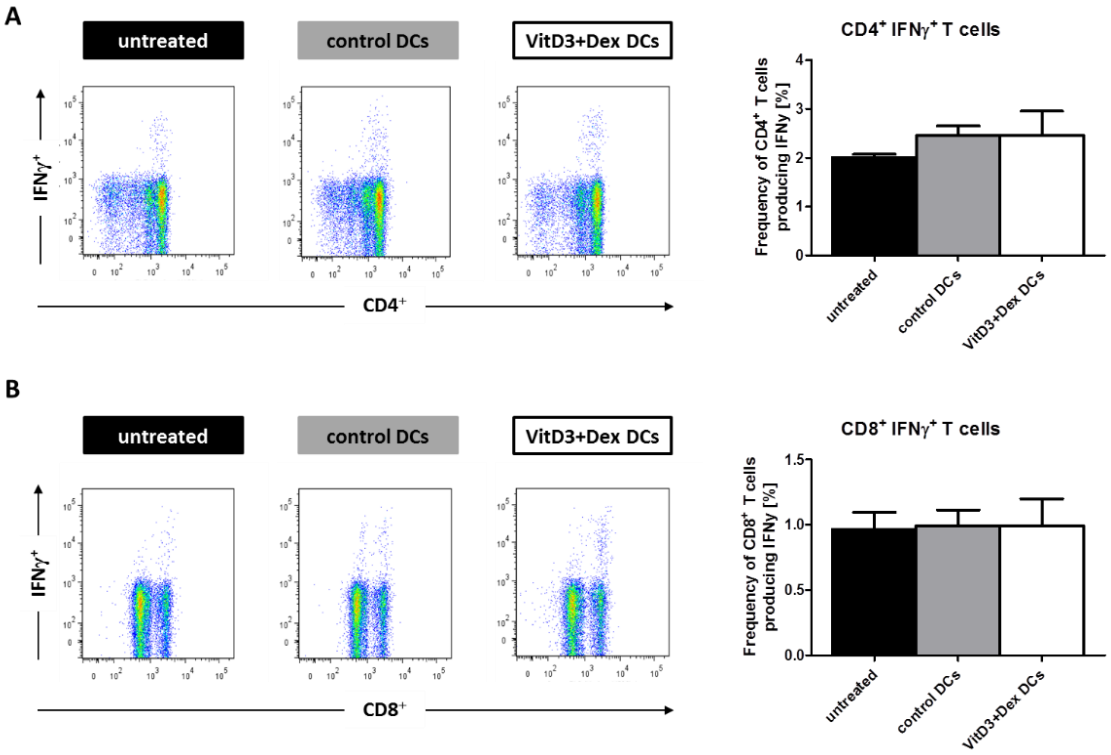

Figure 29: Flow cytometry analysis of hCYP2D6-specific T cells after different DCs injections

Frequency of hCYP2D6-specific $CD4^+$ (A) and $CD8^+$ (B) T cells form mice which received an injection of mature (control) or semi- mature (VitD3+Dex) DCs compared to untreated AIH mice. T cells were stimulated either with the immunodominant $CD4^+$ T cell epitope p6 or the immunodominant $CD8^+$ T cell epitope p21 overnight. N=5.

5.2.2. Nasal administration of hCYP2D6-peptides

The nasal-associated lymphoid tissue (NALT) is part of the lymphoid tissue and is localized at the back of the nose. NALT is an important inductive site for the induction and regulation of mucosal immunity in the upper respiratory tract, similar to Peyer's patch (PP) in the intestinal immune system. It is known that it is involved at the induction and regulation of mucosal immunity in the upper respiratory tract.

Mice were treated five times intranasally with a combination of both peptides p6 and p21 alone or in combination with CpG or Poly IC as adjuvant. Two days after the last intranasal administration the mice were sacrificed to see whether the number of T_{reg} in the NALT has increased (Figure 30).

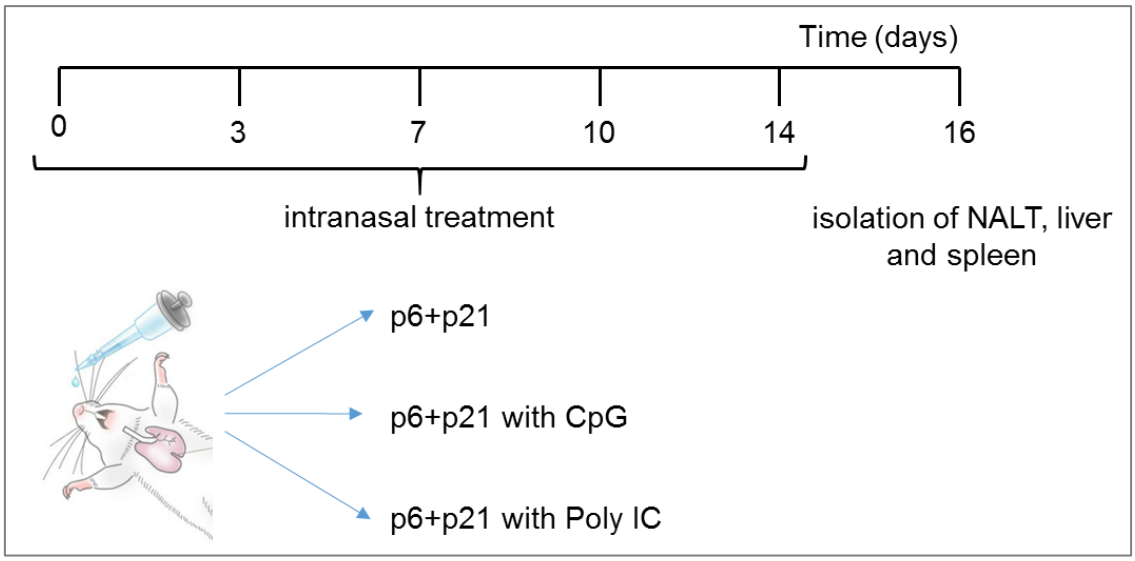

Figure 30: Initial treatment protocol of the tolerance induction via intranasal treatment

Mice were treated five times intranasally with either the both peptides (p6+p21; 100 µg per each administration) or both peptides together with CpG or the combination of both peptides and Poly IC. Two days after the last intranasal administration mice were sacrificed and lymphocytes were isolated from NALT, liver and spleen.

Lymphocytes were isolated from NALT, liver as well as spleen and were stained against $CD4^+$ and $CD8^+$ T cells to evaluate if there is a difference in the absolute amount and overall ratio of $CD4^+$ and $CD8^+$ T cells in the different organs. The frequencies of total lymphocytes in liver and spleen were very similar (Figure 31). Nearly 70% of the total lymphocytes were $CD4^+$ and 20 % were $CD8^+$. In comparison to these organs the frequency of $CD4^+$ T cells in the NALT was about 40 % and less than 20% were $CD8^+$. All groups showed nearly the same frequencies of cell types independent of the treatment regimen (Figure 31).

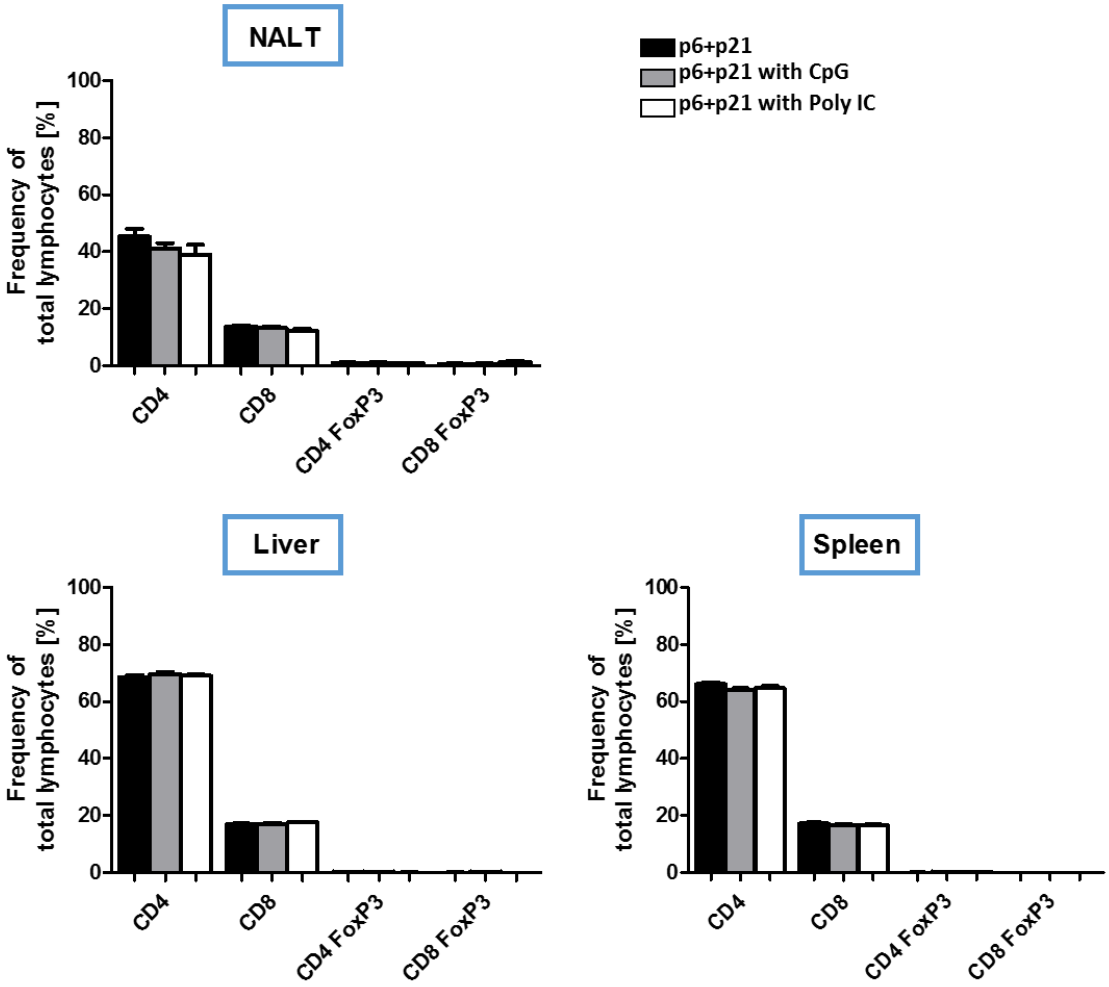

Figure 31: Frequency of total lymphocytes in NALT comparable to liver and spleen after intranasal treatment

Naïve FVB mice were treated five times intranasally with 100 µg per administration of both peptides p6+p21 (black bars) or both peptides together with CpG (grey bars) or Poly IC (white bars). Two days after the last treatment mice were sacrificed and lymphocytes of different organs were isolated. Cells were stained extracellular for $CD4^+$ and $CD8^+$ and intracellular for $FoxP3^+$ and the events were gated first for lymphocytes and then gated for $CD4^+$ and $CD8^+$ T cells and $FoxP3^+$, too. Values are mean ± SEM (n = 5) in % of total $CD4^+$ or $CD8^+$ T cells.

However, the main interest was the assessment of T_{reg} frequencies in the different organs. A closer look at these small amounts of $CD4^+$ or $CD8^+$ $FoxP3^+$ cells showed that although the lowest frequency of $CD4^+$ or $CD8^+$ T cells was in the NALT they had the highest T_{reg} frequency after intranasal treatment (Figure 32). In spleen and liver, the frequency of $FoxP3^+$ T cells was 5 – 10-fold lower than in the NALT. Whereas the frequencies of $CD4^+$ $FoxP3^+$ was similar in the different treatment groups, the peptide

treatment with the adjuvant Poly IC led to a higher $CD8^+$ $FoxP3^+$ frequency compared to the treatment with CpG adjuvant or the peptides alone (Figure 32, right side). T_{reg} are known to have the capacity to induce immune tolerance. In the next experiment it was tested if this high amount of T_{reg} in the NALT has a protective role in our AIH model.

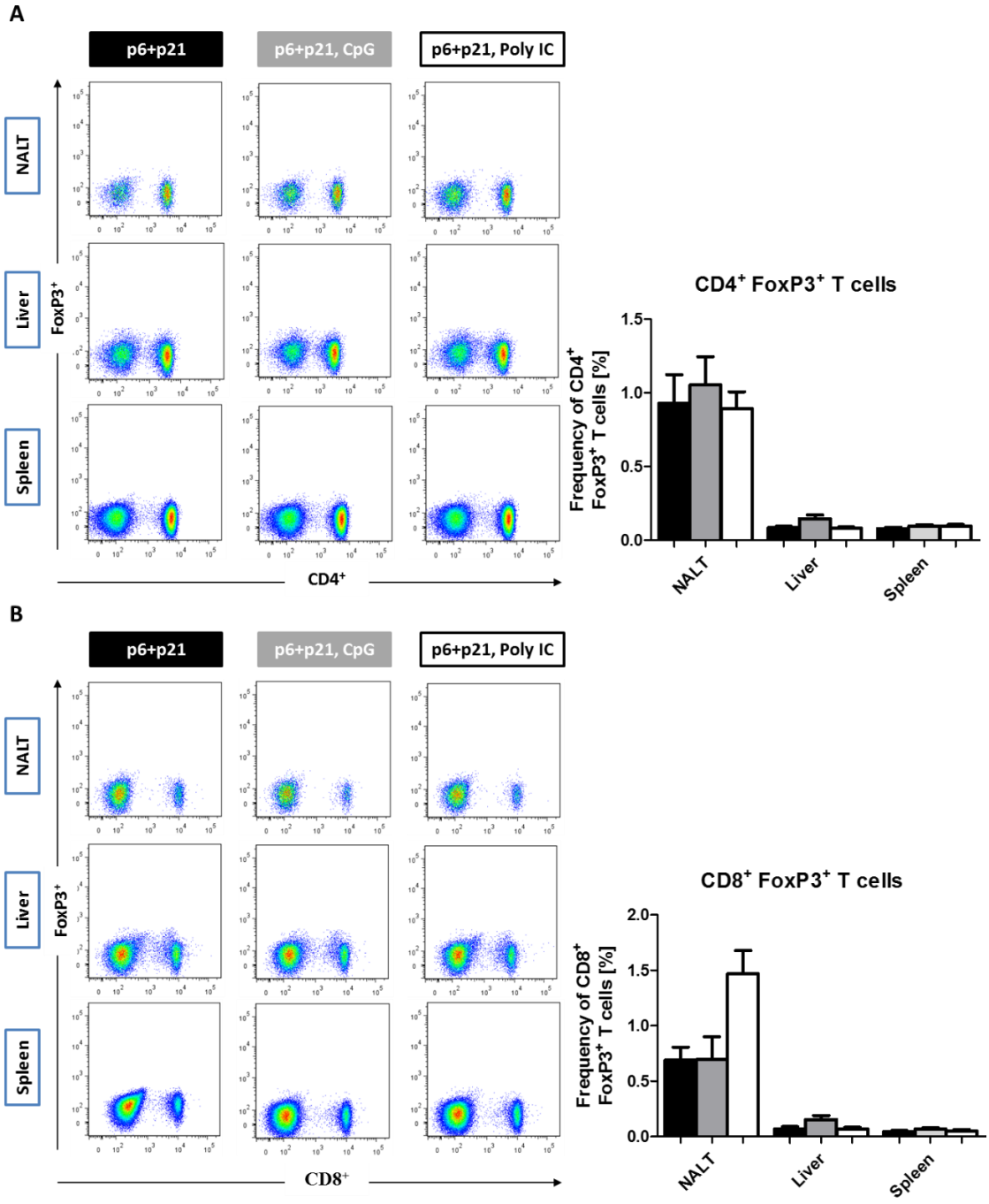

Figure 32: Frequency of $CD4^+$ or $CD8^+$ $FoxP3^+$ T cells in NALT comparable to liver and spleen after intranasal treatment

Naïve FVB mice were treated five times intranasally with 100 µg per administration of both peptides p6+p21 (black bars) or both peptides together with CpG (grey bars) or Poly IC (white bars). Two days after the last treatment mice were sacrificed and lymphocytes of different organs were isolated. Cells were stained for $CD4^+$, $CD8^+$, and

intracellular for FoxP3$^+$. Events were gated first for lymphocytes and then gated for CD4$^+$ FoxP3$^+$ (A) and CD8$^+$ FoxP3$^+$ T cells (B). Values are mean ± SEM (n = 5) in % of total CD4$^+$ or CD8$^+$ T cells.

Thus, in the second treatment protocol the intranasal treatment was combined with a following Ad-2D6 infection. Therefore, mice were treated five times intranasally with either both adjuvants Poly IC and CpG or both adjuvants together with the peptides or only PBS as a control. Two days after the last intranasal administration mice were infected with Ad-2D6 (i.v. and i.p.). Five days after Ad-2D6 injection mice were sacrificed and the isolation of NALT, liver and spleen were done (Figure 33).

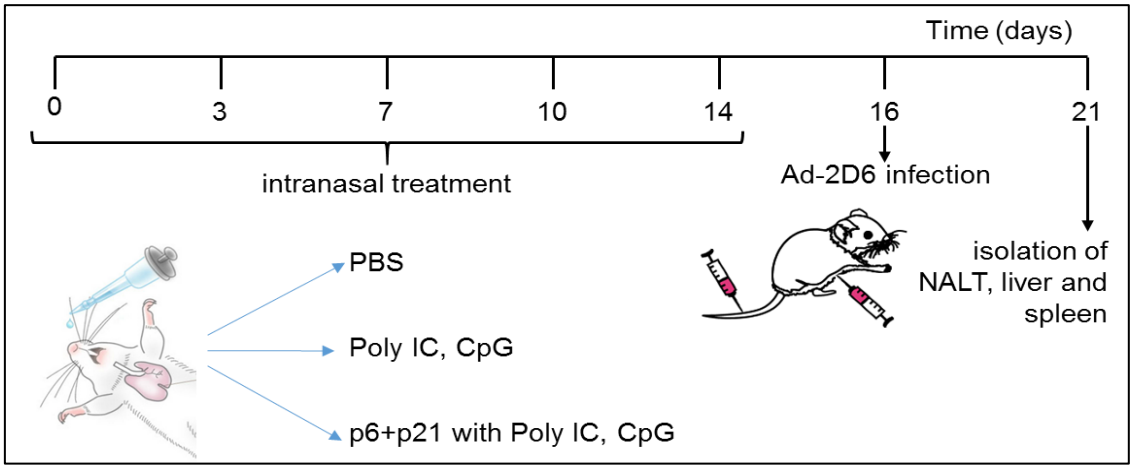

Figure 33: Second treatment protocol of the tolerance induction via intranasal treatment
Mice were treated five times intranasally with either both adjuvants Poly IC and CpG or both adjuvants together with the peptides or only PBS as a control. Two days after the last intranasal administration mice were infected with Ad-2D6 (i.v. and i.p.). Five days after Ad-2D6 injection mice were sacrificed and the isolation of NALT, liver and spleen were done.

Lymphocytes were isolated and stained for CD4$^+$ or CD8$^+$ T cells producing IFNγ or expressing FoxP3. Overall CD4$^+$ FoxP3$^+$ were detected in a higher frequency in liver samples than in NALT samples (Figure 34). In contrast, the frequency of CD8$^+$ FoxP3$^+$ was similar in liver and NALT (Figure 34, B). By comparing this data with the one of the first experiment in which the mice were sacrificed two days after the last intranasal treatment without inducing AIH, it is noticeable that the frequency of T_{reg} in the NALT

has massively decreased and the frequency of T_{reg} in the liver has increased. This observation might indicate that the T_{reg} migrated from the NALT to the inflamed liver.

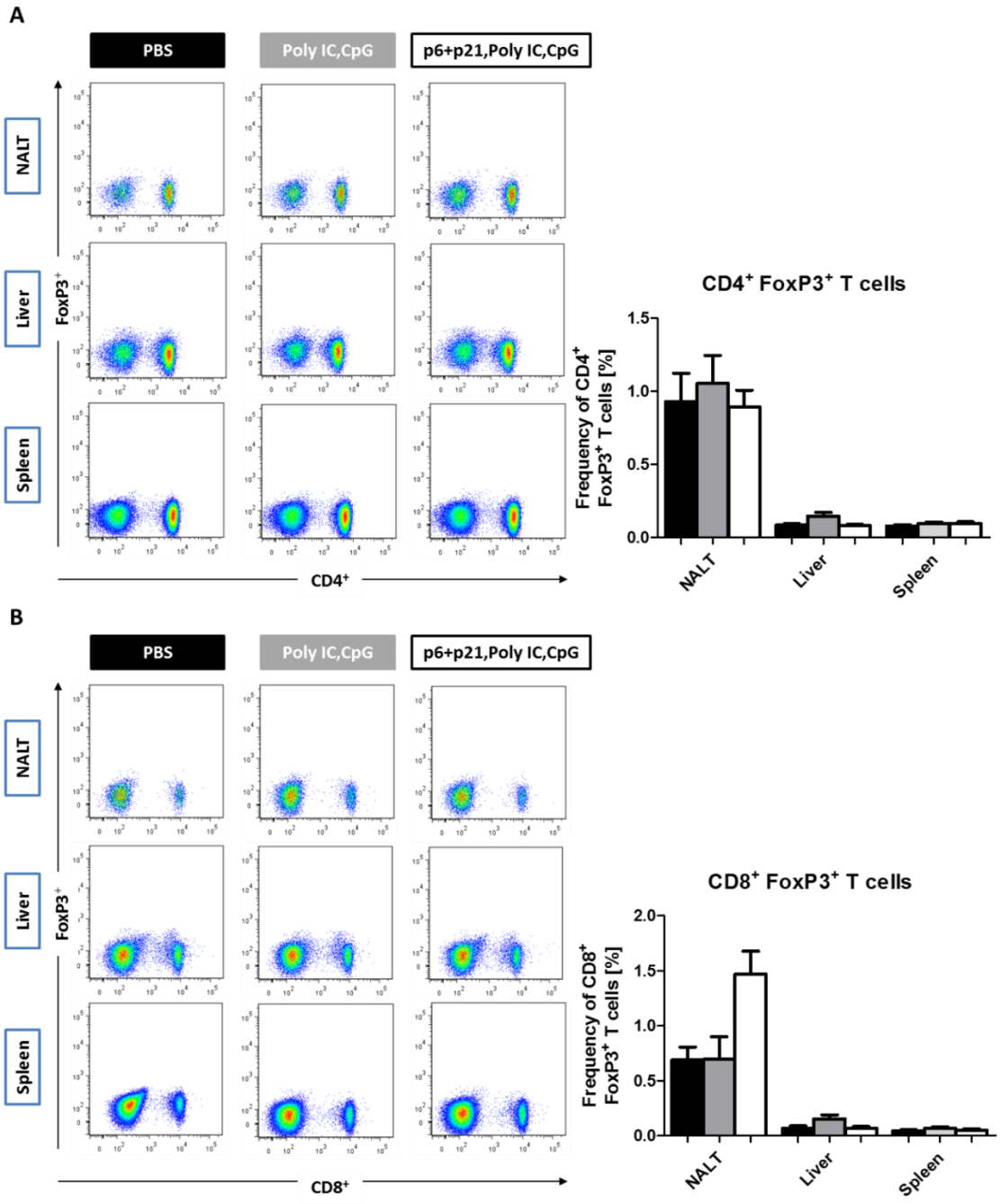

Figure 34: Frequency of $CD4^+$ or $CD8^+$ $FoxP3^+$ T cells in NALT comparable to liver and spleen after intranasal treatment

Naïve FVB mice were treated five times intranasally with PBS (black bars) or Poly IC and CpG (grey bars) or peptide 6 and 21 together with both adjuvants (white bars). Two days after the last intranasal treatment mice were infected with Ad-2D6 (i.v. and i.p.). Five days after the Ad-2D6 injection mice were sacrificed and lymphocytes of different organs were isolated. Cells were stained for $CD4^+$, $CD8^+$, and intracellular for $FoxP3^+$.

Events obtained by flow cytometry were gated first for lymphocytes and then gated for $CD4^+$ $FoxP3^+$ (A) and $CD8^+$ $FoxP3^+$ T cells (B). Values are mean ± SEM (n = 5) in % of total $CD4^+$ or $CD8^+$ T cells.

To see whether these T_{reg} indeed used their capacity to induce immune tolerance, the frequencies of hCYP2D6 specific $CD4^+$ and $CD8^+$ T cells producing IFNγ were determined. Unfortunately, there were no differences in the frequencies of $CD4^+$ or $CD8^+$ T cells producing IFNγ in the different treatment groups (Figure 35).

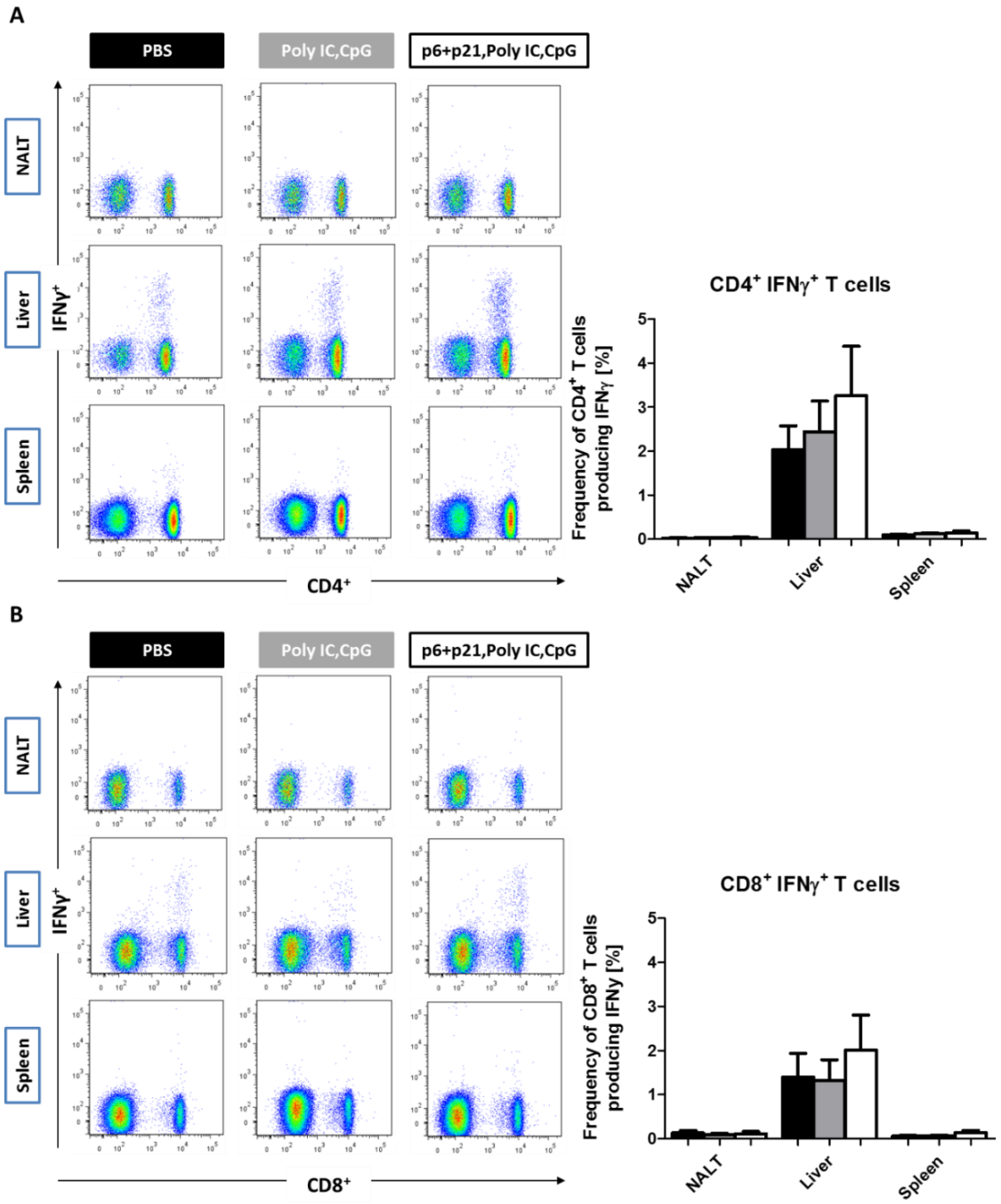

Figure 35: Frequency of CD4⁺ or CD8⁺ IFNγ⁺ T cells in different organs after intranasal treatment

Naïve FVB mice were treated five times intranasally with PBS (black bars) or Poly IC and CpG (grey bars) or peptide 6 and 21 together with both adjuvants (white bars). Two days after the last intranasal treatment mice were infected with Ad-2D6 (i.v. and i.p.). Five days after the Ad-2D6 injection mice were sacrificed and lymphocytes of different organs were isolated. Cells were stained for CD4⁺, CD8⁺, and intracellular for IFNγ⁺. Events obtained by flow cytometry were gated first for lymphocytes and then gated for CD4⁺ IFNγ⁺ (A) and CD8⁺ IFNγ⁺ T cells. Values are mean ± SEM (n = 5) in % of total CD4⁺ or CD8⁺ T cells.

5.2.3. Transfer of hCYP2D6-peptides ECDI-coupled splenocytes

It has been shown that the injection of ECDI-coupled splenocytes loaded with disease specific antigens on the surface, protects EAE mice against the disease. In addition, a phase 1 trial in MS patients showed that this tolerance induced approach was safe and well tolerated and is a promising therapeutic approach.

To test whether this tolerance inducing therapy also worked in a mouse model for AIH, spleens of donor mice were isolated and splenocytes were pooled (Figure 36). Three different preparations of splenocytes with and without crosslinker as well as autoantigen were constructed to analyze the capacity of tolerazing splenocytes. Moreover, the necessity of the crosslink between splenocytes and autoantigens was also analyzed. The first preparation included splenocytes together with the cross-linker and without any autoantigen and worked as a control (SPL+ECDI). The second preparation was the splenocytes together with the cross-linker and the $CD4^+$ immunodominant peptide 6 (SPL+ECDI+p6). This preparation included the virtual approach to test the tolerazing capacity of antigen-coupled splenocytes (Ag-SPL). In the third preparation splenocytes and peptide 6 without the cross-linker were mixed together (SPL+p6). This preparation should identify if the crosslinker is needed to present the peptides on the surface of the cells in the way to reach the tolerazing effect. 40 million cells of one of the three different preparations were i.v. injected into two-weeks old Ad-2D6 infected mice. Two weeks after the splenocytes transfer, mice were sacrificed and liver were isolated.

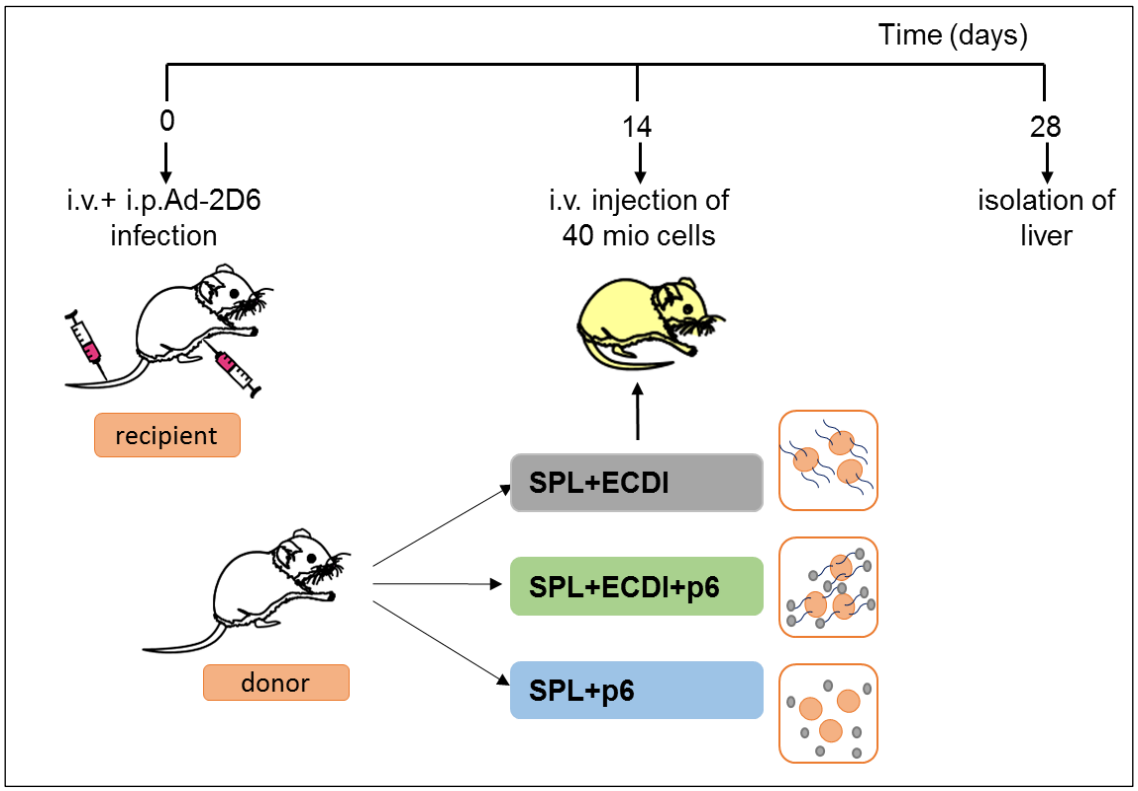

Figure 36: Treatment protocol for the creation of Ag-SPL specific for AIH mice
Recipient mice were infected with Ad-2D6. Two weeks later, livers of donor mice were harvested, splenocytes were isolated and incubated with different components. 40 million cells were injected i.v. into each recipient mouse. Mice were sacrificed two weeks after splenocytes transfer and isolation of liver were done.

To analyze the tolerazing capacity of Ag-SPL, flow cytometry was performed to measure the frequencies of hCYP2D6-specific $CD4^+$ and $CD8^+$ T cells. Figure 37 shows that Ag-SPL led to an increase in the frequency of hCYP2D6 specific $CD4^+$ T cells compared to the group which received splenocytes with the cross-linker but without the peptides. Transfer of splenocytes which were incubated with the peptide but without any cross-linker led also to a higher frequency of specific $CD4^+$ T cells. The frequency of $CD8^+$ T cells producing IFNγ measured in the group which received the Ag-SPL was enhanced compared to the control group. Mice treated with splenocytes and autoantigens without the cross-linker also showed an increase in $CD8^+$ T cells producing IFNγ. Thus, it seems that Ag-SPL did not induce immune tolerance in the AIH mice, but rather boosted the immune response in that way that the mice showed a higher frequency of hCYP2D6 specific T cells.

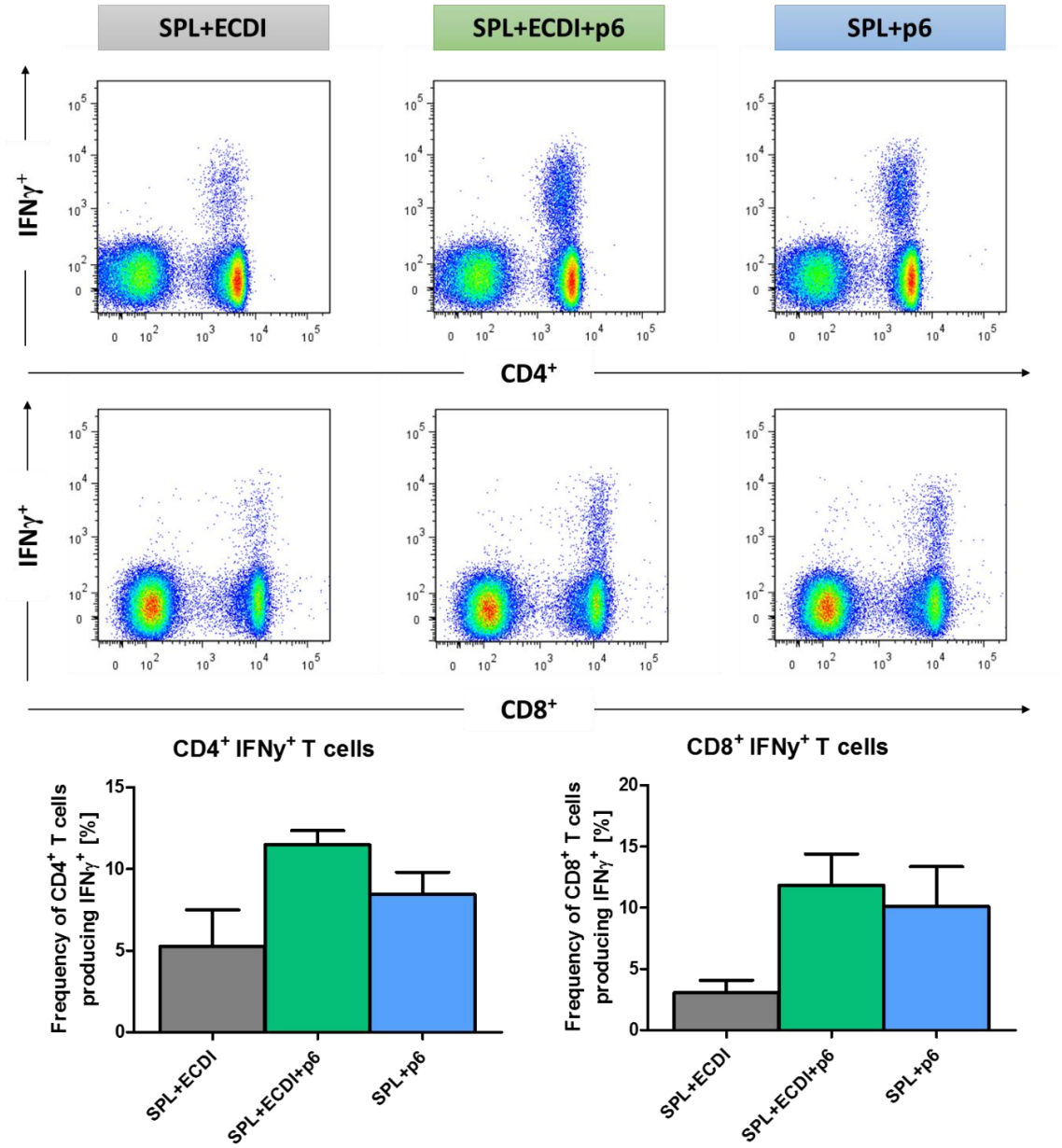

Figure 37: Ag-SPL boosted the frequency of inflammatory CD4⁺ and CD8⁺ T cells
AIH infected mice received intravenously 40 million cells of either splenocytes with cross-linker (grey bars) or Ag-SPL via cross-linker (green bars) or splenocytes with antigen but without cross-linker (blue bars) two weeks after Ad-2D6 infection. Liver lymphocytes were isolated two weeks after splenocytes transfer and were stained for CD4⁺ and CD8⁺ T cells producing IFNγ. Events were gated for lymphocytes and then gated for CD4⁺ or CD8⁺ T cells and finally for IFNγ production. Values are mean ± SEM (n = 4) in % of total CD4⁺ or CD8⁺ T cells.

5.2.4. Nanoparticle-based autoantigen delivery

Due to the failure of Ag-SPL to induce immune tolerance in our AIH model a different approach was tried. Instead of crosslinked splenocytes poly (lactic-co-glycolic acid) (PLG) microparticles encapsulated with disease relevant autoantigens on the surface was used. Nanoparticles specific for AIH which were used in this thesis were created in the lab of Steve Miller, Northwestern University Chicago. At first FVB mice were infected with Ad-2D6 to induce AIH. Two weeks after infection, each mouse received 1.5 mg of i.v. administered NP that encapsulated either the immunodominant $CD4^+$ T cell epitope p6 (NP6) or one of the two immunodominant $CD8^+$ T cell epitopes p25 or p28 (NP25; NP28). Mice were sacrificed one, two, or six weeks after NP injection. Liver lymphocytes were isolated and the frequencies of hCYP2D6-specific T_{reg} and T_{eff} were analyzed by flow cytometry (Figure 38).

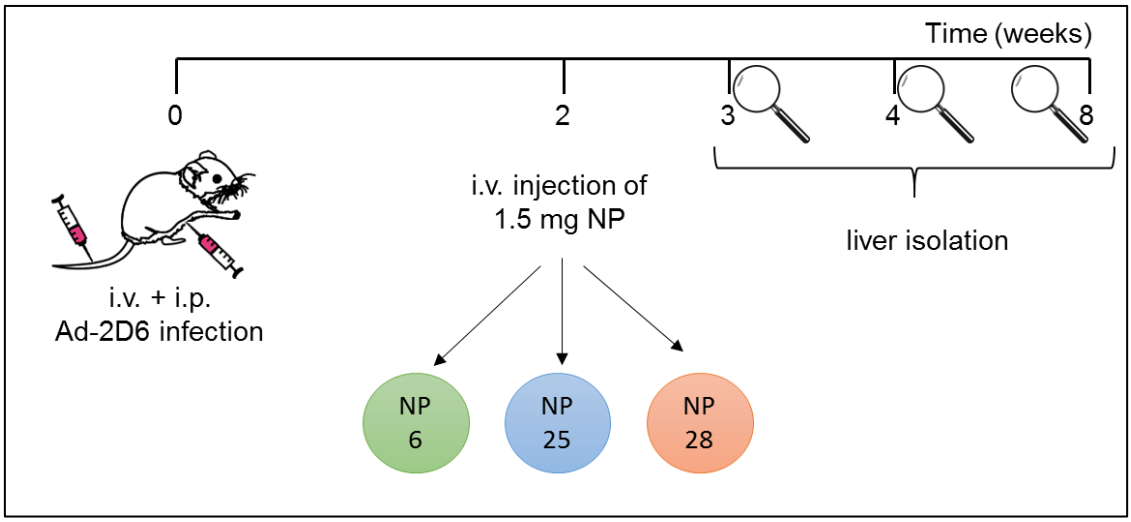

Figure 38: Treatment protocol for nanoparticle therapy to induce tolerance in AIH mice
Ad-2D6 infected mice received 1.5 mg nanoparticle bearing either the immunodominant $CD4^+$ T cell epitope p6 (NP6) or one of the two immunodominant $CD8^+$ T cell epitopes p25 or p28 (NP25; NP28) two weeks after infection. One, two or six weeks after nanoparticle administration livers were harvested and lymphocytes were isolated.

One week after NP administration the results of isolated liver lymphocytes which were first gated for lymphocytes, then for the expression of $CD4^+$ or $CD8^+$ T cells expressing FoxP3 are depicted in Figure 39. Mice which received the $CD4^+$ immunodominant epitope peptide 6 on the surface of NP showed a significantly higher frequency of $CD4^+$

FoxP3$^+$ T cells compared to the untreated control group. Interestingly, NP25 one of the CD8 specific NP had also an effect on CD4$^+$ FoxP3$^+$ T cells and led to a significantly increase in this frequency. In comparison to NP25, the secondary CD8 specific NP28 had no influence in the frequency of CD4$^+$ FoxP3$^+$ T cells.

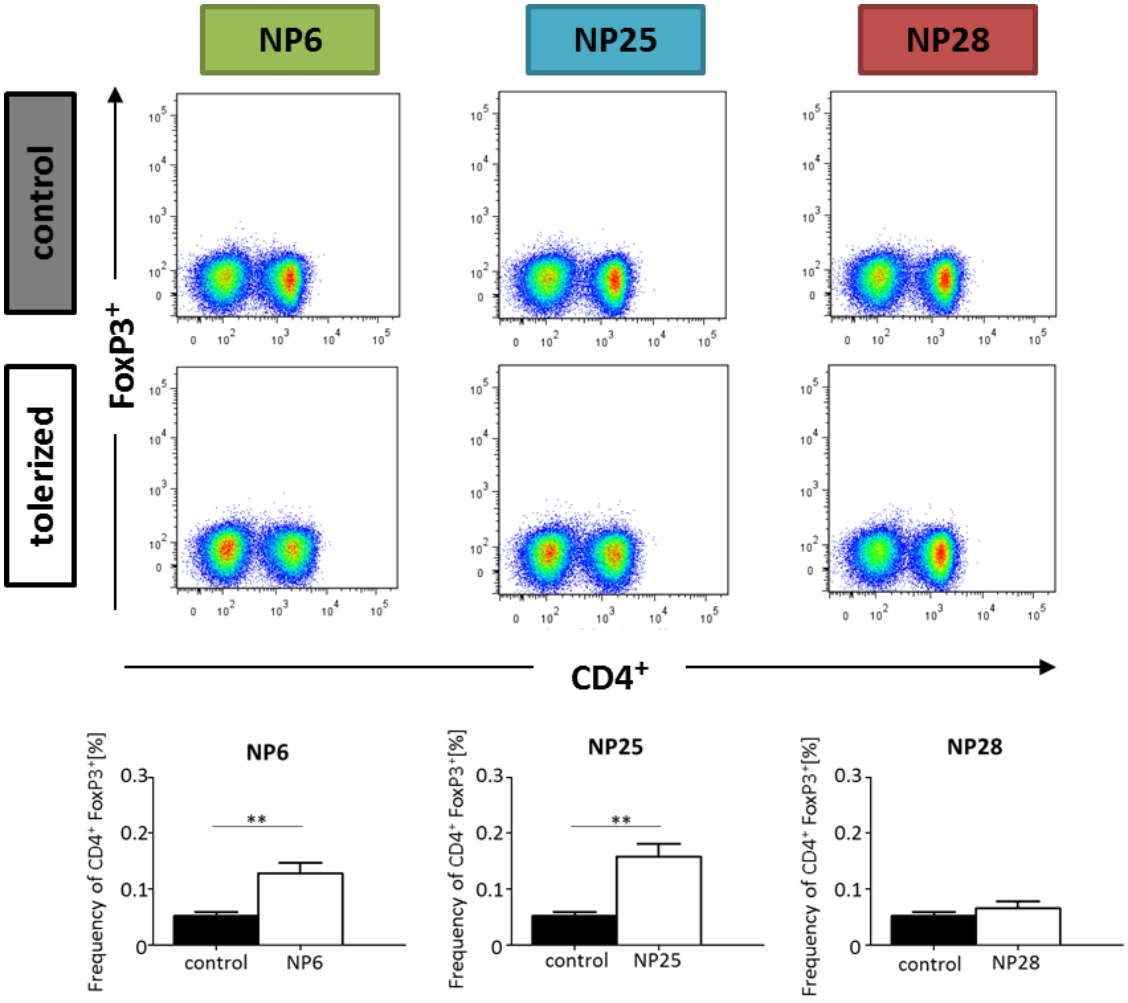

Figure 39: Frequency of CD4$^+$ FoxP3$^+$ T cells one week after NP treatment in AIH
AIH infected mice received i.v. 1.5 mg PLG-nanoparticle bearing either the immunodominant CD4$^+$ T cell epitope (NP6) or one of the two immunodominant CD8$^+$ T cell epitopes (NP25; NP28) two weeks after infection. One week after NP administration liver were harvested, lymphocytes were isolated and stimulated with different hCYP2D6-specific peptides overnight. After stimulation intracellular expression of FoxP3 were then analyzes by flow cytometry. N=5.

The analysis of $CD8^+$ $FoxP3^+$ T cells are depicted in Figure 40. The immunodominant $CD4^+$ epitope peptide NP6 as well as the secondary immunodominant $CD8^+$ NP28 did not increase the frequency of $CD8^+$ $FoxP3^+$ T cells in the tolerized mice. The administration of NP25 led to a slight, non-significant increase in the frequency of $CD8^+$ $FoxP3^+$ T cells. Taken together, NP6 and NP25 had the capacity to increase the frequency of $CD4^+$ $FoxP3^+$ T cells and NP25 also increased the frequency of $CD8^+$ $FoxP3^+$ T cells one week after NP administration.

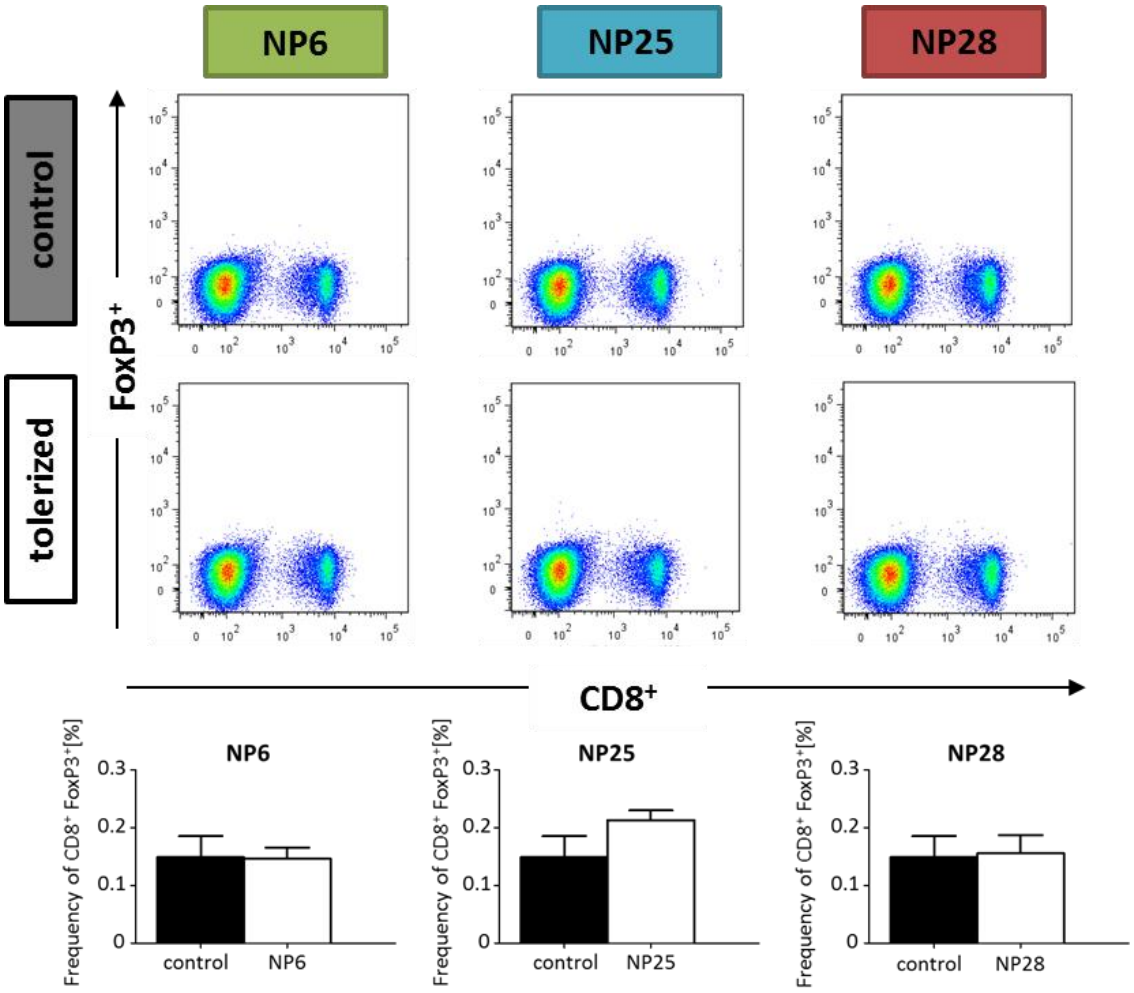

Figure 40: Frequency of $CD8^+$ $FoxP3^+$ T cells one week after NP treatment in AIH
AIH infected mice received i.v. 1.5 mg PLG-nanoparticle bearing either the immunodominant $CD4^+$ T cell epitope (NP6) or one of the two immunodominant $CD8^+$ T cell epitopes (NP25; NP28) two weeks after infection. One week after NP administration liver were harvested, lymphocytes were isolated and stimulated with different hCYP2D6-specific peptides overnight. After stimulation intracellular expression of FoxP3 were then analyzes by flow cytometry. N=5.

After the analysis of NP induced T_{reg} the frequencies of hCYP2D6-specific $CD4^+$ and $CD8^+$ T cells producing IFNγ were determined to see whether the presence of these T_{reg} can regenerate the immune balance. In parallel to the increase in T_{reg}, NP6 administration significantly decreased the frequency of hCYP2D6(p6)-specific $CD4^+$ T cells. Interestingly, the tolerization with the $CD4^+$ epitope (NP6) did also significantly reduce the frequency of hCYP2D6(p25)-specific $CD8^+$ T cells. Indicating that the lack of $CD4^+$ T cell help has an impact on the $CD8^+$ T cell repertoire. Tolerization to the $CD8^+$ epitope 25 with NP25 resulted in a significant and strong decrease of specific $CD8^+$ T cells as well as $CD4^+$ T cells. Tolerization to the second $CD8^+$ epitope 28 did neither decrease the frequency of specific $CD8^+$ nor $CD4^+$ T cells (Figure 41).

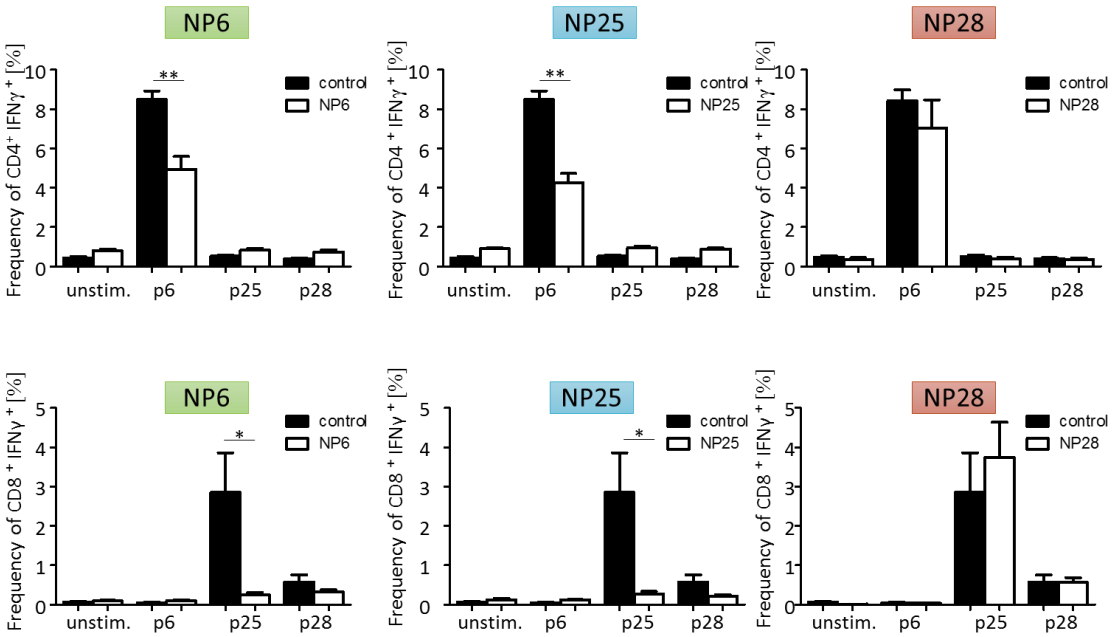

Figure 41: Frequency of hCYP2D6 specific $CD4^+$ and $CD8^+$ T_{eff} one week after NP treatment in AIH mice

AIH infected mice received i.v. 1.5 mg PLG-nanoparticle bearing either the immunodominant $CD4^+$ T cell epitope (NP6) or one of the two immunodominant $CD8^+$ T cell epitopes (NP25; NP28) two weeks after infection. One week after NP administration liver were harvested, lymphocytes were isolated and stimulated with different hCYP2D6-specific peptides overnight. After stimulation intracellular IFNγ production were then analyzes by flow cytometry. N=5.

In addition to the characterization of the frequency of $CD4^+$ and $CD8^+$ T cells expressing $FoxP3^+$ or producing IFNγ at one week after NP administration two later time points were also analyzed to see if the tolerizing effect was long lasting (Figure 42). The tolerizing effect of NP6 one week after NP administration disappeared in the following week but surprisingly the tolerating effect was detectable again at week six after NP administration (Figure 42, upper row).

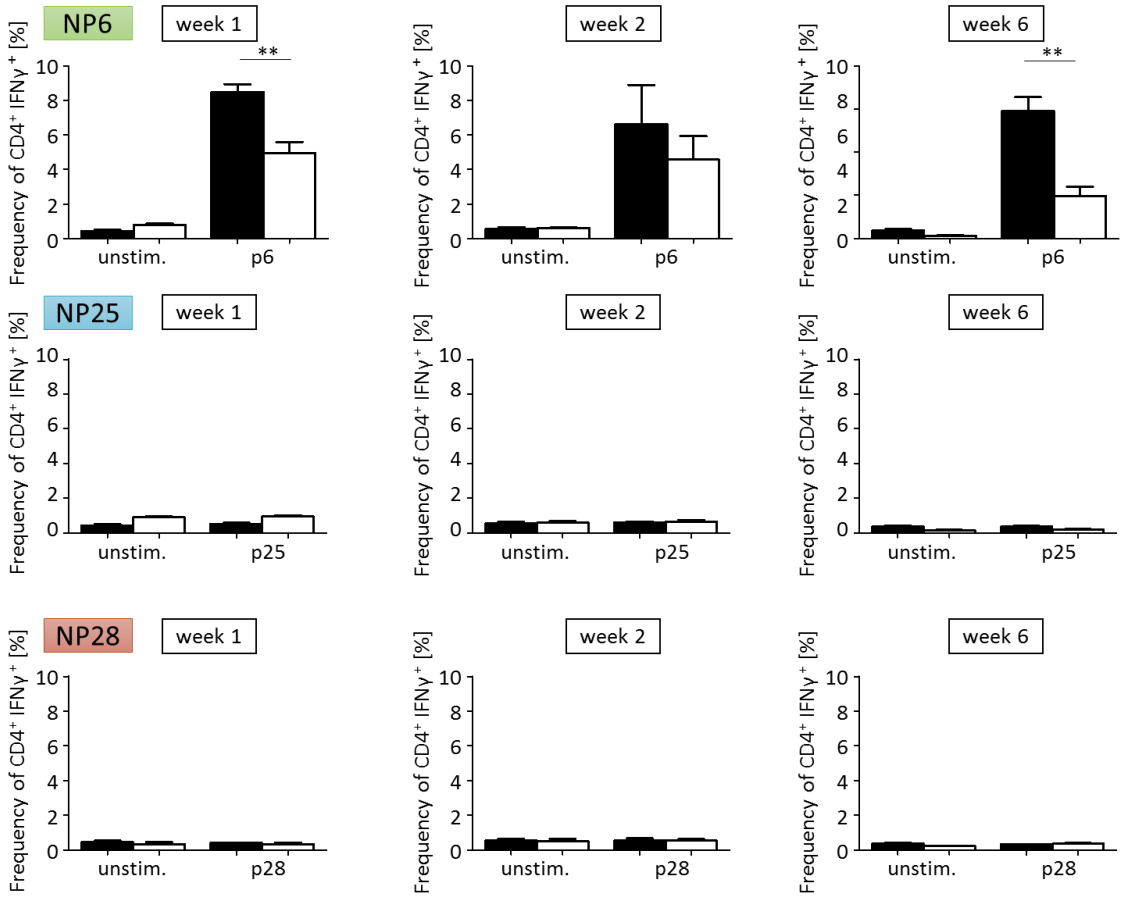

Figure 42: Frequency of hCYP2D6 specific $CD4^+$ T_{eff} in AIH mice over the time
AIH infected mice received i.v. 1.5 mg PLG-nanoparticle bearing either the immunodominant $CD4^+$ T cell epitope (NP6) or one of the two immunodominant $CD8^+$ T cell epitopes (NP25; NP28) two weeks after infection. Livers were harvested on different time points after NP administration. Lymphocytes were isolated and stimulated with different hCYP2D6-specific peptides overnight. After stimulation intracellular IFNγ production were then analyzes by flow cytometry. N=5.

The results of CD8⁺ T cells producing IFNγ one week after NP administration as well as two and six weeks later are shown in Figure 43. The tolerizing effect of NP25 which is shown as a very strong decrease in the frequency of CD8⁺ IFNγ⁺ T cells one week after NP administration disappeared in the following week and was not detectable again at week six after NP administration (Figure 43, middle row). The administration of the second CD8⁺ specific NP has no effect of CD8⁺ T cells producing IFNγ⁺ in tolerized mice at different time points.

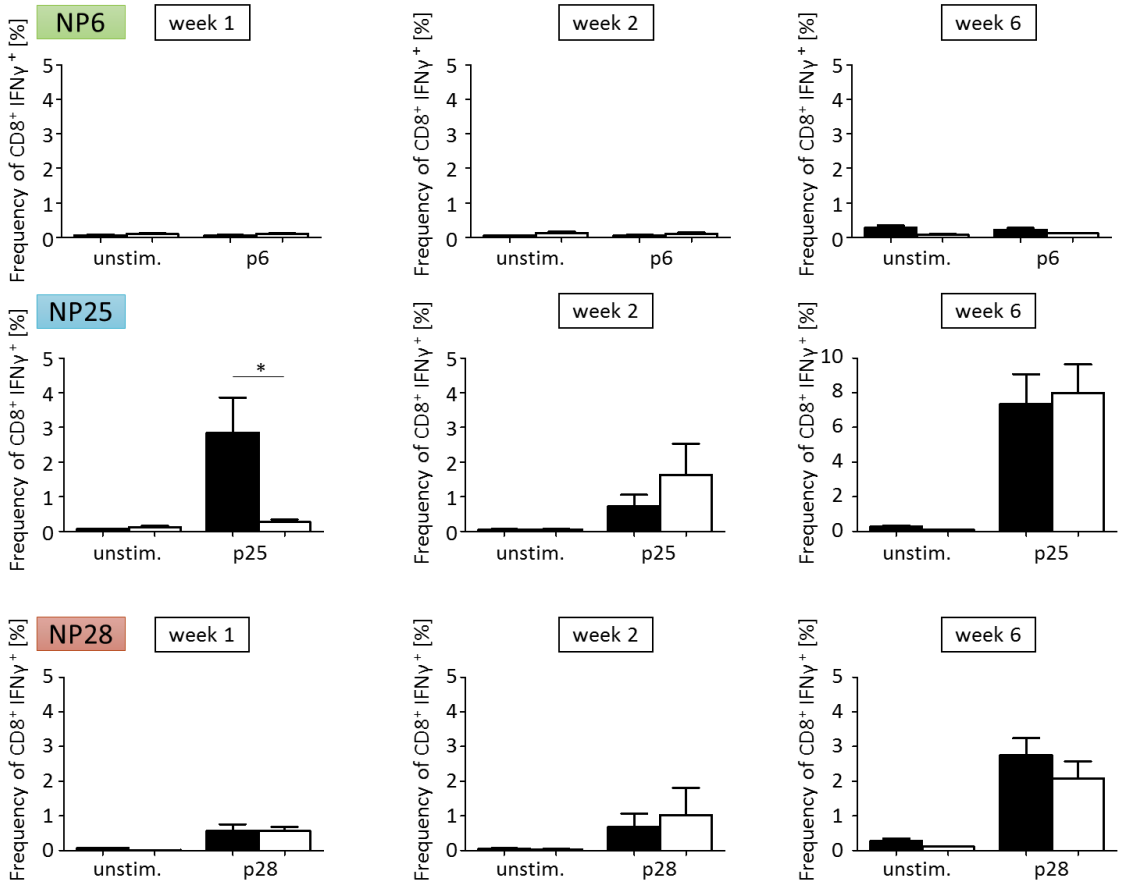

Figure 43: Frequency of hCYP2D6 specific CD8⁺ T_{eff} in AIH mice over the time
AIH infected mice received i.v. 1.5 mg PLG-nanoparticle bearing either the immunodominant CD4⁺ T cell epitope (NP6) or one of the two immunodominant CD8⁺ T cell epitopes (NP25; NP28) two weeks after infection. Livers were harvested on different time points after NP administration. Lymphocytes were isolated and stimulated with different hCYP2D6-specific peptides overnight. After stimulation intracellular IFNγ production were then analyzes by flow cytometry. N=5.

6. Discussion

Autoimmune hepatitis (AIH) and primary sclerosing cholangitis (PSC) are autoimmune diseases of the liver. Both diseases result in liver damage including fibrosis and cirrhosis. To date, there is no AIH- or PSC-specific therapy available to treat or prevent these diseases. In addition, the occurrences of patients who present with an overlapping syndrome (OS) of both diseases further complicate diagnosis as well as treatment. The aims of the study were first the generation of a mouse model which represents the PSC-AIH OS in humans and second to test different pathways of immune tolerance induction to treat AIH in mice.

6.1. Mouse model for human PSC-AIH overlap syndrome

By infecting *Mdr2*$^{-/-}$ mice with adenovirus Ad-2D6, which encodes human Cytochrome P450 2D6 to break immune tolerance, a novel animal model which represents features of human PSC-AIH OS was generated. This new animal model can be used to study PSC-AIH OS development and in addition to test new potential therapeutics for humans suffering from a PSC-AIH OS.

6.1.1. Analysis of laboratory parameters and autoantibodies in solitary PSC and AIH compared to PSC-AIH OS mice

The first characterization of the PSC-AIH OS mouse model included the analysis of liver damage markers, such as presence of liver enzymes in the serum and the detection of autoantibodies. The typical hallmark of PSC is an elevation of AP [258]. In this study, a two to three fold elevation of AP levels in *Mdr2*$^{-/-}$ mice compared to control group was detected. These data are compatible with data from Lammert et al, who showed that female *Mdr2*$^{-/-}$ mice with an age of nine weeks have AP levels about 395 ± 55 [259]. An increased serum level of AP about ≥1.5 times the upper limit of normal for at least six months is the most common biochemical factor detected in human patients with PSC

[260, 261]. In addition to elevated AP levels, a three to fourth fold increase in ALT levels in *Mdr2*$^{-/-}$ mice was measured. A similar elevation can be observed in PSC patients [262, 263]. Thus, the laboratory analysis of liver enzymes in *Mdr2*$^{-/-}$ mice showed that this animal model is very similar to PSC in human. Elevated AP levels were also seen in AIH mice. A condition that has also been observed with a two-fold increase up to normal in 21% of AIH patients [264]. Ad-2D6-infection induced an acute damage to the liver by destruction of hepatocytes which led to the release of ALT at week one to two post-infection [163]. The criteria for a PSC-AIH OS in human patients are elevated AP und ALT levels [265]. Interestingly, these laboratory parameters were highest in PSC-AIH OS mice compared to solitary AIH and PSC mice. ALT levels in the PSC-AIH OS group were increased during the acute phase and were still increased at week three to four post-infection. Further, the observation of the typical kinetic pattern might indicate that one AD of the liver was exacerbating the clinical markers of the other disorder.

In addition to the liver enzymes, total IgG was also elevated in AIH mice. This finding is also compatible with observation in AIH patients, who display levels that are 1.2 – 3 times higher than normal [255]. Hypergammaglobulinemia is not common for PSC patients, only 10 % of human PSC patients show elevated IgG4 values [252, 266]. The analysis of total IgG levels in *Mdr2*$^{-/-}$ mice revealed no elevation compared to control mice. The total IgG levels in the PSC-AIH OS mice were not higher than in mice with solitary AIH. One reason for this could be that in contrast to PSC patients, *Mdr2*$^{-/-}$ mice do not show elevated total IgG levels. Another reason for the missing additional elevation of total IgG levels in PSC-AIH OS mice could be the already very high levels in AIH mice that might be close to saturation and thereby preventing a further increase. The detection of LKM-1-like anti-CYP2D6 antibody was possible and at similar titers in AIH and PSC-AIH OS mice, indicating similar identical hCYP2D6-specific humoral responses in solitary AIH and PSC-AIH OS mice. One reason for this could be that the strong anti-hCYP2D6 response has reached saturation and was not further boosted in PSC-AIH OS mice. In addition, mice with solitary PSC did not form any anti-CYP2D6 antibodies. Thus, the *Mdr2*$^{-/-}$ background has no effect in the generation of LKM-1-like ab. This suggested that PSC-like liver injury triggering cholangitis did not break B cell tolerance to mouse Cyps. If this were the case, a cross-reactivity to hCYP2D6 would happen which might have resulted in a higher antibody titer in the PSC-AIH OS mice.

Moreover, human studies showed no observation of LKM-1 antibodies in PSC patients [267, 268]. The precise specificity of auto-antibodies in PSC is not clearly understood but auto-antibodies against components of the biliary epithelium or neutrophils seem to play an essential role.

The presence of pANCA as a serological marker for PSC, which can be found in up to 90% of PSC patients and is present in 60-90% of AIH patients, was also used to characterize our mouse model [269, 270]. It is known that AIH-1 patients have pANCA-like antibodies which are atypical because they react with peripheral nuclear membrane components [271]. Indeed, pANCA-like antibodies were detected in sera of AIH mice. In contrast, it was not possible to detect pANCA reactivity in sera of *Mdr2*$^{-/-}$ mice at week eleven of age. However, we know from other experiments that sera of *Mdr2*$^{-/-}$ mice with an age of 40 weeks display to a very strong fluorescent signal, indicating that between week eleven and 40 of age tolerance to some neutrophil autoantigens has been broken. Importantly, we found a strong increase in the fluorescent staining from solitary AIH mice to the PSC-AIH OS mice, which confirms the data of human studies in which 81% of the patients with PSC-AIH OS were positive for pANCA [193].

6.1.2. Cholangitis and fibrosis analysis of solitary PSC and AIH compared to PSC-AIH OS mice

It is known that cholangiocytes are the main target of injury leading to cholestatic liver damage [272–274]. Cholestatic liver injury damages bile ducts and induces the proliferation of cholangiocytes that can be linked to hepatic fibrosis [275–277]. *Mdr2*$^{-/-}$ mice represent a mouse model of PSC with a hyperproliferation of cholangiocytes and allow to studing cholestatic liver and bile duct injury. Ad-2D6 infection of *Mdr2*$^{-/-}$ mice resulted in increase of cholangitis suggesting that the severity of a cholestatic disease is enhanced in the concurrent presence of autoimmune-mediated hepatitis. Baghdasaryan et al could also show that *Mdr2*$^{-/-}$ mice develop a strong cholangitis at eight weeks of age [278]. In addition, treating these mice with a selective and potent apical sodium-dependent bile acid transporter (ASBT) inhibitor (A4250) reduced the number of proliferating bile ducts and hepatic inflammation.

In *Mdr2*$^{-/-}$ mice fibrosis started in the periportal region rather than around the central veins and was evolving to bridging fibrosis at later stages of the disease [279]. In AIH mice the fibrosis started around central veins mainly because of the i.v. injection of the virus. Ad-2D6 infection led to an activation of HSCs, which started to produce extracellular matrix components like collagen III resulting in chronic hepatic fibrosis [280]. The fibrotic pattern of the PSC-AIH OS mice nicely showed an overlap of fibrotic events coming from the PSC part (periportal region) and the AIH part (area around the blood vessels).

In addition to the histological analysis other methods to analyze fibrosis have been described. One possibility to determine collagen accumulation and thus the exact stage of fibrosis includes the hepatic hydroxyproline determination which is described as the `gold standard` [281]. Alternatively, the expression levels of fibrotic markers like αSMA, collagen I and collagen III can be analyzed on the protein or on the mRNA level by several methods, including Western blotting, RT-PCR, and protein/gene arrays.

6.1.3. Fibrogenic cell activation was highest in PSC-AIH OS mice

Fibrotic ECM is mostly derived from HSCs or PFs. If fibroblasts get activated by inflammatory mediators, they differentiate into αSMA-positive myofibroblast during fibrogenesis. After western blot analysis of αSMA in the homogenate of eleven weeks old mice an increase of the relative expression levels of αSMA could been observed only in the PSC-AIH OS group, but not in *Mdr2*$^{-/-}$ mice. Our findings are consistent with Ikenaga et al, who compared eight weeks old *Mdr2*$^{-/-}$ mice with FVB wild type mice and could not detect a higher activation of αSMA-positive myofibroblasts [282]. In addition, another group published a strong αSMA expression in two weeks old *Mdr2*$^{-/-}$ mice with a further increase in four weeks old mice. However, the αSMA expression decreased in eight weeks old mice [281]. Thus, the number of activated (αSMA-positive) HSCs seems to change with the age of the mice. A possible reason for this could be that αSMA is needed in the early stages of fibrogenesis and once the periductal fibrous ring had been developed αSMA-positive contractile elements are no longer required. This might explain why there were no activated HSCs in eleven weeks old *Mdr2*$^{-/-}$ mice detectable.

In contrast, a strong increase in the relative expression levels of αSMA in solitary PSC mice compared to PSC-AIH OS mice was seen. From the desmin characterization we know that *Mdr2*$^{-/-}$ mice have a high number of HSCs with the potential to be activated by an injury like Ad2D6-infection. Therefore, in the PSC-AIH OS mice such an elevated relative expression levels of αSMA does not come as a surprise. Taken together, livers of the PSC-AIH OS mice showed the highest fibrosis-specific ECM as well as ductular proliferation which were more than additive. It could be observed that *Mdr2*$^{-/-}$ mice display from a strong upregulation of cholangiocytes proliferation. This enhanced proliferation has been also detected in solitary AIH mice. Interestingly, 20% of AIH patients present with biliary injury and have not been classified as PSC-AIH or PBC-AIH OS [283]. This observation correlated well with the finding of our study. The reason for the strong fibrogenesis in the PSC-AIH OS group could be explained by two distinct activation pathways which may potentiate each other. In solitary AIH mice only HSCs differentiated into myofibroblast, whereas in PSC mice both myofibroblastic HSCs and PFs played a role. This strong fibrogenic cell activation was highest in PSC-AIH OS mice matching observations made in humans suffering from PSC-AIH OS. Such patients tend to develop a more aggressive form of autoimmune liver disease with poorer treatment response and higher risk of cirrhosis [284].

6.1.4. Strongest hepatic infiltration of immune cells was in the PSC-AIH OS model

The characterizations of liver infiltrating innate immune cells like monocytes/macrophages, DCs, and neutrophils showed the highest amount of these cells in the PSC-AIH OS model. Both solitary diseases PSC and AIH triggered a robust increase in monocytes/macrophages, whereas hepatic infiltration of neutrophils was more noticeable in PSC mice. This finding suggests that neutrophils might play a more important role in cholestatic diseases than in AIH. The fact that pANCA antibodies are specific for PSC patients may explain the importance of an increased number of neutrophils in the PSC mouse model. Nakken et al. observed in livers of *Mdr2*$^{-/-}$ versus

wild type mice an over 30-fold increase in mRNA encoding CCL2 which plays a role in neutrophil chemoattractant [285].

A study focusing on the pathological features of PSC patients showed that at the beginning of the disease histological changes of a diffuse mixed of inflammatory cell infiltrate containing neutrophils, but also lymphocytes and plasma cells tend to be located more intense around the bile ducts [286]. This publication confirmed the typical pattern of cell infiltration in *Mdr2*$^{-/-}$ mice which were also predominantly clustered and located around blood vessels and bile ducts. Importantly with regards to the development of a PSC-AIH OS model is that the infiltration of the liver by various leukocytes including CD4^{+} and CD8^{+} T cells was strongest in the PSC-AIH OS mice. Thereby a cumulative effect of the lymphocyte infiltrations from the PSC and AIH part was observed.

6.1.5. Characterization of auto-aggressive immune cells & immune balance

It is widely recognized that autoimmune liver diseases are mainly T cell mediated [287]. In this context it has been also shown that cytokines, such as interleukins, play an important role in the pathogenesis of the disease and can further lead to activation of hepatic innate lymphoid cells and natural killer T cells [288].

The characterization of the overall T cell balance in the PSC-AIH OS mice showed an overlap of the immune response of mice with solitary PSC and AIH. Naïve FVB wild type mice displayed an intact immune balance between type 1 and type 2 CD4^{+} T cells. This was to be expected since under normal physiological conditions, type 1 and type 2 CD4^{+} T cells, as well as the cytokines they secreted are in balance and they can cross-inhibit each other [289]. The strong type 1 CD4^{+} T cell response which was dominant in AIH mice resulted from the virus infection. It has been published already in the 1960s, that virus infections like influenza virus led to a strong induction of IFNs in chick cells [145, 290, 291]. In addition to the influenza virus infection, the infection with the respiratory syncytial virus also resulted in an increased number of respiratory syncytial virus – specific CD4^{+} T cells producing IFNγ [292]. It has been shown in our research group that

the infection with Ad-2D6 shifts the immune response toward a type 1 $CD4^+$ T cell response [163, 293]. All these experiments demonstrated that virus infections are in general responsible for a shift in the immune balance towards a type 1 $CD4^+$ T cell response. Several studies showed high levels of IFNγ expression in human AIH patients [293, 294]. Moreover, the mRNA expression of type 1 $CD4^+$ T cell cytokines was upregulated in AIH in childhood [294]. Immunosuppressive therapy with antagonizing effects of type 1 $CD4^+$ T cell response led to a decreased IFNγ expression in the liver [295]. AIH therapies focused on the downregulation of the type 1 $CD4^+$ T cell - predominant state showed the essential role of the type 1 $CD4^+$ T cell response in the induction of AIH [289]. The CYP2D6 mouse model for AIH represented nicely the dominant type 1 $CD4^+$ T cell response similar to the immune response in human AIH patients.

Type 17 $CD4^+$ T cells play an important role in the defense against fungi and bacteria but it is also known that these are involved in the pathogenesis of many ADs. IL-17A is the product of type 17 $CD4^+$ T cells and is described to promote inflammation and fibrosis in the liver. Yet the consequences of the increased IL-17 levels in the liver are not understood [296]. Studies on human PSC patients show an increased type 17 $CD4^+$ T cell response compared to healthy controls [297, 298]. In our study *Mdr2*$^{-/-}$ mice produced much more IL-17 in comparison to control mice. Our data confirm the results from another group who was measuring the IL-17 levels of *Mdr2*$^{-/-}$ mice via ELISA. In addition, they have shown an reduction of hepatic fibrosis after anti-IL-17A administration [296]. Moreover, Nakken et al., observed that *Mdr2*$^{-/-}$ versus wild type livers showed an over 200-fold upregulation of mRNA encoding CCL20 which is a type 17 T cell chemoattractant [299]. Taken together, the analysis of the overall T cell balance was useful to find an association between cytokine levels and the feature of the disease which further can be used as a treatment target by monoclonal ab, for example, antibodies against IL-12/IL-23 which was successful in ADs of the liver.

The analysis of the hCYP2D6-specific T cell response at week four post-infection showed a significant difference in the hCYP2D6 specific $CD8^+$ T cell response of PSC-AIH OS mice compared to solitary AIH mice. It is likely that the underlying chronic inflammation derived from PSC-like disease is potentiating the hCYP2D6-specific T cell immune response. In this context, it has already been published that *Mdr2*$^{-/-}$ are characterized by

a strong $CD8^+$ T cell response [300]. Unfortunately, until now, it was not possible to characterize the PSC-specific T cell response because the target auto-Ag which were needed for the stimulation have not been identified [301]. Anyhow, some human studies on PSC patients also showed a predominance of $CD8^+$ T cells [302, 303]. In contrast, other studies demonstrated a $CD4^+$ T cell predominance with a type 1 $CD4^+$ T cell response in PSC patients [304]. In a further study no difference in the ratio of $CD4^+/CD8^+$ T cells was observed [305]. These inconsistencies may be explained by the fact that $CD8^+$ T cells are the majority of lobular infiltrate, while $CD4^+$ T cells are mostly present in the portal infiltrate [306]. Studies which showed a higher frequency of $CD8^+$ T cells included PSC patients with a dominant lobular inflammation. The low antigen-specific $CD4^+$ T cell response in PSC-AIH OS mice compared to solitary AIH mice was somewhat surprising. The reason for this may lay in the overall $CD4^+$ T cell response of *Mdr2*$^{-/-}$ mice which showed a stronger type 17 $CD4^+$ T cell response than FVB mice. Ad-2D6 infection resulted in an increase in type 1 $CD4^+$ T cells in both mice strains but this effect was stronger in FVB that in *Mdr2*$^{-/-}$ mice, which carried over the lager type 17 $CD4^+$ T cell compartment. Thus, the overall weaker type 1 $CD4^+$ T cell response in PSC-AIH OS mice may lead to a lower frequency of hCYP2D6-specific $CD4^+$ T cells.

6.1.6. Conclusion Project 1: Generation of a PSC-AIH OS mouse model

The challenge of generating an animal model lays in the fact that it needs to reflect the human disease and its consequences as much as possible. The new mouse model in which *Mdr2*$^{-/-}$ mice were infected with Ad-2D6 was characterized with regards to serological markers like AP and ALT levels. In addition the total IgG was measured as well as the titer of auto-antibodies directed against CYP2D6 (LKM-1-like) and neutrophils (pANCA-like). Fibrosis and cholangitis were analyzed on protein levels and via different immunohistological stains. Moreover, cellular infiltrations of $CD4^+$ and $CD8^+$ T cells, DCs, monocytes/macrophages and neutrophils were determined with immunohistochemistry. Finally, the immune balance and CYP specific T cells were analyzed via flow cytometry. The PSC-AIH OS mouse model which was generated in this study shows the characteristics of both PSC and AIH and mimics features of the human

PSC-AIH OS (Figure 44). The new mouse model allows studying the development of a PSC-AIH OS and how the two overlapping diseases are influencing one another. In this study I have analyzed the influence of a hepatocyte-targeting autoimmune disease and a pre-existing chronic hepatobiliary inflammation in terms of biochemical, serological and immunocellular parameters, but there are still many aspects in need of detailed investigation. It is likely that a complex interplay between a multitude of cell types like B and plasma cells as well as chemokines, cytokines and other factors play a role in the OS. The identification of important driving factors for the OS would allow to evaluate treatment regimens. For example, it would be interesting to use monoclonal antibodies against critical cytokines, such as antibodies against IL-12 or IL-23. Moreover, the administration of dihydroorotate dehydrogenase (DHODH) inhibitor which can block the enzyme for the biosynthesis of pyrimidine nucleotides or RORγ inhibitor are two very promising options to test in the PSC-AIH OS model. RORγ inhibitor which targets the transcriptionfactor of T_H17 cells can maybe reduce the very high amount of type 17 T cell response in the PSC-AIH OS model as well as in solitary PSC. In addition, it would be interesting to see if UDCA has in impact of the OS or can only reduce the PSC part in PSC-AIH OS mice.

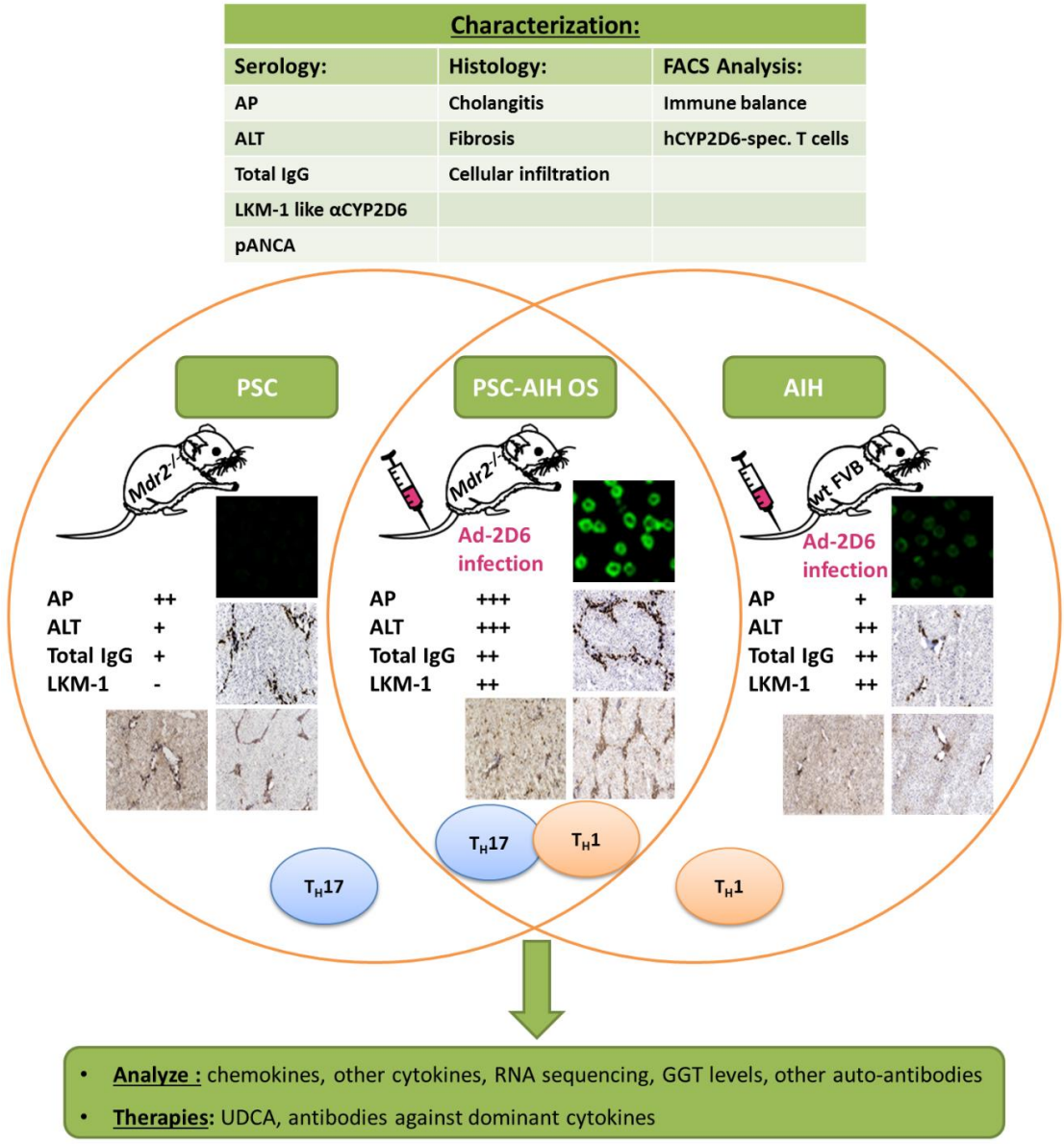

Figure 44: Generation and characterization of the PSC-AIH OS mouse model compared to solitary mouse models of PSC and AIH

6.2. Therapeutic tolerance induction as a therapy for AIH

The second aim of my work was to try different approaches to induce CYP2D6-specific tolerance in an AIH mouse model. In the last past years, it was shown that reestablishment of immune tolerance in patients with ADs is a successful and very promising strategy.

6.2.1. Transfer of VitD3 and Dex-modulated DCs carrying hCYP2D6-peptides

In the last years, many protocols have been published which describe the generation of human monocyte-derived tDCs. In addition, first phase I trials have been done in patients with an ADs like RA, Chron´s disease, and T1D [307–310]. The generation of tDCs which can be used for the restoration of immune tolerance was a promising approach with a high potential to treat AIH in mice.

The stimulation of BMDCs with VitD3 and Dex allows differentiating immature DCs into tDCs [311, 312]. tDCs are characterized by a semi-mature phenotype with a low MHC class II expression as well as a low expression of costimulatory molecule CD86 [313]. Thereby, the combination of both substances VitD3 and Dex leads to a more tolerogenic phenotype than with only one substance [314]. In comparison to the VitD3 and Dex-stimulated tDCs the control DCs expressed high MHC class II levels as well as high costimulatory molecule CD86 which are typical for the expected mature phenotype of DCs [315]. These observations could be confirmed in this study. Moreover, the stimulation with VitD3 is known to increase the expression of PD-L1 [316]. In this study, only a trend towards a stronger PD-L1 expression could be observed by flow cytometry. All in all, the stimulation of BMDCs with IL-4 and GM-CSF together with VitD3 and Dex resulted in tDCs which showed a superior tolerogenic phenotype, similar to published data [311, 312]. After this successful differentiation of tDCs, these cells were injected i.v. into AIH mice on day 12 after Ad-2D6 infection. Thereby, tDCs were compared with mature or stimulatory DCs which were only stimulated with IL-4 and GM-CSF.

It has been shown by others that VitD3 treated DCs are able to activate and induce the expansion of T_{reg}, as well as transfer regulatory properties to T cells or differentiate naïve T cells to T_{reg} [317]. In our hands, the expected higher frequency of T_{reg} and lower frequency of auto-aggressive $CD4^+$ or $CD8^+$ T cells after i.v. injection of tDCs compared to untreated Ad-2D6 infected mice was missing. One reason for this could be that 12 days after Ad-2D6 infection was too late for cell transfer and it did not represent the early-onset of the disease. Second reason could be that the i.v. injection of tDCs was not the right way of application, although it was shown in an EAE model that i.v. injection of tDCs led to a decrease in clinical symptoms in the mice [318, 319]. Another study shows that i.p. injection of tDCs leads to reestablish the immune balance in human patients with Crohn's disease [309]. Third reason could be that the injected number of $2x10^5$ cells was too low to reestablish the immune balance. Another publication shows that the amount of $8x10^5$ cells are able to turn around the immune system [319]. Moreover, another group shows in an experimental model for heart transplantation that the use of $2x10^6$ cells one week before transplantation can promote peripheral transplantation tolerance [320]. Fourth explanation for the failure to succeed could be the loading of the tDCs was not done with the optimal disease specific antigens. Maybe there are other CYP2D6 antigens which are more potential by promoting antigen-specific T_{reg} differentiation.

Taken together, the use of tDCs to induce immune tolerance induction in AIH mice failed. There are many reasons for this including the optimal dose, route of administration, loading the cells with the optimal antigens, and the number of required booster injections [321]. It is therefore planned to adapt the treatment protocol in order to address these problems.

6.2.2. Intranasal treatment to induce immune tolerance in AIH mice

In the second approach, we used i.n. treatment of AIH mice with hCYP2D6 peptides together with two adjuvants. Unfortunately, this approach did not succeed in reestablishing immune tolerance. In this study, mice were treated five times every third day with 100 µg of the immunodominant $CD4^+$ and $CD8^+$ T cell epitopes in combination

with 10 µg of the adjuvants CpG and Poly IC. Afterwards, they got an Ad-2D6 infection and one week later, mice were sacrificed. The result of this approach showed no differences in the frequency of $CD4^+$ or $CD8^+$ $IFN\gamma^+$ T cells between the groups. One reason for the lack of success could be that first the amount of peptides which the mice received was too low. We had chosen to use 100 µg of the immunodominant $CD4^+$ and $CD8^+$ T cell epitopes according to a publication of Anderton et al. which shows that 100 µg peptide per dose every second day before induction of disease was sufficient to induce immune tolerance in an EAE model [322]. In contrast, there are other publications that report treatment with at least 0.5 mg up to 2 mg [323, 324]. In clinical trials, as well as in mouse models of T1D and MS, tolerization with high doses of peptide usually has stronger effects due to induction of IL-10 secretion by T_{reg} but the risk for potential side effects is also increased, especially at the beginning of the therapy [325]. Second, the created treatment protocol regarding the duration of treatment and also the days of application was not the optimal treatment protocol. The previously mention publications describe that the mice received the i.n. application according to several different regimen. Third, it has been demonstrated in an EAE model that not all peptides of MBP and proteolipid protein (PLP) led to tolerance induction. The forth reason for the lack of success could be that T cell epitopes cannot induce immune tolerance. Barbey et al. showed that the i.n. treatment with the complete OVA protein, but not with the major OVA peptide, has the capacity to activate T cells and induce IL-10 production resulting in T cell-specific tolerance via the nasal route [323]. Taken together, the choice of peptide, the dose of peptide, duration of treatment und route of administration were critical factors which could influence the success of the therapy [326–330].

6.2.3. Injection of Ag-coupled splenocytes boosted the frequency of inflammatory T cells

Previous studies in EAE mice show that ECDI-coupled splenocytes loaded with the disease specific antigens on the cell surface is inducing robust antigen-specific tolerance and protect mice against the disease [227, 331].

The transfer of hCYP2D6-peptides with and without ECDI led in both cases to an increase of specific $CD4^+$ and $CD8^+$ T cells compared to the transfer of SP-ECDI without antigen. This observation might suggest that the crosslink probably did not work. However, we used ECDI from two different companies, including the one which our cooperation partner recommended us. One publication focused on the effect and the need of ECDI in which is shown that soluble antigens with splenocytes and without ECDI can interact and were able to create only a weak binding [331]. It is reported in animal experiments in which soluble antigens in comparison to Ag-ECDI-SP were i.v. injected did not result in immune tolerance [236]. Only the Ag-ECDI-SP has the potential to induce immune tolerance. The advantage of ECDI is a nonspecific cross-link of antigens to cells to be perceived by the host in a noninflammatory manner [332]. Soluble injected antigens have the risk to induce an IgE-mediated anaphylaxis which was observed in an EAE model in which the mice died shortly after the injection [236]. In this study the mice did not die from an anaphylactic shock but symptoms of anaphylaxis like skin rashes, shortness of breath, trouble breathing have not been checked. We did not observe obvious symptoms of severe anaphylaxis in mice of this study but a high cytokine production was measured in mice which received the splenocytes and antigens with and without ECDI compared to the group treated with SPL-ECDI. Moreover, it is published that not all antigens led to anaphylaxis. Depend on the fact if the antigens were expressed in the thymus or not. Study on some myelin antigens show that antigens which were not expressed in the thymus led to anaphylaxis [333]. To date, there are no publications available which show whether mouse Cyp are expressed in the thymus or not.

6.2.4. CYP2D6 specific nanoparticles increased the frequency of T_{reg}

In a fourth approach we tried to induce immune tolerance in AIH mice using CYP2D6-peptide coated NP, which were created in the lab of Stephen Miller, Northwestern University Chicago. There are many publications which show the successful treatment of mice with an AD by using antigens coupled NP [101, 243, 244, 248–250]. In this study two out of three different CYP2D6 specific NP were able to significantly increase the amount of CYP2D6 specific $CD4^+$ T_{reg} two weeks after NP injection. At the same time

point, the frequency of $CD4^+$ and $CD8^+$ $IFN\gamma^+$ T cells were significantly reduced in both groups which also showed the increase of T_{reg}. This observation shows that two out of three NP worked. The tolerizing effect of the NP6 which is specific for $CD4^+$ T cells was present one and also six weeks after NP injection but not detectable two weeks after NP injection. In contrast to NP6, the NP25 which is specific for $CD8^+$ T cells displayed a tolerizing effect only one week after NP injection. In addition, the other specific $CD8^+$ T cells NP28 showed no tolerizing effect and did not reduce the frequency of inflammatory T cells. The lacking success after NP28 treatment might be due to its absence in the thymus or the smaller size of the NP on which the antigen was presented, compared to the other NPs which were used in this study.

Many publications show that NP which are i.v. injected will stuck in the liver [101]. Depending on the size of the NP they will be taken up by DCs if they have a size range form 20 – 500 nm [334–336]. If they have a size range from 0.5 – 5 µm NP will be taken up by macrophages [337]. Carambia et al., have shown microscopically that NP are taken up in the liver by LSECs [101]. In this study the size of the NP was 590 nm for N6, 552 nm for NP25 and 482 nm for NP28. The smaller size of the NP28 might be also a reason for the lacking success. Even it is only a small difference in the size of the NP, it could have an influence of the type of cells which take up the NP and present it to other cells. We have not investigated which cells are taking up our NP in this study. However, it has been demonstrated that mice with AIH in the CYP2D6 model, NP are mainly taken up by Kupffer cells and other macrophages [338].

The induction of immune tolerance by using NPs depends on many critical factors which can influence the success of the therapy. First, NPs have to be loaded with the correct antigen. This antigen has to target to APCs and finally needs the capacity to induce immune tolerance by supporting the induction or expansion of T_{reg}. The primary hurdle for antigen-specific immune tolerance induction is the identification of the disease-associated antigens and their epitopes [242]. For AIH-like disease in the CYP2D6 model the epitopes which are associated with the disease have been identified [257]. From other ADs it is known that the appropriate target antigen may change over time due to epitope spreading which make the tolerating strategy much difficult. In a mouse model for T1D it could be prevented by autoantigen-specific immunotherapy in the early stages with the initiating peptide, whereas in the late stage a mixture of several peptides had

to be administered [339]. This demonstrates the frequent increase in the pool of autoantigens during AD. Therefore, it would be worth it to think about to use a pool of different antigens to increase the success rate of immune tolerance induction.

6.2.5. Conclusion Project 2: Therapeutic tolerance induction as a therapy for AIH

Various studies have shown that therapeutic immune tolerance induction can be used to prevent ADs. In the second part of my project I wanted to induce immune tolerance induction in AIH mice on different approaches. The four different approaches were the intranasal peptide administration, injection of tDCs, antigen-coupled splenocytes and antigen-coupled NP. Unfortunately, only the NP approach did induce CYP2D6 specific T_{reg} with a possible capacity to prevent AIH in mice. Two out of three different NPs had the potential to increase the amount of T_{reg} and to reduce the frequency of inflammatory T cells but this effect was not long lasting. However, this moderate shift in immune balance was not sufficient to prevent AIH. Nevertheless, the results represent a first promising approach to induce CYP2D6 specific tolerance in AIH mice but this approach has to be refined in the future. Critical factors like antigen concentration, route and frequency of administration need to be optimized and might play an essential role in influencing the success of the treatment. Moreover, the outcome has to be characterized in more detail. Taken together, it was really surprising that it is so difficult to induce immune tolerance in an organ like the liver that is considered tolerogenic to begin with and contains so many different tolerogenic cells including LSECs and HSCs. In the past many attempts to generate a model for chronic AIH have failed due to the tolerogenic nature of the liver. Thus, one might conclude that once tolerance in the liver has been broken it is particularly difficult to reestablish a healthy state.

7. Materials and Methods

7.1. Materials

7.1.1. Antibodies

ELISA:

Table 1: Antibodies used for ELISA

Antibody	Company
Goat anti-mouse IgG (H+L)-AP conjugate	Bio-Rad; 170-6520
Mouse anti-human SMA (clone 1A4)	Dako, 00053049

FACS-staining:

Table 2: Antibodies used for FACS-staining

Antibody	Company
7-Aminoactinomycin D	Sigma; A9400
Anti-mouse CD3e (clone 145-2C11)	eBioscience; 16-0031-82
V450-anti-mouse CD4 (clone RM4-5)	BD Horizon; 560468
Brilliant Violet 510-anti-mouse CD8a (clone53-6.7)	BioLegend; B231462
Anti-mouse CD16/32	BioLegend; B249157
Anti-mouse CD28 (clone 37.51)	eBioscience; 16-0281-82
PE-Cy7-anti-mouse CD86 BD (clone GL1)	Pharmingen; 560582
APC-anti-mouse CD11c (clone N418)	eBioscience; 17-0114-81
PE-anti-mouse/rat FoxP3 (clone FJK-165)	eBioscience; 12-5773-82
APC-anti-mouse IFNγ	BD Pharmingen; 554412
PE-Cyanine7 IL-4 (clone BVD6-24G2)	eBioscience; E07663-1636
FITC-anti-mouse IL10 (clone JES5-16E3)	eBioscience; 11-7101-82
FITC- IL17 (clone eBio17B7)	eBioscience; 53-7177-81
V450-anti-mouse MHC Class II (clone M5/114.15.2)	eBioscience; 48-5321-82
PE-anti-mouse PDL1 (clone MIH5)	BD Pharmingen; 558091

Histology:

Table 3: Antibodies used for Histology

Antibody	Company
Rat anti-mouse CD4/L3T4 (clone GK 1.5)	BD Pharmingen; 553043
Rat anti-mouse CD8a/Lyt-2 (clone 53-6.7)	BD Pharmingen; 553027
Rat anti-mouse CD11b (clone M1/70)	eBioScience; E015675
Biotin anti-mouse CD11c (clone N418)	eBioScience; 4292345
Rat anti-mouse Ly6G (clone 1A8)	BioXCell; BP0075-1
Mouse anti-mouse α-SMA	Dako; M0851
Rabbit anti-mouse Collagen I	Milipore; 2620158
Rat anti-mouse cytokeratin 19	TROMA-III; AB_2133570
Rabbit anti-mouse Desmin	Abcam, ab15200
Donkey anti-rabbit Alexa Fluor 488	Invitrogen; A21206
Goat anti-rat Alexa Fluor 594	Invitrogen; A11007
Biotinylated anti-goat IgG (H+L)	Vector; BA-5000
Biotinylated anti-rabbit IgG (H+L)	Vector; BA-1000
Biotinylated anti-rat IgG (H+L)	Vector; BA-4001

Western Blot:

Table 4: Antibodies used for Western Blot

Antibody	Company
Mouse anti-α SMA	Dako; M0851
Mouse anti-ß-actin	Sigma; A5441
Rabbit polyclonal Desmin	Abcam; 40324
Goat anti-mouse IgG (H+L)-AP konjugiert	Bio-Rad; 170-6520

7.1.2. Cell lines

AD-293 cells are adherent epithelia cells coming from the human fetal kidney. This cell line was used for the adenovirus production and was ordered by Agilent Technology.

Human promyelocytic leukemic HL-60 cells were cultured in RPMI-1640 plus GlutaMAX containing 10% FCS and 1% antibiotics.

7.1.3. Chemicals

Table 5: Chemicals

Chemical	**Company**
Acetic acid	Sigma Aldrich Chemie GmbH; 33209
Acetone	Sigma Aldrich Chemie GmbH; 32201
Acrylamid (30 %)	Merck Chemicals KGaA; 100639
Ammonium acetate	Merck Chemicals KGaA; 1.01116
Ammonium chloride	Merck; 1.01145
Ammonium peroxide sulphate (APS)	Sigma Aldrich Chemie GmbH; A3678
Ammonium sulphate	Merck Chemicals KGaA; 101211
Aquamount	Merck Chemicals KGaA; 1.08562
β-mercaptoethanol	Gibco; 31350-010
Bisacrylamide (2 %)	Roth; 3029.2
Brefeldin A	Sigma Aldrich Chemie GmbH; B6542
Bromophenol blue	Roth; 512.1
Calcium chloride di-hydrate	Merck Chemicals KGaA; 1.02382
Chloroform	Sigma Aldrich Chemie GmbH; 32211
Dc Protein assay Reagent A Reagent B Reagent S	BioRad 500-0113 500-0114 500-0115
Dimethyl sulfoxide (DMSO)	Sigma Aldrich Chemie GmbH; D5879
Dithiothreitol (DTT)	Fluka; 43817
DMEM + GlutaMax I	Gibco; 61965
DTT (1,4-Dithiothreit)	Roth; 6908.1
ECDI	Merck, S6440507546
ECF substrate	Amersham Bioscience; RPN 5785
Ethylenediamintetraacetic acid (EDTA)	AppliChem; A1103.1000

Ethanol absolute	Sigma Aldrich Chemie GmbH; 24102
FACS Clean	BD Biocience; 340345
FACS Flow	BD Biocience; 342003
FACS Shutdown	BD Biocience; 334224
FCS (Foetal calv serum) heat inactivated	Biochrom AG; S0115
Formaldehyde	Roth; 6749-2
Glycerol	Roth; 3783.1
Glycine	Roth; 3908.2
GM-CSF	R&D; BJ2416101
Haematoxylin	AppliChem A4840.1000
HEPES	Sigma Aldrich Chemie GmbH; H0887
Hydrogen peroxide	Roth; 8070.1
Isoflurane	Abbott; B506
Isopropyl alcohol	Prolabo; R11-36-67
Lipopolysaccharide (LPS)	Sigma Aldrich Chemie GmbH; L 2654
Methanol	Roth; T909.1
Mounting Medium Vectashield Hard Set	Vector Laboratories; H-1400
Non-Essential Amino Acids	Gibco; 11140
OCT solution (Tissue-Tek)	Sakura; 4583
Paraformaldehyde	Merck; 1.04005.1000
PBS	Gibco; 14190
Potassium acetate	Sigma Aldrich Chemie GmbH; P1190
Potassium chloride	Roth; 6781.1
Potassium di-phosphate	Merck; 1.05099
di-Potassium phosphate	Roth; 3904.1
Penicillin-Streptomycin	Gibco; 15140
Percoll	GE Healthcare; 17-0891-01
Peroxidase substrate	Vector; SK-4100
RPMI 1640 + GlutaMax I	Gibco; 61870
Saponin	Sigma Aldrich Chemie GmbH; S7900
Skim milk powder	Töpfer Allgäu; 60226

Sodium azide	Appchem; A1430
Sodium chloride	Sigma Aldrich Chemie GmbH; 31434
Sodium hydroxide	Riedel-de Haën; 30620
di-Sodium phosphate di-hydrate	VWR; 28029.292
Sodium dodecyl sulphate (SDS)	Roth; 2326.2
Sodium pyruvate	Gibco; 11360
TEMED	Roth; 2367.3
Tris	Roth; 4855.2
Tris-HCl	Roth; 9090.2
Triton X-100	Sigma; T8787
Trypan blue	Sigma; T8154
TWEEN 20 (Polyethylen-Sorbitan-Monolaureat)	Sigma Aldrich Chemie GmbH; P7949
Vitamin D_3	Enzo Life Sciences

7.1.4. Laboratory equipment and consumables

Table 6: Laboratory equipment and consumables

Equipment or material	**Company**
70 µm / 100 µm nylon cell strainer	BD Falcon; 352350; 352360
96- well ELISA plates	Anicrin; 3911925
96- well U- and V-bottom plates	Nerbe Plus GmbH; Anicrin 3911924
ALT and AP test stripes	Roche
Anesthesia unit 1200	Univentor
Autoclave v-150	Systec
BD Microtainer SST ™ Tubes	BD Falcon
Capillary (Heparin coated)	Fisher scientific; 02-668-10
Cell culture flasks (25, 75, 175 cm^2)	Cellstar
Cell scraper	Sarstedt; 83.1830
Cell strainer (70 µm, 100 µm)	BD Falcon

Centrifuge, 5804	Eppendorf
Centrifuge. Multifuge 3S-R	Thermo Scientific
Corning®Costar®Stripette®serological pipettes (5 ml, 10 ml, 25 ml, 50 ml)	Sigma-Aldrich Co
Coverslips (24x40 mm)	Menzel-Gläser
Cryomolds	Fisher Scientific
Cryostat Leica CM1850 UV Leica	Biosystem GmbH
Cryotubes, Cryo pure (2 ml)	Sarstedt; 72.379.002
Eppendorf tubes (0.5 ml, 1.5 ml, 2 ml)	Eppendorf
FACS-tubes	BD Falcon; 352052
FACS Unit Canto II	BD
Falcon tubes (15, 50 ml)	Greiner Bio-One
Liquid Blocker Pap-Pen	Daido Sangyo Co
Micro Blood Collection Tubes	Fischer Scientific
Microscope Axiovert 25C	Zeiss
Confocal Microscope LSM 510 META	Zeiss
Microscope Axioskop 2	Zeiss
Microscope Biozero, BZ-8000K	Keyence
Microscope Slides Fischerbrand™ Superfrost™ Plus	Fisher Scientific; J1800AMN
Micro scale, CP153	Sartorius
Microtainer Capillary Blood Collection Tubes	BD Medical
Multichannel pipette	Eppendorf, Hamburg
Needles (23G, 27G, 30G)	Braun Melsungen AG
Pipett tips (10 µl, 20 µl, 200 µl, 1000 µl)	Sarstedt AG & Co
PVDF Transfer Membrane	PolyScreen; NEF1002
Sialin coated slides	Menzel-Gläser; J1800AMN/
Sterile Filter (50, 250, 500 ml)	Millipore
Syringes (0.5, 1, 3, 5, 10, 20 ml)	B.Braun
Tissue culture dishes	Greiner Bio-One
Tissue culture plates (6, 12, 24, 48, 96 well)	Cellstar

Water bath, Isotemp 215	Fisher Scientific
Whatman paper	Whatman International Ltd.

7.1.5. Enzymes and proteins

Table 7: Enzymes and proteins

Protein	**Company**
Collagenase P	Roche; 11 213 857 001
Collagenase IV	Sigma
Cytochrome P450 2D6 recombinant protein	MyBiosoure MBS2009858
Dexamethasone	Sigma; D4902
DNase	Sigma; DN25
GM-CSF (recombinant mouse)	R&D Systems; 415-ML
IL-2	Sigma-Aldrich
IL-4 (recombinant mouse)	Peprotech; 214-14
Protease inhibitor cocktail tablets	Roche; 11 873 580 001

7.1.6. Composition of buffers, solutions and culture media

Table 8: Composition of buffers, solutions and culture media

Solution	**Composition**
ABC reagent solution (Peroxidase Substrate Kit DAB)	5 ml ddH_2O 2 drops of buffer 4 drops of DAB stock solution 2 drops of hydrogen peroxide solution
APS stock (10%)	APS 10 % (w/v) store at 4 °C
Blocking buffer Western Blot	PBS 5 % milk powder 0.1 % Tween-20
Cell freezing medium	90 % FCS

	10 % DMSO
Collagenase buffer	PBS 0.2 mg/ml collagenase IV 0.02 mg/ml DNase 5% FCS
Culture Medium (Ad293)	DMEM + Glutamax I 10 % FCS 1% Pen/Strep 1% NEAA 1% HEPES 1% Pyruvat
DNase stock	20 µg/ml DNase
ELISA blocking buffer	PBS 2 % FCS
ELISA coating buffer	PBS 50 mM Na_2CO_3 50 mM $NaHCO_3$ pH 9.6
ELISA washing buffer	PBS 0.05 % Tween-20 1% FCS
Erythrocyte lysis buffer	0.83 % NH_4Cl in ddH_2O sterile filtrated
Erythrocytes Lysing Solution (10x)	Dissolve in 500 ml H_2O 44.95 g NH_4Cl 5.0 g $KHCO_3$ 1 ml EDTA 0.5 M pH 8.0 Adjust pH to 7.3 sterile filtrated, store at 4°C
FACS fixation buffer	PBS 1 % FCS

	0.1 % NaN_3 1 % PFA pH 7.5
FACS PBS/saponin buffer	PBS 1 % FCS 0.1 % NaN_3 0.1 % saponin pH 7.5
FACS PBS/staining buffer	PBS 1 % FCS 0.1 % NaN_3 pH 7.5
FACS PFA/saponin buffer	PBS 0.1 % saponin 4% PFA pH 7.5
FCS (Foetal calf serum)	Biochrom AG; S0115
H_2O_2 solution	0.3% H_2O_2 0.1 % NaN_3 PBS
Laemmli buffer 2x	50 mM Tris 10% Gycerol 2 % SDS 40 mM DTT pH 6.8
Liver perfusion buffer	RPMI 2 mg/ml collagenase IV 0.02 mg/ml DNase 5 % FCS 1 % HEPES
Lower gel buffer	1.5 M Tris-HCl

	pH 8.8
Phosphate buffered saline (PBS)	140 mM NaCl 10 mM KCl 6.4 mM Na_2HPO_4 2mM KH_2PO_4
Protein sample buffer (4x) reducing	40 % v/v Upper gel buffer 40 % v/v Glycerol 2 mM SDS 40 mM DTT 10 % v/v bromophenol blue
Lysis buffer for Western Blot	ddH_2O 40 mM Tris (pH 7.5) 150 mM NaCl 1 % Triton X-100 6 mM EDTA 10 % Gylcerol 1 % Na-deoxycholate 0.1 % SDS 1 tablet protease inhibitor (Roche) /50 ml
RPMI 1640 + GlutaMax I	Gibco; 61870
RPMI 1640 + GlutaMax I complete	RPMI 1640 (+glutamax-I) 1 % Pen/Strep (100u/ml) 10 % FCS
Running buffer (10x)	250 mM Tris 1.92 M Glycine 1 % SDS pH 8.3
Tissue Culture Medium (TCM)	RPMI 1640 (+glutamax-I) 1 % Pen/Strep 5 % FCS

	$5x10^{-5}$ M β-mercaptoethanol
Tissue Culture Medium without FCS (TCM-)	RPMI 1640 (+glutamax-I) 1 % Pen/Strep 5 % Mouse Serum $5x10^{-5}$ M β-mercaptoethanol
Transfer buffer	1.44 % Glycine 0.3 % Tris 80 % v/v ddH_2O 20 % v/v MeOH
Tris buffer (pH 7.5)	Tris 1 M pH 7.5
Upper gel buffer	0.5 M Tris-HCl pH 6.8
35 % Percoll buffer	35 ml Percoll 4 ml 10x PBS 60 ml 1x PBS sterile filtrated

7.1.7. Kits

Table 9: Kits

Kit	**Company**
ABC-Kit	Vector; PK-7100
Adeno X-rapid Titer Kit	Clontech; 1503860A
Avidin/Biotin blocking kit	Vector; SP-2001
DC Protein Assay	Bio-Rad; 500-0113/-0114/-0115
M.O.M. ™ Immunodetection Kit	Vector; BMK-2202
Peroxidase Substrate Kit DAB	Vector; SK-4100
Reflotron® AP and GPT	Roche; 26780901; 26205401

7.1.8. Mouse stains

AIH model: Wild type FVB/NHsd mice were purchased from the breeding colony of Harlan Netherlands. PSC model: *Mdr2*$^{-/-}$ mice on a FVB/NHsd background and wild type FVB/NHsd mice were from Jackson Laboratory (Jackson Laboratory, Bar Harbor, ME). *Mdr2*$^{-/-}$ mice develop spontaneously progressive biliary fibrosis. Experiments were carried out with age- and sex-matched animals kept under specific pathogen free (SPF) conditions and mice were handled in strict accordance with good animal practice. All animal work was approved by the local Ethic Animal Review Board, Darmstadt, Germany.

7.1.9. Nanoparticles

Table 10: Nanoparticles

Antigen	Batch	Z-avg diameter	Zeta potential	Encapsulation (µg peptide/mg particle)
P6	P6100416	590	-75	5.995+/-1.357
P25	CD8A110816	552	-91	7.197+/-1.04
P28	CD8B100616	482	-79	8.685+/-1.002

7.1.10. Nucleotides and nucleic acids

Table 11: Nucleotides and nucleic acids

Nucleotides and nucleic acids	Company or Reference
CpG	IDT; ODN1826
Poly(I:C)	Sigma; P9582
61x 20mer sequences of cytocrome P450 2D6	Ma et al. Gastroenterology 2006

7.1.11. Peptides

Table 12: Peptides for hCYP2D6 specific stimulation

Name	Sequence	Company
Peptide 6	PGLGNLLHVDFQNTPYCFDQ	GenScript Corporation
Peptide 21	CAAFANHSGRPFRPNGLLDK	GenScript Corporation
Peptide 25	RRFEYDDPRFLRLLDLAQEG	GenScript Corporation
Peptide 28	SGFLREVLNAVPVLLHIPAL	GenScript Corporation

7.1.12. Virus

Mice were infected with an Adenovirus containing the Vector Ad5-hCyp2D6. The virus was grown in Ad-293 cells and titer was determined with the Adeno-X rapid titer kit (Clontech). For the regular CYP2D6 AIH model to find novel tolerogenic therapies, mice were infected with $3x10^8$ pfu intravenously and $3x10^8$ pfu intraperitoneally. The PSC-AIH OS project included only a $3x10^8$ pfu intravenously injection.

7.2. Methods

7.2.1. Cell biological methods

7.2.1.1. Cultivation of cells

Cells were cultured in plastic culture flasks (25, 75 or 175 cm^2) at 37 °C (5 % CO_2, relative humidity 95 %) with appropriate medium. Adherent cells were split when confluent. Medium was removed from the culture flask, the cellular monolayer was rinsed with sterile PBS and the cells were incubated with trypsin-EDTA for five minutes at 37 °C to detach the cells from the plastic. The detached cells were collected by centrifugation at 250 x g for five minutes. Medium was removed and the cells were resuspended in appropriate medium and split.

7.2.1.2. Freezing of cells

Cryotubes were pre-cooled for 30 minutes at 4 °C. The freezing medium was prepared containing 90 % FBS and 10 % DMSO and also pre-cooled at 4 °C. Cells were washed with PBS, trypsinized and centrifuged at 250 x g for five minutes. Supernatant was discarded and the pellet was resuspended to a concentration of 6 x 10^6 cells/ml with pre-cooled freezing medium and 1 ml aliquots were transferred into cryotubes. The aliquots were placed into a polystyrene box to ensure that the cell samples are cooled down to -80 °C at a rate of approx. 1°C/min. After 24 to 48 hours, the cryotubes were transferred to the liquid nitrogen tank (-196 °C).

7.2.1.3. Thawing of cells

A 15 ml tube with 9 ml 37 °C warm medium was prepared. Cell aliquots were taken out of the liquid nitrogen tank and warmed immediately in a water bath (37°C) until cells started to thaw. 1 ml of warm medium was added and liquefied cells were transferred into a 15 ml tube. This step was repeated until all cells were thawed. Cells were step-wise thawed to dilute the liquefied DMSO as fast as possible to avoid cell damage. After centrifuging the cells at 250 x g for five minutes, supernatant was discarded and cells were cultured in appropriate medium.

7.2.1.4. Determining the density of a cell suspension

The cellular density of a suspension was determined by mixing an aliquot of the cell suspension with trypan blue solution. Trypan blue is a diazo dye, which is only incorporated by dead cells, since it cannot pass the cell membrane of viable cells. 10 µl of the dilution were filled into a Neubauer counting chamber and unstained cells were counted under a light microscope (Zeiss). A grid at the bottom of the chamber was used to count the cells and the cell density (cells per ml) was calculated with the following formula:

Cellular density (cells/ml)= number of cells on the grid x dilution factor x 10^4 ml^{-1}

7.2.1.5. Adenovirus production

HEK-293 cells were cultivated in 175 cm^2 flasks in 293-medium, which was DMEM + Glutamax containing 10 % FBS, 1 % streptomycin, 1 % penicillin, 1 % HEPES and 1 % non-essential amino acid. When the cell reached a confluence about 100 %, the virus infection was started. The medium was removed and cells were infected with either Ad-GFP or Ad-2D6 with a MOI of 50 in a total volume of 15 ml 293-medium. After four hours incubation at 37 °C, 5 % CO_2 15 ml pre-warmed 293-medium was added and the cells were incubated at 37 °C, 5 % CO_2 for three days or until most of the cells were detached as clusters. The content of all flasks were transferred to 50 ml falcon tubes and centrifuged at 1100 rpm for five minutes at 4 °C. After centrifugation the supernatant was discarded and three pellets were combined in 1 ml 293-medium. The cells were transferred to cryotubes, snap-frozen in liquid nitrogen and stored for later purification at -80 °C.

7.2.1.6. Adenovirus purification

Cells were lyzed by four rapid thaw steps at 37°C, vortexing and freeze steps in liquid nitrogen. Lysates were pooled in a 15 ml falcon tube and spined at 1500 g for ten minutes at 4°C. In the meantime, CsCl gradients were prepared carefully by overlaying 4 ml of 40 % CsCl in PBS with 4.5 ml of 15 % CsCl in PBS. After centrifugation, supernatant was transfers into a 50 ml falcon tube, filled up to 18 ml with culture medium and mixed. 3 ml of the cleared cell lysate was transferred onto a CsCl gradient and tubes were placed into ultracentrifuge buckets. Cell lysates centrifugation at 25´400 rpm for 17 hours at 4°C led to an upper virus band, which contained the immature, empty virus capsule and a lower band containing the mature virus. The mature virus was collected with a 23G needle connected to a 2 ml syringe below the lower virus band. The virus was transferred to a 3 ml slide-a-lyzer cassette (10 kDa) and dialyzed against two liter cold PBS for six hours. After changing the PBS dialyze continued overnight. At the next day in the morning, virus was collected and transferred to a 15 ml falcon tube on ice. The virus particle concentration was determined by a Bradford protein assay. Then virus was

diluted in PBS and glycerol was added to a 10% final concentration. Finally, virus was transferred to cryotubes, snap-frozen in liquid nitrogen and stored at -80°C.

7.2.1.7. Isolation of liver lymphocytes

Livers of mice were perfused with 5 ml collagenase buffer through the portal vein, dissected and transferred to a 50 ml Falcon tube filled with 10 ml of the collagenase buffer on ice. Under sterile conditions the liver was placed into a petri-dish and cut into small pieces. All the pieces were transferred back into the 50 ml Falcon tube, 10 ml of RPMI 1640 were added and the liver pieces were digested for 45 minutes in a 37 °C water bath. Every 15 minutes the Falcon tube was mixed gently. The reaction was stopped by adding 30 ml ice cold RPMI 1640 followed by a filtration through a 70 µm nylon cell strainer. To remove hepatocytes, the solution was centrifuged at 30 g for three minutes and the supernatant was transferred into a new tube and centrifuged again at 550 g for ten minutes at 4°C. The supernatant was discarded, the cell pellet was resuspended in 20 ml of 35 % Percoll/PBS and centrifuged at 600 x g for 20 minutes at 4 °C. The pellet was washed first with PBS and then with RPMI 1640. To eliminate erythrocytes the cell pellet was resuspended in 7 ml erythrocytes-lysis-buffer and incubated for 5 minutes at RT. To stop the reaction 23 ml of RT RPMI 1640 was added and centrifuged at 550 x g for ten minutes at 4 °C. The supernatant was discarded and the pellet was washed first with PBS and afterwards with RPMI complete. Depending on the pellet size the cells were resuspended in RPMI complete.

7.2.1.8. Isolation of bone marrow derived dendritic cells (BMDCs)

Bone marrow derived dendritic cells (BMDCs) were isolated by removing the femurs of mice and further removing of adhering tissue from femurs. Femurs were transferred into ice-cold PBS and then washed two times more in ice-cold PBS. Bones were transferred to a petridish in which both sides of the bone were cut open. Bone marrow was flushed out by using a 27 G needle and a syringe with 3 ml ice-cold RPMI. Marrow was resuspended and filtered through a nylon cell strainer with a size of 100 µm. Cells were spun down at 400 x g for seven minutes at 4°C (with an acceleration and deceleration of 7). These parameters were used for all subsequent centrifugation steps,

unless mentioned otherwise. The supernatant was discarded, cells were resuspended in 0.83 % NH_4Cl lysis buffer (1+ number of mice = ml of lysis buffer) and incubated four minutes on ice, while shaking occasionally. Cell suspension was filled up to 25 ml with ice-cold PRMI until cells were counted. After counting cells were centrifuged again, supernatant was discarded and cells were adjusted to a concentration of 2×10^7 cells/ml with TCM medium. This cell suspension was diluted 1:50 with TCM containing 20 ng/ml GM-CSF and 20 ng/ ml IL-4. For Vitamin D (VitD3) treatment a concentration of 10^{-8} M was used. Finally 3 ml of the cell suspension was pipetted into each well on a 6-well plate leading to a final concentration of 1.2×10^6 cells per well.

After three days the medium was changed by transferring 1.5 ml of it from each well into a tube and spun down at 400 x g for seven minutes at RT to collect floating cells. Supernatant was discarded and the cell pellet was resuspended in 1.5 ml of fresh TCM containing double the concentration of GM-CSF (40 ng/ml) and IL-4 (40 ng/ml) and transferred back into appropriate wells. For VitD3 treatment a final concentration of $1x10^{-8}$ M and for Dexamethason treatment a final concentration of 1×10^{-6} M was used. Seven days after seeding the cells the medium was removed from each well and transferred into a tube. The well was gently washed with 1 ml of TCM-, which was combined with the removed medium. Afterwards, 900 µl of TCM- that contained 5% mouse serum, 20 ng/ml GM-CSF, 20 ng/ml IL-4 and 100 ng/ml LPS was pipetted to each well. Medium was centrifuged and supernatant was discarded. Cell pellet was resuspended in 100 µl TCM- and added to the corresponding wells. Cells were then stimulated with 10 µg/ml of peptide 6 and peptide 21 overnight.

The next day cells were harvested by vigorous, but carful pipetting. If the cells adhered too much, 1 ml PBS was added and cells were removed with a cell scraper. Next, the wells were washed twice with PBS. Cells were spun down, resuspended and counted. Some cells were stored for phenotype analysis and the main part was used for the animal treatment. Each mouse received 2×10^5 cells via i.v. injection in a volume of 100 µl.

7.2.1.9. Isolation of splenocytes

Spleen cells were isolated by squeezing the spleen through a 70 µm nylon cell strainer in 5 ml RPMI. The suspension was pipetted through the nylon cell strainer twice. The suspension was centrifuged at 550 x g for five minutes at 4 °C. The supernatant was discarded and pellet was resuspended by flicking the tube. To eliminate the red blood cells the pellet was resuspended in 3 ml lysis buffer and incubated for five minutes at RT. The erythrocytes lysis was stopped by adding 11 ml RMPI and the supernatant was carefully transferred into a new Falcon avoiding the clumped cells. The cells were centrifuged at 550 x g for five minutes at 4 °C and the supernatant was discarded. The cell pellet was resuspended in 10 ml cold PBS and centrifuged at 550 x g for five minutes at 4°C. Finally the supernatant was discarded, pellet was resuspended in approximately 0.6 to 1 ml RPMI complete adjusted on the pellet size. The cell suspension was kept at 4 °C until use.

7.2.1.10. Splenocytes-ECDI cross link

Splenocytes were isolated as described in 9.2.1.9 and incubated 1 hour on ice at a concentration of 3.2 x 10^8 cells/ml with and without 1 mg peptide (p6) in the presence of 30 mg/ml 1-ethyl-3-(3-dimethylaminopropyl)-carbodiimide (ECDI) and also without ECDI. Crosslinked splenocytes were washed twice with PBS and 2 x 10^7 cells were injected i.v. into two weeks infected AIH mice.

7.2.1.11. Isolation of NALT associated lymphocytes

Mice were anesthetized with isoflurane and killed by cervical dislocation. After cervical dislocation, mice were decapitated and the lower jaw and tongues were discard. Heads were immobilizes with needles to reveal the upper palate. To visualize the position of the NALT a dissection microscope was used.

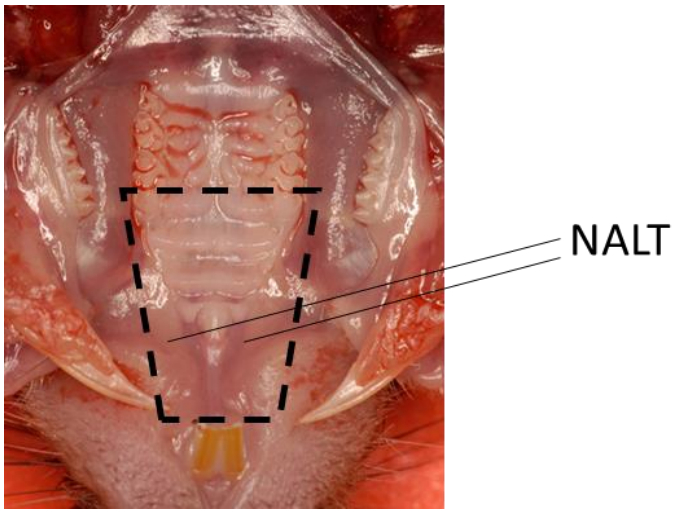

Figure 45: Dissection scheme of nasal-associated lymphoid tissue (NALT)
Occlusal view of the mouth of a mouse showing upper molars. The piece which has to cut out to gain the NALT is showing with the black labeled line. Figure is modified after Bittner-Eddy et al., 2017 [340].

One small piece of the anterior plate was cut out by using a fine forceps and a scalpel to harvest the NALT (see the black line in

Figure 45). Anterior palates were placed immediately into a 3 cm petri dish containing 1 ml ice-cold RMPI complete. NALTs were teased gently into the medium and with the help of two tips cells of the NALT were released out of the NALT. NALT cell suspension was washed twice until they were used for further analysis.

7.2.1.12. Flow cytometry

Cells were harvested and around 10^6 cells were transferred to a V-bottom 96-well plate and centrifuged at 550 x g for five minutes at 4 °C. The supernatant was discarded and the cells were vortexed and resuspended with 150 µl FACS PBS/staining buffer. This step was done twice before the cells were stained with fluorochrome labeled antibodies in 50 µl FACS PBS/staining buffer for 30 minutes at 4°C in the dark. After incubation 100 µl FACS PBS/staining buffer was added and the cells were collected by centrifugation at 550 x g for five minutes at 4°C. The supernatant was discarded. The cells were washed twice by resuspending with 150 µl FACS PBS/staining buffer. After the last washing step the cells were fixed in 200 µl FACS fixation buffer and transferred to FACS tubes to be analyzed by flow cytometry at a BD FACS Canto II.

7.2.1.13. Intra cellular cytokine staining (ICCS)

Coating

The general stimulation of T cells was done by coating a flat-bottom plate with 50 µl anti-CD3 antibodies over night at 4°C. Before plating the cells into the wells, the wells were washed with PBS twice.

Restimulation of lymphocytes

Lymphocytes were isolated as described in 9.2.1.8 and approximal 10^6 cells were added into a well of a V-bottom 96-well plate. Cells were centrifuged at 550 x g for five minutes at 4 °C. Supernatant was discarded, cells were resuspended in RPMI complete containing 2 µg/ml Brefeldin A and MHC class I- or class II-restricted hCYP2D6 peptides (each peptide P6, P21, P25 or P28 2 µg/ml) and transferred into a U-plate for the CYP2D6 specific stimulation. For the general stimulation of T cells an anti-CD3 antibody coated plate was used and anti-CD28 antibody and IL-2 were added in the presence of 2 µg/ml Brefeldin A. Plates were incubated at 37 °C and 5 % CO_2 overnight.

Staining

The cells were transferred to a V-bottom 96-well plate and were centrifuged at 550 x g for five minutes at 4 °C. The supernatant was discarded, plate was vortexed and cells were resuspended with 150 µl FACS PBS/staining buffer. The cells were washed twice before the surface molecules staining with fluorochrome labeled antibodies was done. 50 µl FACS PBS/staining buffer containing the antibodies of choice was added to each well and incubated for 30 minutes at 4 °C in the dark. After incubation 100 µl FACS PBS/staining buffer was added to each well and the plate was centrifuged at 550 x g for three minutes at 4 °C. The cells were washed twice by resuspending with 150 µl FACS PBS/staining buffer. The cells were fixed and permeabilized with 100 µl of PFA/saponin solution for ten minutes at RT. After two additional washes with 150 µl FACS PBS/saponin buffer and spinning at 550 x g for six minutes at 4 °C. The cells were stained intracellular with antibodies against IFNγ and several other cytokines 50 µl FACS PBS/saponin buffer containing the antibodies of choice was added to each well and incubated for 30 minutes at 4 °C in the dark. After incubation 100 µl FACS PBS/saponin buffer was added to each well and the plate was centrifuged at 550 x g for six minutes at 4 °C. The supernatant was discarded and the cells were resuspended with 150 µl FACS

PBS/saponin buffer. The washing step was done twice with FACS PBS/saponin buffer and once with FACS PBS/staining buffer. Finally, the cells were fixed in 200 µl FACS fixation buffer, transferred to FACS tubes and analyzed by flow cytometry with a BD FACS Canto II.

7.2.1.14. Enzyme Linked Immunosorbent Assay (ELISA)

To detect the total amount of IgG or antibodies specific for human CYP2D6, a flat-bottom 96-well microtiter plate was coated overnight with 0.25 µg/ml α-mouse SMA biotinylated antibody or recombinant human CYP2D6 in 100 µl ELISA coating buffer at 4 °C. Afterwards, the plate was washed four times with 150 µl PBS containing 0.05 % Tween-20 and blocked with 200 µl PBS containing 2 % FCS for 90 minutes at RT to block unspecific binding sides. Blocking buffer was removed and the plate was washed four times with 150 µl PBS containing 0.05 % Tween-20. Serial dilutions of a standard IgG or a comparative serum in PBS containing 2 % FCS were performed in order to generate a standard curve. The dilution series for each serum started at 1:1000 for the ELISA of total IgG or 1:100 for the CYP2D6 ELISA, followed by 1:4 or 1:3 dilution steps down to a final dilution of 1:4´096´000 or 1:24´300. 100 µl of each standard dilution and sera were added and were incubated for 90 minutes at 37 °C. After washing the plate four times with ELISA washing buffer 100 µl alkaline-phosphatase-labeled goat anti-mouse IgG antibody diluted 1:2´000 in PBS containing 2 % FCS was added and incubated at 37 °C for 90 minutes. After washing the plate four times with PBS containing 2 % FCS followed by addition of 30 µl ECF substrate which was then incubated for 20 – 30 min at RT. Fluorescence intensity was determined using a Pharos FX molecular imager (Bio-Rad) and signal intensity was quantified using Quantity One software (Bio-Rad).

7.2.1.15. Serum ALT and AP measurements

Alanine aminotransferase (ALT) and alkaline phosphatase (AP) levels were measured with the Reflotron Plus blood analysis system (Roche Diagnostics, Mannheim, Germany). Therefore, 32 µl of serum diluted at least 1:1 in NaCl was added at a Reflotron test reagent stripes and placed into the Reflotron®.

7.2.1.16. pANCA detection

HL60 cells were seeded in 24-well plates on coverslips coated with poly-D-lysine, fixed in ethanol, blocked in 10% FCS/PBS and then incubated in serum diluted in 10% FCS/PBS for two hrs at RT. After incubation, cells were washed and then incubated in FITC-labelled goat anti-human IgG or goat anti-mouse IgG for 1 hr. Cells were washed, mounted in Fluoromount-G and analyzed using a LSM510 META confocal microscope with a 63x oil objective.

7.2.1.17. Nanoparticle preparation

The lyophilized nanoparticles from our cooperation partner were stored in a desiccator at 4°C. Each aliquot was resuspended in 1 ml sterile H_2O and centrifuged at 3000 x g for five minutes. The supernatant was aspirated and the nanoparticles were first resuspended in 200 µl sterile PBS until further 1 ml of sterile PBS was added. Another centrifugation step at 3000 x g for five minutes was done and the supernatant was aspirated. The nanoparticles were resuspended in 200 µl sterile PBS and then brought up to the desired concentration which we wanted to inject.

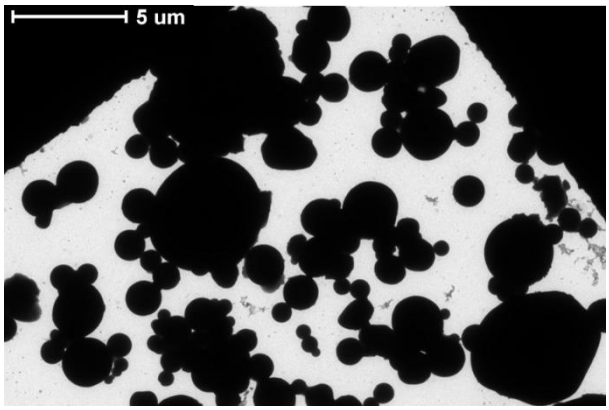

Figure 46: Representative image of a nanoparticle batch
Generation and characterization was done by our cooperation partner Ph.D Tobias Neef, Northwestern University, Chicago.

7.2.2. Histological methods

7.2.2.1. Immunohistochemistry staining

Livers were harvested at times indicated and embedded in Tissue-Tek OCT. OCT was quick-frozen on dry ice and stored at -80 °C. After incubating the samples for one hour at -20 °C 7 µm thick tissue sections were cut using a cryostat and mounted on Microscope Slides Fischerbrand™ Superfrost™ Plus. Consecutive sections were taken and dried at RT. Sections were stored at -20 °C until used.

Fixing:

Tissue sections were fixed in 95 % ethanol or 1:1 diluted ethanol/acetone at -20 °C for 15 minutes. After drying on a paper towel for ten minutes at RT circles were drawn around the specimen by using a wax pencil.

Blocking:

The tissue sections were washed two times in PBS for two minutes and each specimen was incubated in 0.3 % H_2O_2 / 0.1 % Na-azid in PBS for ten minutes at RT. After washing two times in PBS for two minutes one drop of avidin was placed on each specimen and incubated for ten minutes at RT. The tissue sections were washed twice again in PBS for two minutes. After washing one drop of biotin was placed on each specimen and incubated for ten minutes at RT. After an additional washing step, 100 – 200 µl 10 % FBS in PBS was added and incubated for 30 minutes at RT to block unspecific antibody binding.

Staining:

The 10 % FBS in PBS was tapped off and 100 µl of the first antibody diluted 1:50 – 1:1000 in 10 % FBS in PBS were added to each specimen. The sections were incubated for two hours at RT in a humidified chamber in the dark. After tapping the first antibody solution, the sections were washed three times in PBS for four minutes. After washing, 150 µl of biotinylated secondary antibody diluted 1:400 – 1:500 in 10 % FBS in PBS were added to each specimen and was incubated for one hour at RT in a humidified chamber in the dark. The secondary antibody solution was tapped off and sections were washed three times for four minutes in PBS. One drop of ABC reagent solution (Vector Laboratories) was added on each specimen and incubated for 30 minutes at RT. After tapping of the ABC reagent, the sections were washed three times in PBS for four minutes and 120 µl

peroxides substrate was added on each specimen and incubated for two to five minutes at RT. The reaction was stopped by washing in PBS for five minutes and the section were counterstained in hematoxylin solution for three to five minutes at RT. After washing three times in PBS for four minutes two drops of aquamount were added to each section coverslip was placed on each slide. Finally the sections were incubated at RT overnight and pictures were taken at a microscope (Biozero BZ-8000, Keyence / Zeiss).

7.2.2.2. Detection of primary mouse antibodies on murine tissue with the M.O.M. Immunodetection Kit (Vector)

Fixing:

Tissue sections were fixed in 1:1 diluted ethanol/acetone at -20 °C for 15 minutes and after drying on a paper towel for ten minutes circles were drawn around the specimen by using a wax pencil.

Blocking:

After washing two times in PBS for two minutes one drop of avidin was placed on each specimen and incubated for ten minutes at RT. The tissue sections were washed twice again in PBS for two minutes. After washing one drop of biotin was placed on each specimen and incubated for 10 minutes at RT. After two additional washing steps in PBS for two minutes the MOM IgG blocking reagent was added to each slide and incubated for three hours at RT. One drop of the stock solution was mixed with 1.25 ml PBS.

Staining:

After tapping the blocking solution, the sections were washed two times in PBS for two minutes. After washing, the sections were incubated with the MOM diluent solution for exactly five minutes. This solution contains 400 µl protein solution diluted in 5 ml PBS. The tissue sections were washed two times in PBS for two minutes and the secondary antibody was added for exactly five minutes at RT. (1 µl IgG + 1 ml MOM diluent solution). After washing two times in PBS for exactly two minutes one drop of ABC reagent was added to each slide and incubated for 30 minutes at RT. After tapping of the ABC reagent, the sections were washed three times in PBS for four minutes and 120 µl peroxides substrate was added on each specimen and incubated for two to five minutes at RT. The reaction was stopped by washing in PBS for five minutes and the

section were counterstained in hematoxylin solution for five minutes at RT. After washing three times in PBS for four minutes two drops of aquamount were added to each section coverslip was placed on each slide. Finally the sections were incubated at RT overnight and pictures were taken at a microscope (Biozero BZ-8000, Keyence / Zeiss).

7.2.2.3. Immunofluorescence staining

Livers were harvested at different time points after infection and embedded in Tissue-Tek OCT. OCT was quick-frozen on dry ice and stored at -80 °C. After incubating the samples for one hour at -20 °C 7 µm thick tissue sections were cut using a cryostat and mounted slides. Consecutive sections were taken and dried at RT. Sections were stored at -20 °C until used.

Fixing:

Tissue sections were fixed in ethanol at -20 °C for 15 minutes and after drying on a paper towel for ten minutes, circles were drawn around the specimen by using a wax pencil.

Blocking:

After washing two times in PBS for two minutes a few drops of 10% FBS in PBS (PBS/FCS) were added and incubated for 30 min at RT.

Staining:

The blocking solution was tapped off and 1st antibody solution diluted in PBS/FCS was added and incubated for three hours at RT in a humidified chamber. Afterwards, the antibody solution was tapped off and the sections were washed three times in PBS for four minutes. Fluorescent-labeled 2nd antibody diluted in DAPI/FCS/PBS was added and incubated for one hour at RT in a humidified chamber in the dark. After tapping off the 2nd antibody solution sections were washed three times in PBS for four minutes. Finally, the sections were mounted in mounting medium for fluorescent probes and sealed with nail polish. Slides were stored at 4°C in the dark.

Fluorescent signals were analyzed using a LSM510 META confocal microscope with a 40x oil objective and ZEN software (Zeiss, Oberkochen, Germany).

7.2.2.4. Histological quantification

To quantify immunohistochemical staining, pictures were taken with a Keyence microscope and depending on the staining different objectives were used. In order to avoid misinterpretations due to preparation artefacts, such as loss of liver capsule tissue, only parenchymal areas but no capsular regions have been considered. Histological quantification was done by measuring positive areas of immunohistochemical stained tissue with the Macro Hybrid Cell Count tool of the image analysis software BZ-II Analyzer (Keyence). This software allows to automatically measure multiple images under the same conditions. The color distribution was defined for each staining wherein the color analyses were done for all specimens. As an example, the quantification of cholangitis (CK19 stain) is shown below (Figure 47).

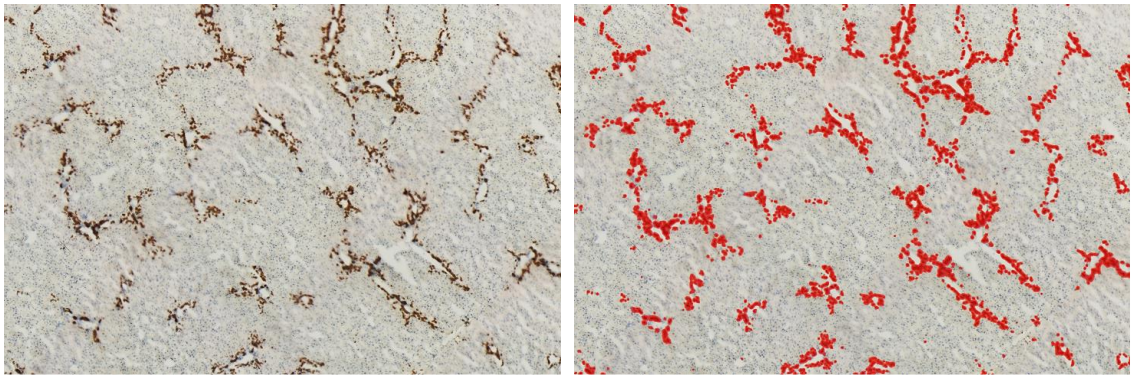

Figure 47: Examples for quantification of anti-CK19 antibody stained area
Original picture of a CK19 staining of a cryosection of a *Mdr2*$^{-/-}$ liver (left side). The same picture after analysis with the Macro Hybrid Cell Count tool of the Keyence image analysis software BZ-II Analyzer. Marked in red are those pixels which were identified as positively stained (right side).

Three pictures per specimen and five animals per group were representative for the particular disease. The area ratio of each tissue component is the sum of positive stained pixels with reference to the total number of pixels. The median area rations of collagen, CK19, CD4, CD8, CD11b, CD11c and neutrophils were calculated and presented in the diagrams.

7.2.3. Molecular biological methods

7.2.3.1. Preparation of protein extraction from liver homogenates

Liver was harvested and homogenized with a tissue homogenizer in 1 ml RIPA-buffer per 100 mg liver tissue containing protease inhibitor.

7.2.3.2. Protein Assay (Lowry Test) Bio-Rad DC Protein Assay

The protein concentration of liver homogenates in detergent solution was measured with the Lowry assay (Bio-Rad DC Protein Assay). Primarily, samples were diluted 1:100 to assure concentrations of the measured samples in the detection ration and standards (0.2 – 1.0 mg/ml) were produced. Then, 20 µl of reagent S to each ml of reagent A was combined to get A´. 20 µl of samples and standards were mixed with 100 µl of reagent A´. 800 µl of reagent B was added to each sample and mixed. 200 µl of reach mix were transferred to a 96-well flat bottom plate. Each probe was measured as triplet and RIPA buffer was used as blank controls. After 15 minutes at RT the absorbance was measured at 650 – 750 nm with an ELISA microplate reader (Sunrise, Tecan).

7.2.3.3. SDS-PAGE

Proteins were separated by SDS-PAGE. An appropriate separating gel was prepared using a 1.5 mm spacer:

Table 13: Separating gel

	10 % one gel	10 % two gels	12 % one gel	12 % two gels
Acrylamide	3.33 ml	5 ml	4 ml	6 ml
Lower gel buffer	2.5 ml	3.75 ml	2.5 ml	3.75 ml
Destilled water	4.07 ml	6.1 ml	3.4 ml	5.1 ml
SDS (20 % w/v)	50 µl	75 µl	50 µl	75 µl
TEMED	5 µl	7.5 µl	5 µl	7.5 µl
APS (10 % w/v)	50 µl	75 µl	50 µl	75 µl

Just after adding the TEMED and APS, the acrylamide solution was poured to about 5 cm from the bottom. During polymerization the solution was overlaid with H_2O. After one hour the overlay was removed and a 3 % stacking gel was prepared:

Table 14: Stacking gel

	3 % one gel	3 % two gels
Acrylamide	0.5 ml	0.75 ml
Lower gel buffer	1.25 ml	1.875 ml
Destilled water	3.25 ml	4.875 ml
SDS (20 % w/v)	25 µl	37.5 µl
TEMED	5 µl	7.5 µl
APS (10 % w/v)	25 µl	37.5 µl

Immediately after pouring, the comb was added. Samples were heated for 5 minutes at 95 °C in 4x Laemmli sapmle buffer. After polymerization, the gels were mounted in the electrophoresis apparature and the inner and outer chamber was filled with 1x Running buffer. The comb was removed and the wells were washed with 1x Running buffer to remove any unpolymerised acrylamide. The samples and 10 µl of the Roti®-Prestained Marker were loaded. Electrophoresis was performed at 140 V until the blue front reached the bottom of the gel (1-1.5 hours).

7.2.3.4. Western Blot

A PVDF membrane (5.2 x 8.5 cm) was prepared and put into methanol for five seconds. The membrane and four of Whatman paper (6 x 9 cm) were equilibrated in transfer buffer for five minutes. The gel and the membrane were put into the blotting apparatus together with the Whatman paper in the following order: two Whatman paper- membrane- gel- two Whatman paper. Air bubbles in between were removed by rolling a plastic pipette over the stock. The proteins were blotted onto the membrane at constant 125 mA per gel, thus set at 250 mA if transferred two gels, for one and a half hours. For blocking, the membrane was incubated for two hours at RT in PBS 5 % milk containing 0.1 % Tween-20 on a shaker. The primary antibody was diluted 1:2000 in PBS

5 % milk containing 0.1 % Tween-20. The membrane was incubated over night at 4 °C together with 10 ml of the antibody solution. After washing six times with PBS 5 % milk containing 0.1 % Tween-20 for five minutes, the second stage antibody was added at a dilution of 1:2000 in 10 ml PBS 5 % milk containing 0.1 % Tween-20. The membrane was incubated with this solution at RT for one and a half hours. After washing three times with PBS 5 % milk containing 0.1 % Tween-20 and three times with PBS for five minutes and once with H_2O. The separated protein bands were visualized with 1 ml ECF reagent and pictures were taken on a Pharos (Pharos FX Plus Molecular Imager, Bio Rad).

7.3. Animal experiments

7.3.1. Blood collection

Mice were anesthetized with 4% isoflurane and blood samples were taken retro-orbitally with a heparin coated capillary (Fisherbrand) and collected in a BD Microtainer® Blood Collection Tubes (BD Falcon). The blood was then incubated on ice for 30 minutes and centrifuged for two minutes at 9500 rpm at 4 °C in a microcentrifuge. The serum was transferred to a new eppendorf tube and stored at -80°C.

7.3.2. Injections

7.3.2.1. Ad-2D6 injection

Mice were infected with an Adenovirus containing the Vector Ad5-hCyp2D6. For the establishment of a PSC-AIH OS mouse model, mice were only infected with $3x10^8$ pfu intravenously. For this injection mice were anesthetized with isoflurane and 100 µl virus were injected with a syringe intravenously. For the regular CYP2D6 AIH model with the aim to find novel tolerogenic therapies, mice were infected with $3x10^8$ pfu intravenously and $3x10^8$ pfu intraperitoneally. For the intraperitoneally injection mice were held in one hand and 100 µl virus were injected with a syringe intraperitoneal.

7.3.2.2. Nanoparticle injection

The nanoparticles were resuspended in 200 µl sterile PBS and then brought up to the desired concentration which was then injected intravenously into two weeks infected AIH mice.

7.3.2.3. DCs injection

After in vitro stimulation of the differentiated DCS and phenotype analysis by FACS measurement cells were set to the appropriate concentration with PBS ($2x10^5$ cells/per mouse). Mice were injected intravenously with 100 µl of the cell suspension. For this a 27G syringe was used to avoid damaging the DCs.

7.3.2.4. SPL-ECDI injection

SPL-ECDI were injected i.v. in an amount of 2×10^7 cells into two weeks infected AIH mice.

7.3.3. Intranasal immunization

Mice were immunized intranasally five times on day 0, 3, 7, 10 and 14. Therefore mice were held in one hand and received 10 µl containing different combination of peptides (p6 and p21, each peptide 100 µg/d) with or without an adjuvant or both of the following adjuvants CpG and Poly IC (each 10 µg/d) in each nares.

7.3.4. Liver perfusion

Mice were anesthetized with isoflurane and killed by cervical dislocation. After the abdomen had been opened the hepatic vein and hepatic artery were cut and the liver was perfused with 5 ml liver perfusion buffer through the hepatic portal vein. The liver was removed into a Falcon containing liver perfusion buffer and one piece of the liver was placed in OCT, quick frozen and appropriately stored for further processing.

7.4. **Statistical evaluations**

All statistics were analyzed using the unpaired, two-tailed t-test (GraphPad Prism 5.02 Software).

8. References

1. Pietropaolo M, Surhigh JM, Nelson PW, Eisenbarth GS. Primer: immunity and autoimmunity. Diabetes. 2008;57:2872–82. doi:10.2337/db07-1691.
2. Martin MU, Resch K. Immunologie. 1st ed. Stuttgart: UTB; 2009.
3. Abbas AK, Lichtman AH, Pillai S. Basic immunology: Functions and disorders of the immune system. Philadelphia, Pa.: Elsevier Saunders; 2014.
4. Murphy KP, Travers P, Walport M, Janeway C, Seidler L, Ehrenstein M, Haußer-Stiller I. Janeway Immunologie. 7th ed. Heidelberg: Spektrum Akademischer Verlag; 2009.
5. Labrecque N, Baldwin T, Lesage S. Molecular and genetic parameters defining T-cell clonal selection. Immunol Cell Biol. 2011;89:16–26. doi:10.1038/icb.2010.119.
6. Ueda H, Howson JMM, Esposito L, Heward J, Snook H, Chamberlain G, et al. Association of the T-cell regulatory gene CTLA4 with susceptibility to autoimmune disease. Nature. 2003;423:506–11. doi:10.1038/nature01621.
7. Hewitt EW. The MHC class I antigen presentation pathway: strategies for viral immune evasion. Immunology. 2003;110:163–9. doi:10.1046/j.1365-2567.2003.01738.x.
8. Gravano DM, Hoyer KK. Promotion and prevention of autoimmune disease by CD8+ T cells. J Autoimmun. 2013;45:68–79. doi:10.1016/j.jaut.2013.06.004.
9. Neefjes J, Jongsma MLM, Paul P, Bakke O. Towards a systems understanding of MHC class I and MHC class II antigen presentation. Nat Rev Immunol. 2011;11:823–36. doi:10.1038/nri3084.
10. Annunziato F, Cosmi L, Liotta F, Maggi E, Romagnani S. Human Th17 cells: are they different from murine Th17 cells? Eur J Immunol. 2009;39:637–40. doi:10.1002/eji.200839050.
11. Jiang S, Dong C. A complex issue on CD4(+) T-cell subsets. Immunol Rev. 2013;252:5–11. doi:10.1111/imr.12041.
12. Zhou L, Chong MMW, Littman DR. Plasticity of CD4+ T cell lineage differentiation. Immunity. 2009;30:646–55. doi:10.1016/j.immuni.2009.05.001.
13. Zhu J, Paul WE. CD4 T cells: fates, functions, and faults. Blood. 2008;112:1557–69. doi:10.1182/blood-2008-05-078154.
14. Hirahara K, Vahedi G, Ghoreschi K, Yang X-P, Nakayamada S, Kanno Y, et al. Helper T-cell differentiation and plasticity: insights from epigenetics. Immunology. 2011;134:235–45. doi:10.1111/j.1365-2567.2011.03483.x.
15. Elser B, Lohoff M, Kock S, Giaisi M, Kirchhoff S, Krammer PH, Li-Weber M. IFN-gamma represses IL-4 expression via IRF-1 and IRF-2. Immunity. 2002;17:703–12.
16. Szabo SJ, Kim ST, Costa GL, Zhang X, Fathman CG, Glimcher LH. A novel transcription factor, T-bet, directs Th1 lineage commitment. Cell. 2000;100:655–69.

17. Reiner SL. Development in motion: helper T cells at work. Cell. 2007;129:33–6. doi:10.1016/j.cell.2007.03.019.
18. Mosmann TR, Cherwinski H, Bond MW, Giedlin MA, Coffman RL. Two types of murine helper T cell clone. I. Definition according to profiles of lymphokine activities and secreted proteins. The Journal of Immunology. 1986;136:2348–57.
19. Holgate ST. Innate and adaptive immune responses in asthma. Nat Med. 2012;18:673–83. doi:10.1038/nm.2731.
20. Biswas PS, Gupta S, Chang E, Song L, Stirzaker RA, Liao JK, et al. Phosphorylation of IRF4 by ROCK2 regulates IL-17 and IL-21 production and the development of autoimmunity in mice. J Clin Invest. 2010;120:3280–95. doi:10.1172/JCI42856.
21. Rutz S, Eidenschenk C, Ouyang W. IL-22, not simply a Th17 cytokine. Immunol Rev. 2013;252:116–32. doi:10.1111/imr.12027.
22. Sato K, Takayanagi H. Osteoclasts, rheumatoid arthritis, and osteoimmunology. Curr Opin Rheumatol. 2006;18:419–26. doi:10.1097/01.bor.0000231912.24740.a5.
23. Dos Passos GR, Sato DK, Becker J, Fujihara K. Th17 Cells Pathways in Multiple Sclerosis and Neuromyelitis Optica Spectrum Disorders: Pathophysiological and Therapeutic Implications. Mediators Inflamm. 2016;2016:5314541. doi:10.1155/2016/5314541.
24. Sakaguchi S, Fukuma K, Kuribayashi K, Masuda T. Organ-specific autoimmune diseases induced in mice by elimination of T cell subset. I. Evidence for the active participation of T cells in natural self-tolerance; deficit of a T cell subset as a possible cause of autoimmune disease. Journal of Experimental Medicine. 1985;161:72–87.
25. Komai T, Inoue M, Okamura T, Morita K, Iwasaki Y, Sumitomo S, et al. Transforming Growth Factor-β and Interleukin-10 Synergistically Regulate Humoral Immunity via Modulating Metabolic Signals. Front Immunol. 2018;9:1364. doi:10.3389/fimmu.2018.01364.
26. Fontenot JD, Gavin MA, Rudensky AY. Foxp3 programs the development and function of CD4+CD25+ regulatory T cells. Nat Immunol. 2003;4:330–6. doi:10.1038/ni904.
27. Hori S, Nomura T, Sakaguchi S. Control of regulatory T cell development by the transcription factor Foxp3. Science. 2003;299:1057–61. doi:10.1126/science.1079490.
28. Abbas AK, Benoist C, Bluestone JA, Campbell DJ, Ghosh S, Hori S, et al. Regulatory T cells: recommendations to simplify the nomenclature. Nat Immunol. 2013;14:307–8. doi:10.1038/ni.2554.
29. Kyewski B, Klein L. A central role for central tolerance. Annu Rev Immunol. 2006;24:571–606. doi:10.1146/annurev.immunol.23.021704.115601.
30. Sakaguchi S, Wing K, Onishi Y, Prieto-Martin P, Yamaguchi T. Regulatory T cells: how do they suppress immune responses? International Immunology. 2009;21:1105–11. doi:10.1093/intimm/dxp095.

31. Gregersen PK, Behrens TW. Genetics of autoimmune diseases--disorders of immune homeostasis. Nat Rev Genet. 2006;7:917–28. doi:10.1038/nrg1944.
32. Münz C, Lünemann JD, Getts MT, Miller SD. Antiviral immune responses: triggers of or triggered by autoimmunity? Nat Rev Immunol. 2009;9:246–58. doi:10.1038/nri2527.
33. Lerner A, Jeremias P, Matthias T. The World Incidence and Prevalence of Autoimmune Diseases is Increasing. IJCD. 2015;3:151–5. doi:10.12691/ijcd-3-4-8.
34. Fairweather D, Rose NR. Women and autoimmune diseases. Emerging Infect Dis. 2004;10:2005–11. doi:10.3201/eid1011.040367.
35. Miller FW, Pollard KM, Parks CG, Germolec DR, Leung PSC, Selmi C, et al. Criteria for environmentally associated autoimmune diseases. J Autoimmun. 2012;39:253–8. doi:10.1016/j.jaut.2012.05.001.
36. Selmi C, Lu Q, Humble MC. Heritability versus the role of the environment in autoimmunity. J Autoimmun. 2012;39:249–52. doi:10.1016/j.jaut.2012.07.011.
37. Ceccarelli F, Agmon-Levin N, Perricone C. Genetic Factors of Autoimmune Diseases. J Immunol Res. 2016;2016:3476023. doi:10.1155/2016/3476023.
38. Zeng H, Zhang R, Jin B, Chen L. Type 1 regulatory T cells: a new mechanism of peripheral immune tolerance. Cell Mol Immunol. 2015;12:566–71. doi:10.1038/cmi.2015.44.
39. Oka S, Furukawa H, Yasunami M, Kawasaki A, Nakamura H, Nakamura M, et al. HLA-DRB1 and DQB1 alleles in Japanese type 1 autoimmune hepatitis: The predisposing role of the DR4/DR8 heterozygous genotype. PLoS ONE. 2017;12:e0187325. doi:10.1371/journal.pone.0187325.
40. Holoshitz J. The rheumatoid arthritis HLA-DRB1 shared epitope. Curr Opin Rheumatol. 2010;22:293–8. doi:10.1097/BOR.0b013e328336ba63.
41. Smikle MF, Pascoe RW, Barton E, Morgan O, Christian N, Dowe G, et al. HLA-DRB3 *0101 is associated with Graves' disease in Jamaicans. Clinical Endocrinology. 2001;55:805–8. doi:10.1046/j.1365-2265.2001.01414.x.
42. Tjernström F, Hellmer G, Nived O, Truedsson L, Sturfelt G. Synergetic effect between interleukin-1 receptor antagonist allele (IL1RN*2) and MHC class II (DR17,DQ2) in determining susceptibility to systemic lupus erythematosus. Lupus. 1999;8:103–8. doi:10.1191/096120399678847560.
43. Pitkänen J, Peterson P. Autoimmune regulator: from loss of function to autoimmunity. Genes Immun. 2003;4:12–21. doi:10.1038/sj.gene.6363929.
44. Peterson P, Nagamine K, Scott H, Heino M, Kudoh J, Shimizu N, et al. APECED: a monogenic autoimmune disease providing new clues to self-tolerance. Immunology Today. 1998;19:384–6. doi:10.1016/S0167-5699(98)01293-6.
45. Anderson MS, Venanzi ES, Klein L, Chen Z, Berzins SP, Turley SJ, et al. Projection of an immunological self shadow within the thymus by the aire protein. Science. 2002;298:1395–401. doi:10.1126/science.1075958.

46. Hardtke-Wolenski M, Taubert R, Noyan F, Sievers M, Dywicki J, Schlue J, et al. Autoimmune hepatitis in a murine autoimmune polyendocrine syndrome type 1 model is directed against multiple autoantigens. Hepatology. 2015;61:1295–305. doi:10.1002/hep.27639.
47. Wahren-Herlenius M, Dörner T. Immunopathogenic mechanisms of systemic autoimmune disease. The Lancet. 2013;382:819–31. doi:10.1016/S0140-6736(13)60954-X.
48. Bogdanos DP, Smyk DS, Rigopoulou EI, Mytilinaiou MG, Heneghan MA, Selmi C, Gershwin ME. Twin studies in autoimmune disease: genetics, gender and environment. J Autoimmun. 2012;38:J156-69. doi:10.1016/j.jaut.2011.11.003.
49. Zheng Z-H, Gao C-C, Wu Z-Z, Liu S-Y, Li T-F, Gao G-M, Liu Z-S. High prevalence of hypovitaminosis D of patients with autoimmune rheumatic diseases in China. Am J Clin Exp Immunol. 2016;5:48–54.
50. Zheng Z-H, Gao C-C, Wu Z-Z, Liu S-Y, Li T-F, Gao G-M, Liu Z-S. High prevalence of hypovitaminosis D of patients with autoimmune rheumatic diseases in China. Am J Clin Exp Immunol. 2016;5:48–54
51. Dankers W, Colin EM, van Hamburg JP, Lubberts E. Vitamin D in Autoimmunity: Molecular Mechanisms and Therapeutic Potential. Front Immunol. 2016;7:697. doi:10.3389/fimmu.2016.00697.
52. Toloza SMA, Cole DEC, Gladman DD, Ibañez D, Urowitz MB. Vitamin D insufficiency in a large female SLE cohort. Lupus. 2010;19:13–9. doi:10.1177/0961203309345775.
53. Bizzaro G, Antico A, Fortunato A, Bizzaro N. Vitamin D and Autoimmune Diseases: Is Vitamin D Receptor (VDR) Polymorphism the Culprit? Isr Med Assoc J. 2017;19:438–43.
54. Ebadi M, Bhanji RA, Mazurak VC, Lytvyak E, Mason A, Czaja AJ, Montano-Loza AJ. Severe vitamin D deficiency is a prognostic biomarker in autoimmune hepatitis. Aliment Pharmacol Ther. 2019;49:173–82. doi:10.1111/apt.15029.
55. Prietl B, Treiber G, Pieber TR, Amrein K. Vitamin D and immune function. Nutrients. 2013;5:2502–21. doi:10.3390/nu5072502.
56. Belkaid Y, Hand TW. Role of the microbiota in immunity and inflammation. Cell. 2014;157:121–41. doi:10.1016/j.cell.2014.03.011.
57. Shamriz O, Mizrahi H, Werbner M, Shoenfeld Y, Avni O, Koren O. Microbiota at the crossroads of autoimmunity. Autoimmun Rev. 2016;15:859–69. doi:10.1016/j.autrev.2016.07.012.
58. Qi C-J, Zhang Q, Yu M, Xu J-P, Zheng J, Wang T, Xiao X-H. Imbalance of Fecal Microbiota at Newly Diagnosed Type 1 Diabetes in Chinese Children. Chin Med J. 2016;129:1298–304. doi:10.4103/0366-6999.182841.
59. Schrumpf E, Kummen M, Valestrand L, Greiner TU, Holm K, Arulampalam V, et al. The gut microbiota contributes to a mouse model of spontaneous bile duct

inflammation. Journal of Hepatology. 2017;66:382–9. doi:10.1016/j.jhep.2016.09.020.
60. Kummen M, Holm K, Anmarkrud JA, Nygård S, Vesterhus M, Høivik ML, et al. The gut microbial profile in patients with primary sclerosing cholangitis is distinct from patients with ulcerative colitis without biliary disease and healthy controls. Gut. 2017;66:611–9. doi:10.1136/gutjnl-2015-310500.
61. Rühlemann MC, Heinsen F-A, Zenouzi R, Lieb W, Franke A, Schramm C. Faecal microbiota profiles as diagnostic biomarkers in primary sclerosing cholangitis. Gut. 2017;66:753–4. doi:10.1136/gutjnl-2016-312180.
62. Miller FW, Alfredsson L, Costenbader KH, Kamen DL, Nelson LM, Norris JM, Roos AJ de. Epidemiology of environmental exposures and human autoimmune diseases: findings from a National Institute of Environmental Health Sciences Expert Panel Workshop. J Autoimmun. 2012;39:259–71. doi:10.1016/j.jaut.2012.05.002.
63. Sharif K, Amital H, Shoenfeld Y. The role of dietary sodium in autoimmune diseases: The salty truth. Autoimmun Rev. 2018;17:1069–73. doi:10.1016/j.autrev.2018.05.007.
64. Chang K, Yang SM, Kim SH, Han KH, Park SJ, Shin JI. Smoking and rheumatoid arthritis. Int J Mol Sci. 2014;15:22279–95. doi:10.3390/ijms151222279.
65. Gorman JD. Smoking and rheumatoid arthritis: another reason to just say no. Arthritis Rheum. 2006;54:10–3. doi:10.1002/art.21576.
66. Kondrashova A, Seiskari T, Ilonen J, Knip M, Hyöty H. The 'Hygiene hypothesis' and the sharp gradient in the incidence of autoimmune and allergic diseases between Russian Karelia and Finland. APMIS. 2013;121:478–93. doi:10.1111/apm.12023.
67. Christen U, Herrath MG von. Infections and Autoimmunity--Good or Bad? The Journal of Immunology. 2005;174:7481–6. doi:10.4049/jimmunol.174.12.7481.
68. Christen U. Editorial: pathogen infection and autoimmunity. Int Rev Immunol. 2014;33:261–5. doi:10.3109/08830185.2014.897345.
69. Herrath MG von, Fujinami RS, Whitton JL. Microorganisms and autoimmunity: making the barren field fertile? Nat Rev Microbiol. 2003;1:151–7. doi:10.1038/nrmicro754.
70. Christen U, Herrath MG von. Initiation of autoimmunity. Curr Opin Immunol. 2004;16:759–67. doi:10.1016/j.coi.2004.09.002.
71. Kaplan MM. Novosphingobium aromaticivorans: a potential initiator of primary biliary cirrhosis. Am J Gastroenterol. 2004;99:2147–9. doi:10.1111/j.1572-0241.2004.41121.x.
72. Tanaka A, Leung PS, Gershwin ME. Environmental basis of primary biliary cholangitis. Exp Biol Med (Maywood). 2018;243:184–9. doi:10.1177/1535370217748893.
73. Faulkner L, Cooper A, Fantino C, Altmann DM, Sriskandan S. The Mechanism of Superantigen-Mediated Toxic Shock: Not a Simple Th1 Cytokine Storm. The Journal of Immunology. 2005;175:6870–7. doi:10.4049/jimmunol.175.10.6870.

74. Maizels RM, McSorley HJ, Smyth DJ. Helminths in the hygiene hypothesis: sooner or later? Clin Exp Immunol. 2014;177:38–46. doi:10.1111/cei.12353.
75. Boyer JL. Bile formation and secretion. Compr Physiol. 2013;3:1035–78. doi:10.1002/cphy.c120027.
76. Bogdanos DP, Gao B, Gershwin ME. Liver immunology. Compr Physiol. 2013;3:567–98. doi:10.1002/cphy.c120011.
77. Ishibashi H, Nakamura M, Komori A, Migita K, Shimoda S. Liver architecture, cell function, and disease. Semin Immunopathol. 2009;31:399–409. doi:10.1007/s00281-009-0155-6.
78. Wick MJ, Leithäuser F, Reimann J. The hepatic immune system. Crit Rev Immunol. 2002;22:47–103.
79. Kita H, Mackay IR, van de Water J, Gershwin ME. The lymphoid liver: considerations on pathways to autoimmune injury. Gastroenterology. 2001;120:1485–501.
80. Calne RY, Sells RA, Pena JR, Davis DR, Millard PR, Herbertson BM, et al. Induction of immunological tolerance by porcine liver allografts. Nature. 1969;223:472–6.
81. KNOLLE P, Schlaak J, Uhrig A, Kempf P, Zum Meyer Büschenfelde KH, GERKEN G. Human Kupffer cells secrete IL-10 in response to lipopolysaccharide (LPS) challenge. Journal of Hepatology. 1995;22:226–9.
82. Lauwerys BR, Garot N, Renauld JC, Houssiau FA. Cytokine production and killer activity of NK/T-NK cells derived with IL-2, IL-15, or the combination of IL-12 and IL-18. The Journal of Immunology. 2000;165:1847–53.
83. Itoh Y, Morita A, Nishioji K, Fujii H, Nakamura H, Kirishima T, et al. Time course profile and cell-type-specific production of monokine induced by interferon-gamma in Concanavalin A-induced hepatic injury in mice: comparative study with interferon-inducible protein-10. Scand J Gastroenterol. 2001;36:1344–51.
84. Crispe IN. Hepatic T cells and liver tolerance. Nat Rev Immunol. 2003;3:51–62. doi:10.1038/nri981.
85. Schwabe RF, Schnabl B, Kweon YO, Brenner DA. CD40 activates NF-kappa B and c-Jun N-terminal kinase and enhances chemokine secretion on activated human hepatic stellate cells. The Journal of Immunology. 2001;166:6812–9.
86. Viñas O, Bataller R, Sancho-Bru P, Ginès P, Berenguer C, Enrich C, et al. Human hepatic stellate cells show features of antigen-presenting cells and stimulate lymphocyte proliferation. Hepatology. 2003;38:919–29. doi:10.1053/jhep.2003.50392.
87. Winau F, Hegasy G, Weiskirchen R, Weber S, Cassan C, Sieling PA, et al. Ito cells are liver-resident antigen-presenting cells for activating T cell responses. Immunity. 2007;26:117–29. doi:10.1016/j.immuni.2006.11.011.
88. Gao B. Basic liver immunology. Cell Mol Immunol. 2016;13:265–6. doi:10.1038/cmi.2016.09.

89. Crispe IN. Liver antigen-presenting cells. Journal of Hepatology. 2011;54:357–65. doi:10.1016/j.jhep.2010.10.005.
90. Thomson AW, Knolle PA. Antigen-presenting cell function in the tolerogenic liver environment. Nat Rev Immunol. 2010;10:753–66. doi:10.1038/nri2858.
91. Sørensen KK, McCourt P, Berg T, Crossley C, Le Couteur D, Wake K, Smedsrød B. The scavenger endothelial cell: a new player in homeostasis and immunity. Am J Physiol Regul Integr Comp Physiol. 2012;303:R1217-30. doi:10.1152/ajpregu.00686.2011.
92. Limmer A, Ohl J, Kurts C, Ljunggren HG, Reiss Y, Groettrup M, et al. Efficient presentation of exogenous antigen by liver endothelial cells to CD8+ T cells results in antigen-specific T-cell tolerance. Nat Med. 2000;6:1348–54. doi:10.1038/82161.
93. KNOLLE P, SCHMITT E, JIN S, GERMANN T, DUCHMANN R, HEGENBARTH S, et al. Induction of cytokine production in naive CD4+ T cells by antigen-presenting murine liver sinusoidal endothelial cells but failure to induce differentiation toward Th1 cells☆, ☆☆. Gastroenterology. 1999;116:1428–40. doi:10.1016/S0016-5085(99)70508-1.
94. Ju C, McCoy JP, Chung CJ, Graf MLM, Pohl LR. Tolerogenic role of Kupffer cells in allergic reactions. Chem Res Toxicol. 2003;16:1514–9. doi:10.1021/tx0341761.
95. Ju C, Pohl LR. Tolerogenic role of Kupffer cells in immune-mediated adverse drug reactions. Toxicology. 2005;209:109–12. doi:10.1016/j.tox.2004.12.017.
96. Knolle, Uhrig, Hegenbarth, LOser, Schmitt, Gerken, Lohse. IL-10 down-regulates T cell activation by antigen-presenting liver sinusoidal endothelial cells through decreased antigen uptake via the mannose receptor and lowered surface expression of accessory molecules. Clin Exp Immunol. 1998;114:427–33. doi:10.1046/j.1365-2249.1998.00713.x.
97. Breous E, Somanathan S, Vandenberghe LH, Wilson JM. Hepatic regulatory T cells and Kupffer cells are crucial mediators of systemic T cell tolerance to antigens targeting murine liver. Hepatology. 2009;50:612–21. doi:10.1002/hep.23043.
98. Knoll P, Schlaak J, Uhrig A, Kempf P, Zum Büschenfelde K-HM, Gerken G. Human Kupffer cells secrete IL-10 in response to lipopolysaccharide (LPS) challenge. Journal of Hepatology. 1995;22:226–9. doi:10.1016/0168-8278(95)80433-1.
99. Wiegard C, Frenzel C, Herkel J, Kallen K-J, Schmitt E, Lohse AW. Murine liver antigen presenting cells control suppressor activity of CD4+CD25+ regulatory T cells. Hepatology. 2005;42:193–9. doi:10.1002/hep.20756.
100. Lüth S, Huber S, Schramm C, Buch T, Zander S, Stadelmann C, et al. Ectopic expression of neural autoantigen in mouse liver suppresses experimental autoimmune neuroinflammation by inducing antigen-specific Tregs. J Clin Invest. 2008;118:3403–10. doi:10.1172/JCI32132.
101. Carambia A, Freund B, Schwinge D, Bruns OT, Salmen SC, Ittrich H, et al. Nanoparticle-based autoantigen delivery to Treg-inducing liver sinusoidal

endothelial cells enables control of autoimmunity in mice. Journal of Hepatology. 2015;62:1349–56. doi:10.1016/j.jhep.2015.01.006.
102. Mastoraki A, Papantoni E, Papanikolaou IS, Kotsilianou O, Kanakis D, Sakorafas G, Safioleas M. Facing the Challenge of Acute Autoimmune Liver Disease: Report of a Case and Review of the Literature. Gastroenterology Res. 2009;2:183–7. doi:10.4021/gr2009.05.1295.
103. Trivedi PJ, Hirschfield GM. Treatment of autoimmune liver disease: current and future therapeutic options. Ther Adv Chronic Dis. 2013;4:119–41. doi:10.1177/2040622313478646.
104. Kaplan MM, Gershwin ME. Primary biliary cirrhosis. N Engl J Med. 2005;353:1261–73. doi:10.1056/NEJMra043898.
105. Griffiths L, Dyson JK, Jones DEJ. The new epidemiology of primary biliary cirrhosis. Semin Liver Dis. 2014;34:318–28. doi:10.1055/s-0034-1383730.
106. Gershwin ME, Selmi C, Worman HJ, Gold EB, Watnik M, Utts J, et al. Risk factors and comorbidities in primary biliary cirrhosis: a controlled interview-based study of 1032 patients. Hepatology. 2005;42:1194–202. doi:10.1002/hep.20907.
107. Corpechot C, Chrétien Y, Chazouillères O, Poupon R. Demographic, lifestyle, medical and familial factors associated with primary biliary cirrhosis. Journal of Hepatology. 2010;53:162–9. doi:10.1016/j.jhep.2010.02.019.
109. Smyk DS, Rigopoulou EI, Bogdanos DP. Potential Roles for Infectious Agents in the Pathophysiology of Primary Biliary Cirrhosis: What's New? Curr Infect Dis Rep. 2013;15:14–24. doi:10.1007/s11908-012-0304-2.
110. Prince MI, Ducker SJ, James OFW. Case-control studies of risk factors for primary biliary cirrhosis in two United Kingdom populations. Gut. 2010;59:508–12. doi:10.1136/gut.2009.184218.
111. Mantaka A, Koulentaki M, Chlouverakis G, Enele-Melono JM, Darivianaki A, Tzardi M, Kouroumalis EA. Primary biliary cirrhosis in a genetically homogeneous population: disease associations and familial occurrence rates. BMC Gastroenterol. 2012;12:110. doi:10.1186/1471-230X-12-110.
112. Li M, Zheng H, Tian Q-b, Rui M-n, Liu D-w. HLA-DR polymorphism and primary biliary cirrhosis: evidence from a meta-analysis. Arch Med Res. 2014;45:270–9. doi:10.1016/j.arcmed.2014.03.002.
113. Purohit T, Cappell MS. Primary biliary cirrhosis: Pathophysiology, clinical presentation and therapy. World J Hepatol. 2015;7:926–41. doi:10.4254/wjh.v7.i7.926.
114. Oertelt S, Rieger R, Selmi C, Invernizzi P, Ansari AA, Coppel RL, et al. A sensitive bead assay for antimitochondrial antibodies: Chipping away at AMA-negative primary biliary cirrhosis. Hepatology. 2007;45:659–65. doi:10.1002/hep.21583.
115. Katsumi T, Tomita K, Leung PSC, Yang G-X, Gershwin ME, Ueno Y. Animal models of primary biliary cirrhosis. Clin Rev Allergy Immunol. 2015;48:142–53. doi:10.1007/s12016-015-8482-y.

116. Hirschfield GM, Gershwin ME. The immunobiology and pathophysiology of primary biliary cirrhosis. Annu Rev Pathol. 2013;8:303–30. doi:10.1146/annurev-pathol-020712-164014.
117. Leung PSC, Wang J, Naiyanetr P, Kenny TP, Lam KS, Kurth MJ, Gershwin ME. Environment and primary biliary cirrhosis: electrophilic drugs and the induction of AMA. J Autoimmun. 2013;41:79–86. doi:10.1016/j.jaut.2012.12.007.
118. Mao TK, Davis PA, Odin JA, Coppel RL, Gershwin ME. Sidechain biology and the immunogenicity of PDC-E2, the major autoantigen of primary biliary cirrhosis. Hepatology. 2004;40:1241–8. doi:10.1002/hep.20491.
119. Tanaka A, Gershwin ME. Finding the cure for primary biliary cholangitis - Still waiting. Liver Int. 2017;37:500–2. doi:10.1111/liv.13344.
120. Chascsa D, Carey EJ, Lindor KD. Old and new treatments for primary biliary cholangitis. Liver Int. 2017;37:490–9. doi:10.1111/liv.13294.
121. Halilbasic E, Fuchs C, Hofer H, Paumgartner G, Trauner M. Therapy of Primary Sclerosing Cholangitis--Today and Tomorrow. Dig Dis. 2015;33 Suppl 2:149–63. doi:10.1159/000440827.
122. Beuers U. Crosstalk of liver, bile ducts and the gut. Clin Rev Allergy Immunol. 2009;36:1–3. doi:10.1007/s12016-008-8084-z.
123. Zenouzi R, Weismüller TJ, Hübener P, Schulze K, Bubenheim M, Pannicke N, et al. Low risk of hepatocellular carcinoma in patients with primary sclerosing cholangitis with cirrhosis. Clin Gastroenterol Hepatol. 2014;12:1733–8. doi:10.1016/j.cgh.2014.02.008.
124. Molodecky NA, Kareemi H, Parab R, Barkema HW, Quan H, Myers RP, Kaplan GG. Incidence of primary sclerosing cholangitis: a systematic review and meta-analysis. Hepatology. 2011;53:1590–9. doi:10.1002/hep.24247.
125. Hirschfield GM, Karlsen TH, Lindor KD, Adams DH. Primary sclerosing cholangitis. The Lancet. 2013;382:1587–99. doi:10.1016/S0140-6736(13)60096-3.
126. Kaplan GG, Laupland KB, Butzner D, Urbanski SJ, Lee SS. The burden of large and small duct primary sclerosing cholangitis in adults and children: a population-based analysis. Am J Gastroenterol. 2007;102:1042–9. doi:10.1111/j.1572-0241.2007.01103.x.
127. Rizvi S, Eaton JE, Gores GJ. Primary Sclerosing Cholangitis as a Premalignant Biliary Tract Disease: Surveillance and Management. Clin Gastroenterol Hepatol. 2015;13:2152–65. doi:10.1016/j.cgh.2015.05.035.
128. Chapman R, Cullen S. Etiopathogenesis of primary sclerosing cholangitis. WJG. 2008;14:3350. doi:10.3748/wjg.14.3350.
129. Spurkland A, Saarinen S, Boberg KM, Mitchell S, Broome U, Caballeria L, et al. HLA class II haplotypes in primary sclerosing cholangitis patients from five European populations. Tissue Antigens. 1999;53:459–69. doi:10.1034/j.1399-0039.1999.530502.x.

130. Janse M, Lamberts LE, Franke L, Raychaudhuri S, Ellinghaus E, Muri Boberg K, et al. Three ulcerative colitis susceptibility loci are associated with primary sclerosing cholangitis and indicate a role for IL2, REL, and CARD9. Hepatology. 2011;53:1977–85. doi:10.1002/hep.24307.
131. Lazaridis KN, LaRusso NF. Primary Sclerosing Cholangitis. N Engl J Med. 2016;375:1161–70. doi:10.1056/NEJMra1506330.
132. Horsley-Silva JL, Carey EJ, Lindor KD. Advances in primary sclerosing cholangitis. Lancet Gastroenterol Hepatol. 2016;1:68–77. doi:10.1016/S2468-1253(16)30010-3.
133. Chapman R, Fevery J, Kalloo A, Nagorney DM, Boberg KM, Shneider B, Gores GJ. Diagnosis and management of primary sclerosing cholangitis. Hepatology. 2010;51:660–78. doi:10.1002/hep.23294.
134. Tischendorf JJW, Hecker H, Krüger M, Manns MP, Meier PN. Characterization, outcome, and prognosis in 273 patients with primary sclerosing cholangitis: A single center study. Am J Gastroenterol. 2007;102:107–14. doi:10.1111/j.1572-0241.2006.00872.x.
135. Hov JR, Boberg KM, Karlsen TH. Autoantibodies in primary sclerosing cholangitis. WJG. 2008;14:3781. doi:10.3748/wjg.14.3781.
136. Lammert F, Wang DQ-H, Hillebrandt S, Geier A, Fickert P, Trauner M, et al. Spontaneous cholecysto- and hepatolithiasis in Mdr2-/- mice: a model for low phospholipid-associated cholelithiasis. Hepatology. 2004;39:117–28. doi:10.1002/hep.20022.
137. Degiorgio D, Crosignani A, Colombo C, Bordo D, Zuin M, Vassallo E, et al. ABCB4 mutations in adult patients with cholestatic liver disease: impact and phenotypic expression. J Gastroenterol. 2016;51:271–80. doi:10.1007/s00535-015-1110-z.
138. Mauad TH, van Nieuwkerk CMJ, Dingemans KP, Smit JJM, Schinkel AH, Notenboom RGE, et al. Mice with Homozygous Disruption of the mdr2 P-Glycoprotein Gene A Novel Animal Model for Studies of Nonsuppurative Inflammatory Cholangitis and Hepatocarcinogenesis. Am J Pathol. 1994;145:1237–45.
139. Fickert P, Fuchsbichler A, Wagner M, Zollner G, Kaser A, Tilg H, et al. Regurgitation of bile acids from leaky bile ducts causes sclerosing cholangitis in Mdr2 (Abcb4) knockout mice. Gastroenterology. 2004;127:261–74. doi:10.1053/j.gastro.2004.04.009.
140. Trauner M, Fickert P, Wagner M. MDR3 (ABCB4) defects: a paradigm for the genetics of adult cholestatic syndromes. Semin Liver Dis. 2007;27:77–98. doi:10.1055/s-2006-960172.
141. Fickert P, Zollner G, Fuchsbichler A, Stumptner C, Weiglein AH, Lammert F, et al. Ursodeoxycholic acid aggravates bile infarcts in bile duct–ligated and Mdr2 knockout mice via disruption of cholangioles. Gastroenterology. 2002;123:1238–51. doi:10.1053/gast.2002.35948.

142. Carrasco-Avino G, Schiano TD, Ward SC, Thung SN, Fiel MI. Primary sclerosing cholangitis: detailed histologic assessment and integration using bioinformatics highlights arterial fibrointimal hyperplasia as a novel feature. Am J Clin Pathol. 2015;143:505–13. doi:10.1309/AJCPVKFVIPRBXQR2.
143. Smit JJM, Schinkel AH, Elferink RPJO, Groen AK, Wagenaar E, van Deemter L, et al. Homozygous disruption of the murine MDR2 P-glycoprotein gene leads to a complete absence of phospholipid from bile and to liver disease. Cell. 1993;75:451–62. doi:10.1016/0092-8674(93)90380-9.
144. Pollheimer MJ, Fickert P. Animal models in primary biliary cirrhosis and primary sclerosing cholangitis. Clin Rev Allergy Immunol. 2015;48:207–17. doi:10.1007/s12016-014-8442-y.
145. Hintermann E, Holdener M, Bayer M, Loges S, Pfeilschifter JM, Granier C, et al. Epitope spreading of the anti-CYP2D6 antibody response in patients with autoimmune hepatitis and in the CYP2D6 mouse model. J Autoimmun. 2011;37:242–53. doi:10.1016/j.jaut.2011.06.005.
146. Mieli-Vergani G, Vergani D. Autoimmune paediatric liver disease. WJG. 2008;14:3360. doi:10.3748/wjg.14.3360.
147. Mieli-Vergani G, Vergani D, Baumann U, Czubkowski P, Debray D, Dezsofi A, et al. Diagnosis and Management of Pediatric Autoimmune Liver Disease. Journal of Pediatric Gastroenterology and Nutrition. 2018;66:345–60. doi:10.1097/MPG.0000000000001801.
148. Dong Y, Potthoff A, Klinger C, Barreiros AP, Pietrawski D, Dietrich CF. Ultrasound findings in autoimmune hepatitis. World J Gastroenterol. 2018;24:1583–90. doi:10.3748/wjg.v24.i15.1583.
149. Zachou K, Muratori P, Koukoulis GK, Granito A, Gatselis N, Fabbri A, et al. Review article: autoimmune hepatitis -- current management and challenges. Aliment Pharmacol Ther. 2013;38:887–913. doi:10.1111/apt.12470.
150. Manns MP, Czaja AJ, Gorham JD, Krawitt EL, Mieli-Vergani G, Vergani D, Vierling JM. Diagnosis and management of autoimmune hepatitis. Hepatology. 2010;51:2193–213. doi:10.1002/hep.23584.
151. Oo YH, Hubscher SG, Adams DH. Autoimmune hepatitis: new paradigms in the pathogenesis, diagnosis, and management. Hepatol Int. 2010;4:475–93. doi:10.1007/s12072-010-9183-5.
152. Liberal R, Grant CR, Mieli-Vergani G, Vergani D. Autoimmune hepatitis: a comprehensive review. J Autoimmun. 2013;41:126–39. doi:10.1016/j.jaut.2012.11.002.
153. Grønbæk L, Vilstrup H, Jepsen P. Autoimmune hepatitis in Denmark: incidence, prevalence, prognosis, and causes of death. A nationwide registry-based cohort study. Journal of Hepatology. 2014;60:612–7. doi:10.1016/j.jhep.2013.10.020.

154. Sebode M, Weiler-Normann C, Liwinski T, Schramm C. Autoantibodies in Autoimmune Liver Disease-Clinical and Diagnostic Relevance. Front Immunol. 2018;9:609. doi:10.3389/fimmu.2018.00609.
155. Christen U, Hintermann E. Autoantibodies in Autoimmune Hepatitis: Can Epitopes Tell Us about the Etiology of the Disease? Front Immunol. 2018;9:163. doi:10.3389/fimmu.2018.00163.
156. Christen U. The role of autoantibodies in autoimmune hepatitis type 2. Immunotherapy. 2013;5:247–56. doi:10.2217/imt.13.5.
157. Yamamoto AM, Mura C, Lemos-Chiarandini C de, Krishnamoorthy R, Alvarez F. Cytochrome P450IID6 recognized by LKM1 antibody is not exposed on the surface of hepatocytes. Clin Exp Immunol. 1993;92:381–90.
158. Manns MP, Griffin KJ, Sullivan KF, Johnson EF. LKM-1 autoantibodies recognize a short linear sequence in P450IID6, a cytochrome P-450 monooxygenase. J. Clin. Invest. 1991;88:1370–8. doi:10.1172/JCI115443.
159. Liberal R, Vergani D, Mieli-Vergani G. Paediatric Autoimmune Liver Disease. Dig Dis. 2015;33 Suppl 2:36–46. doi:10.1159/000440708.
160. Christen U, Hintermann E. Immunopathogenic Mechanisms of Autoimmune Hepatitis: How Much Do We Know from Animal Models? Int J Mol Sci 2016. doi:10.3390/ijms17122007.
161. Donaldson P. Susceptibility to autoimmune chronic active hepatitis: Human leukocyte antigens DR4 and A1-B8-DR3 are independent risk factors. Hepatology. 1991;13:701–6. doi:10.1016/0270-9139(91)92567-R.
162. Ma Y, Bogdanos DP, Hussain MJ, Underhill J, Bansal S, Longhi MS, et al. Polyclonal T-cell responses to cytochrome P450IID6 are associated with disease activity in autoimmune hepatitis type 2. Gastroenterology. 2006;130:868–82. doi:10.1053/j.gastro.2005.12.020.
163. Holdener M, Hintermann E, Bayer M, Rhode A, Rodrigo E, Hintereder G, et al. Breaking tolerance to the natural human liver autoantigen cytochrome P450 2D6 by virus infection. J Exp Med. 2008;205:1409–22. doi:10.1084/jem.20071859.
164. Bowen DG, Zen M, Holz L, Davis T, McCaughan GW, Bertolino P. The site of primary T cell activation is a determinant of the balance between intrahepatic tolerance and immunity. J. Clin. Invest. 2004;114:701–12. doi:10.1172/JCI200421593.
166. Yamamoto AM, MURA C, De Lemos-Chiarandini C. Krishnamoorthy R, Alvarez . Cytochrome P450IID6 recognized by LKMl antibody is not exposed on the surface of hepatocytes. Clinical & Experimental Immunology Volume 92, Issue 3. 1993
167. Kerkar N, Choudhuri K, Ma Y, Mahmoud A, Bogdanos DP, Muratori L, et al. Cytochrome P4502D6193-212: A New Immunodominant Epitope and Target of Virus/Self Cross-Reactivity in Liver Kidney Microsomal Autoantibody Type 1-Positive Liver Disease. The Journal of Immunology. 2003;170:1481–9. doi:10.4049/jimmunol.170.3.1481.

168. EASL Clinical Practice Guidelines: Autoimmune hepatitis. Journal of Hepatology. 2015;63:971–1004. doi:10.1016/j.jhep.2015.06.030.
169. Czaja AJ, Manns MP. Advances in the diagnosis, pathogenesis, and management of autoimmune hepatitis. Gastroenterology. 2010;139:58-72.e4. doi:10.1053/j.gastro.2010.04.053.
170. Terziroli Beretta-Piccoli B, Mieli-Vergani G, Vergani D. Autoimmune hepatitis: Standard treatment and systematic review of alternative treatments. World J Gastroenterol. 2017;23:6030–48. doi:10.3748/wjg.v23.i33.6030.
171. Czaja AJ. Advances in the current treatment of autoimmune hepatitis. Dig Dis Sci. 2012;57:1996–2010. doi:10.1007/s10620-012-2151-2.
172. Strassburg CP, Manns MP. Treatment of autoimmune hepatitis. Semin Liver Dis. 2009;29:273–85. doi:10.1055/s-0029-1233534.
173. Schramm C, Lohse AW. Role of mycophenolate mofetil in the treatment of autoimmune hepatitis. Journal of Hepatology. 2011;55:510–1. doi:10.1016/j.jhep.2011.01.012.
174. Baven-Pronk AMC, Coenraad MJ, van Buuren HR, Man RA de, van Erpecum KJ, Lamers MMH, et al. The role of mycophenolate mofetil in the management of autoimmune hepatitis and overlap syndromes. Aliment Pharmacol Ther. 2011;34:335–43. doi:10.1111/j.1365-2036.2011.04727.x.
175. Chatur N, Ramji A, Bain VG, Ma MM, Marotta PJ, Ghent CN, et al. Transplant immunosuppressive agents in non-transplant chronic autoimmune hepatitis: the Canadian association for the study of liver (CASL) experience with mycophenolate mofetil and tacrolimus. Liver Int. 2005;25:723–7. doi:10.1111/j.1478-3231.2005.01107.x.
176. Inductivo-Yu I, Adams A, Gish RG, Wakil A, Bzowej NH, Frederick RT, Bonacini M. Mycophenolate mofetil in autoimmune hepatitis patients not responsive or intolerant to standard immunosuppressive therapy. Clin Gastroenterol Hepatol. 2007;5:799–802. doi:10.1016/j.cgh.2007.02.030.
177. Devlin SM, Swain MG, Urbanski SJ, Burak KW. Mycophenolate Mofetil for the Treatment of Autoimmune Hepatitis in Patients Refractory to Standard Therapy. Canadian Journal of Gastroenterology. 2004;18:321–6. doi:10.1155/2004/504591.
178. Richardson PD, James PD, Ryder SD. Mycophenolate mofetil for maintenance of remission in autoimmune hepatitis in patients resistant to or intolerant of azathioprine. Journal of Hepatology. 2000;33:371–5. doi:10.1016/S0168-8278(00)80271-8.
179. Christen U, Herrath MG von. Initiation of autoimmunity. Curr Opin Immunol. 2004;16:759–67. doi:10.1016/j.coi.2004.09.002.
180. Holdener M, Hintermann E, Bayer M, Rhode A, Rodrigo E, Hintereder G, et al. Breaking tolerance to the natural human liver autoantigen cytochrome P450 2D6 by virus infection. J Exp Med. 2008;205:1409–22. doi:10.1084/jem.20071859.

181. Rust C, Beuers U. Overlap syndromes among autoimmune liver diseases. WJG. 2008;14:3368. doi:10.3748/wjg.14.3368.
182. Boberg KM, Chapman RW, Hirschfield GM, Lohse AW, Manns MP, Schrumpf E. Overlap syndromes: the International Autoimmune Hepatitis Group (IAIHG) position statement on a controversial issue. Journal of Hepatology. 2011;54:374–85. doi:10.1016/j.jhep.2010.09.002.
183. Czaja AJ. Diagnosis and Management of the Overlap Syndromes of Autoimmune Hepatitis. Canadian Journal of Gastroenterology. 2013;27:417–23. doi:10.1155/2013/198070.
184. McNair A. Autoimmune hepatitis overlapping with primary sclerosing cholangitis in five cases. Am J Gastroenterol. 1998;93:777–84. doi:10.1016/S0002-9270(98)00104-X.
185. Buuren HRv, Hoogstraten HJFv, Terkivatan T, Schalm SW, Vleggaar FP. High prevalence of autoimmune hepatitis among patients with primary sclerosing cholangitis. Journal of Hepatology. 2000;33:543–8. doi:10.1016/S0168-8278(00)80005-7.
186. Gregorio GV, Portmann B, Karani J, Harrison P, Donaldson PT, Vergani D, Mieli-Vergani G. Autoimmune hepatitis/sclerosing cholangitis overlap syndrome in childhood: a 16-year prospective study. Hepatology. 2001;33:544–53. doi:10.1053/jhep.2001.22131.
187. Kuiper EMM, Zondervan PE, van Buuren HR. Paris criteria are effective in diagnosis of primary biliary cirrhosis and autoimmune hepatitis overlap syndrome. Clin Gastroenterol Hepatol. 2010;8:530–4. doi:10.1016/j.cgh.2010.03.004.
188. EASL Clinical Practice Guidelines: management of cholestatic liver diseases. Journal of Hepatology. 2009;51:237–67. doi:10.1016/j.jhep.2009.04.009.
189. Autoimmune Hepatitis-Primary Biliary Cirrhosis Overlap Syndrome: Current Trends in Diagnosis and Treatment.
190. Corpechot C, Abenavoli L, Rabahi N, Chrétien Y, Andréani T, Johanet C, et al. Biochemical response to ursodeoxycholic acid and long-term prognosis in primary biliary cirrhosis. Hepatology. 2008;48:871–7. doi:10.1002/hep.22428.
191. Czaja AJ. Review article: The prevention and reversal of hepatic fibrosis in autoimmune hepatitis. Aliment Pharmacol Ther. 2014;39:385–406. doi:10.1111/apt.12592.
192. Czaja AJ. The overlap syndromes of autoimmune hepatitis. Dig Dis Sci. 2013;58:326–43. doi:10.1007/s10620-012-2367-1.
193. Lüth S, Kanzler S, Frenzel C, Kasper HU, Dienes HP, Schramm C, et al. Characteristics and long-term prognosis of the autoimmune hepatitis/primary sclerosing cholangitis overlap syndrome. J Clin Gastroenterol. 2009;43:75–80. doi:10.1097/MCG.0b013e318157c614.
194. Floreani A, Rizzotto ER, Ferrara F, Carderi I, Caroli D, Blasone L, Baldo V. Clinical course and outcome of autoimmune hepatitis/primary sclerosing cholangitis

overlap syndrome. Am J Gastroenterol. 2005;100:1516–22. doi:10.1111/j.1572-0241.2005.41841.x.

195. Fontenot JD, Rudensky AY. A well adapted regulatory contrivance: regulatory T cell development and the forkhead family transcription factor Foxp3. Nat Immunol. 2005;6:331–7. doi:10.1038/ni1179.

196. Sakaguchi S, Miyara M, Costantino CM, Hafler DA. FOXP3+ regulatory T cells in the human immune system. Nat Rev Immunol. 2010;10:490–500. doi:10.1038/nri2785.

197. Fontenot JD, Gavin MA, Rudensky AY. Foxp3 programs the development and function of CD4+CD25+ regulatory T cells. Nat Immunol. 2003;4:330–6. doi:10.1038/ni904.

198. Hori S, Nomura T, Sakaguchi S. Control of regulatory T cell development by the transcription factor Foxp3. Science. 2003;299:1057–61. doi:10.1126/science.1079490.

199. Khattri R, Cox T, Yasayko S-A, Ramsdell F. An essential role for Scurfin in CD4+CD25+ T regulatory cells. Nat Immunol. 2003;4:337–42. doi:10.1038/ni909.

200. Cao X, Cai SF, Fehniger TA, Song J, Collins LI, Piwnica-Worms DR, Ley TJ. Granzyme B and perforin are important for regulatory T cell-mediated suppression of tumor clearance. Immunity. 2007;27:635–46. doi:10.1016/j.immuni.2007.08.014.

201. Gondek DC, Lu L-F, Quezada SA, Sakaguchi S, Noelle RJ. Cutting Edge: Contact-Mediated Suppression by CD4+CD25+ Regulatory Cells Involves a Granzyme B-Dependent, Perforin-Independent Mechanism. The Journal of Immunology. 2005;174:1783–6. doi:10.4049/jimmunol.174.4.1783.

202. Vignali DAA, Collison LW, Workman CJ. How regulatory T cells work. Nat Rev Immunol. 2008;8:523–32. doi:10.1038/nri2343.

203. Liu J, Cao X. Regulatory dendritic cells in autoimmunity: A comprehensive review. J Autoimmun. 2015;63:1–12. doi:10.1016/j.jaut.2015.07.011.

204. Inaba K, Inaba M, Deguchi M, Hagi K, Yasumizu R, Ikehara S, et al. Granulocytes, macrophages, and dendritic cells arise from a common major histocompatibility complex class II-negative progenitor in mouse bone marrow. Proc Natl Acad Sci U S A. 1993;90:3038–42.

205. Inaba K. Generation of large numbers of dendritic cells from mouse bone marrow cultures supplemented with granulocyte/macrophage colony-stimulating factor. Journal of Experimental Medicine. 1992;176:1693–702. doi:10.1084/jem.176.6.1693.

206. Anderson AE, Sayers BL, Haniffa MA, Swan DJ, Diboll J, Wang X-N, et al. Differential regulation of naïve and memory CD4+ T cells by alternatively activated dendritic cells. J Leukoc Biol. 2008;84:124–33. doi:10.1189/jlb.1107744.

207. Anderson AE, Swan DJ, Sayers BL, Harry RA, Patterson AM, Delwig A von, et al. LPS activation is required for migratory activity and antigen presentation by

tolerogenic dendritic cells. J Leukoc Biol. 2009;85:243–50. doi:10.1189/jlb.0608374.

208. Bosma BM, Metselaar HJ, Nagtzaam NMA, Haan R de, Mancham S, van der Laan LJW, et al. Dexamethasone transforms lipopolysaccharide-stimulated human blood myeloid dendritic cells into myeloid dendritic cells that prime interleukin-10 production in T cells. Immunology. 2008;125:91–100. doi:10.1111/j.1365-2567.2008.02824.x.

209. Harry RA, Anderson AE, Isaacs JD, Hilkens CMU. Generation and characterisation of therapeutic tolerogenic dendritic cells for rheumatoid arthritis. Ann Rheum Dis. 2010;69:2042–50. doi:10.1136/ard.2009.126383.

210. O'Flynn L, Treacy O, Ryan AE, Morcos M, Cregg M, Gerlach J, et al. Donor bone marrow-derived dendritic cells prolong corneal allograft survival and promote an intragraft immunoregulatory milieu. Mol Ther. 2013;21:2102–12. doi:10.1038/mt.2013.167.

211. Domogalla MP, Rostan PV, Raker VK, Steinbrink K. Tolerance through Education: How Tolerogenic Dendritic Cells Shape Immunity. Front Immunol. 2017;8:1764. doi:10.3389/fimmu.2017.01764.

212. Audiger C, Rahman MJ, Yun TJ, Tarbell KV, Lesage S. The Importance of Dendritic Cells in Maintaining Immune Tolerance. J Immunol. 2017;198:2223–31. doi:10.4049/jimmunol.1601629.

213. Hirsch DL, Ponda P. Antigen-based immunotherapy for autoimmune disease: current status. Immunotargets Ther. 2015;4:1–11. doi:10.2147/ITT.S49656.

214. Machen J, Harnaha J, Lakomy R, Styche A, Trucco M, Giannoukakis N. Antisense Oligonucleotides Down-Regulating Costimulation Confer Diabetes-Preventive Properties to Nonobese Diabetic Mouse Dendritic Cells. The Journal of Immunology. 2004;173:4331–41. doi:10.4049/jimmunol.173.7.4331.

215. Krege J, Seth S, Hardtke S, Davalos-Misslitz ACM, Förster R. Antigen-dependent rescue of nose-associated lymphoid tissue (NALT) development independent of LTbetaR and CXCR5 signaling. Eur J Immunol. 2009;39:2765–78. doi:10.1002/eji.200939422.

216. Kiyono H, Fukuyama S. NALT- versus Peyer's-patch-mediated mucosal immunity. Nat Rev Immunol. 2004;4:699–710. doi:10.1038/nri1439.

217. Jain R, Waldvogel-Thurlow S, Darveau R, Douglas R. Differences in the paranasal sinuses between germ-free and pathogen-free mice. Int Forum Allergy Rhinol. 2016;6:631–7. doi:10.1002/alr.21712.

218. Heritage PL, Underdown BJ, Arsenault AL, Snider DP, McDermott MR. Comparison of murine nasal-associated lymphoid tissue and Peyer's patches. Am J Respir Crit Care Med. 1997;156:1256–62. doi:10.1164/ajrccm.156.4.97-03017.

219. Lee H, Ruane D, Law K, Ho Y, Garg A, Rahman A, et al. Phenotype and function of nasal dendritic cells. Mucosal Immunol. 2015;8:1083–98. doi:10.1038/mi.2014.135.

220. Mutoh M, Kimura S, Takahashi-Iwanaga H, Hisamoto M, Iwanaga T, Iida J. RANKL regulates differentiation of microfold cells in mouse nasopharynx-associated lymphoid tissue (NALT). Cell Tissue Res. 2016;364:175–84. doi:10.1007/s00441-015-2309-2.
221. WU H-Y, NGUYEN HH, RUSSELL MW. Nasal Lymphoid Tissue (NALT) as a Mucosal Immune Inductive Site. Scand J Immunol. 1997;46:506–13. doi:10.1046/j.1365-3083.1997.d01-159.x.
222. Unger WWJ. Nasal tolerance induces antigen-specific CD4+CD25- regulatory T cells that can transfer their regulatory capacity to naive CD4+ T cells. International Immunology. 2003;15:731–9. doi:10.1093/intimm/dxg069.
223. Fourlanos S, Perry C, Gellert SA, Martinuzzi E, Mallone R, Butler J, et al. Evidence that nasal insulin induces immune tolerance to insulin in adults with autoimmune diabetes. Diabetes. 2011;60:1237–45. doi:10.2337/db10-1360.
224. Chai J-G, James E, Dewchand H, Simpson E, Scott D. Transplantation tolerance induced by intranasal administration of HY peptides. Blood. 2004;103:3951–9. doi:10.1182/blood-2003-11-3763.
225. Ronan EO, Lee LN, Tchilian EZ, Beverley PCL. Nasal associated lymphoid tissue (NALT) contributes little to protection against aerosol challenge with Mycobacterium tuberculosis after immunisation with a recombinant adenoviral vaccine. Vaccine. 2010;28:5179–84. doi:10.1016/j.vaccine.2010.05.075.
226. DEBERTIN AS, TSCHERNIG T, TONJES H, KLEEMANN WJ, TROGER HD, PABST R. Nasal-associated lymphoid tissue (NALT): frequency and localization in young children. Clin Exp Immunol. 2003;134:503–7. doi:10.1111/j.1365-2249.2003.02311.x.
227. Miller SD, Wetzig RP, Claman HN. The induction of cell-mediated immunity and tolerance with protein antigens coupled to syngeneic lymphoid cells. Journal of Experimental Medicine. 1979;149:758–73.
228. Turley DM, Miller SD. Prospects for antigen-specific tolerance based therapies for the treatment of multiple sclerosis. Results Probl Cell Differ. 2010;51:217–35. doi:10.1007/400_2008_13.
229. Eagar TN, Turley DM, Padilla J, Karandikar NJ, Tan L, Bluestone JA, Miller SD. CTLA-4 Regulates Expansion and Differentiation of Th1 Cells Following Induction of Peripheral T Cell Tolerance. The Journal of Immunology. 2004;172:7442–50. doi:10.4049/jimmunol.172.12.7442.
230. Luo X, Pothoven KL, McCarthy D, DeGutes M, Martin A, Getts DR, et al. ECDI-fixed allogeneic splenocytes induce donor-specific tolerance for long-term survival of islet transplants via two distinct mechanisms. Proc Natl Acad Sci U S A. 2008;105:14527–32. doi:10.1073/pnas.0805204105.
231. Miller SD, Turley DM, Podojil JR. Antigen-specific tolerance strategies for the prevention and treatment of autoimmune disease. Nat Rev Immunol. 2007;7:665–77. doi:10.1038/nri2153.

232. Turley DM, Miller SD. Peripheral Tolerance Induction Using Ethylenecarbodiimide-Fixed APCs Uses both Direct and Indirect Mechanisms of Antigen Presentation for Prevention of Experimental Autoimmune Encephalomyelitis. The Journal of Immunology. 2007;178:2212–20. doi:10.4049/jimmunol.178.4.2212.
233. Fife BT, Guleria I, Gubbels Bupp M, Eagar TN, Tang Q, Bour-Jordan H, et al. Insulin-induced remission in new-onset NOD mice is maintained by the PD-1-PD-L1 pathway. J Exp Med. 2006;203:2737–47. doi:10.1084/jem.20061577.
234. Gregorian SK, Clark L, Heber-Katz E, Amento EP, Rostami A. Induction of peripheral tolerance with peptide-specific anergy in experimental autoimmune neuritis. Cell Immunol. 1993;150:298–310. doi:10.1006/cimm.1993.1198.
235. Dua HS, Gregerson DS, Donoso LA. Inhibition of experimental autoimmune uveitis by retinal photoreceptor antigens coupled to spleen cells. Cell Immunol. 1992;139:292–305.
236. Smith CE, Eagar TN, Strominger JL, Miller SD. Differential induction of IgE-mediated anaphylaxis after soluble vs. cell-bound tolerogenic peptide therapy of autoimmune encephalomyelitis. Proc Natl Acad Sci U S A. 2005;102:9595–600. doi:10.1073/pnas.0504131102.
237. Pedotti R, Mitchell D, Wedemeyer J, Karpuj M, Chabas D, Hattab EM, et al. An unexpected version of horror autotoxicus: anaphylactic shock to a self-peptide. Nat Immunol. 2001;2:216–22. doi:10.1038/85266.
238. Getts DR, Turley DM, Smith CE, Harp CT, McCarthy D, Feeney EM, et al. Tolerance induced by apoptotic antigen-coupled leukocytes is induced by PD-L1+ and IL-10-producing splenic macrophages and maintained by T regulatory cells. J Immunol. 2011;187:2405–17. doi:10.4049/jimmunol.1004175.
239. Musyanovych A, Landfester K. Polymer micro- and nanocapsules as biological carriers with multifunctional properties. Macromol Biosci. 2014;14:458–77. doi:10.1002/mabi.201300551.
240. Getts DR, Terry RL, Getts MT, Deffrasnes C, Müller M, van Vreden C, et al. Therapeutic inflammatory monocyte modulation using immune-modifying microparticles. Sci Transl Med. 2014;6:219ra7. doi:10.1126/scitranslmed.3007563.
241. Danhier F, Ansorena E, Silva JM, Coco R, Le Breton A, Préat V. PLGA-based nanoparticles: an overview of biomedical applications. J Control Release. 2012;161:505–22. doi:10.1016/j.jconrel.2012.01.043.
242. Getts DR, Shea LD, Miller SD, King NJC. Harnessing nanoparticles for immune modulation. Trends Immunol. 2015;36:419–27. doi:10.1016/j.it.2015.05.007.
243. Hunter Z, McCarthy DP, Yap WT, Harp CT, Getts DR, Shea LD, Miller SD. A biodegradable nanoparticle platform for the induction of antigen-specific immune tolerance for treatment of autoimmune disease. ACS Nano. 2014;8:2148–60. doi:10.1021/nn405033r.

244. Getts DR, Martin AJ, McCarthy DP, Terry RL, Hunter ZN, Yap WT, et al. Microparticles bearing encephalitogenic peptides induce T-cell tolerance and ameliorate experimental autoimmune encephalomyelitis. Nat Biotechnol. 2012;30:1217–24. doi:10.1038/nbt.2434.
245. Hunter Z, McCarthy DP, Yap WT, Harp CT, Getts DR, Shea LD, Miller SD. A biodegradable nanoparticle platform for the induction of antigen-specific immune tolerance for treatment of autoimmune disease. ACS Nano. 2014;8:2148–60. doi:10.1021/nn405033r.
246. Barbucci R, Giani G, Fedi S, Bottari S, Casolaro M. Biohydrogels with magnetic nanoparticles as crosslinker: characteristics and potential use for controlled antitumor drug-delivery. Acta Biomater. 2012;8:4244–52. doi:10.1016/j.actbio.2012.09.006.
247. Ponzio RA, Marcato YL, Gómez ML, Waiman CV, Chesta CA, Palacios RE. Crosslinked polymer nanoparticles containing single conjugated polymer chains. Methods Appl Fluoresc. 2017;5:24001. doi:10.1088/2050-6120/aa6405.
248. Lewis JS, Dolgova NV, Zhang Y, Xia CQ, Wasserfall CH, Atkinson MA, et al. A combination dual-sized microparticle system modulates dendritic cells and prevents type 1 diabetes in prediabetic NOD mice. Clin Immunol. 2015;160:90–102. doi:10.1016/j.clim.2015.03.023.
249. Yeste A, Nadeau M, Burns EJ, Weiner HL, Quintana FJ. Nanoparticle-mediated codelivery of myelin antigen and a tolerogenic small molecule suppresses experimental autoimmune encephalomyelitis. Proc Natl Acad Sci U S A. 2012;109:11270–5. doi:10.1073/pnas.1120611109.
250. Maldonado RA, LaMothe RA, Ferrari JD, Zhang A-H, Rossi RJ, Kolte PN, et al. Polymeric synthetic nanoparticles for the induction of antigen-specific immunological tolerance. Proc Natl Acad Sci U S A. 2015;112:E156-65. doi:10.1073/pnas.1408686111.
251. Hintermann E, Ehser J, Bayer M, Pfeilschifter JM, Christen U. Mechanism of autoimmune hepatic fibrogenesis induced by an adenovirus encoding the human liver autoantigen cytochrome P450 2D6. J Autoimmun. 2013;44:49–60. doi:10.1016/j.jaut.2013.05.001.
252. Chapman RW, Arborgh BA, Rhodes JM, Summerfield JA, Dick R, Scheuer PJ, Sherlock S. Primary sclerosing cholangitis: a review of its clinical features, cholangiography, and hepatic histology. Gut. 1980;21:870–7. doi:10.1136/gut.21.10.870.
253. Chapman R, Fevery J, Kalloo A, Nagorney DM, Boberg KM, Shneider B, Gores GJ. Diagnosis and management of primary sclerosing cholangitis. Hepatology. 2010;51:660–78. doi:10.1002/hep.23294.
254. Desmet VJ, Gerber M, Hoofnagle JH, Manns M, Scheuer PJ. Classification of chronic hepatitis: Diagnosis, grading and staging. Hepatology. 1994 Jun;19(6):1513-20.

255. Czaja AJ. Behavior and significance of autoantibodies in type 1 autoimmune hepatitis. Journal of Hepatology. 1999;30:394–401.
256. Terjung B, Spengler U, Sauerbruch T, Worman HJ. “Atypical p-ANCA” in IBD and hepatobiliary disorders react with a 50-kilodalton nuclear envelope protein of neutrophils and myeloid cell lines. Gastroenterology. 2000;119:310–22. doi:10.1053/gast.2000.9366.
257. Ehser J, Holdener M, Christen S, Bayer M, Pfeilschifter JM, Hintermann E, et al. Molecular mimicry rather than identity breaks T-cell tolerance in the CYP2D6 mouse model for human autoimmune hepatitis. J Autoimmun. 2013;42:39–49. doi:10.1016/j.jaut.2012.11.001.
258. Gidwaney NG, Pawa S, Das KM. Pathogenesis and clinical spectrum of primary sclerosing cholangitis. World J Gastroenterol. 2017;23:2459–69. doi:10.3748/wjg.v23.i14.2459.
259. Lammert F, Wang DQ-H, Hillebrandt S, Geier A, Fickert P, Trauner M, et al. Spontaneous cholecysto- and hepatolithiasis in Mdr2-/- mice: a model for low phospholipid-associated cholelithiasis. Hepatology. 2004;39:117–28. doi:10.1002/hep.20022.
260. Chandok N, Hirschfield GM. Management of Primary Sclerosing Cholangitis: Conventions and Controversies. Canadian Journal of Gastroenterology. 2012;26:261–8. doi:10.1155/2012/426430.
261. Eaton JE, Talwalkar JA, Lazaridis KN, Gores GJ, Lindor KD. Pathogenesis of primary sclerosing cholangitis and advances in diagnosis and management. Gastroenterology. 2013;145:521–36. doi:10.1053/j.gastro.2013.06.052.
262. Chapman R, Fevery J, Kalloo A, Nagorney DM, Boberg KM, Shneider B, Gores GJ. Diagnosis and management of primary sclerosing cholangitis. Hepatology. 2010;51:660–78. doi:10.1002/hep.23294.
263. Talwalkar JA, Lindor KD. Primary sclerosing cholangitis. Inflamm Bowel Dis. 2005;11:62–72.
264. Czaja AJ. Autoimmune hepatitis--approach to diagnosis. MedGenMed. 2006;8:55.
265. Czaja AJ. Diagnosis and Management of the Overlap Syndromes of Autoimmune Hepatitis. Canadian Journal of Gastroenterology. 2013;27:417–23. doi:10.1155/2013/198070.
266. Benito de Valle M, Müller T, Björnsson E, Otten M, Volkmann M, Guckelberger O, et al. The impact of elevated serum IgG4 levels in patients with primary sclerosing cholangitis. Dig Liver Dis. 2014;46:903–8. doi:10.1016/j.dld.2014.06.010.
267. Ballot E, Homberg JC, Johanet C. Antibodies to soluble liver antigen: an additional marker in type 1 auto-immune hepatitis. Journal of Hepatology. 2000;33:208–15.
268. Miyakawa H, Kawashima Y, Kitazawa E, Kawaguchi N, Kato T, Kikuchi K, et al. Low frequency of anti-SLA/LP autoantibody in Japanese adult patients with

autoimmune liver diseases: analysis with recombinant antigen assay. J Autoimmun. 2003;21:77–82.
269. Vierling JM. Animal models for primary sclerosing cholangitis. Best Pract Res Clin Gastroenterol. 2001;15:591–610. doi:10.1053/bega.2001.0207.
270. McFarlane IG. Definition and classification of autoimmune hepatitis. Semin Liver Dis. 2002;22:317–24. doi:10.1055/s-2002-35702.
271. Vergani D, Mieli-Vergani G. Autoimmune hepatitis: Diagnostic criteria and serological testing. Clinical Liver Disease. 2014;3:38–41. doi:10.1002/cld.321.
272. Glaser S, Meng F, Han Y, Onori P, Chow BK, Francis H, et al. Secretin stimulates biliary cell proliferation by regulating expression of microRNA 125b and microRNA let7a in mice. Gastroenterology. 2014;146:1795-808.e12. doi:10.1053/j.gastro.2014.02.030.
273. Lee S-O. Physiologic and pathologic experimental models for studying cholangiocytes. Korean J Hepatol. 2008;14:139–49. doi:10.3350/kjhep.2008.14.2.139.
274. Yoo K-S, Lim WT, Choi HS. Biology of Cholangiocytes: From Bench to Bedside. Gut Liver. 2016;10:687–98. doi:10.5009/gnl16033.
275. Jones H, Hargrove L, Kennedy L, Meng F, Graf-Eaton A, Owens J, et al. Inhibition of mast cell-secreted histamine decreases biliary proliferation and fibrosis in primary sclerosing cholangitis Mdr2(-/-) mice. Hepatology. 2016;64:1202–16. doi:10.1002/hep.28704.
276. Graf A, Meng F, Hargrove L, Kennedy L, Han Y, Francis T, et al. Knockout of histidine decarboxylase decreases bile duct ligation-induced biliary hyperplasia via downregulation of the histidine decarboxylase/VEGF axis through PKA-ERK1/2 signaling. Am J Physiol Gastrointest Liver Physiol. 2014;307:G813-23. doi:10.1152/ajpgi.00188.2014.
277. Kennedy LL, Hargrove LA, Graf AB, Francis TC, Hodges KM, Nguyen QP, et al. Inhibition of mast cell-derived histamine secretion by cromolyn sodium treatment decreases biliary hyperplasia in cholestatic rodents. Lab Invest. 2014;94:1406–18. doi:10.1038/labinvest.2014.129.
278. Baghdasaryan A, Fuchs CD, Österreicher CH, Lemberger UJ, Halilbasic E, Påhlman I, et al. Inhibition of intestinal bile acid absorption improves cholestatic liver and bile duct injury in a mouse model of sclerosing cholangitis. Journal of Hepatology. 2016;64:674–81. doi:10.1016/j.jhep.2015.10.024.
279. Bataller R, Brenner DA. Liver fibrosis. J. Clin. Invest. 2005;115:209–18. doi:10.1172/JCI200524282.
280. Kallis YN, Forbes SJ. The bone marrow and liver fibrosis: friend or foe? Gastroenterology. 2009;137:1218–21. doi:10.1053/j.gastro.2009.08.026.
281. Popov Y, Patsenker E, Fickert P, Trauner M, Schuppan D. Mdr2 (Abcb4)-/- mice spontaneously develop severe biliary fibrosis via massive dysregulation of pro- and

antifibrogenic genes. Journal of Hepatology. 2005;43:1045–54. doi:10.1016/j.jhep.2005.06.025.
282. Ikenaga N, Liu SB, Sverdlov DY, Yoshida S, Nasser I, Ke Q, et al. A new Mdr2(-/-) mouse model of sclerosing cholangitis with rapid fibrosis progression, early-onset portal hypertension, and liver cancer. Am J Pathol. 2015;185:325–34. doi:10.1016/j.ajpath.2014.10.013.
283. Trivedi PJ, Hirschfield GM. Review article: overlap syndromes and autoimmune liver disease. Aliment Pharmacol Ther. 2012;36:517–33. doi:10.1111/j.1365-2036.2012.05223.x.
284. Aguilar-Nájera O, Velasco-Zamora JA, Torre A. Overlap syndromes of autoimmune hepatitis: diagnosis and treatment. Revista de Gastroenterología de México (English Edition). 2015;80:150–9. doi:10.1016/j.rgmxen.2015.07.001.
285. Nakken KE, Nygård S, Haaland T, Berge KE, Arnkvaern K, Ødegaard A, et al. Multiple inflammatory-, tissue remodelling- and fibrosis genes are differentially transcribed in the livers of Abcb4 (-/ -) mice harbouring chronic cholangitis. Scand J Gastroenterol. 2007;42:1245–55. doi:10.1080/00365520701320521.
286. Portmann, C B. MINI-SYMPOSIUM: LIVER AND BILIARY TREE: Primary biliary cirrhosis and sclerosing cholangitis.
287. Montano-Loza AJ, Czaja AJ. Cell mediators of autoimmune hepatitis and their therapeutic implications. Dig Dis Sci. 2015;60:1528–42. doi:10.1007/s10620-014-3473-z.
288. Akberova D, Kiassov AP, Abdulganieva D. Serum Cytokine Levels and Their Relation to Clinical Features in Patients with Autoimmune Liver Diseases. J Immunol Res. 2017;2017:9829436. doi:10.1155/2017/9829436.
289. Behfarjam F, Sanati MH, Nasseri Moghaddam S, Ataei M, Nikfam S, Jadali Z. Role of Th1/Th2 cells and related cytokines in autoimmune hepatitis. Turk J Gastroenterol. 2017;28:110–4. doi:10.5152/tjg.2017.17501.
290. Gregory SM, Nazir SA, Metcalf JP. Implications of the innate immune response to adenovirus and adenoviral vectors. Future Virol. 2011;6:357–74. doi:10.2217/fvl.11.6.
291. Béládi I, Pusztai R. Interferon-like substance produced in chick fibroblast cells inoculated with human adenoviruses. Z Naturforsch B. 1967;22:165–9.
292. Schijf MA, Kruijsen D, Bastiaans J, Coenjaerts FEJ, Garssen J, van Bleek GM, van't Land B. Specific dietary oligosaccharides increase Th1 responses in a mouse respiratory syncytial virus infection model. J Virol. 2012;86:11472–82. doi:10.1128/JVI.06708-11.
293. Löhr HF, Schlaak JF, Lohse AW, Böcher WO, Arenz M, GERKEN G, Zum Meyer Büschenfelde KH. Autoreactive CD4+ LKM-specific and anticlonotypic T-cell responses in LKM-1 antibody-positive autoimmune hepatitis. Hepatology. 1996;24:1416–21. doi:10.1002/hep.510240619.

294. Kawashima H, Kato N, Ioi H, Nishimata S, Watanabe C, Kashiwagi Y, et al. mRNA expression of T-helper 1, T-helper 2 cytokines in autoimmune hepatitis in childhood. Pediatr Int. 2008;50:284–6. doi:10.1111/j.1442-200X.2008.02584.x.
295. Ferreyra Solari NE, Galoppo C, Cuarterolo M, Goñi J, Fernández-Salazar L, Arranz LE, et al. The simultaneous high expression of Vα24, IFN-γ and FoxP3 characterizes the liver of children with type I autoimmune hepatitis. Clin Immunol. 2010;137:396–405. doi:10.1016/j.clim.2010.08.013.
296. Tedesco D, Thapa M, Chin CY, Ge Y, Gong M, Li J, et al. Alterations in Intestinal Microbiota Lead to Production of Interleukin 17 by Intrahepatic γδ T-Cell Receptor-Positive Cells and Pathogenesis of Cholestatic Liver Disease. Gastroenterology. 2018;154:2178–93. doi:10.1053/j.gastro.2018.02.019.
297. Katt J, Schwinge D, Schoknecht T, Quaas A, Sobottka I, Burandt E, et al. Increased T helper type 17 response to pathogen stimulation in patients with primary sclerosing cholangitis. Hepatology. 2013;58:1084–93. doi:10.1002/hep.26447.
298. Sebode M, Peiseler M, Franke B, Schwinge D, Schoknecht. Reduced FOXP3(1) regulatory T cells in patients with primary sclerosing cholangitis are associated with IL2RA gene polymorphisms.
299. Nakken KE, Nygård S, Haaland T, Berge KE, Arnkvaern K, Ødegaard A, et al. Multiple inflammatory-, tissue remodelling- and fibrosis genes are differentially transcribed in the livers of Abcb4 (-/ -) mice harbouring chronic cholangitis. Scand J Gastroenterol. 2007;42:1245–55. doi:10.1080/00365520701320521.
300. Peng Z-W, Rothweiler S, Wei G, Ikenaga N, Liu SB, Sverdlov DY, et al. The ectonucleotidase ENTPD1/CD39 limits biliary injury and fibrosis in mouse models of sclerosing cholangitis. Hepatol Commun. 2017;1:957–72. doi:10.1002/hep4.1084.
301. Trauner M. · Fickert P. · Baghdasaryan A. · Claudel T. · Halilbasic E. · Moustafa T. · Wagner M. · Zollner G. New Insights into Autoimmune Cholangitis through Animal Models.
302. Si L, Whiteside TL, Schade RR, Starzl TE, van Thiel DH. T-lymphocyte subsets in liver tissues of patients with primary biliary cirrhosis (PBC), patients with primary sclerosing cholangitis (PSC), and normal controls. J Clin Immunol. 1984;4:262–72. doi:10.1007/BF00915293.
303. Whiteside TL, Lasky S, Si L, van Thiel DH. Immunologic analysis of mononuclear cells in liver tissues and blood of patients with primary sclerosing cholangitis. Hepatology. 1985;5:468–74. doi:10.1002/hep.1840050321.
304. Bo X. Tumour necrosis factor alpha impairs function of liver derived T lymphocytes and natural killer cells in patients with primary sclerosing cholangitis. Gut. 2001;49:131–41. doi:10.1136/gut.49.1.131.
305. Snook JA, Chapman RW, Sachdev GK, Heryet A, Kelly PMA, Fleming KA, Jewell DP. Peripheral blood and portal tract lymphocyte populations in primary sclerosing

cholangitis. Journal of Hepatology. 1989;9:36–41. doi:10.1016/0168-8278(89)90073-1.

306. Hashimoto E1, Lindor KD, Homburger HA, Dickson ER, Czaja AJ, Wiesner RH, Ludwig J. Immunohistochemical characterization of hepatic lymphocytes in primary biliary cirrhosis in comparison with primary sclerosing cholangitis and autoimmune chronic active hepatitis.

307. Anderson AE, Swan DJ, Wong OY, Buck M, Eltherington O, Harry RA, et al. Tolerogenic dendritic cells generated with dexamethasone and vitamin D3 regulate rheumatoid arthritis CD4+ T cells partly via transforming growth factor-β1. Clin Exp Immunol. 2017;187:113–23. doi:10.1111/cei.12870.

308. Domogalla MP, Rostan PV, Raker VK, Steinbrink K. Tolerance through Education: How Tolerogenic Dendritic Cells Shape Immunity. Front Immunol. 2017;8:1764. doi:10.3389/fimmu.2017.01764.

309. Jauregui-Amezaga A, Cabezón R, Ramírez-Morros A, España C, Rimola J, Bru C, et al. Intraperitoneal Administration of Autologous Tolerogenic Dendritic Cells for Refractory Crohn's Disease: A Phase I Study. J Crohns Colitis. 2015;9:1071–8. doi:10.1093/ecco-jcc/jjv144.

310. Dáňová K, Grohová A, Strnadová P, Funda DP, Šumník Z, Lebl J, et al. Tolerogenic Dendritic Cells from Poorly Compensated Type 1 Diabetes Patients Have Decreased Ability To Induce Stable Antigen-Specific T Cell Hyporesponsiveness and Generation of Suppressive Regulatory T Cells. J Immunol. 2017;198:729–40. doi:10.4049/jimmunol.1600676.

311. Rigby WF, Waugh M, Graziano RF. Regulation of human monocyte HLA-DR and CD4 antigen expression, and antigen presentation by 1,25-dihydroxyvitamin D3. Blood. 1990;76:189–97.

312. Piemonti L, Monti P, Allavena P, Sironi M, Soldini L, Leone BE, et al. Glucocorticoids affect human dendritic cell differentiation and maturation. The Journal of Immunology. 1999;162:6473–81.

313. Kim SH, Jung HH, Lee CK. Generation, Characteristics and Clinical Trials of Ex Vivo Generated Tolerogenic Dendritic Cells. Yonsei Med J. 2018;59:807–15. doi:10.3349/ymj.2018.59.7.807.

314. Ferreira GB, Kleijwegt FS, Waelkens E, Lage K, Nikolic T, Hansen DA, et al. Differential protein pathways in 1,25-dihydroxyvitamin d(3) and dexamethasone modulated tolerogenic human dendritic cells. J Proteome Res. 2012;11:941–71. doi:10.1021/pr200724e.

315. Maldonado RA, Andrian UH von. How tolerogenic dendritic cells induce regulatory T cells. Adv Immunol. 2010;108:111–65. doi:10.1016/B978-0-12-380995-7.00004-5.

316. Unger WWJ, Laban S, Kleijwegt FS, van der Slik AR, Roep BO. Induction of Treg by monocyte-derived DC modulated by vitamin D3 or dexamethasone: differential role for PD-L1. Eur J Immunol. 2009;39:3147–59. doi:10.1002/eji.200839103.

317. Nikolic T, Roep BO. Regulatory multitasking of tolerogenic dendritic cells - lessons taken from vitamin d3-treated tolerogenic dendritic cells. Front Immunol. 2013;4:113. doi:10.3389/fimmu.2013.00113.
318. Mansilla MJ, Contreras-Cardone R, Navarro-Barriuso J, Cools N, Berneman Z, Ramo-Tello C, Martínez-Cáceres EM. Cryopreserved vitamin D3-tolerogenic dendritic cells pulsed with autoantigens as a potential therapy for multiple sclerosis patients. J Neuroinflammation. 2016;13:113. doi:10.1186/s12974-016-0584-9.
319. Xie Z, Chen J, Zheng C, Wu J, Cheng Y, Zhu S, et al. 1,25-dihydroxyvitamin D3 - induced dendritic cells suppress experimental autoimmune encephalomyelitis by increasing proportions of the regulatory lymphocytes and reducing T helper type 1 and type 17 cells. Immunology. 2017;152:414–24. doi:10.1111/imm.12776.
320. Fu F, Li Y, Qian S, Lu L, Chambers F, Starzl TE, et al. Costimulatory molecule-deficient dendritic cell progenitors (MHC class II+, CD80dim, CD86-) prolong cardiac allograft survival in nonimmunosuppressed recipients. Transplantation. 1996;62:659–65.
321. García-González P, Ubilla-Olguín G, Catalán D, Schinnerling K, Aguillón JC. Tolerogenic dendritic cells for reprogramming of lymphocyte responses in autoimmune diseases. Autoimmun Rev. 2016;15:1071–80. doi:10.1016/j.autrev.2016.07.032.
322. Anderton SM, Wraith DC. Hierarchy in the ability of T cell epitopes to induce peripheral tolerance to antigens from myelin. Eur J Immunol. 1998;28:1251–61. doi:10.1002/(SICI)1521-4141(199804)28:04<1251::AID-IMMU1251>3.0.CO;2-O.
323. Barbey C, Donatelli-Dufour N, Batard P, Corradin G, Spertini F. Intranasal treatment with ovalbumin but not the major T cell epitope ovalbumin 323-339 generates interleukin-10 secreting T cells and results in the induction of allergen systemic tolerance. Clin Exp Allergy. 2004;34:654–62. doi:10.1111/j.1365-2222.2004.1929.x.
324. Pellaton-Longaretti C, Boudousquié C, Barbier N, Barbey C, Argiroffo CB, Donati Y, et al. CD4+CD25-mTGFbeta+ T cells induced by nasal application of ovalbumin transfer tolerance in a therapeutic model of asthma. International Immunology. 2011;23:17–27. doi:10.1093/intimm/dxq453.
325. Sabatos-Peyton CA, Verhagen J, Wraith DC. Antigen-specific immunotherapy of autoimmune and allergic diseases. Curr Opin Immunol. 2010;22:609–15. doi:10.1016/j.coi.2010.08.006.
326. Chen Y, Kuchroo VK, Inobe J, Hafler DA, Weiner HL. Regulatory T cell clones induced by oral tolerance: suppression of autoimmune encephalomyelitis. Science. 1994;265:1237–40.
327. Cottrez F, Groux H. Regulation of TGF-beta response during T cell activation is modulated by IL-10. The Journal of Immunology. 2001;167:773–8.

328. Groux H, O'Garra A, Bigler M, Rouleau M, Antonenko S, Vries JE de, Roncarolo MG. A CD4+ T-cell subset inhibits antigen-specific T-cell responses and prevents colitis. Nature. 1997;389:737–42. doi:10.1038/39614.
329. Janssen EM, van Oosterhout AJ, Nijkamp FP, van Eden W, Wauben MH. The efficacy of immunotherapy in an experimental murine model of allergic asthma is related to the strength and site of T cell activation during immunotherapy. The Journal of Immunology. 2000;165:7207–14.
330. Strobel S, Mowat AM. Immune responses to dietary antigens: oral tolerance. Immunology Today. 1998;19:173–81.
331. Wetzig R, Hanson DG, Miller SD, Claman HN. Binding of ovalbumin to mouse spleen cells with and without carbodiimide. Journal of Immunological Methods. 1979;28:361–8. doi:10.1016/0022-1759(79)90201-1.
332. Luo X, Miller SD, Shea LD. Immune Tolerance for Autoimmune Disease and Cell Transplantation. Annu Rev Biomed Eng. 2016;18:181–205. doi:10.1146/annurev-bioeng-110315-020137.
333. Pedotti R, Mitchell D, Wedemeyer J, Karpuj M, Chabas D, Hattab EM, et al. An unexpected version of horror autotoxicus: anaphylactic shock to a self-peptide. Nat Immunol. 2001;2:216–22. doi:10.1038/85266.
334. Xiang SD, Scholzen A, Minigo G, David C, Apostolopoulos V, Mottram PL, Plebanski M. Pathogen recognition and development of particulate vaccines: does size matter? Methods. 2006;40:1–9. doi:10.1016/j.ymeth.2006.05.016.
335. Foged C, Brodin B, Frokjaer S, Sundblad A. Particle size and surface charge affect particle uptake by human dendritic cells in an in vitro model. Int J Pharm. 2005;298:315–22. doi:10.1016/j.ijpharm.2005.03.035.
336. Joshi VB, Geary SM, Salem AK. Biodegradable particles as vaccine delivery systems: size matters. AAPS J. 2013;15:85–94. doi:10.1208/s12248-012-9418-6.
337. Zhao L, Seth A, Wibowo N, Zhao C-X, Mitter N, Yu C, Middelberg APJ. Nanoparticle vaccines. Vaccine. 2014;32:327–37. doi:10.1016/j.vaccine.2013.11.069.
338. Violatto MB, Casarin E, Talamini L, Russo L, Baldan S, Tondello C, et al. Dexamethasone Conjugation to Biodegradable Avidin-Nucleic-Acid-Nano-Assemblies Promotes Selective Liver Targeting and Improves Therapeutic Efficacy in an Autoimmune Hepatitis Murine Model. ACS Nano 2019. doi:10.1021/acsnano.8b09655.
339. Vanderlugt CL, Miller SD. Epitope spreading in immune-mediated diseases: implications for immunotherapy. Nat Rev Immunol. 2002;2:85–95. doi:10.1038/nri724.
340. Bittner-Eddy PD, Fischer LA, Tu AA, Allman DA, Costalonga M. Discriminating between Interstitial and Circulating Leukocytes in Tissues of the Murine Oral Mucosa Avoiding Nasal-Associated Lymphoid Tissue Contamination. Front Immunol. 2017;8:1398. doi:10.3389/fimmu.2017.01398.

Effects of adenovirus-induced hepatocyte damage on chronic bile duct inflammation in a sclerosing cholangitis mouse model.

Sina Fuchs[1], Monika Bayer[1], Richard Taubert[2], Michael P. Manns[2], Josef M. Pfeilschifter[1], Urs Christen[1], and Edith Hintermann[1#]

[1]Pharmazentrum Frankfurt / ZAFES, Goethe University Hospital Frankfurt, Frankfurt am Main, Germany; [2]Department of Gastroenterology, Hepatology and Endocrinology, Hannover Medical School, Hannover, Germany

 # Corresponding address:

Edith Hintermann, Ph.D.; Pharmazentrum Frankfurt; Goethe University Hospital Frankfurt; Theodor-Stern Kai 7; 60590 Frankfurt am Main; Germany; Phone: +49-69-6301-83105; Fax: +49-69-6301-7663; Email: hintermann@med.uni-frankfurt.de

Word count: 4991

Number of figures: 7

Abbreviations:

AIH, autoimmune hepatitis; Ad, adenovirus; hCYP2D6, human Cytochrome P450 2D6; PSC, primary sclerosing cholangitis; PBC, primary biliary cholangitis; *Mdr2*, multidrug resistance gene 2; AST, aspartate aminotransferase; ALT, alanine aminotransferase; LKM-1, type 1 liver/kidney microsomal; AP, alkaline phosphatase; pANCA, perinuclear anti-neutrophil cytoplasmic antibody; SC, sclerosing cholangitis; CK19, cytokeratin 19; HSC, hepatic stellate cell; PF, portal fibroblast; αSMA, α-smooth muscle actin

Conflict of interest: The authors declare no competing financial interests.

Financial support:

Supported by grant HI 1837/1-1 and the KFO250 project 7 from the German Research Foundation, by the Young Faculty program from Hannover Medical School, by the Goethe University Hospital Frankfurt and by the Else Kröner-Fresenius Foundation, Germany.

Acknowledgments

This work was supported by grant HI 1837/1-1 to E. H. and by the KFO250 project 7 from the German Research Foundation and by the Goethe University Hospital Frankfurt. R.T was supported by the Young Faculty program from Hannover Medical School. S.F. was the recipient of a fellowship of the Else Kröner-Fresenius Foundation (EKFS), Germany, Research Training Group Translational Research Innovation - Pharma (TRIP).

Abstract

Background & Aims: Four major autoimmune diseases target the liver. They develop due to bile duct destruction, leading to chronic cholestasis or result from hepatocyte damage like autoimmune hepatitis (AIH). Interestingly, some patients simultaneously show features of both cholangitis and AIH. Our goal was to mimic such concurrent characteristics in a mouse model that would help deciphering mechanisms possibly involved in an inflammatory crosstalk between cholestatic disease and hepatitis. ***Methods:*** *Mdr2*$^{-/-}$ mice, which spontaneously develop sclerosing cholangitis due to accumulation of toxic bile salts, were infected with adenovirus (Ad) encoding human Cytochrome P4502D6 (hCYP2D6), the major target autoantigen in type-2 AIH, to trigger hepatocyte injury. Wildtype FVB mice were controls. ***Results:*** Resulting Ad-*Mdr2*$^{-/-}$ mice presented with cholangitis, fibrosis, and cellular infiltrations that were higher than in *Mdr2*$^{-/-}$ or Ad-FVB mice. Increased levels of anti-neutrophil cytoplasmic antibodies but similar anti-hCYP2D6 antibody titers were detected in Ad-*Mdr2*$^{-/-}$ compared to *Mdr2*$^{-/-}$ and Ad-FVB mice, respectively. IFNγ-expressing hCYP2D6-specific CD4 T cells declined, whereas hCYP2D6-specific CD8 T cells increased in Ad-*Mdr2*$^{-/-}$ compared to Ad-FVB mice. The overall T cell balance in Ad-*Mdr2*$^{-/-}$ mice was a combination of a type 17 T cell response typically found in *Mdr2*$^{-/-}$ mice with a type 1 dominated T cell response characteristic for Ad-FVB mice. Simultaneously, the type 2 T cell compartment was markedly reduced. ***Conclusions:*** Experimental hepatitis induction in a mouse with sclerosing cholangitis results in a disorder which represents not simply the sum of the individual characteristics but depicts a more complex entity which urges on further analysis.

Word count: 250

Keywords:
autoimmune liver disease, autoimmune hepatitis, primary sclerosing cholangitis

Lay summary

We show that mice which suffer from chronic bile duct injury can develop concurrently autoimmune liver inflammation when hepatocytes get damaged by a specific virus. The result is an increased activation of the immune system and therefore stronger liver damage and fibrosis.

1. Introduction

Four major autoimmune diseases target the liver and lead to progressive tissue destruction and eventually liver failure if untreated: Autoimmune hepatitis (AIH), which is characterized predominantly by hepatocyte damage as well as primary sclerosing cholangitis (PSC), primary biliary cholangitis (PBC)[1, 2] and IgG4-associated cholangitis[3-5], which develop due to bile duct destruction resulting in chronic cholestasis. The etiological triggers and pathogenic mechanisms leading to these diseases are not yet fully understood,[6] making it difficult to develop tailor-made therapies. Common consent has found the idea that environmental factors combined with genetic predisposition breakdown self-tolerance to liver tissue resulting in autoaggressive hepatic injury.[6, 7]

AIH is characterized by interface hepatitis with plasma and T cell infiltration, piecemeal necrosis and variable stages of fibrosis.[8-11] Patients show increased serum levels of aspartate aminotransferase (AST) and alanine aminotransferase (ALT), increased γ-globulin concentrations and usually the generation of autoantibodies with specificities for different liver antigens. Historically, type 1 AIH has been characterized by the presence of anti-nuclear and/or anti-smooth muscle autoantibodies, whereas type 1 liver/kidney microsomal (LKM-1) and/or liver cytosol type 1 autoantibodies have been considered as the hallmark of type 2 AIH.[12, 13] AIH is associated with specific HLA alleles, is more common in females and affects all ages though with a higher occurrence and a more aggressive course of type 2 AIH in children.[14, 15] The current standard therapy is glucocorticoid treatment alone or in combination with other immunosuppressive drugs like azathioprine or non-approved salvage therapies.[9, 15-17]

PSC is characterized by chronic inflammation of intra- and extrahepatic bile ducts, resulting in fibrotic lesions and bile duct strictures and eventually develops into cirrhosis with

portal hypertension.[18-20] In up to 80% of cases PSC goes along with inflammatory bowel disease.[21] Biochemical features are increased levels of alkaline phosphatase (AP) and gamma glutamyl transferase, a slight increase in ALT/AST levels and a rise in serum bilirubin in advanced stages.[18-20] Diagnosis is made by bile duct imaging since no disease-specific autoantibodies have been identified, but antibodies to biliary and colonic epithelial proteins and several ubiquitous self-antigens can be detected at low titers[22] with perinuclear anti-neutrophil cytoplasmic antibodies (pANCAs) being the most frequent reactivity.[23] Genetic susceptibility is associated with up to 20 loci e.g. certain HLA alleles, genes of the IL-2 pathway or *MDR3* and the disease is more common in men than women.[18-20, 24, 25] To date, no effective treatment for PSC is available besides liver transplantation, as immunosuppressive drugs and the administration of ursodeoxycholic acid do not improve disease.[18-20, 26]

In some patients, hepatocellular damage and cholestasis coexist and have developed either simultaneously or consecutively.[13, 26-30] For example, 14–18% of patients with classical AIH show features of cholestatic diseases, designated AIH-PBC or AIH-PSC overlap syndrome. Likewise, when PSC is the dominant phenotype and AIH the secondary phenotype, the disease is called PSC-AIH overlap syndrome or variant form of PSC.[14, 27-31]

The goal of our study was to investigate how a pre-existing chronic hepatobiliary inflammation and an experimentally induced hepatocyte-targeting disease would influence each other in terms of biochemical, serological and immunocellular parameters. We used *Mdr2*$^{-/-}$ mice on a FVB/NHsd (FVB) background, which suffer from a PSC-like disease, since they lack the ATP binding cassette transporter ABCB4, a phospholipid flippase that causes biliary excretion of phosphatidylcholine, which is used to pack bile acids into micelles. In the absence of phosphatidylcholine, bile acids leak into portal tracts and harm surrounding cells, which leads spontaneously to a chronic biliary liver disease with sclerosing cholangitis (SC).[32, 33] *Mdr2*$^{-/-}$ mice were infected with adenovirus Ad-2D6, which encodes human

cytochrome P450 2D6 (hCYP2D6), the major target autoantigen in type 2 AIH.[34] We have previously shown that infection with Ad-2D6 but not a control virus encoding green fluorescence protein breaks tolerance to the murine CYP homologues, inducing an autoimmune liver disease with hCYP2D6-specific T cells, a hCYP2D6-specific B cell response and liver fibrosis.[35, 36] In Ad-2D6 infected *Mdr2*$^{-/-}$ (Ad-*Mdr2*$^{-/-}$) mice, serologic liver damage markers were not dramatically increased but cholangitis, fibrosis, and cellular infiltration were higher than in uninfected *Mdr2*$^{-/-}$ and Ad-FVB mice. Increased pANCA levels were detected in Ad-*Mdr2*$^{-/-}$ animals compared to *Mdr2*$^{-/-}$ mice, whereas anti-hCYP2D6 titers were similar in Ad-FVB and Ad-*Mdr2*$^{-/-}$ mice. The Ad-*Mdr2*$^{-/-}$ T cell balance united the *Mdr2*$^{-/-}$-specific type 17 T cell response with the Ad-FVB-specific type 1 T cell response, simultaneously decreasing type 2 T cells. These findings suggest that the severity of an existing cholestatic liver disease is enhanced when an autoimmune-mediated hepatitis is induced. Concomitantly, hepatocyte-specific autoimmunity is enhanced by a pre-existing SC.

2. Materials and Methods

Mouse strains and adenovirus treatment

Mice were handled in strict accordance with good animal practice. Animal work was approved by the Ethics Animal Review Board, Darmstadt, Germany (Reference number V54-19c20/15-FU1150). Cohoused 8-week-old females on standard chow were used. *Mdr2*$^{-/-}$ mice on a FVB/NHsd background and wild type FVB/NHsd mice were from Jackson Laboratory (Jackson Laboratory, Bar Harbor, ME). Adenovirus infection: Mice were injected intravenously with 3 x 10^8 pfu of Ad-2D6 and were sacrificed 4 weeks later. Ad-2D6 was generated as described[36] and virus titer was determined with the Adeno-X rapid titer kit (Clontech, Palo Alto, USA).

Patient material

Human sera were from the prospective serum library and liver biopsies from the liver tissue library of the Department of Gastroenterology, Hepatology and Endocrinology, Hannover Medical School, Hannover, Germany. The blood procurement protocol and analysis as well as biopsy collection and analysis have been approved by the Ethics Committee of the Medical School of Hannover. Patients have been clinically diagnosed with AIH or PSC and written informed consent was obtained from each patient.

Cell line and pANCA detection

For pANCA detection, human promyelocytic leukemia HL-60 cells were used as described in Supporting Information.

Anti-hCYP2D6 antibody titer determination

Anti-hCYP2D6 antibody titers were determined using recombinant hCYP2D6 (MyBiosource, San Diego, CA, USA) as described in Supporting Information.

Serum ALT and AP measurements

ALT and AP levels were measured with the Reflotron Plus blood analysis system (Roche Diagnostics, Mannheim, Germany). Blood was collected with heparin-coated capillary tubes (Natelson tubes, Kimble Chase, Rockwood, TN, USA), centrifuged in Microtainer SST tubes (BD Biosciences, Heidelberg, Germany) and serum was stored at -80°C until used.

Isolation of liver lymphocytes and flow cytometric analysis

Liver lymphocytes were isolated according.[35] Protein expression was detected and analyzed as described in Supporting Information.

Protein Immunoblotting, immunohistochemistry and quantification of stained areas

Total liver protein extracts were prepared and analyzed by immunoblotting as described in Supporting Information. Paraffin-embedded biopsy sections were deparaffinized and rehydrated before hematoxylin staining was performed. Cryosections of mouse livers were fixed in ethanol or ethanol/acetone (1:1). Staining procedures and data analysis are described in Supporting Information.

Quantification of collagen III mRNA expression levels by RT-PCR

Collagen III mRNA was quantified as described in Supporting Information using probe Col3α1 (Mm01254476_m1, Applied Biosystems, Waltham, MA, USA), TaqMan Fast

Advanced Master Mix (Applied Biosystems) and the 7500 Fast Real-Time PCR System (Applied Biosystems).

Statistical analysis

Statistical significance was analyzed using two-tailed unpaired t-test performed with GraphPad Prism software (GraphPad Software, San Diego, USA).

3. Results

3.1 Infection of Mdr2$^{-/-}$ mice with Ad-2D6 triggers increased alkaline phosphatase and serum aminotransferase levels.

To study how preexisting chronic bile duct inflammation and the development of experimental AIH influence each other, we used 8-week-old *Mdr2*$^{-/-}$ mice, which suffer from SC (Figure S1A) and infected them with Ad-2D6, which initiates hCYP2D6-specific AIH in FVB mice[36] (Figure S1B), resulting in Ad-*Mdr2*$^{-/-}$ mice. As controls, uninfected (naïve) FVB or *Mdr2*$^{-/-}$ mice and Ad-FVB mice were used. As serological disease markers we analyzed AP activity, which relates to biochemical symptoms of cholestasis and ALT activity, which is typically elevated in AIH. During the course of disease, we observed a slight increase of AP activity and a stronger elevation of ALT activity (Figure 1A). Both activity levels were highest in Ad-*Mdr2*$^{-/-}$ mice (Figure 1A). Interestingly, in Ad-*Mdr2*$^{-/-}$ mice, the kinetic pattern of ALT activity seemed to follow the one found in Ad-FVB mice (AIH model) with a peak at week 1 post-infection. Similarly, the kinetic pattern found for AP activity in Ad-*Mdr2*$^{-/-}$ mice followed the one from *Mdr2*$^{-/-}$ mice (cholangitis model) (Figure 1A). This finding might indicate that one autoimmune liver disease is exacerbating the clinical markers of the other disorder.

3.2 Ad-2D6 infection initiates autoantibody production in Mdr2$^{-/-}$ mice.

Next, we analyzed sera collected at week 4 after Ad-2D6 infection for the presence of AIH- and PSC-specific autoantibodies. Titers of LKM-1-like anti-hCYP2D6 antibodies were similar in Ad-FVB and Ad-*Mdr2*$^{-/-}$ mice, as assessed by ELISA (Figure 1B), indicating similar hCYP2D6-specific humoral responses in both models. As expected, uninfected mice generated no anti-hCYP2D6 antibodies. Although the specificity of autoantibodies in PSC is

controversially discussed, autoantibodies against components of the biliary epithelium and neutrophils seem to be of relevance, yet the latter are also reported in AIH.[22] To identify pANCAs, we used human promyelocytic leukemia HL-60 cells as target[37] and found higher reactivity with sera of Ad-*Mdr2*$^{-/-}$ mice than *Mdr2*$^{-/-}$ or Ad-FVB mice (Figure 1C). These findings suggest that the strong anti-hCYP2D6 response (titers > 20,000) is not further boosted when AIH is induced on top of a pre-existing cholangitis. This in contrast to the weak pANCA response, which is amplified in Ad-*Mdr2*$^{-/-}$ mice, either because a second B cell response targeting the liver is initiated or due to pro-inflammatory cytokines released after the Ad-2D6 infection.

3.3 Ad-2D6 infected Mdr2$^{-/-}$ *mice show enhanced cholangiocyte proliferation and hepatic fibrosis.*

We have previously shown that adenovirus infection *per se* triggers acute but transient liver injury, whereas virus-driven expression of hCYP2D6 led to persistent liver damage and associated fibrogenesis.[36, 38] In contrast to our regular hCYP2D6 mouse model for AIH, we infected mice in this study via the intravenous route only in order to avoid massive sub-capsular fibrosis that is observed after the additional intraperitoneal infection.[38] Four weeks after Ad-2D6 administration, livers were harvested and subjected to immunohistochemical analysis. Cytokeratin 19 (CK19) staining revealed that cholangiocyte hyperproliferation, a hallmark of the *Mdr2*$^{-/-}$ cholangitis model, is further increased in Ad-*Mdr2*$^{-/-}$ livers (Figure 2A, B), suggesting that the severity of a cholestatic disease is enhanced in the concurrent presence of autoimmune-mediated hepatitis. Similarly, fibrosis-associated extracellular matrix remodelling was strongest in Ad-*Mdr2*$^{-/-}$ mice, as these livers showed the highest collagen III signal (Figure 2A, B). Fibrogenesis was still ongoing 4 weeks after Ad-2D6 infection indicated by collagen III mRNA levels that were higher in all three liver disease models than

in naïve FVB mice (Figure 2C). Notably, the highest collagen III mRNA level was found in livers of Ad-*Mdr2*$^{-/-}$ mice (Figure 2C). Fibroblasts, which get activated and differentiate into αSMA-positive myofibroblasts during fibrogenesis, are responsible for such fibrotic extracellular matrix deposition. To confirm the intense fibrotic activity in Ad-*Mdr2*$^{-/-}$ livers, we analysed αSMA protein expression by immunoblotting and observed the strongest αSMA signal in livers of Ad-*Mdr2*$^{-/-}$ mice (Figure 2D). Myofibroblasts originate from different liver fibroblast types, e.g. hepatic stellate cells (HSCs), which are desmin-positive cells, and portal fibroblasts (PFs), which express elastin.[39] Desmin staining revealed that the number of perivascular HSCs in *Mdr2*$^{-/-}$ mice was rather high compared to FVB mice and that infection triggered only a slight increase of HSCs in Ad-FVB and Ad-*Mdr2*$^{-/-}$ mice (Figure 3A). These findings were confirmed in immunoblotting experiments (Figure 3B). Co-staining experiments with antibodies to desmin and CK19 showed that HSC proliferation and accumulation occurred in portal fields in periductular areas (Figure 3C), where also strong collagen III signals have been observed (Figure 2A). Elastin staining demonstrated that PFs were scarce in livers of FVB and Ad-FVB mice (Figure 4A, B). However, hepatic elastin signal increased substantially in portal fields of *Mdr2*$^{-/-}$ mice and seemed even stronger in Ad-*Mdr2*$^{-/-}$ mice (Figure 4A, B). Taken together, the most dramatic fibrotic changes were detected in livers of Ad-*Mdr2*$^{-/-}$ mice and were the result of an additive effort of activated HSCs and PFs.

3.4 Characterization of liver infiltrating innate immune cells in Ad-Mdr2$^{-/-}$ *mice.*

Next, we sought to compare the numbers of liver infiltrating innate immune cells in the different disease models by immunohistochemical staining and automated quantification. Visualization of CD11b, CD11c and Ly6G demonstrated that hepatic infiltration of monocytes/macrophages, dendritic cells and neutrophils respectively, was increased in Ad-

FVB and *Mdr2*$^{-/-}$ mice, compared to FVB mice and was most severe in livers of Ad-*Mdr2*$^{-/-}$ mice (Figure 5A, B), which exhibit the chronic inflammation leading to strong fibrotic tissue remodeling (Figure 2A).

3.5 Characterization of the hCYP2D6-specific T cell response and the overall T cell balance in Ad-Mdr2$^{-/-}$ *mice.*

In a similar approach we analyzed liver-infiltrating cells of the adaptive immune system in the different animal models. As shown in Figures 6A/B, the highest number of CD4 and CD8 T cells, respectively, was found in livers of Ad-*Mdr2*$^{-/-}$ mice. Since to date no PSC-specific target antigens have been identified, no disease-specific T cell responses can be analyzed. To characterize the hCYP2D6-specific T cell response, we stimulated isolated liver lymphocytes with the immunodominant CD4 and CD8 epitopes, which we had mapped earlier[40], and analyzed IFNγ expression by flow cytometry (Figure 6C). Interestingly, Ad-*Mdr2*$^{-/-}$ mice generated less IFNγ-expressing CD4 T cells than Ad-FVB mice, whereas the hCYP2D6-specific CD8 T cell response was boosted in Ad-*Mdr2*$^{-/-}$ compared to Ad-FVB mice (Figure 6C). These changes led us to ask how the overall T cell balance differs in the 3 disease models. Thus, we stimulated liver-infiltrating cells with anti-CD3 / anti-CD28 antibodies and IL-2 and analyzed the frequencies of type 1 (IFNγ), type 2 (IL-4), type 17 (IL-17), and regulatory (IL-10) T cells by intracellular cytokine staining (Figure 7). Naïve FVB mice carried an almost even distribution of type 1 and type 2 CD4 T cells, with a small fraction of type 17 CD4 T cells and about 6% CD4 T cells with a regulatory phenotype (Figure 7A). Naive *Mdr2*$^{-/-}$ mice showed also equally frequent type 1 and type 2 CD4 T cells, but in addition they displayed a substantial fraction of type 17 CD4 T cells (Figure 7A). In contrast, in Ad-FVB mice, type 1 CD4 T cells were dominating, followed by a much lower frequency of type 2 CD4 T cells and a rather low percentage of type 17 CD4 T cells. Ad-*Mdr2*$^{-/-}$ mice

showed a veritable overlap of the T cell distributions found in *Mdr2*$^{-/-}$ and Ad-FVB mice. Besides a disbalance towards type 1 CD4 T cell domination like in Ad-FVB, Ad-*Mdr2*$^{-/-}$ mice also carried a considerable proportion of type 17 CD4 T cells. Regulatory CD4 T cells were equally frequent in all models. Overall, the CD8 T cell balance was more dominated by type 1 T cells compared to the CD4 T cell balance (Figure 7B). Just like for CD4 T cells, Ad-2D6-infection of FVB mice expanded the type 1 CD8 T cell fraction. In Ad-*Mdr2*$^{-/-}$ mice, the frequency of type 1 CD8 T cells further increased, whereas less type 2 CD8 T cells were seen. Furthermore, the percentage of type 17 CD8 T cells was similar in *Mdr2*$^{-/-}$ and Ad-*Mdr2*$^{-/-}$ mice. Taken together, the hepatic T cell response observed in Ad-*Mdr2*$^{-/-}$ mice is a superposition of the responses typical for *Mdr2*$^{-/-}$ and Ad-FVB mice.

4. Discussion

We have studied the evolution of chronic biliary inflammation into a disease with features of both AIH and SC. To this end, *Mdr2*$^{-/-}$ mice, which suffer from biliary injury due to defective biliary phospholipid secretion, have been infected with adenovirus Ad-2D6 to break tolerance to the major autoantigen in type 2 AIH hCYP2D6 and its mouse homologues, provoking hepatocyte damage by autoimmune processes. Though Ad-2D6 caused no long-lasting increase in ALT/AP levels, the chronic nature of the autoimmune insult resulted in an overall increase in cellular infiltration by various immune cells and a more pronounced fibrosis in livers of Ad-*Mdr2*$^{-/-}$ mice. In addition, a humoral response was initiated which led to the generation of anti-hCYP2D6 antibodies and pANCAs. The total T cell pool was dominated by type 1 T cells and showed a considerable amount of type 17 T cells. Also, a hCYP2D6-specific T cell response was generated. These data suggest that the initial cholangitis has evolved into an autoimmune-driven chronic inflammation with both hepatocellular and biliary targets, probably resembling human AIH-PSC overlap syndrome. Overlap syndromes of autoimmune liver diseases describe clinical observations rather than pathological entities with defined manifestations. They could be atypical variants of e.g. classical PSC, represent a transitional stage from e.g. AIH to PSC, describe two concurrent separate classical diseases or even constitute new diseases.[28] Due to this complexity, identifying the underlying pathogenic mechanisms will be difficult in men, making it necessary to develop animal models suitable to dissect such diverse diseases into better defined entities. In the described setup we study simultaneously SC, experimentally induced AIH, and the combination thereof, an approach which in the long-run allows to identify pathways which are either SC or AIH specific or universally valid for autoinflammatory liver pathogenesis. The use of Ad-2D6 to induce type 2 AIH has the advantages that disease onset

(time of infection) and target antigen (hCYP2D6 and mouse homologues) are known. We have previously shown that Ad-2D6 infection of wild type mice generates strong inflammatory responses with liver-infiltrating leukocytes,[38] production of hCYP2D6-specific LKM-1 antibodies[36], and hCYP2D6-specific T cells.[40]

The data presented here demonstrate that various aspects of an inflammatory disease with autoimmune features seem to be influenced differently by the simultaneous presence of hepatitis and cholangitis. (1) Infiltration of the liver by various leukocytes was strongest in Ad-*Mdr2*$^{-/-}$ mice and a cumulative effect was observed. Both SC and AIH triggered a robust increase in monocytes/macrophages and dendritic cells, whereas hepatic infiltration by neutrophils was more pronounced in SC, suggesting a certain specificity for the cholestatic disease. Further studies will show whether disease-specific chemotactic factors can be identified, which may become the target of therapeutic intervention. In this regard, one should consider the work by Nakken et al., which shows an over 30-fold increase in mRNA encoding CCL2 (neutrophil chemoattractant) and an over 200-fold upregulation of mRNA encoding CCL20 (type 17 T cell chemoattractant) in *Mdr2*$^{-/-}$ versus wild type livers.[41]

(2) Interestingly, the increments in ductular proliferation and in fibrosis-specific extracellular matrix production were more than additive in Ad-*Mdr2*$^{-/-}$ livers. The upregulation of cholangiocyte proliferation was typically detected in *Mdr2*$^{-/-}$ livers but was also seen in Ad-FVB mice. This observation correlates well with the finding that up to 20% of AIH patients present with biliary injury, which is not classified as PBC or PSC overlap syndrome.[42] Fibrogenesis in Ad-*Mdr2*$^{-/-}$ mice may be driven by two distinct activation pathways, which may potentiate each other, as in AIH only HSCs differentiate into myofibroblasts, whereas in SC both myofibroblastic HSCs and PFs are involved. These strong fibrotic changes detected in Ad-*Mdr2*$^{-/-}$ mice match with the observation that patients with

overlap syndromes tend to develop a more aggressive form of autoimmune liver disease with poorer treatment responses and higher rates of cirrhosis.[43]

(3) The hCYP2D6-specific B cell response is a parameter that was similar in Ad-FVB and Ad-*Mdr2*$^{-/-}$ mice. This suggests that liver injury triggering cholangitis does not break B cell tolerance to mouse Cyps, which otherwise most probably would have resulted in cross-reactivity to hCYP2D6 over time and the development of augmented hCYP2D6 antibody titers in Ad-*Mdr2*$^{-/-}$ mice. In contrast to the humoral response, the hCYP2D6-specific CD8 T cell response was boosted in Ad-*Mdr2*$^{-/-}$ versus Ad-FVB mice. Here it is likely that the fertile inflammatory field in *Mdr2*$^{-/-}$ mouse livers resulted in an accelerated expansion of liver autoantigen-specific CD8 T cells.

(4) Surprisingly, one aspect of the antigen-specific autoimmune response was blocked in Ad-*Mdr2*$^{-/-}$ mice compared to Ad-FVB mice, namely the hCYP2D6-specific CD4 T cell response. A closer look at the overall CD4 T cell balance may explain this result: Naïve *Mdr2*$^{-/-}$ mice present with a stronger type 17 CD4 T cell response than FVB mice. Infection with Ad-2D6 increases the compartment of type 1 CD4 T cells in both mice strains but this effect is stronger in FVB than in *Mdr2*$^{-/-}$ mice, which carry over a larger type 17 CD4 T cell compartment. Thus, the overall weaker type 1 CD4 T cell response in Ad-*Mdr2*$^{-/-}$ mice may lead to a lower percentage of hCYP2D6-specific CD4 T cells. Importantly, IL17A expressing lymphocytes have been localized in periductal areas in PSC patients.[44]

The presented data illustrate that our experimentally induced SC-AIH model offers the possibility to study a multitude of cell types, cytokines, chemokines, and other factors, as well as treatment regimens, which impact on autoimmune-driven liver injury. Additional such animal models can be envisioned. For example, feeding lithogenic diets which result in bile duct injury and biliary fibrosis[45] could be easily combined with Ad-2D6 infection. Cholangitis

and AIH could be induced simultaneously or consecutively in alternate order, giving the opportunity to analyze further aspects of overlap syndromes.

References

1. Hirschfield GM, Gershwin ME. Primary biliary cirrhosis: one disease with many faces. Isr Med Assoc J 2011; 13: 55-59.
2. Tanaka A, Gershwin ME. Finding the cure for primary biliary cholangitis - Still waiting. Liver Int 2017; 37: 500-502.
3. Hubers LM, Beuers U. IgG4-related disease of the biliary tract and pancreas: clinical and experimental advances. Curr Opin Gastroenterol 2017; 33: 310-314.
4. Hubers LM, Maillette de Buy Wenniger LJ, Doorenspleet ME, et al. IgG4-associated cholangitis: a comprehensive review. Clin Rev Allergy Immunol 2015; 48: 198-206.
5. Trampert DC, Hubers LM, van de Graaf SFJ, et al. On the role of IgG4 in inflammatory conditions: lessons for IgG4-related disease. Biochim Biophys Acta Mol Basis Dis 2018; 1864: 1401-1409.
6. Liaskou E, Hirschfield GM, Gershwin ME. Mechanisms of tissue injury in autoimmune liver diseases. Semin Immunopathol 2014; 36: 553-568.
7. Christen U, Hintermann E. Pathogens and autoimmune hepatitis. Clin Exp Immunol 2019; 195(1): 35-51.
8. Liberal R, Grant CR, Mieli-Vergani G, et al. Autoimmune hepatitis: A comprehensive review. J Autoimmun 2013; 41: 126-139.
9. Manns MP, Czaja AJ, Gorham JD, et al. Diagnosis and management of autoimmune hepatitis. Hepatology 2010; 51: 2193-2213.
10. Oo YH, Hubscher SG, Adams DH. Autoimmune hepatitis: new paradigms in the pathogenesis, diagnosis, and management. Hepatol Int 2010; 4: 475-493.
11. Schramm C, Lohse AW. Autoimmune hepatitis on the rise. J Hepatol 2014; 60: 478-479.

12. Christen U, Hintermann E. Autoantibodies in Autoimmune Hepatitis: Can Epitopes Tell Us about the Etiology of the Disease? Frontiers in Immunology 2018; 9: 163

13. Sebode M, Weiler-Normann C, Liwinski T, et al. Autoantibodies in Autoimmune Liver Disease-Clinical and Diagnostic Relevance. Front Immunol 2018; 9: 609.

14. Mieli-Vergani G, Vergani D. Autoimmune paediatric liver disease. World J Gastroenterol 2008; 14: 3360-3367.

15. Mieli-Vergani G, Vergani D, Czaja AJ, et al. Autoimmune hepatitis. Nat Rev Dis Primers 2018; 4: 18017.

16. Czaja AJ, Manns MP. Advances in the Diagnosis, Pathogenesis and Management of Autoimmune Hepatitis. Gastroenterology 2010; 139(1): 58-72.

17. European Association for the Study of the L. EASL Clinical Practice Guidelines: Autoimmune hepatitis. J Hepatol 2015; 63: 971-1004.

18. Hirschfield GM, Karlsen TH, Lindor KD, et al. Primary sclerosing cholangitis. Lancet 2013; 382: 1587-1599.

19. Horsley-Silva JL, Carey EJ, Lindor KD. Advances in primary sclerosing cholangitis. Lancet Gastroenterol Hepatol 2016; 1: 68-77.

20. Lazaridis KN, LaRusso NF. Primary Sclerosing Cholangitis. N Engl J Med 2016; 375: 1161-1170.

21. Chapman R, Cullen S. Etiopathogenesis of primary sclerosing cholangitis. World J Gastroenterol 2008; 14: 3350-3359.

22. Hov JR, Boberg KM, Karlsen TH. Autoantibodies in primary sclerosing cholangitis. World J Gastroenterol 2008; 14: 3781-3791.

23. Bogdanos DP, Invernizzi P, Mackay IR, et al. Autoimmune liver serology: current diagnostic and clinical challenges. World J Gastroenterol 2008; 14: 3374-3387.

24. Jungst C, Lammert F. Cholestatic liver disease. Dig Dis 2013; 31: 152-154.

25. Karlsen TH, Kaser A. Deciphering the genetic predisposition to primary sclerosing cholangitis. Semin Liver Dis 2011; 31: 188-207.

26. Maillette de Buy Wenniger L, Beuers U. Bile salts and cholestasis. Dig Liver Dis 2010; 42: 409-418.

27. Boberg KM, Chapman RW, Hirschfield GM, et al. Overlap syndromes: the International Autoimmune Hepatitis Group (IAIHG) position statement on a controversial issue. J Hepatol 2011; 54: 374-385.

28. Czaja AJ. Diagnosis and management of the overlap syndromes of autoimmune hepatitis. Can J Gastroenterol 2013; 27: 417-423.

29. Rust C, Beuers U. Overlap syndromes among autoimmune liver diseases. World J Gastroenterol 2008; 14: 3368-3373.

30. Schramm C, Lohse AW. Overlap syndromes of cholestatic liver diseases and autoimmune hepatitis. Clin Rev Allergy Immunol 2005; 28: 105-114.

31. Silveira MG, Lindor KD. Overlap syndromes with autoimmune hepatitis in chronic cholestatic liver diseases. Expert Rev Gastroenterol Hepatol 2007; 1: 329-340.

32. Fickert P, Fuchsbichler A, Wagner M, et al. Regurgitation of bile acids from leaky bile ducts causes sclerosing cholangitis in Mdr2 (Abcb4) knockout mice. Gastroenterology 2004; 127: 261-274.

33. Lammert F, Wang DQ, Hillebrandt S, et al. Spontaneous cholecysto- and hepatolithiasis in Mdr2-/- mice: a model for low phospholipid-associated cholelithiasis. Hepatology 2004; 39: 117-128.

34. Christen U, Holdener M, Hintermann E. Cytochrome P450 2D6 as a model antigen. Dig Dis 2010; 28: 80-85.

35. Hintermann E, Ehser J, Christen U. The CYP2D6 Animal Model: How to Induce Autoimmune Hepatitis in Mice. J Vis Exp 2012; 60: 1-7.

36. Holdener M, Hintermann E, Bayer M, et al. Breaking tolerance to the natural human liver autoantigen cytochrome P450 2D6 by virus infection. J Exp Med 2008; 205: 1409-1422.

37. Terjung B, Spengler U, Sauerbruch T, et al. "Atypical p-ANCA" in IBD and hepatobiliary disorders react with a 50-kilodalton nuclear envelope protein of neutrophils and myeloid cell lines. Gastroenterology 2000; 119: 310-322.

38. Hintermann E, Ehser J, Bayer M, et al. Mechanism of autoimmune hepatic fibrogenesis induced by an adenovirus encoding the human liver autoantigen cytochrome P450 2D6. J Autoimmun 2013; 44: 49-60.

39. Wells RG. The portal fibroblast: not just a poor man's stellate cell. Gastroenterology 2014; 147: 41-47.

40. Ehser J, Holdener M, Christen S, et al. Molecular mimicry rather than identity breaks T-cell tolerance in the CYP2D6 mouse model for human autoimmune hepatitis. J Autoimmun 2013; 39-49.

41. Nakken KE, Nygard S, Haaland T, et al. Multiple inflammatory-, tissue remodelling- and fibrosis genes are differentially transcribed in the livers of Abcb4 (-/ -) mice harbouring chronic cholangitis. Scand J Gastroenterol 2007; 42: 1245-1255.

42. Trivedi PJ, Hirschfield GM. Review article: overlap syndromes and autoimmune liver disease. Aliment Pharmacol Ther 2012; 36: 517-533.

43. Aguilar-Najera O, Velasco-Zamora JA, Torre A. Overlap syndromes of autoimmune hepatitis: diagnosis and treatment. Rev Gastroenterol Mex 2015; 80: 150-159.

44. Katt J, Schwinge D, Schoknecht T, et al. Increased T helper type 17 response to pathogen stimulation in patients with primary sclerosing cholangitis. Hepatology 2013; 58: 1084-1093.

45. Trauner M, Fickert P, Baghdasaryan A, et al. New insights into autoimmune cholangitis through animal models. Dig Dis 2010; 28: 99-104.

Figure Legends

Figure 1: Laboratory parameters and autoantibodies were highest in Ad-Mdr2$^{-/-}$ mice.

(A) Alkaline phosphatase (AP) and alanine aminotransferase (ALT) levels in naïve and Ad-2D6 infected FVB and *Mdr2*$^{-/-}$ mice were determined in 10 mice per group over a period of 4 weeks (mean ± SEM, n = 10). Note that *Mdr2*$^{-/-}$ mice displayed strongly elevated enzyme levels already before infection (week 0). Infection resulted in a further increase in serum AP and ALT levels at week 1 post-infection, and these levels remained highest in the Ad-*Mdr2*$^{-/-}$ mice at all times. (B) Detection of anti-hCYP2D6 antibodies by ELISA using recombinant hCYP2D6 as target for sera of naïve and Ad-2D6 infected FVB and *Mdr2*$^{-/-}$ mice at week 4 after infection. Sera of 5 mice per group are shown. Note that anti-hCYP2D6 antibodies were generated at similar titers in Ad-2D6 infected FVB and *Mdr2*$^{-/-}$ mice. (C) The presence of pANCAs in serum of naïve and Ad-2D6 infected FVB and *Mdr2*$^{-/-}$ mice at week 4 after infection was analyzed using human promyelocytic leukemia HL-60 cells. Two examples out of 10 mice per group are depicted. Serum dilution was 1:20. Note that sera of Ad-*Mdr2*$^{-/-}$ mice showed the highest reactivity. Sera of diagnosed PSC patients and of healthy volunteers (3 per group) served as control. Patient sera were diluted 1:80 and control sera 1:40. Presence of pANCAs was visualized with a fluorochrome-labelled secondary anti-mouse or human antibody (green).

Figure 2: Ductular proliferation and fibrosis were strongest in livers of Ad-Mdr2$^{-/-}$ mice.

(A) Livers were harvested 4 weeks after Ad-2D6 infection of FVB and *Mdr2*$^{-/-}$ mice. Naïve littermates were used as control. Cryosections were stained for the cholangiocyte marker cytokeratin 19 (CK19, upper row) or for collagen III (lower row). Representative pictures of liver sections of 10 mice per group are depicted. Bar, 50 µm. (B) Quantification of CK19 and collagen III signals in % of total area was performed with Keyence BZ-II Analyzer software.

Presented values are the mean ± SEM (n = 5) of whole liver sections excluding the capsule with 5 mice per group. Significant differences ($p < 0.05$, unpaired, two-tailed t-test) are indicated (*). (C) Relative collagen III mRNA levels at week 4 after infection determined by quantitative RT-PCR are shown. Naïve and Ad-2D6 infected FVB and *Mdr2*$^{-/-}$ mice were analyzed. Data were normalized to GAPDH signals and are presented as mean ± SD (n = 5) of fold increase relative to naïve FVB mice. (D) Immunoblot detection of αSMA in total liver homogenates. Livers of 4 mice per group were analyzed at week 4 after infection. Depicted are 3 representative examples per group. β-actin was used as loading control. Expression levels of naïve FVB mice were set at 1 (mean ± SD, n = 4). Significant differences ($p < 0.05$, unpaired, two-tailed t-test) are indicated (*).

Figure 3: Ad-Mdr2$^{-/-}$ *livers contained the highest level of HSCs.*

(A) Desmin as marker of HSCs was stained in cryosections of livers from naïve or Ad-2D6 infected FVB or *Mdr2*$^{-/-}$ mice at week 4 after infection. Note the strong accumulation of HSCs in the portal fields of Mdr2$^{-/-}$ and Ad-*Mdr2*$^{-/-}$ livers compared to Ad-FVB livers and naïve FVB controls. Representative pictures of liver sections of 10 mice per group. Bar, 50 µm. (B) Immunoblot detection of desmin in total liver homogenates. Livers of 4 mice per group were analyzed at week 4 after infection. Depicted are 3 representative examples per group. β-actin was used as loading control. Expression levels of naïve FVB mice were set at 1 (mean ± SD, n = 4). Significant differences ($p < 0.05$, unpaired, two-tailed t-test) are indicated (*). (C) Co-staining of desmin (green) and CK19 (red) in liver sections described in (A) confirmed the concentration of HSCs in periductular areas in *Mdr2*$^{-/-}$ and Ad-*Mdr2*$^{-/-}$ livers. Nuclei are stained with DAPI (blue). Upper row shows merged pictures and lower row the desmin signal only. Bar, 20 µm. Representative pictures of liver sections of 10 mice per group.

Figure 4: Activated PFs accumulated numerously in Mdr2$^{-/-}$ and Ad-Mdr2$^{-/-}$ livers.

(A) Elastin, a marker of activated PFs, was stained in livers of naïve or Ad-2D6 infected FVB and *Mdr2*$^{-/-}$ mice at week 4 after infection. Representative pictures of liver sections of 10 mice per group. Bar, 50 µm. (B) Co-staining experiments visualizing elastin (green) and CK19 (red) were performed with the livers described in (A). Note that in FVB and Ad-FVB livers, the elastin signal, which surrounded blood vessels, resulted mainly from smooth muscle cells (arrow heads). In *Mdr2*$^{-/-}$ and Ad-*Mdr2*$^{-/-}$ livers, elastin-positive cells corresponded to activated PFs (arrows) due to their location in periductular areas and they contributed considerably to the strong elastin staining. Nuclei are stained with DAPI (blue). Upper row shows merged pictures and lower row the elastin signal only. Bar, 20 µm

Figure 5: Cellular infiltrations were most prominent in livers of Ad-Mdr2$^{-/-}$ mice.

(A) Livers of Ad-2D6 infected FVB and *Mdr2*$^{-/-}$ mice or naïve littermates were harvested at week 4 after infection. Liver sections were stained for the presence of monocytes/macrophages (CD11b, upper row), dendritic cells (CD11c, middle row) or neutrophils (Ly6G, lower row). Representative pictures of liver sections of 10 mice per group are shown. Bar, 50 µm. (B) Quantification of CD11b, CD11c and Ly6G signals is presented in % of total area. Values are the mean ± SEM (n = 15) of 3 pictures per liver section per mouse with 5 mice per group. Significant differences ($p < 0.05$, unpaired, two-tailed t-test) are indicated (*).

Figure 6: General and CYP2D6-specific T cell analyses show SC and AIH linked differences.

(A) Livers were collected from Ad-2D6 infected FVB or *Mdr2*$^{-/-}$ mice or naïve littermates at week 4 after infection and cryosections were stained for CD4 T cells (CD4, upper row) or CD8 T cells (CD8, lower row). Representative pictures of liver sections of 10 mice per group

are shown. Bar, 50 µm. (B) Quantification of CD4 and CD8 T cell signals in % of total area is presented. Values are the mean ± SEM (n = 15) of 3 pictures per liver section per mouse with 5 mice per group. Significant differences ($p < 0.05$, unpaired, two-tailed t-test) are indicated (*). (C) Livers were harvested from mice treated as described in (A) and lymphocytes were isolated. They were stimulated with hCYP2D6-specific CD4 or CD8 peptides, stained for IFNγ production and analyzed by flow cytometry. Cells gated for lymphocytes have been further gated for CD4 T cells (red) and CD8 T cells (blue). Values are mean ± SEM (n = 12) in % of total CD4 or CD8 T cells. Significant differences ($p < 0.05$, unpaired, two-tailed t-test) are indicated (*). Note that the frequency of hCYP2D6-specific CD4 T cells was reduced whereas the frequency of hCYP2D6-specific CD8 T cells was two-fold enhanced in Ad-*Mdr2*$^{-/-}$ mice compared to Ad-FVB mice.

Figure 7: Characterization of the overall T cell immune balance in naïve and Ad-2D6 infected FVB and Mdr2$^{-/-}$ *mice.*

(A, B) Livers were collected from Ad-2D6 infected FVB or *Mdr2*$^{-/-}$ mice or naïve littermates at week 4 after infection. Lymphocytes were isolated, stimulated with anti-CD3 IgG, anti-CD28 IgG and IL-2 and stained for intracellular IL-10, IFNγ, IL-4 or IL-17 production before analysis by flow cytometry. Cells gated for lymphocytes have been further gated for CD4 T cells (A) and CD8 T cells (B). Pie charts were calculated using the mean of data from 6 - 10 mice per group. Representative dot blots are shown in Figure S2.

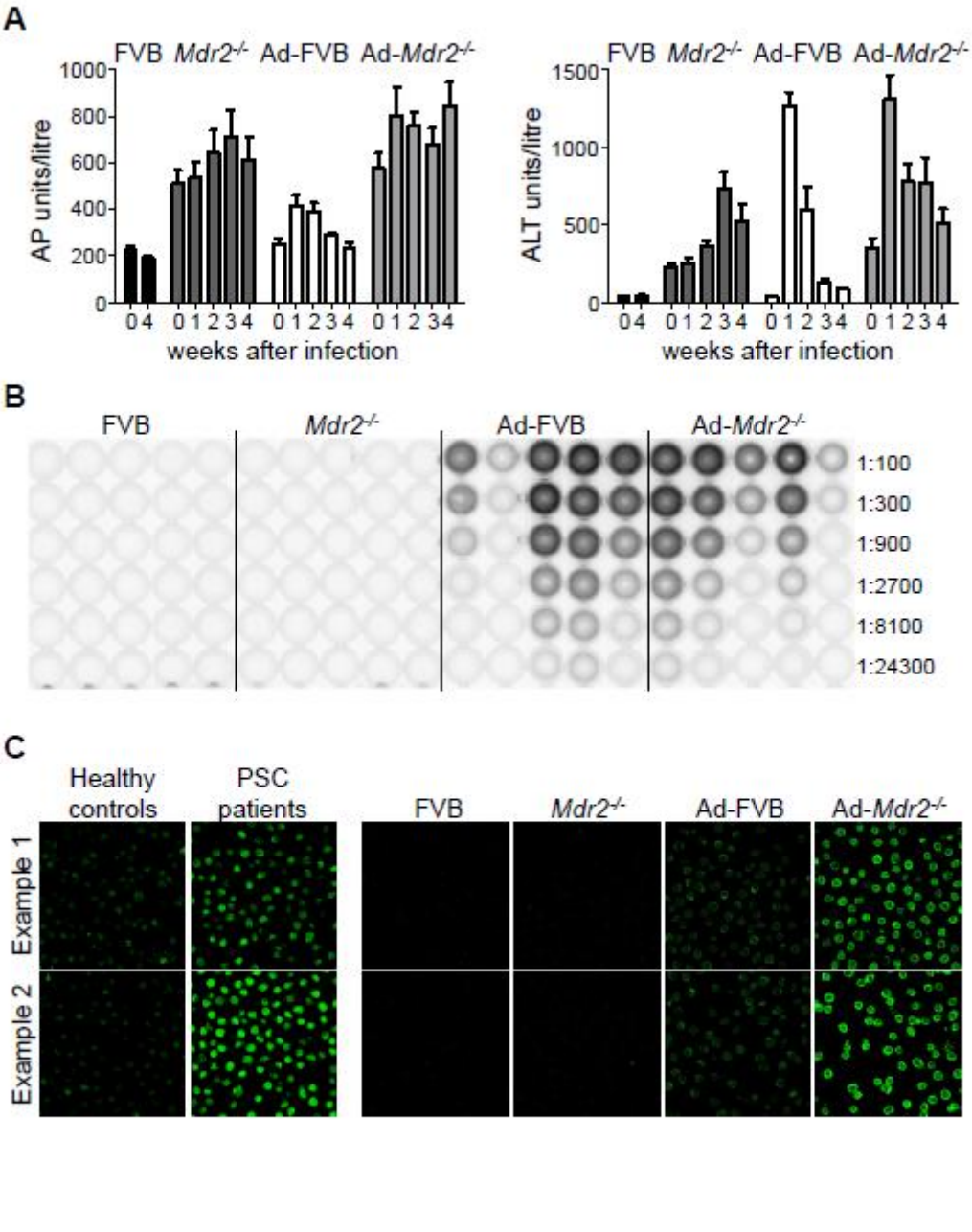

Fig. 1, Fuchs et al.

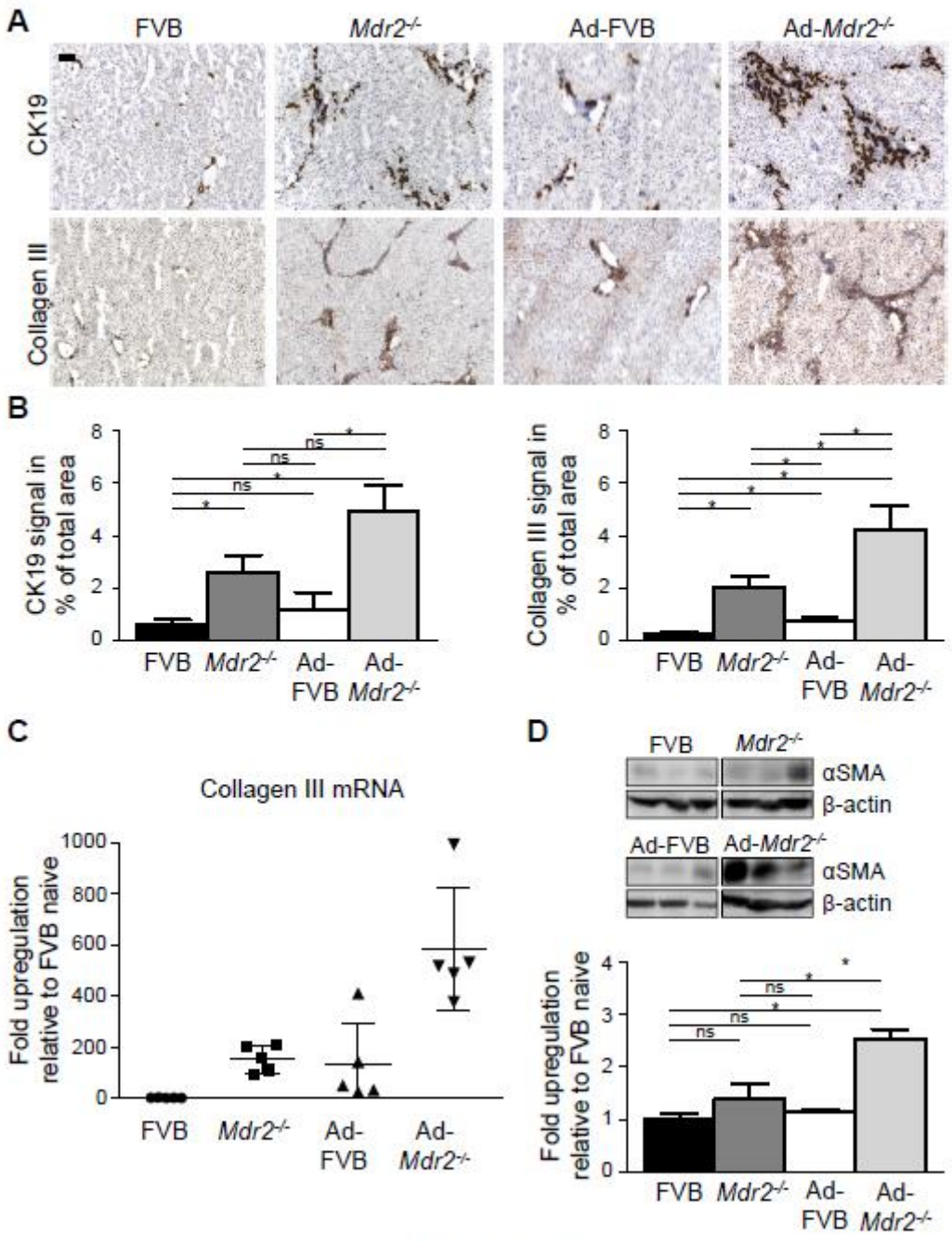

Fig. 2, Fuchs et al.

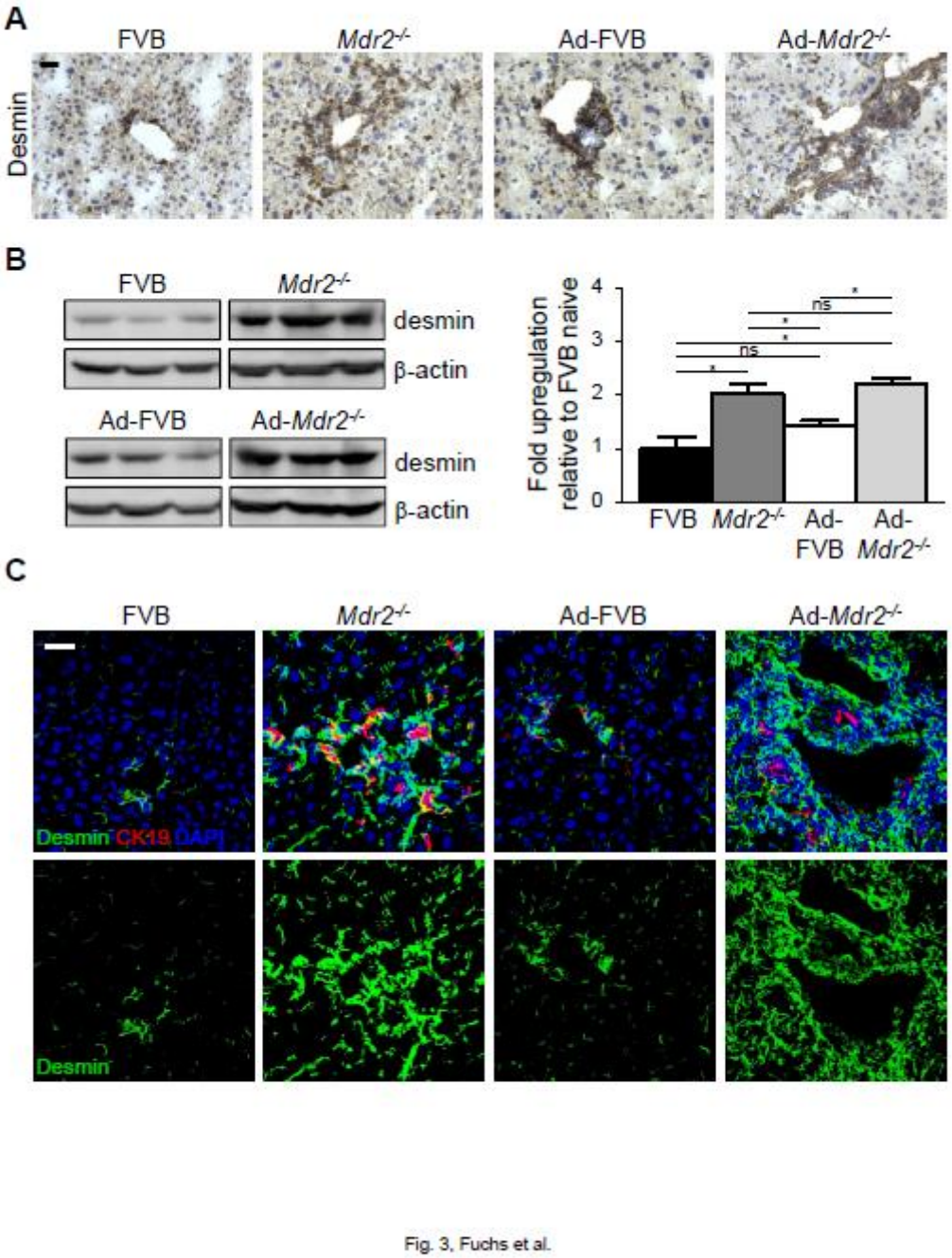

Fig. 3, Fuchs et al.

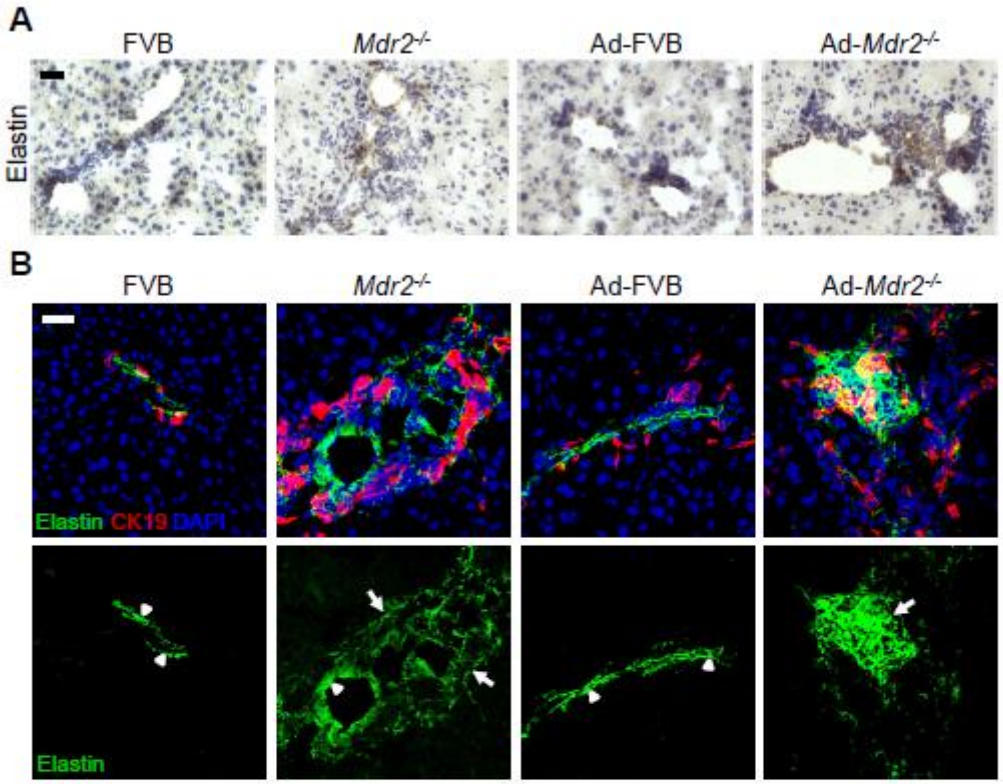

Fig. 4, Fuchs et al.

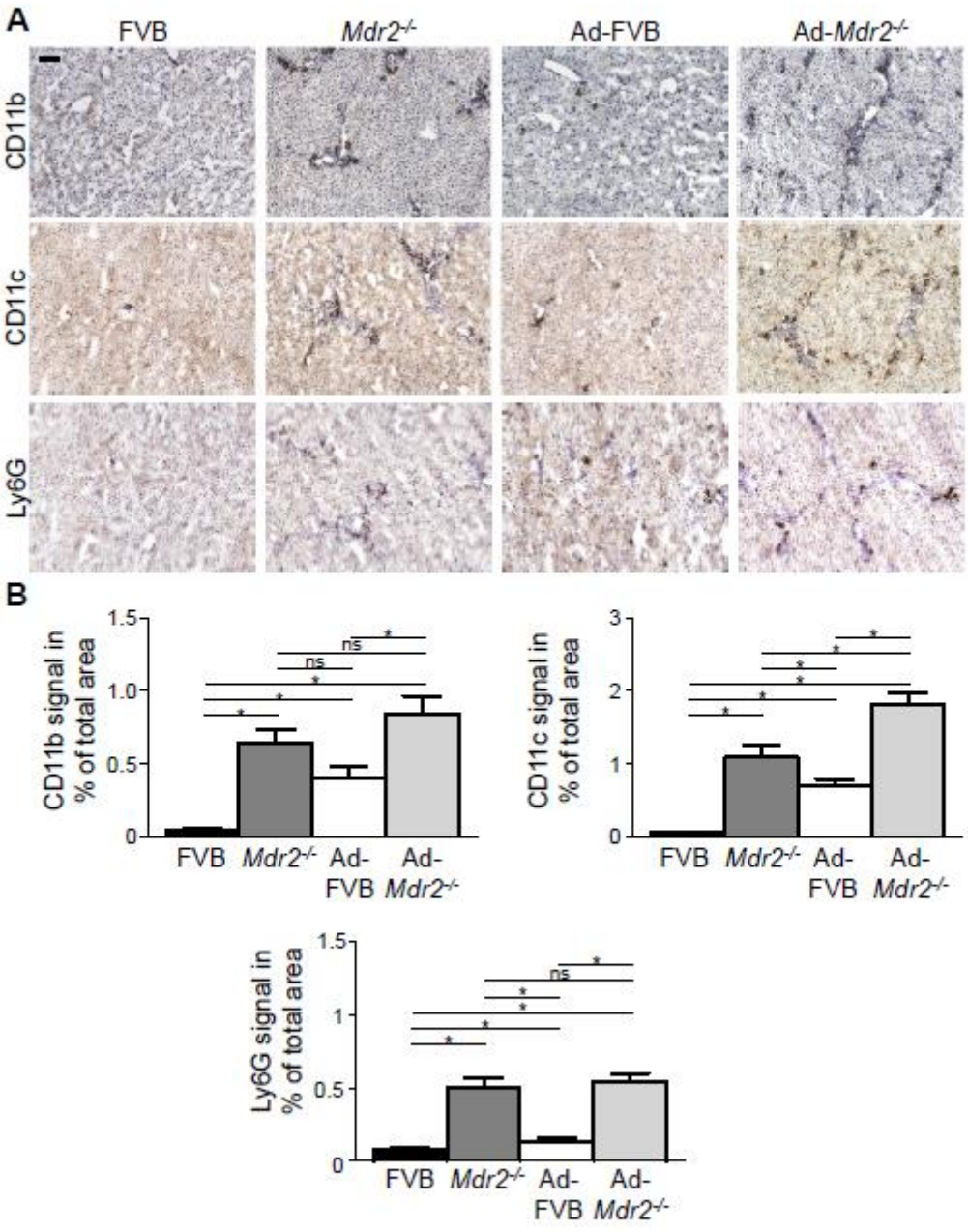

Fig. 5, Fuchs et al.

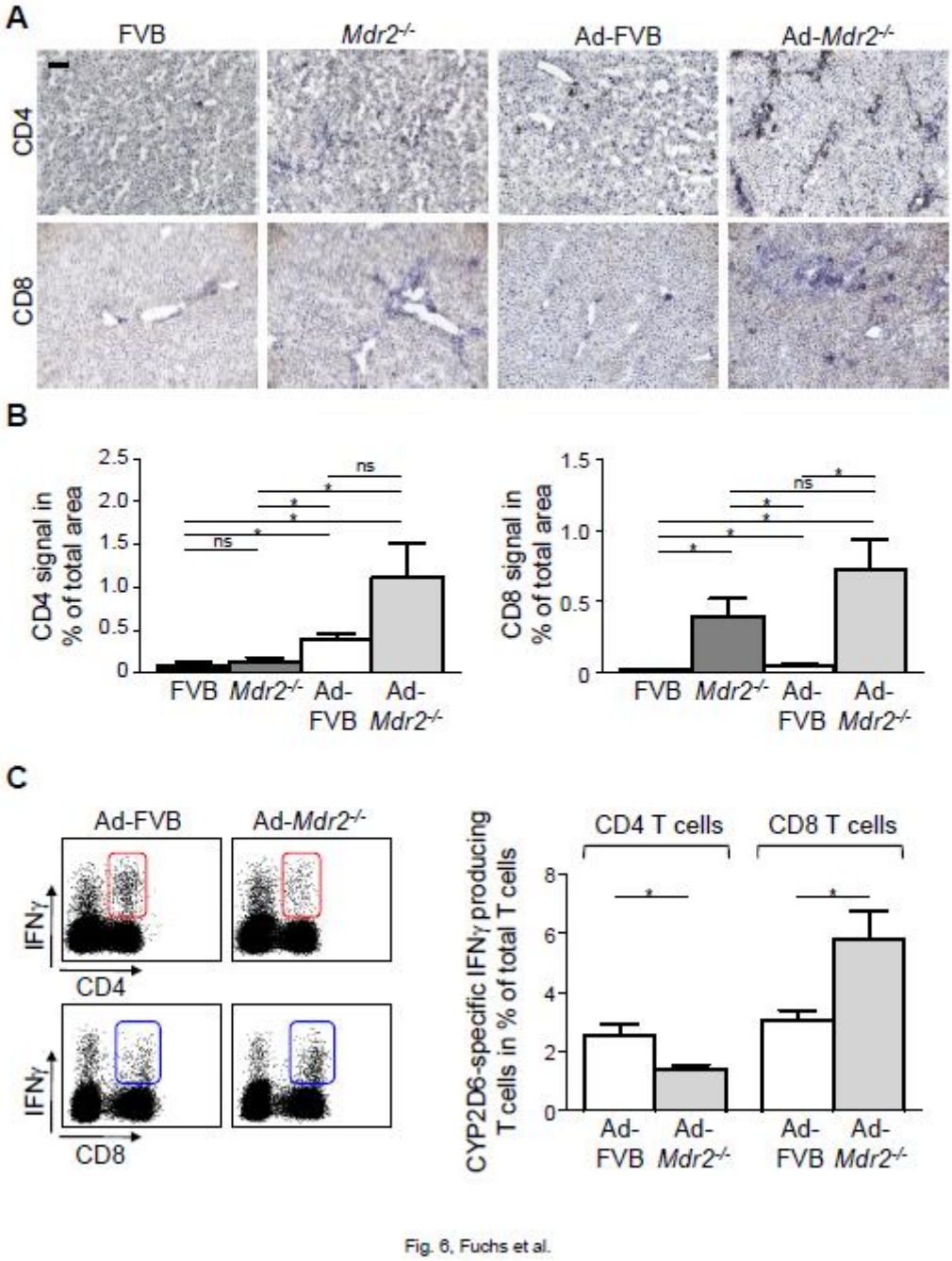

Fig. 6, Fuchs et al.

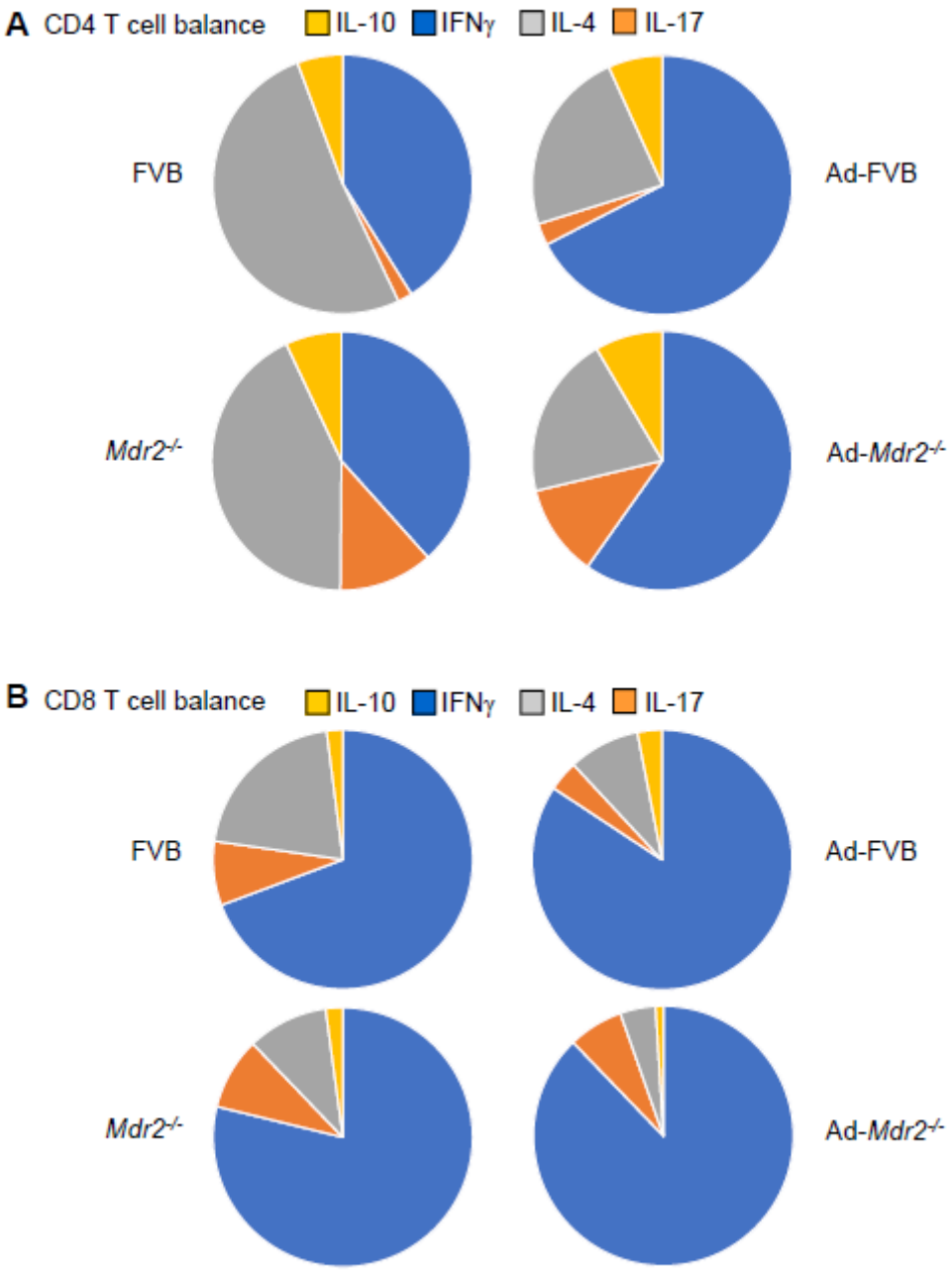

Fig. 7, Fuchs et al.

8.1. **Declaration of academic honesty**

Except where stated otherwise by reference or acknowledgment, the work presented was generated by myself under the supervision of my advisors during my doctoral studies. All contributions from colleagues are explicitly referenced in the thesis.

The material listed below was obtained in the context of collaborative research:

Fig. 15: Serum reactivity of pANCA- like antibodies to human promyelocytic leukemic HL-60 cells, PD Dr. Edith Hintermann, Pharmazentrum Frankfurt. She did the staining and I created the figure.

Frankfurt,